

BOTTOM CURRENTS AND ABYSSAL SEDIMENTATION  
PROCESSES SOUTH OF ICELAND

by

Alexander N. Shor

A. B., Harvard University

(1974)

Submitted in partial fulfillment of the  
requirements for the degree of  
Doctor of Philosophy

at the

Massachusetts Institute of Technology

and the

Woods Hole Oceanographic Institution

October 1979

*via February 1980*

*1 2/1*

Signature of Author:

.....  
Joint Program in Oceanography, Massachu-  
setts Institute of Technology - Woods  
Hole Oceanographic Institution, and  
Department of Earth & Planetary Sciences  
and Department of Meteorology, Massachu-  
setts Institute of Technology

*o o*

Certified by:

.....  
Thesis Supervisor

Accepted by:

.....  
Chairman, Joint Oceanography Committee  
in the Earth Sciences, Massachusetts  
Institute of Technology - Woods Hole  
Oceanographic Institution

**WITHDRAWN**  
MASSACHUSETTS INSTITUTE  
OF TECHNOLOGY  
**FROM**  
MAY 3 1980  
**MIT LIBRARIES**  
LIBRARIES



Room 14-0551  
77 Massachusetts Avenue  
Cambridge, MA 02139  
Ph: 617.253.5668 Fax: 617.253.1690  
Email: docs@mit.edu  
<http://libraries.mit.edu/docs>

## **DISCLAIMER OF QUALITY**

Due to the condition of the original material, there are unavoidable flaws in this reproduction. We have made every effort possible to provide you with the best copy available. If you are dissatisfied with this product and find it unusable, please contact Document Services as soon as possible.

Thank you.

**There are numerous pages within this thesis  
that contain poor greyscale image reproduction.  
This is the best copy available.**

BOTTOM CURRENTS AND ABYSSAL SEDIMENTATION PROCESSES SOUTH OF ICELAND

by Alexander Noble Shor

Submitted to the Massachusetts Institute of Technology-Woods Hole Oceanographic Institution Joint Program in Oceanography on October 31, 1979, in partial fulfillment of the requirements for the degree of Doctor of Philosophy.

ABSTRACT

An investigation was carried out to observe the geologic effects of steady bottom currents on sediments of East Katla Ridge on the southern insular rise of Iceland. Near-bottom southwest to west-flowing currents exceeded  $20 \text{ cm sec}^{-1}$  for two weeks over a 25-kilometer wide section of the ridge flank between approximately 1400 and 1800 meters water depth; maximum density and minimum temperature were observed at 1800 meters. Total transport of Iceland-Scotland Overflow Water was calculated to be  $5.0 \times 10^6 \text{ m}^3 \text{ sec}^{-1}$ ; suspended sediment transport is approximately  $0.4 \times 10^6 \text{ grams sec}^{-1}$ , with a net deposition of 10 to 15 cm/1000 years estimated from the flux difference in and out of the station array.

Sediment distribution patterns indicate that the current axis, where flow exceeds approximately  $15 \text{ cm sec}^{-1}$ , is a site of erosion and winnowing (sand layer formation) while the current margin is a site of rapid accumulation (from observed Holocene rates of 25 to 35 cm per 1000 yr to estimated rates of greater than 100 cm/1000 yr based on 3.5 kHz echosounder records). Holocene silty turbidites are locally thick in a submarine channel; sandy turbidites and current-winnowed 'sandy contourites' are present in the axis of the major submarine canyon.

'Sandy contourite' deposits beneath the axis of the Iceland-Scotland Overflow Current are very poorly sorted muddy sands lacking primary sedimentary structures. Bioturbation is inferred to cause the unique characteristics of these deposits, as well as the absence of fine silt laminae in 'muddy contourites' at the current margin.

Thesis Supervisor: Dr. Charles D. Hollister  
Title: Senior Scientist

#### ACKNOWLEDGEMENTS

I thank Drs. Charles Hollister and David Johnson, who provided the support and encouragement for this thesis study, and for many other stimulating projects along the way. I appreciate also the efforts of L. Valentine Worthington, Peter Lonsdale and John Southard, who also served on my thesis committee.

I am grateful for the support provided by the crew and scientific party during ATLANTIS II Cruise 94-1, especially to David Johnson (chief scientist) and David Casiles (master) who helped make the expedition a great success. The able technical assistance provided by Warren Witzell and Alan Driscoll was appreciated greatly, as was the support of David Porter, who operated the CTD system, and Jerry Graham, who was in charge of current meter moorings. I thank all the personnel for their assistance.

Financial support for shipboard operations and most of the post-cruise data analysis was provided by NSF Grant OCE76-81491 to Dr. Charles Hollister. Sediment trap and hydrocast operations received partial support under ONR Contract N00014-74-C-0262.

Dr. A. H. Bouma of the U. S. Geological Survey generously provided his box corer and supplies. Arrangements for rental and operation of the CTD system were made by R. Millard. Current meter rental was arranged with the assistance of G. Anderson and S. Ferreira of the Marine Life Research Group (Scripps Institution). Rental of the Lamont-Doherty



nephelometer system was provided through the courtesy of L. G. Sullivan and P. E. Biscaye.

I appreciate the assistance of numerous members of the Woods Hole scientific staff and of my student colleagues for the many discussions and critiques which helped me focus my ideas and understand the implications of the results we obtained south of Iceland. I am particularly grateful to Roger Flood, Wilf Gardner, and Mary Jo Richardson for their interest and help with my work, and for their unselfish cooperation during our time as students together.

The assistance of Cynthia Brown-Stanton and Elaine Ellis in typing the manuscript is greatly appreciated, as is the acquisition of a Wang word processing system by WHOI.

And finally, I am most overwhelmingly grateful to Nancy and Caleb, my wife and son, who suffered even more than I in the final stages of this thesis. To both of you, please accept my promise that I shall never write another thesis. I love you both too much.

TABLE OF CONTENTS

	<u>Page</u>
ABSTRACT.....	2
ACKNOWLEDGEMENTS.....	3
LIST OF FIGURES.....	7
LIST OF TABLES.....	10
CHAPTER I: INTRODUCTION.....	12
A. Statement of the Problem.....	12
B. Previous Work: "Contourites".....	18
C. Objectives.....	20
D. Iceland Basin: Regional Setting.....	21
E. Description of Shipboard Program.....	31
CHAPTER II: THE DEEP CIRCULATION OVER EAST KALTA RIDGE.....	36
A. Direct Current Measurements.....	36
B. Indirect Current Indicators.....	44
C. Volume Transport.....	48
D. Water Masses.....	55
E. Bottom Mixed Layers and Near-Bottom Density Distribution.....	57
F. Suspended Sediment Flux.....	69
G. Summary of Deep Circulation.....	76
CHAPTER III: SEDIMENT DISTRIBUTION PATTERNS.....	78
A. Echo Character: Definition of Acoustic Units.....	78
B. Geographic Distribution of Acoustic Units.....	105
C. Surface Sediment Lithology.....	110
D. Summary of Sediment Distribution.....	120
CHAPTER IV: SEDIMENTATION PROCESSES -- OBSERVATIONS AND INTERPRETATION.....	123
A. Bottom Bedforms: Photographic Evidence.....	123
B. Stratigraphy: Recognition of Holocene Deposits.....	131
C. Accumulation Rates of Holocene Sediments.....	142
D. Primary Sedimentary Structures.....	145
E. Bioturbation.....	157
F. Sediment Size Analysis.....	171
G. Contourites: Recognition and Characteristics.....	184
H. Summary: 'Contourite' Characteristics in the Katla Ridge Region.....	197

	<u>Page</u>
CHAPTER V: SUMMARY AND CONCLUSIONS.....	199
A. Summary.....	199
B. Conclusions.....	204
REFERENCES.....	205
APPENDIX I: STATION LOCATIONS.....	212
APPENDIX II: FLOW CALCULATIONS.....	225
APPENDIX III: CARBONATE CONTENT OF PISTON CORES.....	231
APPENDIX IV: SAND CONTENT OF PISTON CORES.....	237
APPENDIX V: PALEOMAGNETIC ORIENTATION OF CORES.....	241

LIST OF FIGURES

<u>Figure</u>	<u>Page</u>
1.1 Bathymetry of Iceland Basin.....	13
1.2 Bathymetry of Katla Ridge survey area.....	15
1.3 Physiographic provinces of Katla Ridge region.....	25
1.4 Airgun section across East and West Katla Ridges.....	29
2.1 Current meter and hydrographic stations.....	38
2.2 Current velocity vectors from six current meters.....	40
2.3 Progressive vectors from six current meters.....	42
2.4 Potential temperature vs. salinity.....	46
2.5 Geostrophic velocity profiles for station pairs.....	49
2.6 Potential temperature, salinity and light scattering along northern CTD section.....	51
2.7 Potential density: Myrdalsjokull Canyon.....	58
2.8 Potential density: east flank, East Katla Ridge.....	61
2.9 Potential density: southeast of West Katla Ridge.....	64
2.10 Potential density distribution around Katla Ridges at 100 meters above bottom.....	66
2.11 Correlation of suspended sediment concentration with light scattering for Katla Ridge stations.....	72
3.1 Echo character map of Katla Ridge survey area.....	79
3.2 Bathymetry of Katla Ridge survey area, showing track coverage of AII-94-1.....	81
3.3 Examples of 3.5 kHz echograms: transparent sediments.....	83
3.4 Examples of 3.5 kHz echograms: laminated sediments.....	85

<u>Figure</u>		<u>Page</u>
3.5	Examples of 3.5 kHz echograms: acoustically impenetrable sediments.....	87
3.6	Examples of 3.5 kHz echograms: 'multi-laminated' sediments...	89
3.7	Examples of 3.5 kHz echograms: asymmetric sediment waves.....	91
3.8	Examples of 3.5 kHz echograms: symmetric sediment waves.....	93
3.9	Examples of 3.5 kHz echograms: 'dissected terrain'.....	95
3.10	Examples of 3.5 kHz echograms: small-scale surface roughness and hyperbolae.....	97
3.11	Examples of 3.5 kHz echograms: surface erosion.....	99
3.12	Examples of 3.5 kHz echograms: slumps, v-channels, and scarps.....	101
3.13	Echo character map of Katla Ridge survey area.....	106
3.14	Carbonate content of piston core sediments.....	112
3.15	Sand-size component of piston core sediments.....	114
4.1	Bottom photograph, East Katla Ridge crest.....	124
4.2	Bottom photograph, East Katla Ridge current axis.....	126
4.3	Bottom photograph, East Katla Ridge lower east flank.....	129
4.4	Bottom photograph, Myrdalsjokull Channel.....	132
4.5	Stratigraphy of cores 3PC, 4PC.....	135
4.6	<u>Globigerina pachyderma</u> in cores 1PC, 4PC, 12PC.....	137
4.7	X-radiographs of turbidite sand layers, east flank of East Katla Ridge.....	148
4.8	Photograph of face of core 10BC (multi-laminated channel sediments).....	151

<u>Figure</u>	<u>Page</u>
4.9 X-radiograph of core 10BC (multi-laminated channel sediments) showing deep burrows and silt laminae.....	153
4.10 X-radiograph of core 9PC, showing cross-laminated sands from Myrdalsjokull Canyon axis.....	155
4.11 X-radiograph of core 9BC, showing bioturbation effects in transparent sediments adjacent to Myrdalsjokull Channel.....	159
4.12 X-radiograph of core 11BC, showing bioturbation effects in transparent sediments adjacent to Myrdalsjokull Channel.....	161
4.13 Photograph of face of core 11BC, showing structureless silt deposit with deep, open burrows.....	163
4.14 Photograph of face of core 15BC, showing extensively burrowed muddy sand surface layer.....	166
4.15 Photograph of core top of core 3BC, showing effects of both winnowing and bioturbation on sediments beneath the bottom current.....	169
4.16 Size frequency distribution, surface sediment samples.....	174
4.17 Size frequency, fine fraction of surface sediments.....	177
4.18 Cumulative frequency and statistics for model mixture of sand plus mud.....	180
AI-1 Station locations: Current meters, CTD lowerings.....	221
AI-2 Station locations: Nephelometer, hydrographic lowerings, sediment trap moorings.....	223
AI-3 Station locations: Piston cores, box cores, camera lowerings.....	225
AV-1 Box core orientation.....	242

LIST OF TABLES

<u>Table</u>	<u>Page</u>
1.1 Principal characteristics of turbidite and contourite sand or silt, modified from Hollister and Heezen (1972).....	19
2.1 Current meter data.....	37
2.2 Volume transport rates of Norwegian Sea Overflow Water and Norwegian Sea Deep Water.....	54
2.3 Suspended sediment concentration vs. light scattering.....	71
2.4 Suspended sediment transport rates for Katla Ridge stations...	75
4.1 Radiocarbon dates, core 4PC.....	141
4.2 Summary of grain size distribution in surface sediments.....	173
4.3 Sandy contourites: sedimentary characteristics.....	185
4.4 Muddy contourites: sedimentary characteristics.....	194
AI-1 CTD stations.....	213
AI-2 Nephelometer stations.....	214
AI-3 Hydrocasts.....	215
AI-4 Camera stations.....	216
AI-5 Current meters.....	217
AI-6 Sediment trap moorings.....	218
AI-7 Piston cores.....	219
AI-8 Box cores.....	220
AII-1 Station information for flow calculations.....	226
AII-2 Velocity calculations.....	227
AII-3 Volume transport below reference level.....	229

<u>Table</u>		<u>Page</u>
AIII-1	Carbonate summary.....	232
AIV-1	Coarse fraction.....	238
AV-1	Summary of mean orientation of box cores.....	244
AV-2	Paleomagnetic determinations, box cores.....	245



## CHAPTER I: INTRODUCTION

### A. Statement of the Problem

The initial goal of this research project was to test the hypothesis "can bottom current deposits be distinguished from turbidity current deposits based on primary sedimentary structures in Holocene sediments from the insular rise and slope southeast of Iceland?"

The Iceland margin was chosen as the study area because: (1) A bottom current originating at the Iceland-Faroe Ridge is known to flow through the region (Steele et al., 1962; Worthington and Volkmann, 1965) with velocities in the range  $10-30 \text{ cm sec}^{-1}$ . Experimental work suggests that such velocities are competent to resuspend and transport fine-grained sediments (Southard et al., 1971; Lonsdale and Southard, 1974). (2) Volcanic activity in the Vestmann Island (Surtsey) on the Iceland outer shelf and historical subglacial eruptions and resulting sediment-laden floods on Iceland ("jokulhlaups") suggest that turbidity currents have been active in post-glacial and probably historical times through one or both of two major submarine canyons incised into the Katla Ridges (Figures 1.1, 1.2).

The research problem was intended as a test of the contour current model of continental rise genesis proposed by Heezen et al. (1966) and developed further by Hollister (1967), Hollister and Heezen (1972) and others from work on the continental rise of eastern North America.

FIGURE 1.1: Bathymetry of Iceland Basin. Locations of the Katla Ridges and submarine canyons on the southern Iceland margin are indicated. Contours are in corrected meters. Bathymetry after Lonsdale (unpublished data) and NAVOCEANO World Relief Map NA 5.

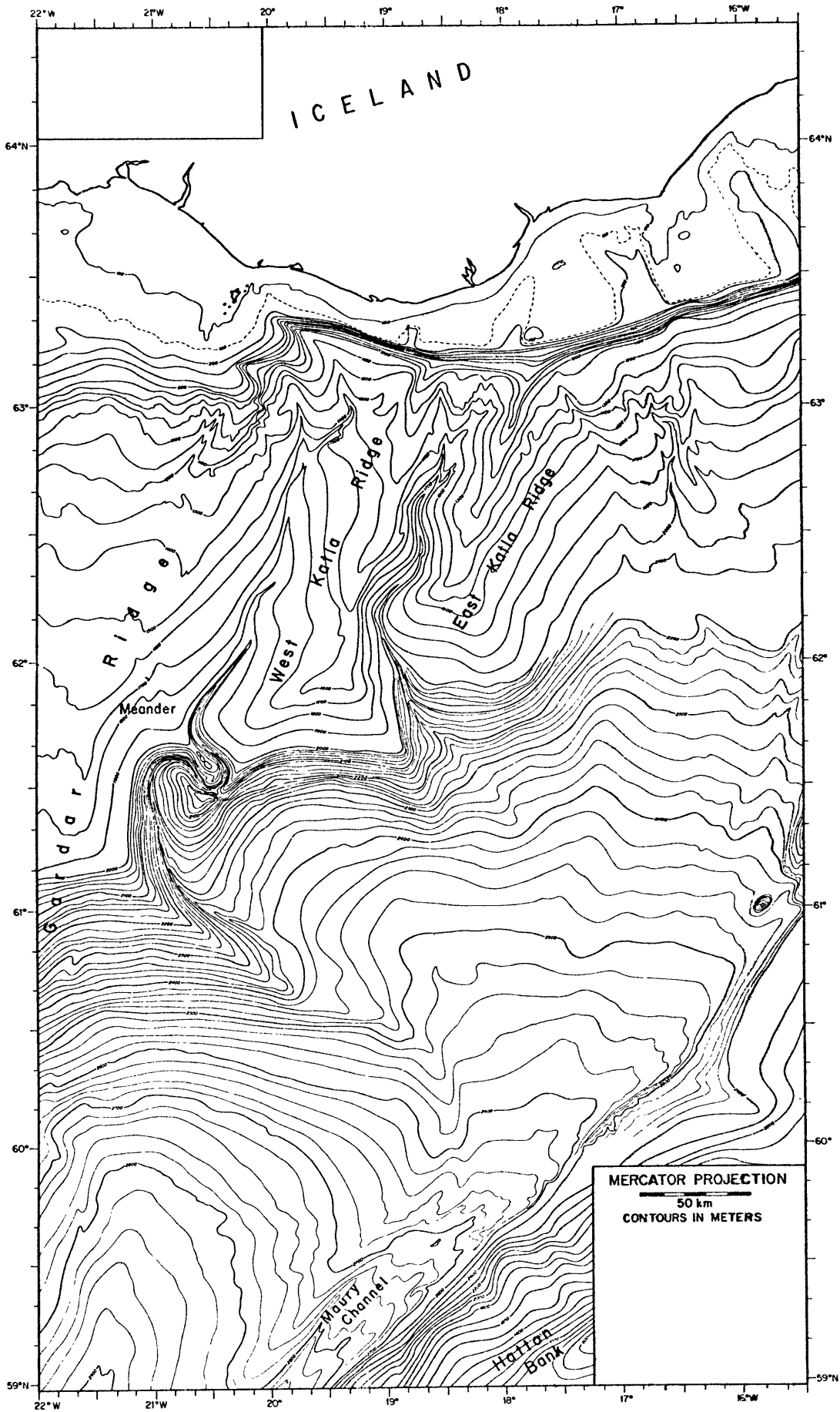
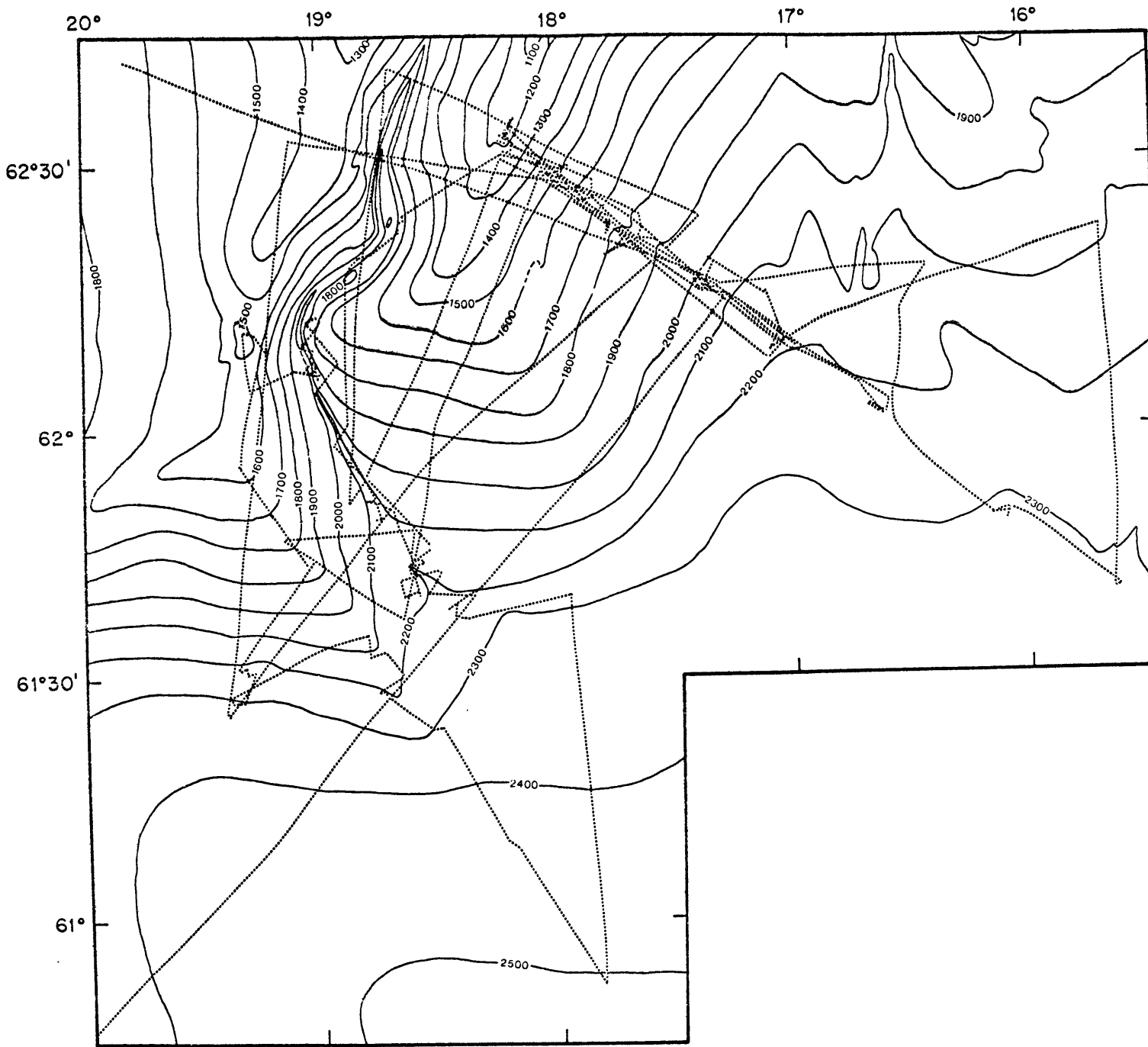


FIGURE 1.2: Bathymetry of Katla Ridge survey area. Track lines indicate extent of echosounder coverage obtained during Atlantis II Cruise 94-1. Contours in regions of insufficient track coverage are based on NAVOCEANO World Relief Map NA 5. Contours in corrected meters.



The basic assumptions involved in this model are:

- 1) The primary source of continental rise sediments is the continental shelf and upper slope where land-derived terrigenous muds are deposited;
- 2) Sediments are transported downslope by turbidity currents, with the bulk of the coarse sediment bypassing the continental rise towards ultimate deposition as turbidites in abyssal plains; and
- 3) A portion of the fine fraction of the turbidites is removed by bottom currents ("contour currents") flowing parallel to the continental rise bathymetric contours. This material is deposited from a turbulent nepheloid layer as a sediment wedge (the continental rise) striking parallel to the continental margin.

Studies on the North American rise have concentrated on demonstrating the presence of an otherwise poorly documented "contour current" (Western Boundary Undercurrent) using bottom photographs and sediment structures of continental rise sediments and contrasting these structures with those in sediments from the adjacent abyssal plains. Provenance of sediments in each sedimentary province has generally been deduced from composition (clay mineralogy, heavy mineral assemblages, distinctive color), or assumed. However, since this region has few unique mineral assemblages which may be unambiguously used for provenance determination, this task has been only marginally successful.

The present investigation, by contrast, was undertaken in a region in which the dominant terrigenous sediment source is local and well

defined (submarine canyons originating on the Icelandic shelf) and in which a "steady" bottom current is known to be currently active (Steele et al, 1962) and is inferred to have been so on independent evidence at least since the retreat of pack ice from the Iceland-Faroe Ridge following the last glacial maximum (Worthington, 1970; Ruddiman and Glover, 1975; McIntyre et al., 1972; Kellogg, 1976; 1977). The purpose of this study is to delineate the characteristics of sediment deposits developed under a known current field and with well defined sediment source characteristics.

B. Previous Work: "Contourites"

Analysis of cored continental rise sediments has led to the classification of a sediment type referred to as "contourite" which is characteristic of the rise province, and which differs in certain respects from "turbidites" commonly recovered from abyssal plain environments. The characteristic sedimentary structures and compositional differences between "contourite" and turbidite as defined by Hollister and Heezen (1972), Field and Pilkey (1971) and Fritz and Pilkey (1975) for sediments off eastern North America are found in Table 1.1.

Although distinct differences can often be discerned between these two types of deposits it should be stressed that transitional or overlapping depositional structures are observed, and our understanding of the depositional history of the continental rise has relied heavily on surface morphology, acoustic stratigraphy and geologic inference. Uncertainties in these inferences are largely due to a poor understanding of the variability of the Western Boundary Undercurrent on a geologic time scale.

TABLE 1.1: Principal characteristics of turbidite and contourite sand or silt, modified from Hollister and Heezen (1972).

	Turbidite	Contourite
Size Sorting	moderate to poorly sorted >1.50 (Folk)	well to very well sorted < 0.75 (Folk)
Bed Thickness	usually 10-100 cm	usually < 5 cm
Grading	normal grading ubiquitous, bottom contacts sharp, upper contacts poorly defined	normal and reverse grading, bottom and top contacts sharp
Cross laminations	common, accentuated by concentrations of lutite	common, accentuated by concentrations of heavy minerals
Horizontal laminations	common in upper portion only, accentuated by concentration of lutite	common throughout, accentuated by concentrations of heavy minerals of foraminifera shells
Massive Bedding	common, particularly in lower portion	absent
Grain Fabric	little or no preferred grain orientation in massive graded portions	preferred grain orientation parallel to the bedding plane is ubiquitous throughout bed
Matrix (<2 $\mu$ )	10 to 20%	0 to 5%
Microfossils	common and well preserved, sorted by size throughout bed	rare and usually worn or broken, often size sorted in placers
Plant and skeletal remains	common and well preserved, sorted by size throughout bed, shallow fauna often found	rare and usually worn or broken, shallow fauna absent
Heavy minerals	high variability within single units, unstable minerals common (garnet, epidote)	low variability; stable suites (zircon, tourmaline, rutile)
Classification (Pettijohn)	graywacke and sub-graywacke and orthoquartzite	sub-graywacke, arkose and orthoquartzite



The work on the North American continental rise suffers from the neglect of proximal turbidites and the large spatial separation of the rise and abyssal plain cores on which "contourite" and turbidite characteristics were determined. This may explain why investigations of continental rise sediments and morphology in the vicinity of submarine channels and fans (e.g. Stanley et al., 1971, Damuth and Kumar, 1975) have arrived at different conclusions regarding the relative importance of downslope and along-slope transport of sediments in continental rise genesis. No detailed work has previously been carried out with the goal of correlating sediment texture with sedimentary provinces defined by bottom current measurements and surface echo sounding in a region with a volumetrically important local source of terrigenous sediment.

### C. Objectives

The goal of this study is to describe the geologic effects of a bottom current on the sea bed in a region of strong, unidirectional flow. This study concentrates on the past 13,000 years (which is the approximate termination of the last glacial period at this site) in order to avoid the problem of changes in deep circulation and sediment input from Iceland which have been predicted to occur across this climatic boundary (e.g. Weyl, 1968; Kellogg, 1976; 1977; Ruddiman and Bowles, 1978; and others).

Specific goals of this research are:

1. To define the modern flow of Iceland-Scotland Overflow Water (ISOW) through the Katla Ridge region;

2. To describe the regional distribution of Holocene sediments in the region and observe whether deposition and erosion may be uniquely related to bottom current flow; and
3. To characterize the sedimentary deposits lying beneath the current in hopes of using these criteria for subsequent identification of current deposits where flow conditions are not directly observed.

D. Iceland Basin: Regional Setting

Iceland Basin is bordered on the north by the Iceland-Faroe Ridge, on the east by Rockall Plateau and on the west by Iceland and Reykjanes Ridge (Figure 1.1). It opens to the south into the European Basin without a geographical barrier. The deepest part of the basin is Maury Channel, which lies east of the center and immediately west of Hatton Drift, a sediment pile on the southwest flank of Rockall Plateau. The Iceland Basin plunges to the south, with a maximum depth at the southern end of Rockall Plateau of about 3000 meters. The Iceland-Faroe Ridge has several sills between 500 and 600 meters deep connecting Iceland Basin with the Norwegian Sea. Reykjanes Ridge plunges southward from above sea level on Iceland to approximately 1000 meters at  $56^{\circ}\text{N}$ ; Rockall Plateau likewise rises above 1000 meters north of  $56^{\circ}\text{N}$ .

Two elongate, north-south striking sediment drifts are developed in Iceland Basin (Johnson and Schneider, 1969; Jones et al., 1970; Davies and Laughton, 1972). Gardar Drift is continuous from the southern slope of Iceland (approximately  $62^{\circ} 30'\text{N}$ ) to at least  $54^{\circ}\text{N}$ , where it becomes difficult to follow due to the irregular bathymetry associated

with Charlie-Gibbs Fracture Zone. The strike of Gardar Drift is approximately  $210^{\circ}$ , nearly parallel to Reykjanes Ridge over its entire length. Several smaller, subparallel drifts are developed between Gardar Drift and Reykjanes Ridge south of  $60^{\circ}\text{N}$ .

Hatton Drift extends along the western flank of Rockall Plateau from its southern limit to somewhat north of  $61^{\circ}\text{N}$ . It appears to wrap around the southern edge of the plateau and connect with Feni Drift in Rockall Trough. The northern extension is poorly defined, probably due to the gradual shallowing of the basin.

Hydrographic studies (Fuglister, 1960; Steele et al., 1962; Worthington and Volkmann, 1965; Worthington and Wright, 1970; Hollister et al., 1976) reveal a well-developed deep thermohaline current flowing southward along the eastern flank of Reykjanes Ridge from its origin in the Norwegian Sea (Worthington, 1970) to Charlie-Gibbs Fracture Zone near  $53^{\circ}\text{N}$  (Worthington and Volkmann, 1965; Garner, 1972; Shor et al., 1980 (in press)). The flow originates through several channels and sills across the Iceland-Faroe and Scotland-Faroe Ridges, and is driven by downslope flow of high density Norwegian Sea Deep Water brought to shallow depths by convective winter overturning (Worthington, 1970). This dense water mixes with warmer, more saline water as it flows downslope (Worthington and Volkmann, 1965; Steele et al., 1962).

At least some of the overflow may be episodic over short periods (weeks to years) (Lee and Ellett, 1965; Ellett and Roberts, 1973; Crease, 1965), although the Faroe Bank Channel appears to maintain a steady flow (Crease, 1965). Episodic overflow may account for the variable volume

transport calculated by Worthington and Volkmann (1965) along the length of the flow (from 2.0 to  $7.6 \times 10^6 \text{ m}^3 \text{ sec}^{-1}$ ), although problems associated with choice of an appropriate reference level may explain some of the uncertainty (Ivers, 1975). Velocities measured within the overflow current along the western margin of the Iceland Basin (Steele et al., 1962; Worthington and Volkmann, 1965) are typically in the range 10-30  $\text{cm sec}^{-1}$ .

Gardar and Hatton Drifts are presumed to originate from sediment transported along the margins of the basin by bottom currents of Iceland-Scotland Overflow Water (Jones et al, 1973; Johnson and Schneider; 1969, Ruddiman, 1972). The morphology of the drifts ranges from smooth, convex piles to irregular deposits with mudwaves and scour, and from sharply peaked to nearly flat. Similar features have been described in the Argentine Basin (Ewing et al., 1971); the western North Atlantic (Johnson and Schneider, 1969; Ewing and Hollister, 1972; Flood, 1978) and in Rockall Trough (Johnson and Schneider, 1969; Jones et al., 1973; Flood, 1978) in regions swept by deep thermohaline currents.

A major study of sedimentation processes on the east flank of Reykjanes Ridge by Ruddiman (1972) concluded that sediment deposition between  $53^{\circ}$  and  $60^{\circ}\text{N}$  along the ridge has been almost entirely a result of bottom current flow, with major accumulations in fracture zones and along the current margin (Gardar Drift). He inferred that current activity has been important in controlling sedimentation since at least 17 my BP based on the age of the youngest crust beneath the deposits interpreted as current-deposited in seismic reflection profiles.

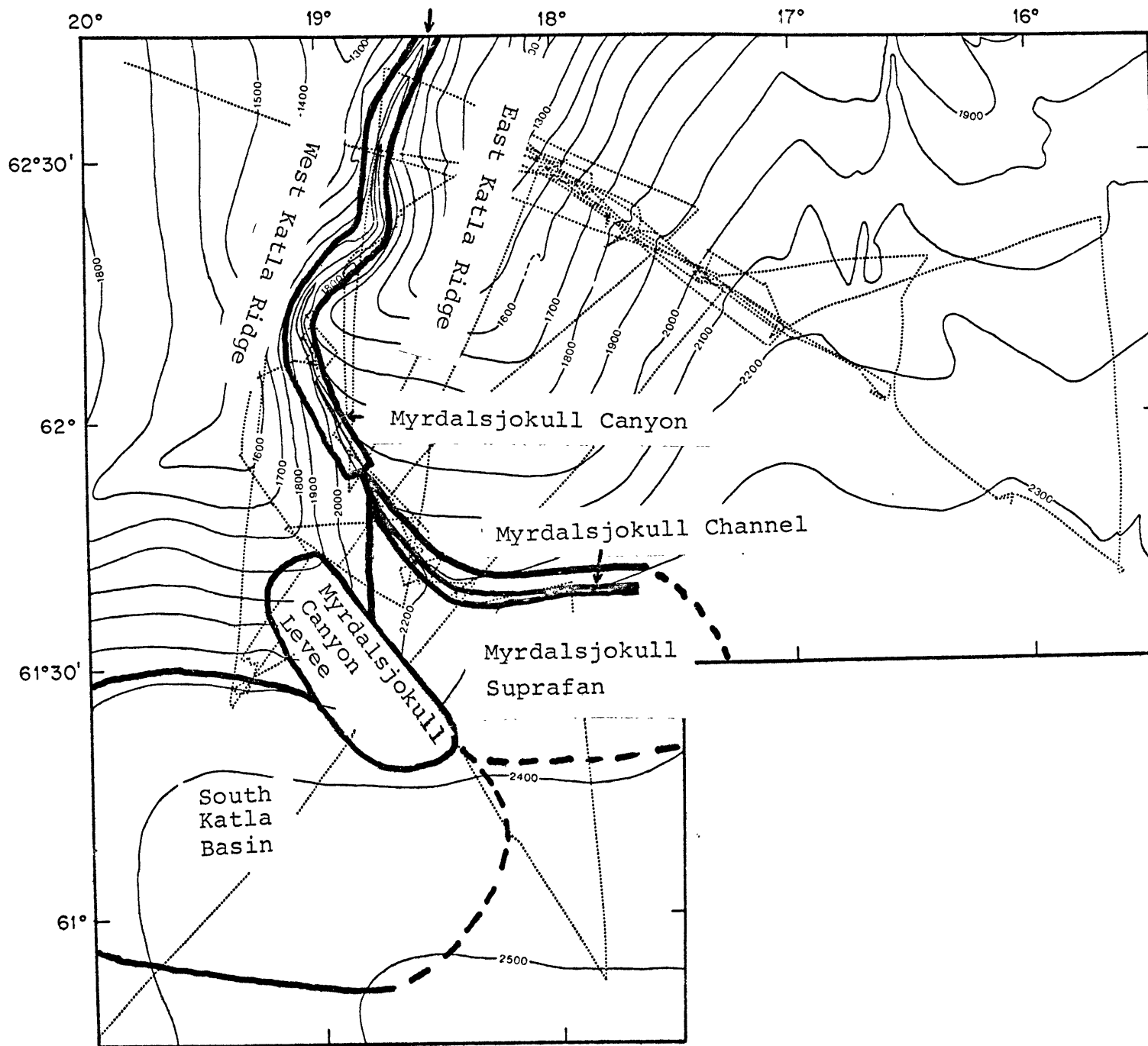
### Katla Ridges

The Katla Ridges (Malmborg, 1974) are a pair of thick sediment deposits located on the insular rise south of Iceland (Figure 1.2). They cover an area of approximately 20,000 km<sup>2</sup>, and they strike about 210° from the insular slope. They may be distinguished morphologically between water depths of approximately 1000 and 2300 meters. The two ridges are separated by Myrdalsjokull Canyon (Egloff & Johnson, 1979; Johnson and Palmasson, In prep.), a deep narrow turbidity-current pathway originating on the Iceland shelf. A second major canyon (Reynidsjup Canyon) bounds West Katla Ridge to the west. It also originates on the Iceland shelf in the vicinity of the Vestmann Islands (Hollister and Lonsdale, 1977).

Previous works by Malmborg (1974), Egloff and Johnson (1979) and Johnson and Palmasson (In prep.) have designated the names 'Katla Ridges' (East and West) to the two sediment drifts, and the names Myrdalsjokull and Reynidsjup Canyons to the two canyons which bound them (Figure 1.3). Two additional features outside the immediate study area (Gardar Ridge, discussed at length by Johnson et al, 1970 and Ruddiman, 1972), and Maury Channel (Cherkis, et al, 1973) are major morphologic features of Iceland Basin which are inferred to be related to the ridge/channel morphology of the Iceland Rise.

For the purpose of this study several additional morphologic features in the vicinity of East Katla Ridge are assigned generic names. These include (as illustrated in Figure 1.3): Myrdalsjokull Suprafan, Myrdalsjokull Canyon Levee, Myrdalsjokull Channel, and South Katla

FIGURE 1.3: Physiographic provinces of Katla Ridge region. See text for discussion.



Basin. The following criteria have been used for the identification of the geomorphic units named above:

1) Myrdalsjokull Suprafan extends from the mouth of Myrdalsjokull Canyon at approximately 2120 meters axial depth towards the east out of our survey area. It is bounded on the south by Myrdalsjokull Canyon Levee, and has been the site of deposition of turbidites for an indeterminate period. Over 0.25 sec ( >250 meters) of deposition has occurred in the former erosional extension of Myrdalsjokull Canyon at 18°25'W (Figure 5 in Johnson and Shor, 1977).

2) Myrdalsjokull Canyon Levee: This SE-trending spur of West Katla Ridge is a barrier to southward flow of turbidity currents. The southwest flank is mantled with asymmetric sediment waves.

3) Myrdalsjokull Channel is a depositional feature approximately one kilometer wide extending from the mouth of Myrdalsjokull Canyon (61°58'N, 18°48'W) towards the southeast (trend 140°). It is recognized as both a local depression in bathymetry and as the site of deposition of a unique acoustically-defined sediment type ('multi-laminated'). The channel undergoes a major change in trend (to 090°) and acoustic character at 18°20'W where the topographic expression of the channel continues eastward. The acoustically 'multi-laminated' sediment fill characteristic of the western end of the channel terminates, apparently due to the ability of turbidity currents to breach the Myrdalsjokull Canyon Levee and flow to the south.

4) South Katla Basin is a cul-de-sac basin bounded on the north by West Katla Ridge and Myrdalsjokull Canyon Levee, on the west by a submarine

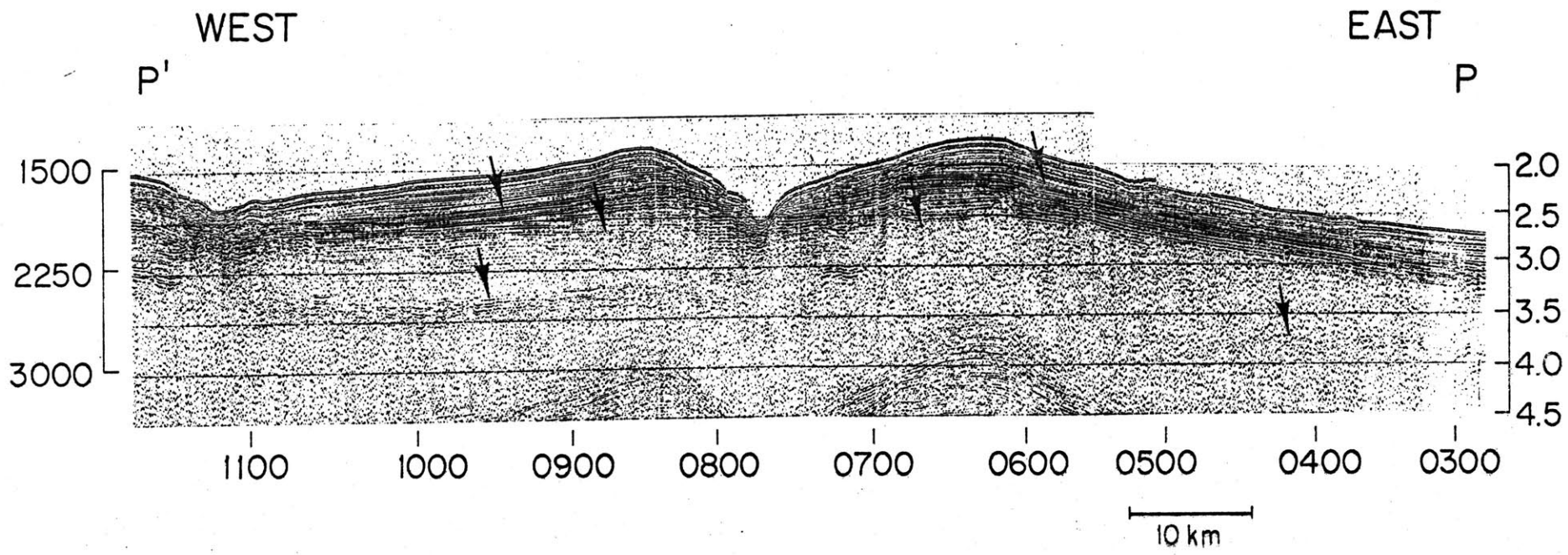


meander at the mouth of Reynidsjup Canyon (Lonsdale and Hollister, 1979, in press) and on the south by a levee extending eastwards from Reynidsjup Canyon. South Katla Basin is open at its eastern end, and merges with the central portion of Iceland Basin and the Maury Channel/Fan complex.

The Katla Ridges are smooth features with accumulation of sediment beneath the crests in excess of 1.5 kilometers (Figure 1.3). Their mode of formation is inferred to result from the rapid denudation of Iceland during the Neogene, sediment transport to the base of the slope by turbidity currents and subsequent entrainment and transport southwestward by the flow of Iceland-Scotland Overflow Water. The development of the ridges has very likely not been a continuous process, however, and major fluctuations in both turbidity current (input) and bottom current activity (redistribution) since the Early-Middle Miocene are likely (e.g. Shor & Poore, 1978).

Development of the Katla Ridges as levees built by Plio/Pleistocene turbidity currents, as suggested by Johnson and Palmason (in prep.), does not appear reasonable. Our profile (Figure 1.4) across both East and West Katla Ridges shows that the convex ridge morphology is evident in deep reflectors to approximately 0.75 sec subbottom (> 0.75 km), which would imply accumulations rates since 3 myBP (during ridge growth) of >250 meters per million years (25 cm/1000 yr) if the sea level fluctuations of the glacial Pliocene and Pleistocene are solely responsible for the turbidity currents inferred to be responsible for the development of the canyon/ridge morphology. It seems more plausible that the ridge and canyon system began to develop considerably earlier, during the Early to

FIGURE 1.4: Airgun section across East and West Katla Ridges (Profile P-P' of Johnson and Shor, 1977). This reflection profile was obtained during AII-94-1 with a 40 cubic inch airgun, and crosses the ridge crests at approximately 62°30' N. Arrows beneath each ridge indicate (starting with the deepest): 1) acoustic basement, 2) the shallowest flat-lying reflector, which is inferred to predate ridge formation, and 3) the highly reflective group of reflectors within the convex ridge sequence, which is tentatively inferred to be a Pliocene unconformity (see text).



Middle Miocene, a time when evidence from both tectonic studies (Vogt 1972) and sedimentary studies (Ruddiman, 1972; Shor and Poore, 1978) indicate that a major reorganization of sea floor spreading and bottom circulation occurred in the North Atlantic. A set of strong reflections at approximately 0.3 sec subbottom may be an unconformity related to the changing sea level on Iceland and the resultant increase in turbidity current flow (Figure 1.4). This feature is well above the deepest ridge reflections, however.

The Katla Ridges are located on crust whose presumed age ranges from ca. 35 to 50 myBP based on extrapolation of magnetic lineations from the south (e.g. Vogt & Avery, 1974). Magnetic anomaly 18 is observed in both AII-94 data and LDGO data (Talwani et al, 1974) beneath the east flank of East Katla Ridge (Schouten, personal communication).

Basement depths throughout the northern North Atlantic (north of  $53^{\circ}\text{N}$ ) are shallow relative to the worldwide averages for crust of equivalent age (Luyendyk et al, 1978; Parsons & Sclater, 1977; and others). However, subsidence rates are not observed to be different. Instead, the entire Reykjanes Ridge appears to be shallow, and to have been so at least since 36 myBP. The crest dips from above sea level on Iceland to normal (approximately 2000 meters) depth at the Charlie-Gibbs Fracture Zone near  $53^{\circ}\text{N}$ . Thus the shallow depth of our study area is a regional tectonic feature, and not a local anomaly.

#### E. Description of Shipboard Program

During June and July of 1977, the author spent 15 days in the Katla Ridge region of Iceland Basin during Atlantis II cruise 94-1 (Johnson and

Shor, 1977) to study the influence of abyssal currents on accumulation patterns of Holocene sediments on the Katla Ridges and to investigate the impact of turbidity currents as both direct and indirect sources of sediment on and around the fan seaward of Myrdalsjokull Canyon. Operations on this cruise are summarized below:

#### Navigation

A combination of satellite and LORAN C navigation was used. Fixes with LORAN C were taken (automatically) every 10 minutes, and were supplemented with fixes recorded manually. Satellite data was routinely recorded by the mate on watch. Both systems worked well, and the only problems were caused by weather interference with the LORAN. Most of these fixes proved to be correctable, however. Navigation in all portions of the survey area may be considered to have a precision of approximately  $\pm 0.1$  n.m.

#### Station Data

1. CTD profiles. Twenty-six CTD profiles were obtained in the Iceland Basin region using the Neil Brown<sup>R</sup> CTD system modified by R. Millard and L. Armi at Woods Hole. Twenty-two of these profiles provided usable pressure, temperature and salinity data from the surface to near-bottom. Three stations (CTD #16, 17, 18) provided only temperature data due to failure of the conductivity cell, while one station (CTD #20) did not profile the entire water column, but was a test station using a second instrument at the site of CTD #19.

CTD data was reduced on shore under the direction of Robert Millard of WHOI. Problems with data acquisition were resolved for the 22 good

stations and data quality is comparable to that expected for this Neil Brown<sup>R</sup> instrument (accuracy of  $t \pm .001^{\circ}\text{C}$ ,  $S \pm .003^{\circ}/\text{oo}$ ,  $P \pm 0.1$  dbar; precision of  $S \pm .001^{\circ}/\text{oo}$  for each cast). Salinities were calibrated against samples obtained at each station with Niskin and Nansen bottles to correct for drift in the conductivity sensor.

Ten good CTD lowerings were made on the northern section of stations at nine locations extending from the ridge crest at approximately 1180 meters to the center of the basin at approximately 2320 meters. CTD #32 was a reoccupation of CTD #11. Seven stations were occupied on a transect extending SE from the crest of West Katla Ridge, four lowerings were made in Myrdalsjokull Canyon and Channel, and one lowering was in the current axis on the southern flank of W. Katla Ridge (all station locations are tabulated and figured in Appendix I).

2. Nephelometer profiles. A total of 27 nephelometer profiles were obtained in the Iceland Basin region using the system developed at Lamont-Doherty Geological Observatory by Thorndike (1975). In general the locations of the nephelometer stations correspond with the CTD lowerings, with the nephelometer attached to the wire 10 meters above the CTD (Appendix I).

3. Hydrocasts. Twenty-four hydrographic stations were occupied, each of which consisted of between five and fifteen water samples (using 5-liter bottles and 30-liter bottles) (Appendix I). Water samples were filtered through 0.6 micron Nuclepore<sup>R</sup> filters for analysis of the concentration and composition of suspended particulates and the underlying surface sediments. The measurements of total concentration of suspended

particulates were used to calibrate the nephelometer profiles. Temperature and salinity from hydrocasts were used to calibrate the salinity data acquired on adjacent CTD lowerings. Details of suspended sediment studies will be reported by M. J. Richardson (Ph.D. dissertation in progress; WHOI/MIT Joint Program in Oceanography).

4. Bottom current measurement. Three current meters, of the type developed by the Scripps Institution of Oceanography Marine Life Research Group (Schick et al, 1968) were deployed at a total of six locations on the east flank of the East Katla Ridge to measure the speed and direction of the thermohaline current flowing along the ridge. Each instrument was positioned 10 meters above the sea floor, and recorded currents over a period of approximately one week. The location of the transect of current meters corresponds with the western end of the northern transect of CTD stations (Appendix I).

5. Coring. Twelve standard piston cores and fourteen box cores were obtained in the Katla Ridge area (Appendix I). The box core used is that described by Bouma (1969, p. 339-342). Generally the box corer functioned well, although poor penetration resulted in poor or no recovery at 4 stations (#2, 5, 13, 14 BC). The locking compass used for core orientation was lost during a test station, and was not used during the cruise. Paleomagnetic declination was used for azimuthal orientation of the cores. All piston cores were rigged with 40 feet (13 meters) of core barrel, and generally penetrated completely with only a minor amount of flow-in. Piston core 7 PC did not trip properly, and recovered only disturbed sediments.

6. Bottom photography. Nine camera stations in the Katla Ridge area yielded one or more useable exposures, and a total of 42 useable exposures were obtained in the region. The camera used (Benthos Model 371 Utility Camera System) was extensively tested in shallow water and consistently performed in a satisfactory manner, but failed repeatedly during the Iceland Basin work, despite extensive efforts by electronics technicians to remedy the problems. Camera station locations and number of usable exposures at each are listed in Appendix I.

7. Sediment trap moorings. In order to estimate the vertical flux of suspended particulates, three moorings of sediment traps were deployed in the Katla Ridge region: two along the East Katla Ridge transect, and one near the turbidity current channel (Appendix I). This data is part of a study of sedimentation processes by M. J. Richardson and will be discussed in her Ph.D. dissertation.

#### Underway data

Routine collection of 3.5 kHz echosounder profiles was carried out throughout the cruise, weather permitting. During periods when storms prevented use of the 3.5 kHz system, the 12 kHz backup system was used. Overall quality of records was good, although some record sections are noisy due to poor weather conditions.

Airgun (40 cubic inch) and magnetometer data was gathered on a number of profiles within the survey area. The airgun data is summarized and illustrated in Johnson and Shor (1977).



## CHAPTER II: THE DEEP CIRCULATION OVER EAST KATLA RIDGE

Circulation of Iceland-Scotland Overflow Water (ISOW) around and over East Katla Ridge is inferred from a series of current meters, hydrographic sections, and bottom photographs.

### A. Direct Current Measurements

Direct current measurements were made 10 meters above bottom at six locations on the east flank of East Katla Ridge (Figure 2.1). This section was composed of three current meters moored for one week followed by redeployment of the same meters at alternating depths down the flank for one additional week. These current meters show a velocity core (a flow greater than 20 centimeters per second) flowing somewhat upslope of the contours (up to  $45^{\circ}$ ) flanked on either side by reduced velocities. This indicates that our section encompassed most or all of the main flow of the ISOW through the East Katla Ridge region.

Velocity information measured at current meter deployments on the east flank of East Katla Ridge is summarized in Table 2.1 and Figures 2.2 and 2.3. Current meters moored in 1400, 1600 and 1800 meters water depth all recorded steady, unidirectional flow towards the west to southwest (CM 6, 2, 5 respectively). Vector mean velocities exceeded  $18 \text{ cm sec}^{-1}$  over the recording period (5.5 to 6.75 days). Maximum speeds observed during 15-minute digitizing intervals were  $29 \text{ cm sec}^{-1}$ . Flow was directed upslope from the contours by 30 to  $45^{\circ}$ .

The shallowest current meter (CM 3, 1177 meters) on the ridge crest displayed a strong M2 tidal component, with mean flow towards the west

TABLE 2.1: Current meter data.

	<u>HT ABOVE</u>	<u>DURATION</u>	<u>VECTOR MEAN</u>		<u>MEAN SPEED</u>	<u>VELOCITY @ 217°</u>
	<u>BOTTOM</u>		speed	direction	(cm/sec)	(cm/sec)
	(meters)	(hours)				
CM 1	10	162	10.6 cm/sec	227°T	14.0	10.4
CM 2	10	151	20.9 cm/sec	226°T	21.0	13.7
CM 3	10	144	13.3 cm/sec	282°T	14.5	5.4
CM 4	10	156	5.8 cm/sec	273°T	8.8	3.2
CM 5	10	152	20.0 cm/sec	247°T	20.4	17.3
CM 6	10	132	18.7 cm/sec	265°T	21.5	12.5

	<u>LATITUDE</u>	<u>LONGITUDE</u>	<u>WATER DEPTH</u>	<u>GMT</u>
CM 1	62°17.4'N	17°24.6'W	2000 (meters)	2300/26 June- 1900/03 July
CM 2	62°28.3'N	17°53.5'W	1600	0400/27 June- 1330/03 July
CM 3	62°34.9'N	18°15.0'W	1177	0820/27 June- 1000/03 July
CM 4	62°10.8'N	17°03.6'W	2171	0300/04 July- 1800/10 July
CM 5	62°23.2'N	17°42.4'W	1796	0825/04 July- 1200/10 July
CM 6	62°30.8'N	18°04.8'W	1393	1930/04 July- 0800/10 July

FIGURE 2.1: Current meter and hydrographic stations. Locations of all CTD stations occupied during AII-94-1 plus 6 current meter moorings are indicated. Mean vector velocity for period of current meter deployments are indicated. Solid line encloses the 17-station array which is used for volume transport and suspended sediment flux calculations. Figure from Shor, 1978.

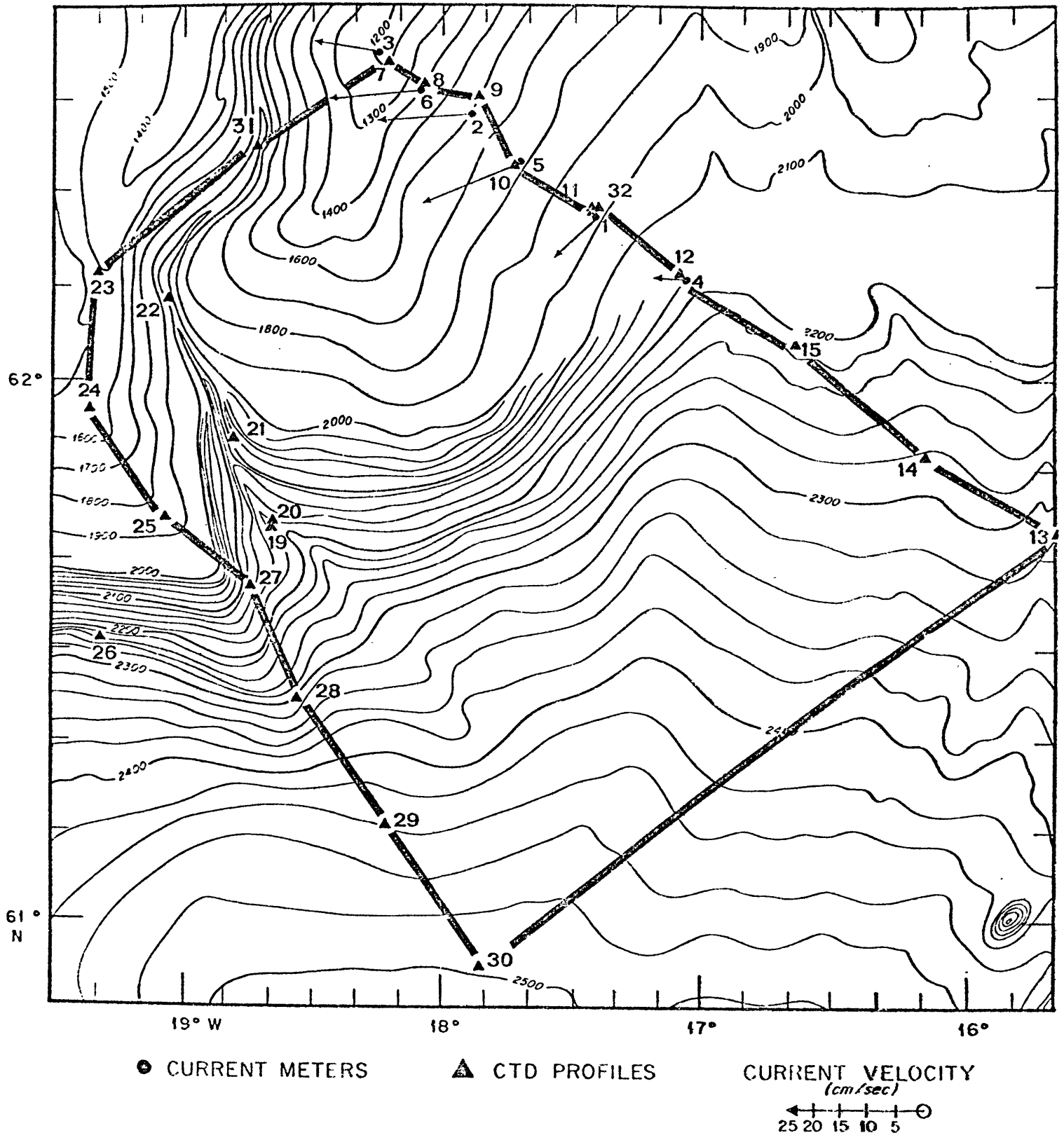


FIGURE 2.2: Current velocity vectors from six current meters. Current meter locations are indicated in Figure 5. Velocity vectors are plotted against date(GMT), and 30-minute averages are plotted every hour. Tidal components have not been removed. Compass orientation is as indicated; vertical vectors are perpendicular to the CTD station line strike ( $127^{\circ}$ ) for comparison with velocity estimated by geostrophic calculations. Note uniformity of current direction and speed at the three meters located within the axis of the ISOC flow (CM 6, 2, 5).

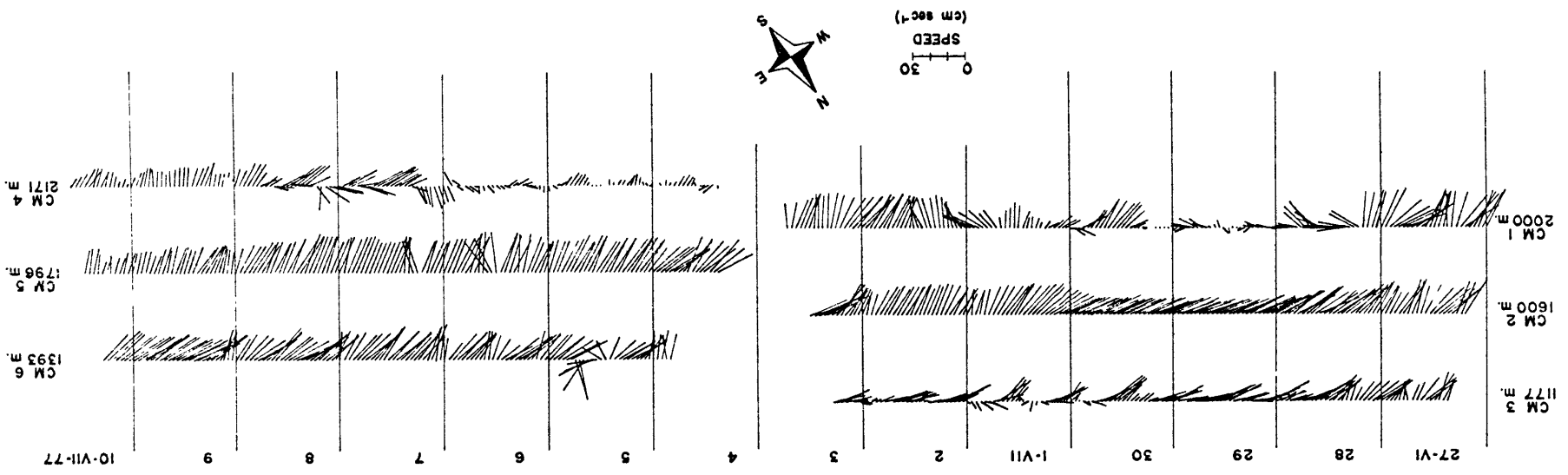
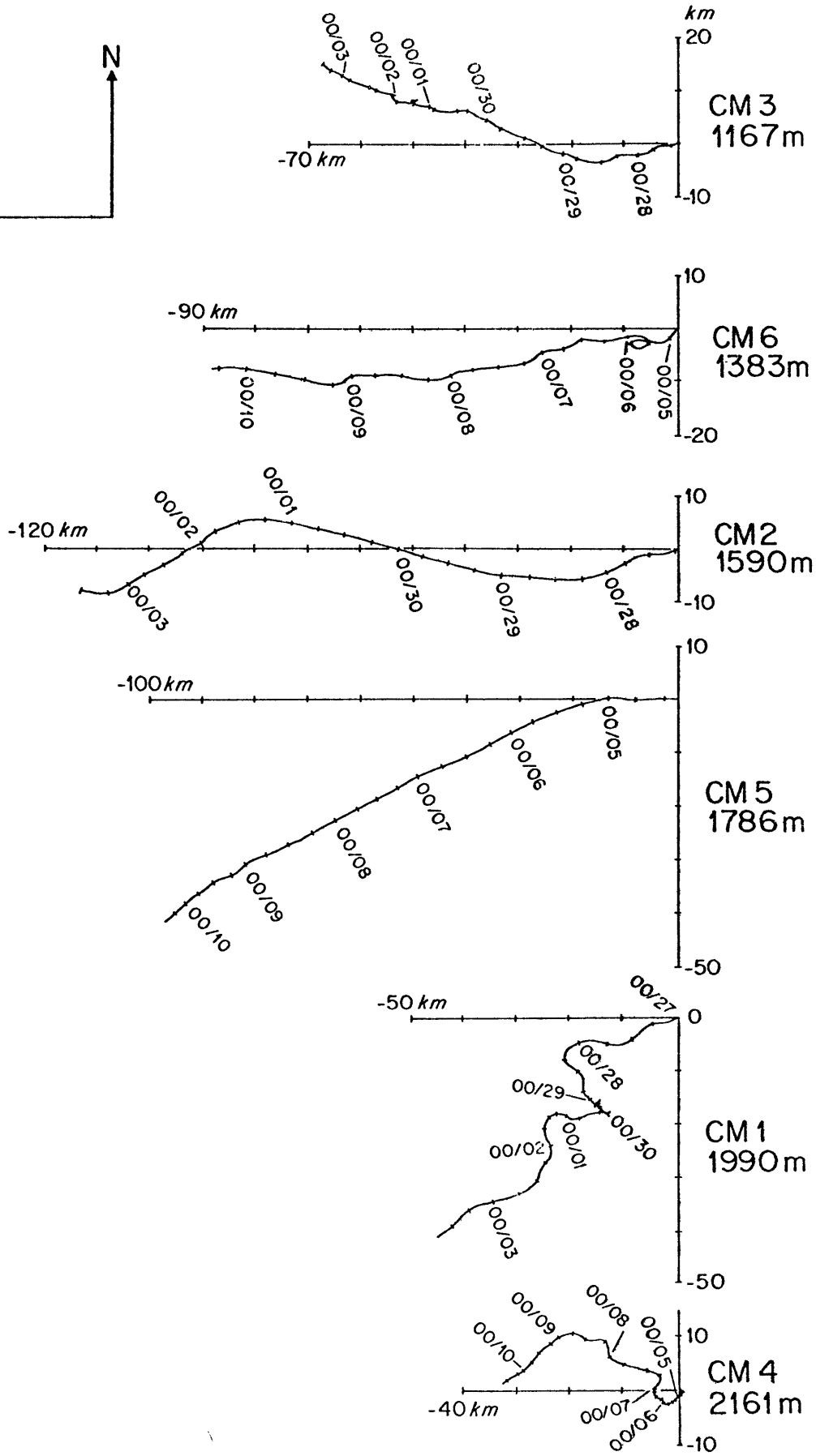
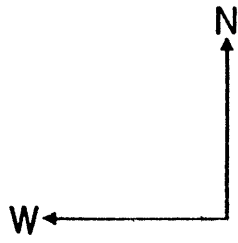


FIGURE 2.3: Progressive vectors from six current meters. Velocity data as in Table 2.1 and Figure 2.2 plotted as progressive vectors every 30 minutes. Flow at the shallowest meter is uniform in direction, although speed varies considerably; the two deepest meters show considerable fluctuation in both speed and direction. The three meters in the flow axis show remarkably little fluctuation in direction or speed throughout the deployments.





(282°). Periodic stalls and occasional current reversals reduced the vector mean velocity to only 13 cm sec<sup>-1</sup>, and suggest that 1200 meters is near the minimum depth of cross-ridge flow of the bottom current.

The current meter at 2000 meters (CM 1) recorded a period of approximately 2 days of low velocities and stalls which was both preceded and followed by strong (>20 cm/sec) flow. The current meter record shows eastward flow preceding the stall, and we infer that water from the current axis (upslope) moved into the position of the station and stalled.

The deepest current meter (CM 4; 2171 meters) shows low westerly flow ( $\bar{v} = 5.8 \text{ cm sec}^{-1}$ ) for the duration of the record, and is assumed to lie outside of the main body of the bottom current.

Velocity components along the azimuth 217° are listed in Table 2.1; the vector stick diagram (Figure 2.2) is also plotted relative to 217°. This is the azimuth normal to the mean line of CTD stations 7 to 15 to which geostrophic velocities are compared.

#### B. Indirect Current Indicators

Various methods were used to determine flow direction and estimate velocity in other portions of the survey regions. Bottom photographs obtained on the east flank of East Katla Ridge show good agreement between directions inferred from surface sculpturing and current meter measurements. Similarly, bottom photographs from the saddle of West Katla Ridge indicate westward flow. Photographs from the Myrdalsjokull Canyon axis and two additional sites within the channel extending eastward from the canyon show evidence of northward flow (into the canyon). Because no exit exists for deep flow towards the north in the canyon, we

expect that the presence of ripples and scouring pointing northwards indicates strong tidal flow within the canyon region.

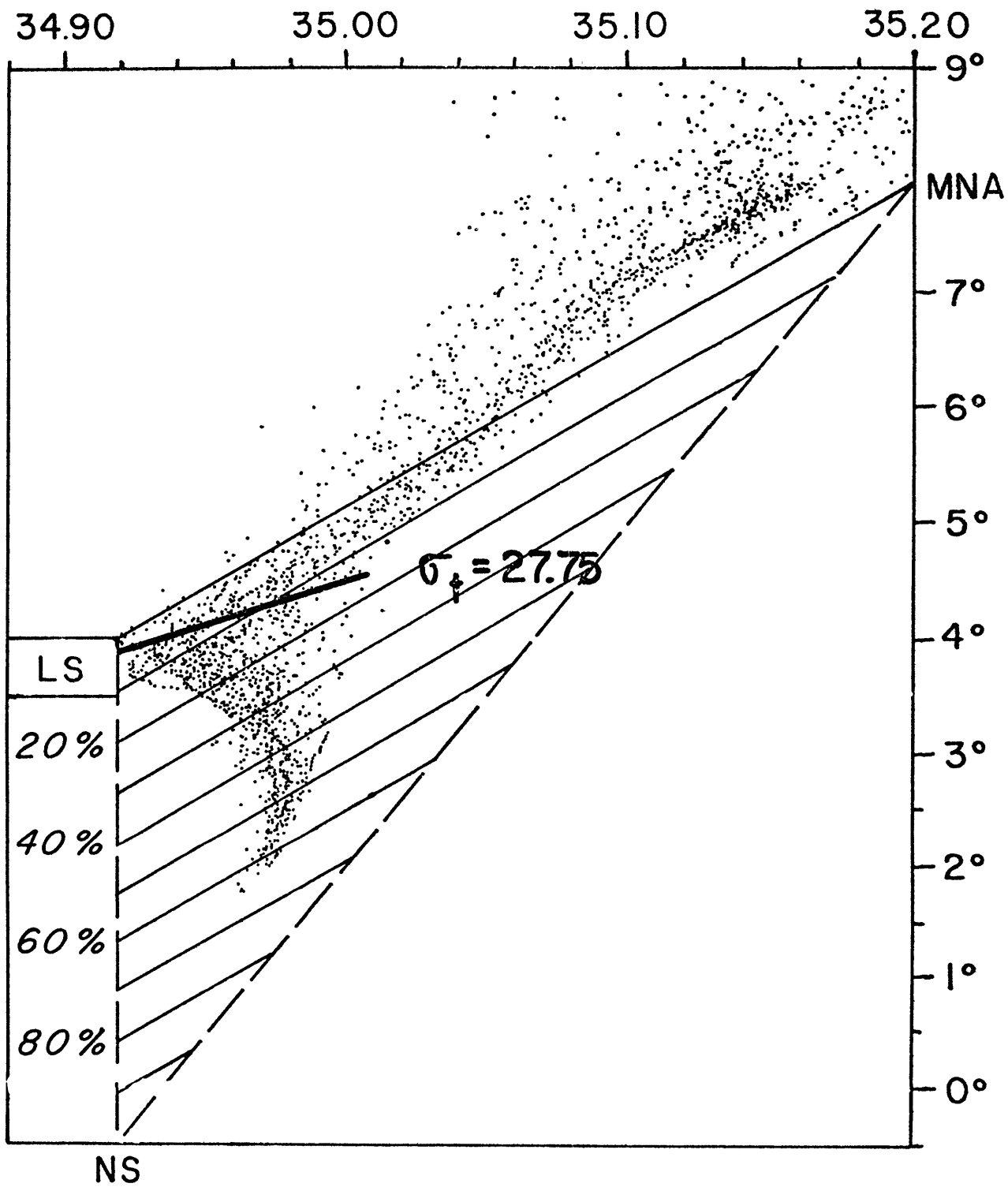
Hydrographic stations were used to extend the measured velocity section from the East Katla Ridge. Seventeen lowerings with a Neil Brown CTD<sup>R</sup> instrument were made in two sections. The northern section coincides with the current meter locations, and extends an additional 80 kilometers eastward to the basin center. The second line was located off the southeast flank of West Katla Ridge, extending a comparable distance towards the southeast (Figure 2.1). Velocities were calculated based on the geostrophic assumption, according to the formula

$$v = \frac{100 g (\Delta D)}{2 \Omega (\Delta x) \sin \phi} \text{ cm sec}^{-1}$$

Where  $g$  = gravitational acceleration ( $983 \text{ cm sec}^{-2}$ );  
 $\Omega$  = angular velocity of the earth ( $0.729 \times 10^{-4} \text{ sec}^{-1}$ );  
 $\phi$  = site latitude  
 $\Delta D$  = dynamic height difference (units of meters) between stations relative to the reference level (where  $\Delta D = 0$ ); and  
 $\Delta x$  = station separation (meters).

A reference level was chosen based on both measured velocities along the northern line and on previous work (Steele, Barrett and Worthington, 1962). We used a level corresponding to the density interface  $\sigma_t$  equals 27.75 for a 'level of no motion'. This level produces good agreement between calculated and measured velocities, and allows us to extrapolate our results to regions where direct measurements are absent. This reference surface corresponds to a major break in the temperature-salinity curve (Figure 2.4), and is comparable to the level used by Steele et al (1962) based on 'salinity anomaly'.

FIGURE 2.4: Potential temperature vs. salinity. All CTD stations occupied during AII-94-1 within the Katla Ridge survey area are included. Water masses are abbreviated as in the text. Percentages of Norwegian Sea Deep Water (NS) are indicated on the left margin, after the method of Hermann (1967). Heavy line indicates the approximate position of the reference surface used in velocity and volume transport calculations. Salinity is horizontal axis; potential temperature is vertical.



General features of the calculated velocity profiles are observed in Figure 2.5. They are as follows:

1. A tendency toward increasing southwest velocities towards the bottom is observed at all stations pairs except the northernmost two pairs on the east flank;
2. Maximum velocities near the bottom are observed between 1600 and 1800 meters on the east flank of East Katla Ridge, and between 1800 and 2100 meters on the east flank of West Katla Ridge;
3. The velocity maximum coincides with a local minimum in potential temperature (which is also the maximum in potential density) (Figure 2.6);
4. The apparent decrease in near-bottom velocity near the top of East Katla Ridge may perhaps be explained as being due to flow shifting towards the west and northwest, nearly parallel to our section, as observed at current meters at 1177, 1393 and 1600 meters.

C. Volume transport. Seventeen CTD stations were included in a closed array encompassing the flow of ISOW along East Katla Ridge for volume transport calculations (Figure 2.1). A reference level  $\sigma_t = 27.75$  was used as a level of no motion.

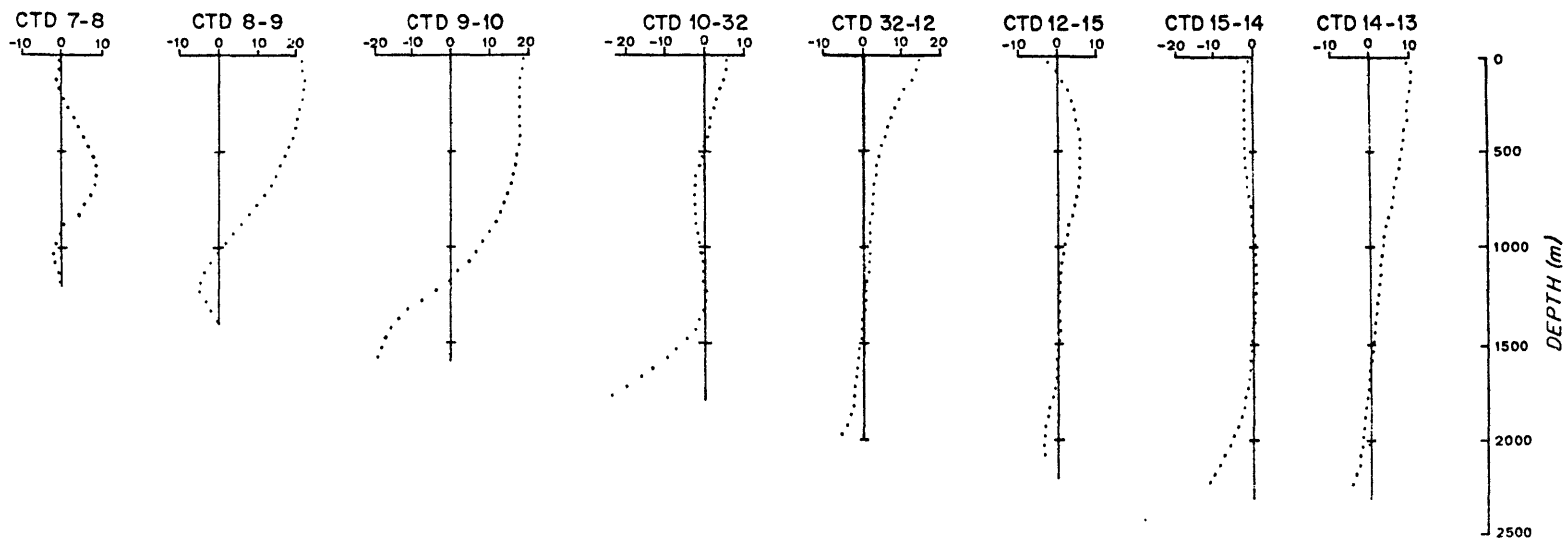
Volume transport was computed every 50 meters below the reference level for each consecutive station pair by the standard equation for geostrophic flow:

$$VT_{50} = \frac{50 \text{ g} (\Delta D)}{2 \Omega \sin \phi} \text{ m}^3 \text{ sec}^{-1}$$

where  $VT_{50}$  is the flow through a 50-meter thick layer between adjacent stations. The symbols and reference level are as defined previously for

FIGURE 2.5: Geostrophic velocity profiles for station pairs along the two lines of CTD stations indicated in Figure 2.1. Velocities are calculated as discussed in the text, using a reference "level of no motion" at  $\sigma_t$  equals 27.75.

# NORTHERN LINE



# SOUTHERN LINE

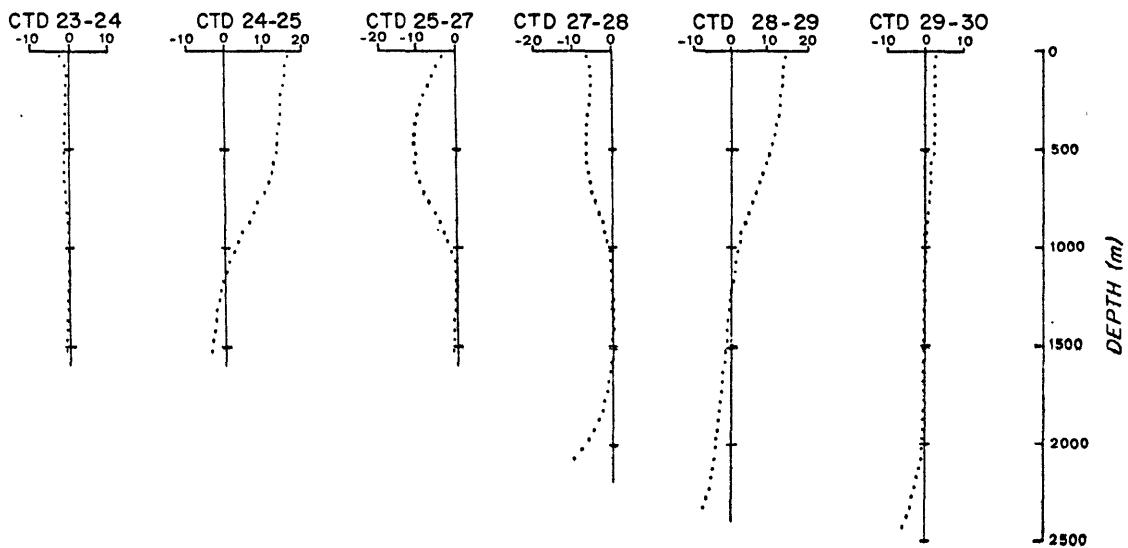
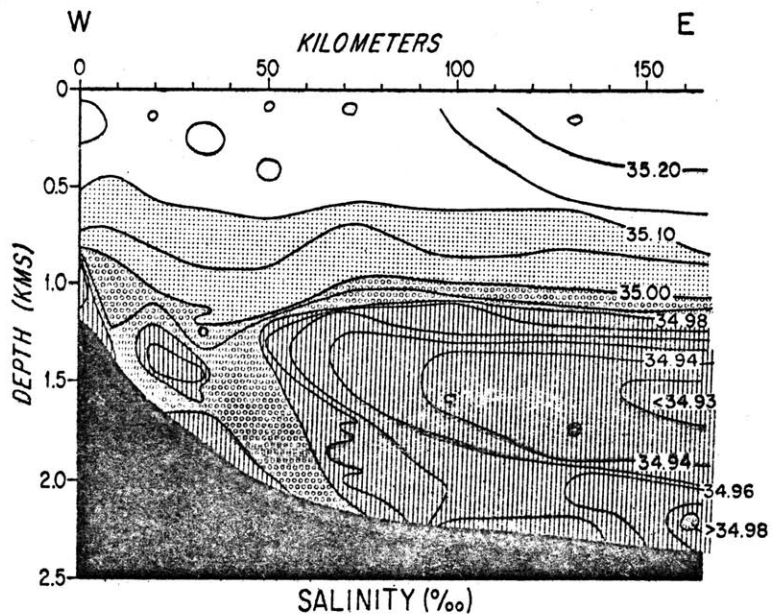
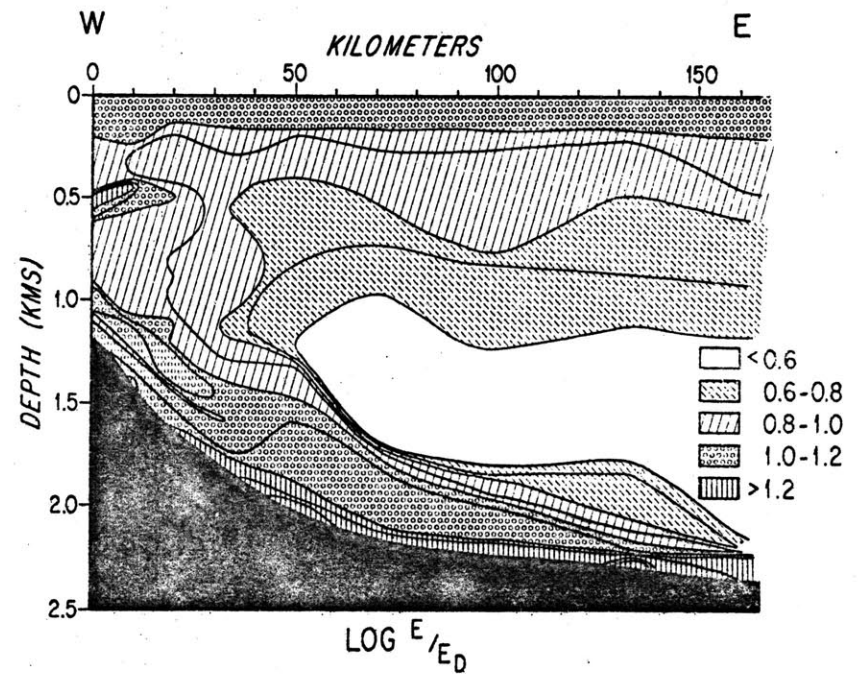
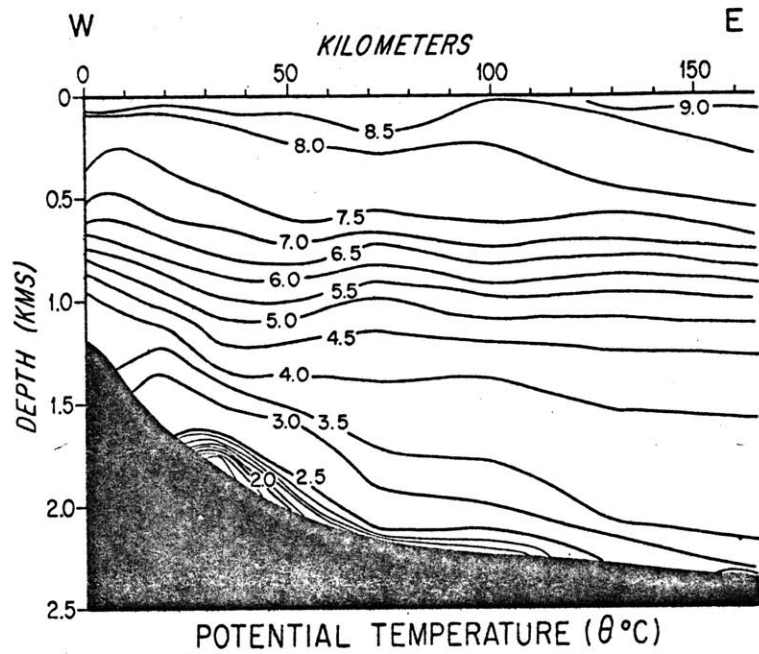


FIGURE 2.6: Potential temperature, salinity and light scattering along northern CTD section. Note core of cold water in vicinity of 1800 meters water depth, where potential temperature is less than 2° C. Salinity within the current is higher than at comparable depths in the basin to the east. Light scattering ( $\log E/E_D$ ) is uniformly higher throughout the water column within 50 kilometers of the ridge crest than to the east. This station is based on data from CTD stations 7 to 15 and the associated nephelometer lowerings.





velocity. Volume transport below the reference level for each station pair ( $\Sigma VT_{50}$ ) is listed in Table 2.2.

Because the stations are located on a sloping bottom, a considerable volume of water is missed by the above calculation, and must be estimated in a slightly different manner. Dynamic heights at the deepest measurement of the shallower CTD lowering are used to calculate flow velocity at that level. The calculated velocity is then multiplied by the area below the deepest incremental calculated volume transport to give the "bottom flow volume" ( $VT_B$ ) for each station pair (Table 2.2).

Once the volume transport has been calculated for each station pair, the total transport of the deep current may be estimated by summing all station pairs on each section across the current. In addition, we may test our choice of a reference level by determining whether mass is conserved through the array.

Volume transport for the northern and southern lines of stations (below the reference level) are  $5.02$  and  $4.19 \times 10^6 \text{ m}^3/\text{sec}$  respectively (Table 2.2). The lower value for the southern line apparently indicates that our stations did not extend far enough to the east to encompass the total flow. This is supported by the calculated transport of  $0.82 \times 10^6 \text{ m}^3/\text{sec}$  (east) between the easternmost stations on the northern and southern lines (stations 13 and 30). Flow across the western line is small ( $0.15 \times 10^6 \text{ m}^3/\text{sec}$ ) and poorly determined due to the geometry of Myrdalsjokull Canyon, which separates the East and West Katla Ridges. Only a minor portion of the flow is likely to be able to escape across the ridges on the western margin of the study area, with

TABLE 2.2: Volume transport rates of Iceland-Scotland Overflow Water and Norwegian Sea Deep Water. Values in  $10^6 \text{ m}^3/\text{second}$ .

Station Pair(CTD)	VT <sub>50</sub>	VT <sub>B</sub>	VT <sub>total</sub>	VT <sub>NS</sub>	IN/OUT
<u>NORTHERN LINE</u>					
7-8	-.029	-.002	-.031	-.006	in
8-9	-.124	+.001	-.123	-.037	in
9-10	-.708	-.286	-.994	-.430	in
10-32	-.937	-.226	-1.163	-.613	in
32-12	-.291	-.468	-.759	-.177	in
12-15	-.297	-.059	-.356	-.155	in
15-14	-.916	-.235	-1.151	-.428	in
14-13	-.363	-.095	-.458	-.134	in
TOTAL	-3.665	-1.370	<u>-5.035</u>	<u>-1.980</u>	IN
<u>SOUTHERN LINE</u>					
23-24	-.055	-.018	-.073	-.025	out
24-25	-.206	-.226	-.432	-.125	out
25-27	-.715	-.451	-1.166	-.455	out
27-28	-.471	-.311	-.782	-.316	out
28-29	-.936	-.187	-1.123	-.438	out
29-30	-.518	-.095	-.613	-.263	out
TOTAL	-2.901	-1.288	<u>-4.189</u>	<u>-1.622</u>	OUT
<u>EASTERN LINE</u>					
13-30 (total)	+.630	+.190	<u>+.820</u>	<u>+.256</u>	OUT
<u>WESTERN LINE</u>					
7-31	-.055	-.298	-.353	----	out
31-23	+.116	+.092	+.208	----	in
TOTAL	+.061	-.206	<u>-.145</u>	----	OUT

the remainder of the water recirculating in the canyon. We feel that the mass balance supports our choice of a reference level at  $\sigma_t = 27.75$ .

CTD 11 (at 2000 meters) was taken during a period of near-zero flow (1000 GMT, 30 June--see Figure 2.2). The record shows a thick bottom layer of low temperature gradient which is considerably different from the record of CTD 32 taken at the same place 10 days later. For this reason, we chose to substitute CTD 32 (at the same location) into the northern line, feeling that calculations made using CTD 11 would give a poor representation of the geostrophic flow due to advection. If CTD 11 is substituted into the northern line, a total flow of  $5.6 \times 10^6$  m<sup>3</sup>/sec is obtained for the northern line. The increased flow is due mainly to the shallowing of the reference surface in CTD 11 as compared with CTD 32.

#### D. Water Masses

The principal water masses involved in the deep circulation of Iceland Basin are as follows:

- (1) Norwegian Sea Deep Water (NS).  $\theta = -0.5^\circ\text{C}$ ;  $S = 34.92^\circ/\text{oo}$ . The principal deep water mass of the Norwegian Sea.
- (2) Modified North Atlantic Water (MNA).  $\theta = 8.0^\circ\text{C}$ ;  $S = 35.20^\circ/\text{oo}$ . A water mass whose  $\theta$  and  $S$  properties vary regionally. Values used are typical of the eastern Iceland-Faroe Ridge where most of the ISOW is formed.

- (3) North Icelandic Winter Water (NI) and Irminger Sea Water (AI), generally considered together as NI/AI due to their similar properties.  $\theta = 2.5$  to  $3.0^{\circ}\text{C}$ ;  $S = 34.88$  to  $34.90^{\circ}/\text{oo}$ .  
Meincke (1977) observed a freshening of this water mass near the Faroe Islands in 1977 with  $\theta = 3.0^{\circ}\text{C}$ ;  $S = 34.78^{\circ}/\text{oo}$ .
- (4) Labrador Sea Water (LS).  $\theta = 3.5$  to  $4.0^{\circ}\text{C}$ ;  $S = 34.90$  to  $34.94^{\circ}/\text{oo}$ . The principal deep water mass of the central Iceland Basin, defined as a pronounced salinity minimum on  $\theta$  vs.  $S$  curves.
- (5) Iceland-Scotland Overflow Water (ISOW). This water mass results from the mixing of the 4 water masses above in various proportions.  $\theta$  varies from  $2.0$  to  $4.0^{\circ}\text{C}$ ;  $S$  from  $34.95$  to  $35.00^{\circ}/\text{oo}$  in the Katla Ridge area. Typical values far from the source (e.g. in the Charlie-Gibbs Fracture Zone) are  $\theta = 2.8$  to  $3.0^{\circ}\text{C}$ ;  $S = 34.98$  o/oo.

Because four water masses are involved in the mixing process which leads to the formation of ISOW, it is not possible to precisely determine the fraction of each in the final mixture using only temperature and salinity. However, since MNA, NI/AI and LS all fall on an approximately straight line, it is possible to estimate the fraction of NS at a given station. This has been done for the 17 stations studied (Figure 2.4).

The fraction of Norwegian Sea Deep Water (NS) was calculated at 50 meter intervals for each station according to the method described by Hermann (1967). The mixing triangle was constructed using MNA, LS and NS as endpoints. The substitution of NI/AI for LS does not significantly

change the results. However, ambiguities in defining the endmembers precisely introduce a possible error of approximately 10% to the total flow calculation.

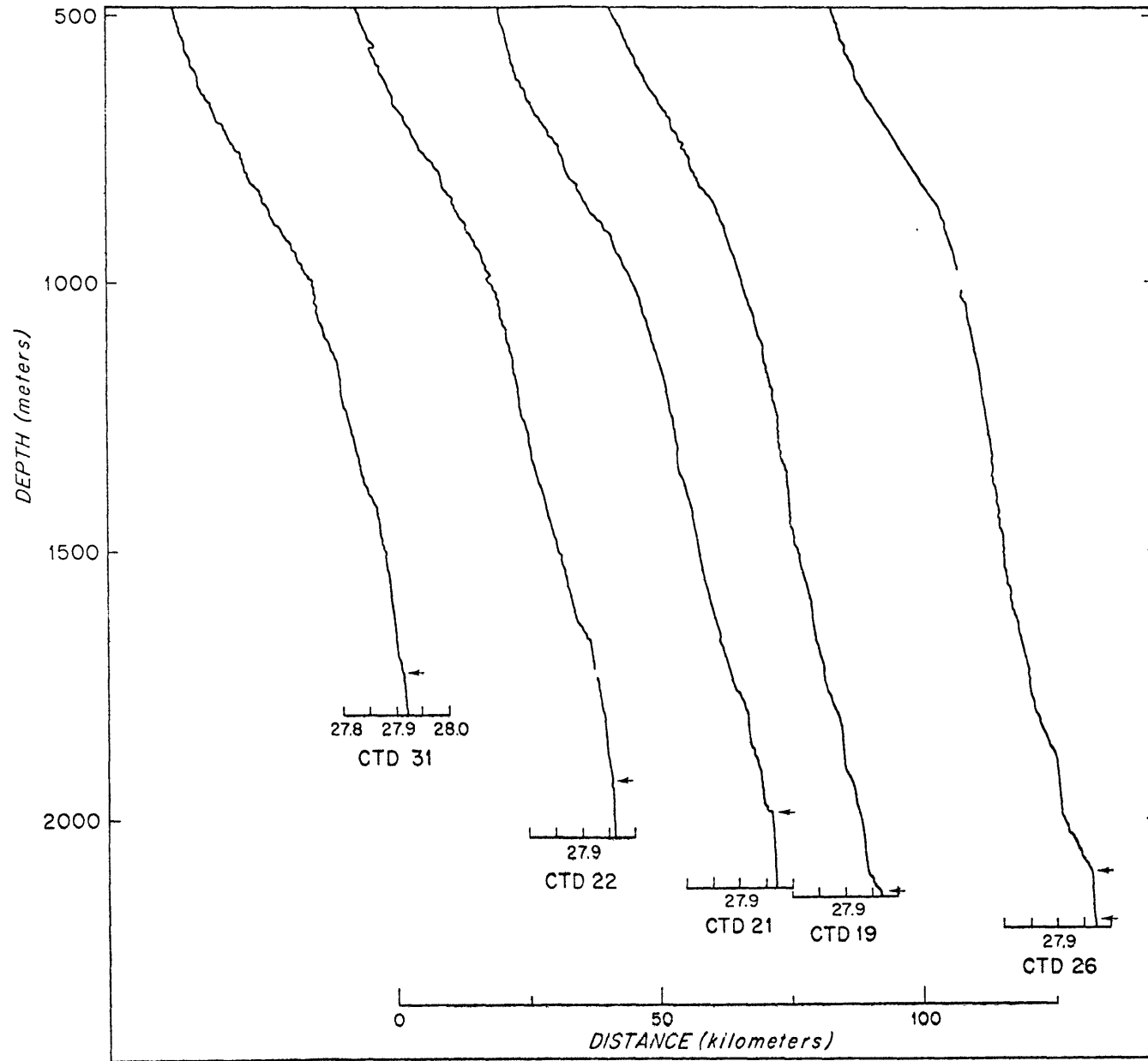
The flow volume of NS is calculated by multiplying the mean fraction at a given depth by the total transport at that depth for each station pair (VT<sub>50</sub>). The calculated transports are listed in Table 2.2. The transport across the northern line is approximately  $2.0 \times 10^6 \text{ m}^3 \text{ sec}^{-1}$ . This compares favorably with the value of  $2.2 \times 10^6 \text{ m}^3 \text{ sec}^{-1}$  NS independently estimated by the members of the 'OVERFLOW 73' working group at the meeting held in Oban, Scotland in May 1978 (Conseil International pour l'Investigation de la Mer, 1979).

#### E. Bottom Mixed Layers and Near-Bottom Density Distribution

One additional feature of the hydrographic data which bears on the question of current flow is the presence and thickness of near-bottom mixed layers. These layers of constant or nearly constant potential density are interpreted to form only in locations where sufficiently rapid flow intersects the bottom (Armi and Millard, 1976; Armi, 1978). Mixed layers are a ubiquitous feature of CTD profiles in the Katla Ridge region. They are observed both immediately adjacent to the bottom and as detached layers somewhat above. The thickest layers are those observed within the axis of Myrdalsjokull Canyon. Two lowerings (CTD No. 21, 22) display mixed layers thicker than 120 meters (Figure 2.7). These canyon mixed layers are formed of high density overflow water, comparable in density to that observed in the core of the flow to the north. It appears that the cascading of dense water from the flow axis into the

FIGURE 2.7: Potential density: Myrdalsjokull Canyon. Vertical profiles of potential density from within the canyon (CTD 31, 22, 21, and 19) and within the current southwest of the canyon mouth (CTD 26) demonstrate the strong influence of mixing processes within the canyon on the structure of the lower 100 meters of the water column. Bottom mixed layer height is indicated by arrows. The upper arrow on CTD 26 indicates the top of the layer of potential density equal to 27.96 which is inferred to have been advected from the canyon. The thin layer at CTD 19 indicates that this station is located east of the point at which the main body of the current turns westwards as it exits the canyon. Distance measured along the canyon axis is indicated, and is aligned to the isopycnal 27.9. See Figure 2.1 for station locations.

POTENTIAL DENSITY ( $\sigma_\theta$ ): CANYON PLUS CTD 26





canyon as it rounds the southern end of East Katla Ridge may result in the stirring of these waters and the formation of thick mixed layers. An alternate hypothesis is that tidal flow within the canyon is responsible for forming the thick layers.

The density of bottom water along the southern line of stations, which records the flow exiting from the canyon, is much more uniform to greater distances from the ridge than that on the northern section. This suggests that the canyon exerts a strong influence across the entire width of the flow, and is influential in producing the uniform property distributions observed further to the south.

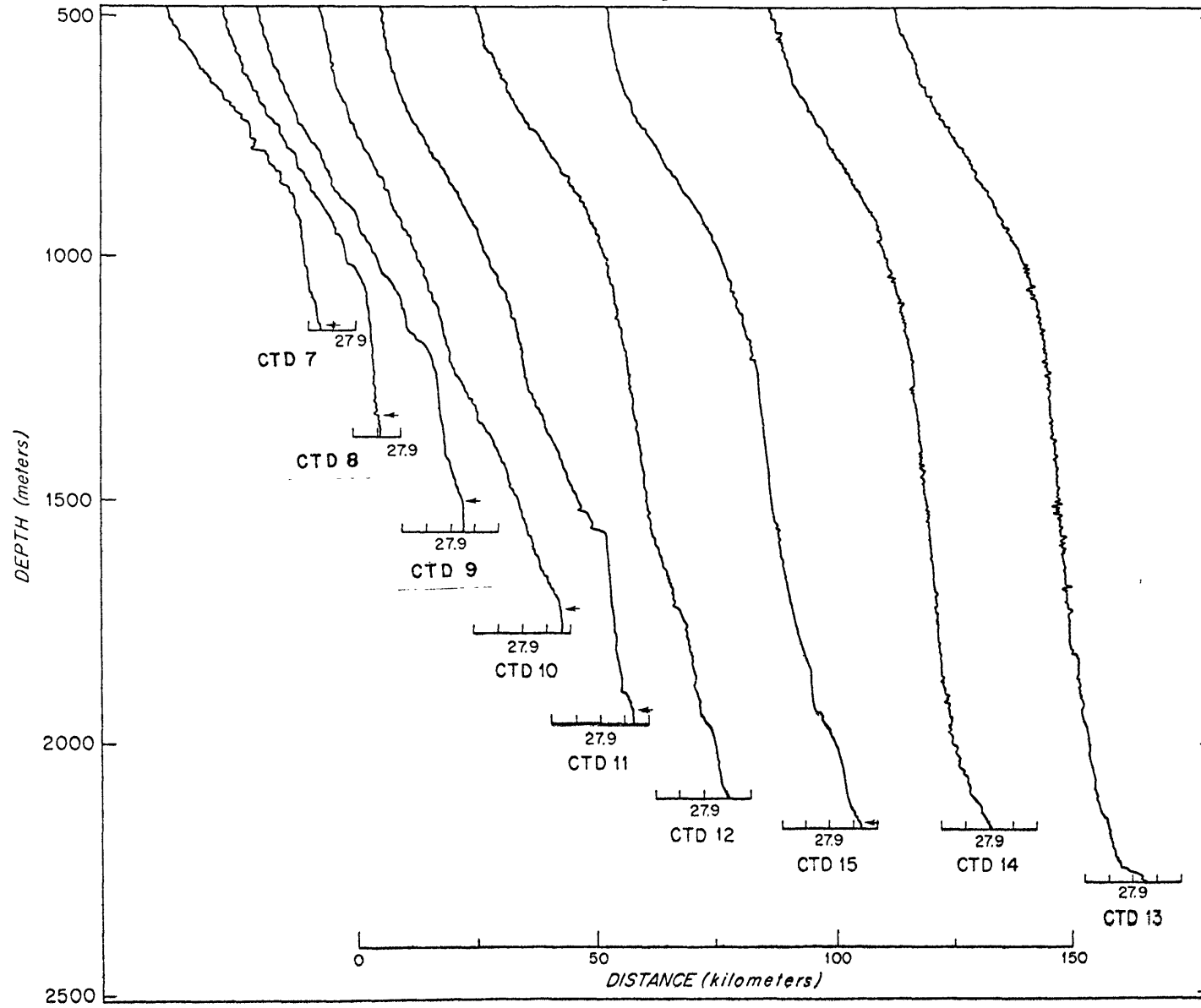
Mixed layers observed on the northern line show somewhat different characteristics (Figure 2.8). Near bottom mixed layers are observed to be thickest in the flow axis, attaining maximum heights of 30 to 50 meters above the bottom. Mean thicknesses at locations both up and down slope from the axis are approximately 10 to 20 meters.

Bottom mixed layers are observed at CTD lowerings 7, 8, 9, 10, 32, and 15. These lowerings all correspond to periods of flow  $>10$  cm  $\text{sec}^{-1}$  at adjacent current meters. No mixed layers are observed at CTD lowerings 14 and 13 which were located deeper than our deepest current meter. Bottom photographs from this portion of the survey area indicate little evidence for bottom flow, however (camera lowerings #6, 7, 8). CTD lowering 12 did not reach bottom, and does not show a near-bottom mixed layer above an estimated height of 20 meters above bottom.

CTD lowering 11 was made immediately following a stall at the adjacent current meter (CM 1). Although the lower 60-70 meters of the water

FIGURE 2.8: Potential density: east flank, East Katla Ridge. Vertical profiles of potential density, as in Figure 2.7. Mixed layer height may be observed to be maximum at CTD 9 (1600 meters), decreasing both up and down the slope. Potential density maximum (in excess of 27.98) is observed at CTD 10, at 1800 meters water depth. Shape of lower 400 meters of CTD 11 is inferred to result from advection and stall of water from the current axis (upslope)(see text). See Figure 2.1 for station locations.

POTENTIAL DENSITY ( $\sigma_\theta$ ): NORTHERN LINE



column constitute a layer of cold water which has apparently penetrated following the stall, mixing has not been complete. The lower 25 meters does appear to be developing into a single layer, however.

#### Bottom layers on southern line of station

No stations from the southern line (Figure 2.9) have mixed layers more than 20 meters thick. CTD stations 19, 23, and 24 have no bottom mixed layers, while CTD #25, 27, 28, 29, and 30 over the depth range 1850 to 2550 meters all have layers 10-20 meters thick. The lack of bottom mixed layers at CTD stations 19 and 24 may be due to their locations near points of exchange between canyon water and outside. The presence of mixed layers along most of the southern line suggests that currents in this region were flowing at comparable rates to flow measured near CTD lowerings 7, 8, 32 and 15 (about 10-20 cm sec<sup>-1</sup>). However, direct measurements were not made at these stations.

#### Density distribution of bottom water

Water observed in Myrdalsjokull Canyon is separated into two major mixed units, one of density  $\sigma_{\theta} = 27.96$  and one of 27.90. The layer of  $\sigma_{\theta} = 27.96$ , observed with thickness in excess of 100 meters at CTD #21 and 22, has its origin in the most dense waters observed on the east flank of E. Katla Ridge (CTDs #10 and 11). This water appears to rise from the 1800 meter isobath to approximately 1600 meters as it rounds the SE nose of E. Katla Ridge; it then plunges upon entering the canyon to approximately 2000 meters (CTD 21, 22) and is diverted to the south by the western canyon wall (Figure 2.10). A thick layer of quite uniform density is observed within the canyon. The density distribution is altered in the

FIGURE 2.9: Potential density: southeast of West Katla Ridge. Vertical profiles of potential density, as in Figures 2.8 and 2.9. Thin bottom mixed layers are typical of this section of stations, which apparently misses the main axis of flow exiting the canyon. Near-bottom potential density is uniformly greater than 27.95 for all stations deeper than 1700 meters, in contrast to the northern line of stations (Figure 2.8) on which the deepest water at the easternmost stations are less dense. See Figure 2.1 for station locations.

POTENTIAL DENSITY ( $\sigma_\theta$ ): SOUTHERN LINE

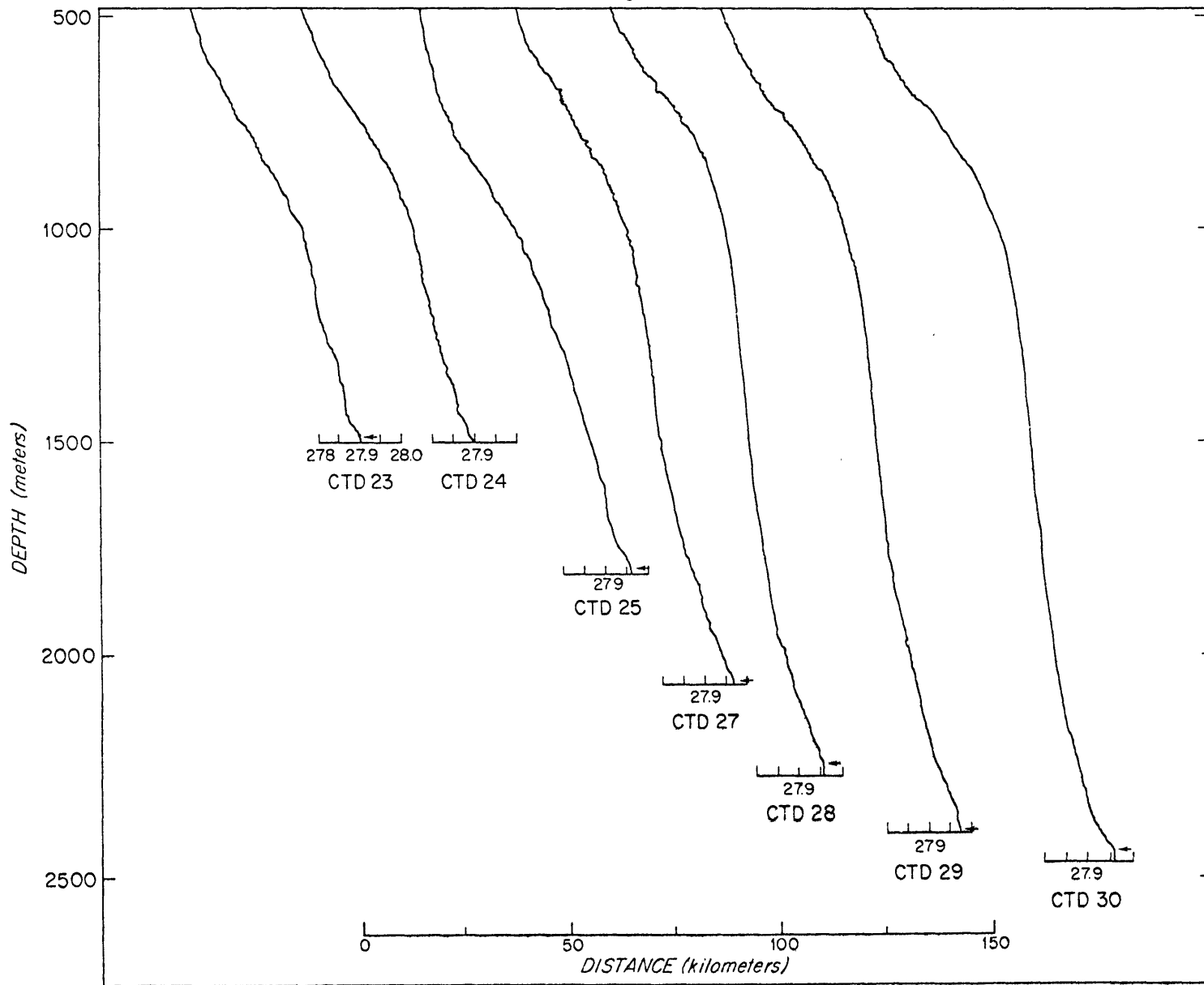
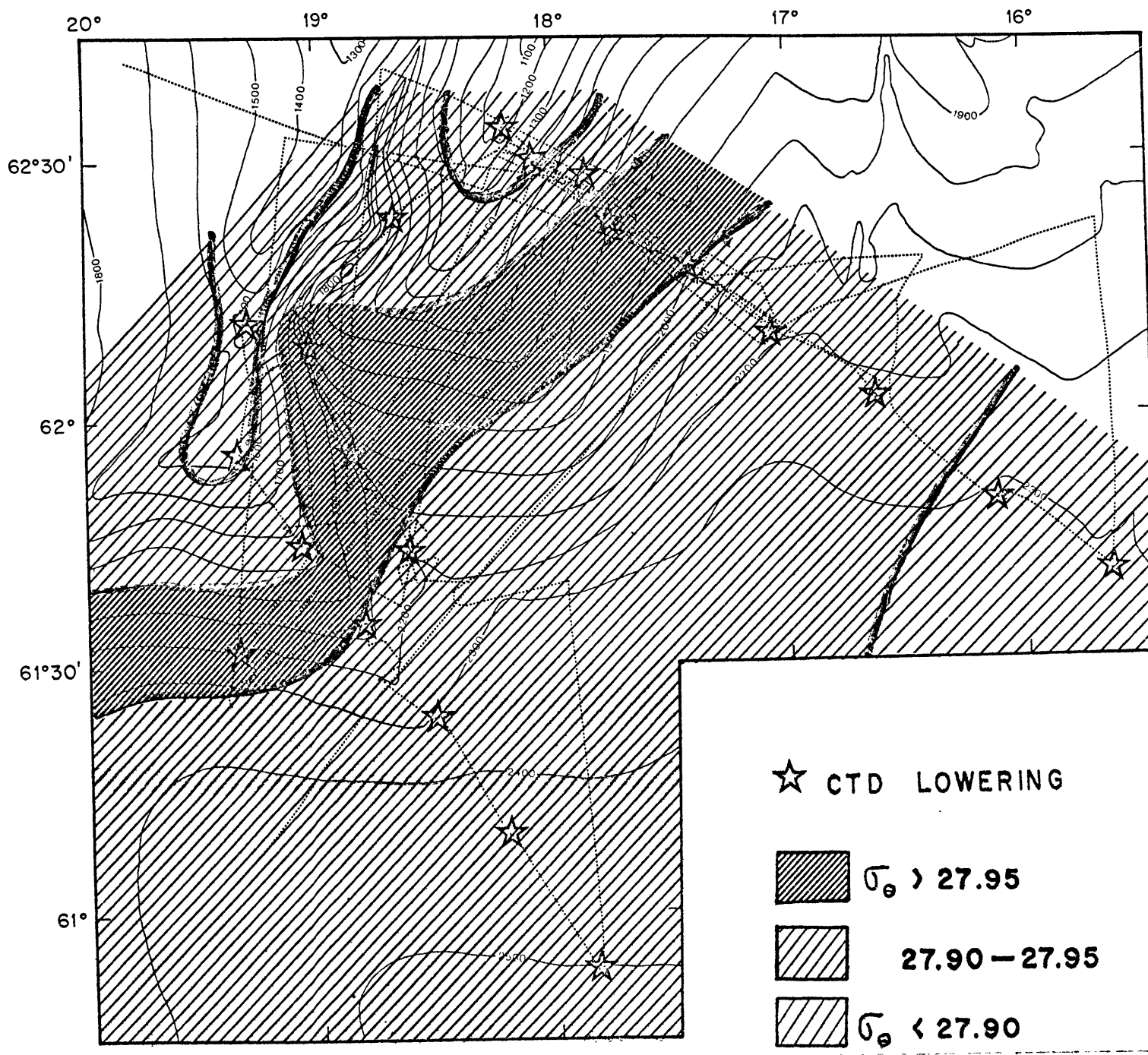


FIGURE 2.10: Potential density distribution around the Katla Ridges at 100 meters above bottom. Waters in which potential density exceeds 27.95 corresponds to the inferred axis of the current. Note the penetration of the dense water into Myrdalsjokull Canyon. The current axis is inferred to shallow as it crosses the southern end of East Katla Ridge (based on current measurements) and to deepen as it exits the canyon (see text).





exiting water, with  $\sigma_{\theta} > 27.95$  observed at the bottom from CTD #25 to 30 (1850-2500 meters; Figure 2.9). This contrasts with the deeper stations on the east flank, where no water this dense is observed deeper than 2220 meters (CTD #15). It appears that the effect of the canyon on the flow is to divert the dense axis of flow to greater depths (2000 to 2300 meters--see CTD #26, Figure 2.7) and spread the dense water over a greater depth range on the south flank of W. Katla Ridge.

A second mixed unit of  $\sigma_{\theta} = 27.90$  seems to form from the waters observed at 1400-1600 meters on E. Katla Ridge (CTD #8, 9). This water is observed on the bottom at CTD #31 (north of the bend in the canyon at  $62^{\circ} 13' N$ ) and as a thin bottom layer at CTDs #23, 24 where it crosses the nose of W. Katla Ridge.

"Fossil" mixed layers. "Fossil" mixed layers are defined by Armi (1978) as mixed layers which are separated from the bottom at the point of observation. Because the mixing process involved in formation of isopycnal layers is assumed to require that water is in contact with the bottom at the point of formation, Armi (1978) has explained these detached layers as representing previous episodes of mixing (hence 'fossil' herein implying an age measured in days or weeks).

Data from the Katla Ridge area indicates that fossil mixed layers are common on the northern line from the ridge crest to approximately 2200 meters (CTD 15). Profiles from lowerings 14 and 13 show little evidence for either new or fossil mixed layers within the bottom current.

Intermediate layers ( $\sigma_{\theta} = 27.92 - 27.94$ ) are observed off the bottom at canyon CTDs #22 and 21 and CTDs #25 and 26 on the W. Katla Ridge south

flank; at the latter two stations a thick layer of 27.90 water is also present.

Detached mixed layers are poorly developed at CTD stations #27-30, where horizontal mixing has smeared the discrete layers into a smoother density gradient over the lower several hundred meters. Discrete layers 10-20 meters thick are still observed within 200 meters of the bottom at some stations, however (e.g. CTD #28; Figure 2.9).

#### F. Suspended Sediment Flux

The rate of transport of suspended sediments in the ISOC may be estimated by combining the flow rate of ISOW with measurements of suspended particle concentration. The data used for the concentrations was obtained by M. J. Richardson as part of a study of sediment flux for her Ph.D. dissertation (in progress). Suspended sediments were vacuum-filtered onto 0.6  $\mu$  Nuclepore<sup>R</sup> filters from a known volume of water, and a 'dregs' correction was applied to the data by making a separate determination for water below the spigot of the Niskin bottle (Gardner, 1977).

Because of the poor vertical distribution of suspended sediment samples within the 17-station array, I have used 16 nephelometer profiles obtained at the site of each CTD station (except station CTD 28) to estimate suspended sediment concentration. Correlation of nephelometer and particle concentration data has been discussed by Biscaye and Eittrheim (1972) and is currently under investigation in our data by Richardson.

The first step in the advective flux calculation is the correlation of suspended sediment concentration and light scattering intensity in such a way that light scattering ( $\log E/E_D$ ) may be used to predict

concentration (C). This relationship is established as follows:

- 1) Suspended sediment concentrations (micrograms per liter) are determined for all sites at which CTD lowerings were obtained for use in volume transport calculations.
- 2) Nephelometer light scattering intensity is determined at 50-meter intervals at each lowering.
- 3) Suspended sediment concentrations are averaged over increments of 0.1 units of  $\log E/E_D$  (Table 2.3).
- 4) A linear regression of  $\log C$  on  $\log E/E_D$  is calculated using average concentrations within the 0.1 unit  $\log E/E_D$  window.
- 5) Estimates of predictive error of regression are calculated following standard methods (Stanley and Gray, 1973).

The relationship  $\log C = 0.917 (\log E/E_D) + 0.929$ , or  $C (\mu\text{gm/liter}) = 8.49 (E/E_D)^{.917}$  is significant at the 95% confidence level ( $r^2 = 0.445^*$ ,  $n=11$ ) (Figure 2.11). Estimated error of regression for predicted values of  $\log C$  are 0.175 to 0.193 (95% confidence limit) over the observed range of light scattering. Using a maximum error estimate ( $\pm 0.195$ ) indicates that concentrations may be considered accurate to  $\hat{C}/1.5 < C < 1.5\hat{C}$  where  $\hat{C}$  is the predicted concentration and  $C$  is the actual concentration.

The second step in calculating advective flux of suspended sediments is to combine the volume transport of ISOW with the concentration data such that  $C_{50} \times VT_{50} = SST_{50}$  (suspended sediment transport over 50 meter vertical steps). Light scattering values ( $\log E/E_D$ ) at each station pair are averaged over the depth interval, converted to concentration

TABLE 2.3: Suspended sediment concentration vs light scattering.

<u>Log E/E<sub>D</sub></u>	<u>Log C (mean + s.d.)</u>	<u>n</u>
0.4 - 0.5	1.25 + .06	3
0.5 - 0.6	1.54 + .16	11
0.6 - 0.7	1.53 + .20	9
0.7 - 0.8	1.71 + .06	5
0.8 - 0.9	1.70 + .14	10
0.9 - 1.0	1.75 + .14	13
1.0 - 1.1	1.86 + .26	24
1.1 - 1.2	2.00 + .17	13
1.2 - 1.3	1.99 + .20	8
1.3 - 1.4	2.27 + .20	6
1.4 - 1.5	2.26 + .21	6
Total =		108

Linear regression:  $\log C = .917 \log (E/E_D) + .929$        $r^2 = 0.445^*$

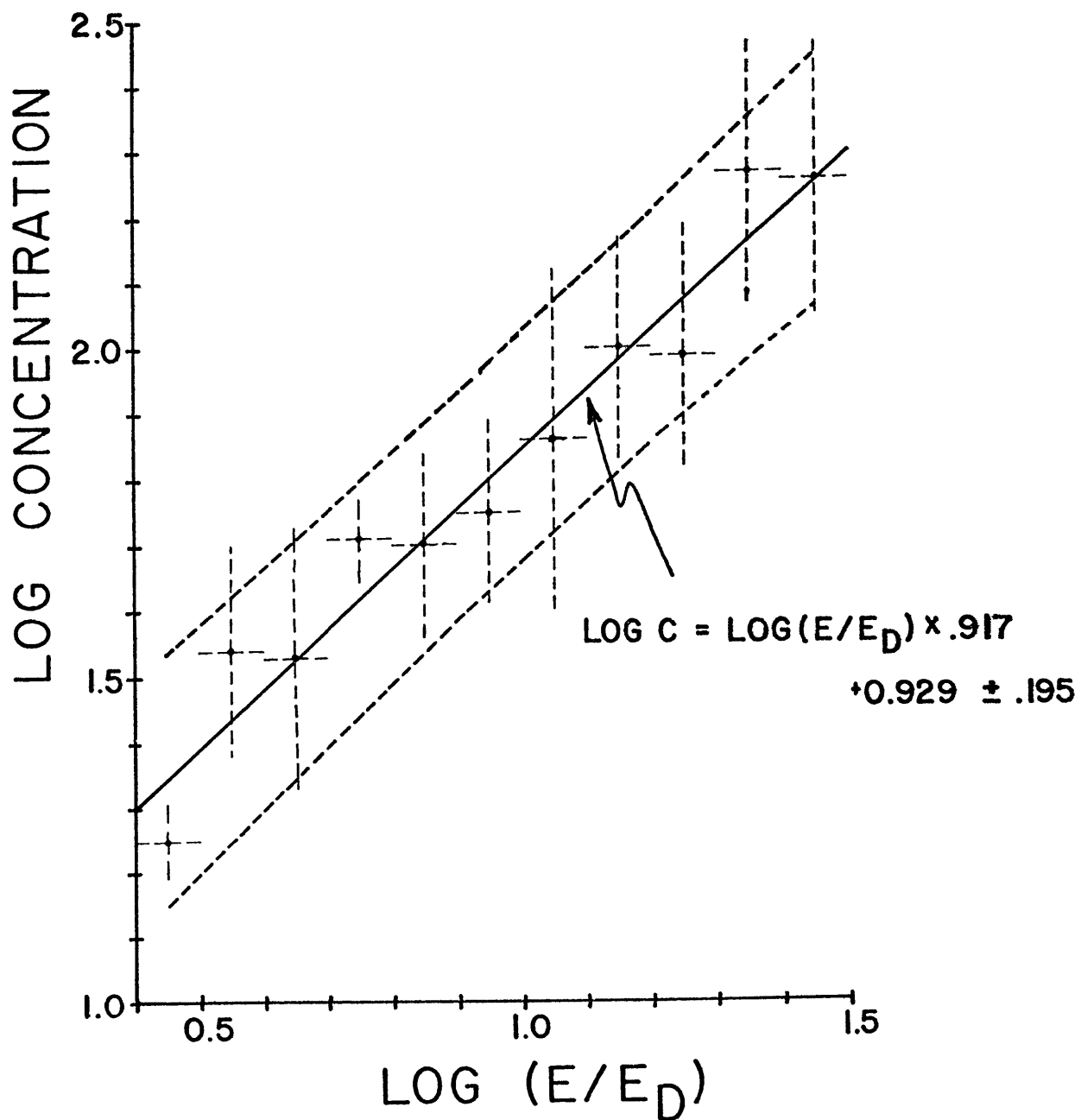
95% confidence on prediction of C:

0.175 at  $\log E/E_D = 0.95$   
 0.193 at  $\log E/E_D = 0.45, 1.45$

Stations used in correlation: 17, 18, 19, 20, 22, 23, 25, 26, 28, 29, 30, 31, 32, 33, 34, 36, 39, 40, 47, 55, 59, 63, 74, 75, 76, 81, 85.  
 (See Appendix 1 for appropriate CTD, nephelometer and hydrographic station numbers.)

Statistics after Stanley and Gray, 1973.

FIGURE 2.11: Correlation of suspended sediment concentration with light scattering for Katla Ridge stations. See text for discussion.



( $C_{50}$ ) and multiplied by volume transport ( $VT_{50}$ ) (Appendix II). The deepest flow and flux are computed in a similar manner to that described previously for volume transport, using all light scattering data below the deepest 50-meter increment as an average to estimate  $C_B$  (bottom concentration). Hence  $SST_B = C_B \times VT_B$ , and total suspended sediment flux for each station pair  $\Sigma SST = SST_{50} + SST_B$ .

The relationship used for calculating suspended sediment flux was calculated as discussed above, but used a slightly different set of concentration data. (Several generations of improved quality have been produced by Richardson; for the final correlation and discussion of accuracy we must await completion of her Ph.D. dissertation.)

The resulting regression ( $\log C = .814 \log E/E_D + 1.073$ ) was based on 144 pairs of data points, and has a predictive error in  $\log C$  of approximately 0.25. The difference between the two regression equations is small throughout the range 0.4 to 1.5 units of  $\log E/E_D$  which encompasses most of the light scattering values observed in Iceland Basin (e.g. Figure 2.6).

Transport rates of suspended sediment below the reference level at  $\sigma_t = 27.75$  determined for each station pair are listed in Table 2.4. There is a net flux observed into the station array of approximately 90,000 gm/sec, resulting from the observed difference between 454,000 gm/sec entering across the northern section and 365,000 gm/sec leaving via the other three sections. This flux corresponds to a mean accumulation rate of 12.5 cm/1000 yr (assuming a sediment density of 1.5 gm/cm<sup>3</sup>).

TABLE 2.4: Suspended sediment transport rates for Katla Ridge stations. Values in kilograms per second. In/Out is flux direction in or out of station array.

STATION PAIR(CTD)	SST <sub>50</sub>	SST <sub>B</sub>	SST <sub>total</sub>	IN/OUT
<u>NORTHERN LINE</u>				
7-8	-2.4	-6.1	-8.5	in
8-9	-11.3	+0.1	-11.2	in
9-10	-64.4	-27.9	-92.3	in
10-32	-65.4	-59.2	-124.6	in
32-12	-24.1	-16.7	-40.8	in
12-15	-27.7	-7.8	-35.5	in
15-14	-66.8	-38.7	-105.5	in
14-13	-21.1	-14.4	-35.5	in
TOTAL	-283.2	-170.9	<u>-454.1</u>	IN
<u>SOUTHERN LINE</u>				
23-24	-2.5	-1.2	-3.7	out
24-25	-9.3	-21.2	-30.5	out
25-27	-51.9	-46.7	-98.6	out
27-28				
28-29	-61.4	-70.9	-132.3	out
29-30	-29.7	-15.9	-45.6	out
TOTAL	-154.8	-155.9	<u>-310.7</u>	OUT
<u>EASTERN LINE</u>				
13-30 (total)	+19.4	+24.6	<u>+44.0</u>	OUT
<u>WESTERN LINE</u>				
7-31	-4.0	-21.5	-25.5	out
31-23	+7.5	+8.2	+15.7	in
TOTAL	3.5	-13.3	<u>-9.8</u>	OUT



G. Summary of Deep Circulation

Steady near-bottom west to southwesterly flow was recorded at approximately  $20 \text{ cm sec}^{-1}$  near bottom between 1400 and 1800 meters water depth on the east flank of East Katla Ridge. The upslope flow direction of the current suggests that the axis of maximum density rises from a water depth of approximately 1800 meters on the east flank to about 1600 meters on the southern end of the ridge. The density distribution of water in the canyon axis suggests that the flow axis plunges approximately 300 to 400 meters upon encountering the canyon and north wall of West Katla Ridge: the depth of the 27.90 through 27.96 potential density surfaces in the canyon are all deeper than at the comparable stations on the east flank, and a thick mixed layer with a potential density of 27.96 is present in the canyon indicating mixing of the lower 100 to 150 meters of the water column.

Dense water exiting the canyon and resuming a westward flow is shifted to somewhat greater depths than on the East Katla Ridge east flank. Thin layers with potential density greater than 27.96 are guided well to the east of our section, causing a broadening of the most dense stratum. The thick mixed layers originating in the canyon are entrained in the main flow in the vicinity of 2200 meters water depth where they flow towards the west along West Katla Ridge towards Gardar sediment drift. The deepest strata flowing westwards in South Katla Basin are expected to be diverted back towards the south and east along the levee extending eastward from Reynidsjup Canyon.

The influence of Myrdalsjokull Canyon on the flow of the ISOC appears to be twofold. It is responsible for mixing of the lower 100 to 150 meters of the water column, the beginning of the process which alters the cold ( $\theta < 2^{\circ}\text{C}$ ), fresh ( $S = 34.96\%$ ) core surrounded by warmer, more saline water into the uniform waters observed at  $53^{\circ}\text{N}$  in Charlie-Gibbs Fracture Zone ( $\theta = 2.8^{\circ}\text{C}$ ,  $S = 34.98\%$ ). Myrdalsjokull Canyon is also responsible for broadening the deep current by diverting dense water to the east along Myrdalsjokull Canyon Levee.

Total flow of ISOW is approximately  $5.0 \times 10^6 \text{ m}^3 \text{ sec}^{-1}$ , of which approximately  $2.0 \times 10^6 \text{ m}^3 \text{ sec}^{-1}$  is the most dense Norwegian Sea Deep Water ( $\theta = -0.5^{\circ}\text{C}$ ,  $S = 34.92\%$ ) and the remainder admixed waters of the southern Norwegian Sea and northern North Atlantic. Approximately  $0.4 \times 10^6 \text{ grams sec}^{-1}$  of sediment is transported through the survey area; a net loss of  $0.1 \times 10^6 \text{ grams/sec}$  is observed within our station grid which corresponds to a net deposition rate of 10 to 15 cm/1000 yrs.

### CHAPTER III: SURFACE SEDIMENT DISTRIBUTION PATTERNS

#### A. Echo Character: Definition of Acoustic Units

3.5 kHz echo sounding has been used to define regions of distinct acoustic sediment types in the Katla Ridge region (Figures 3.1, 3.2), and has proved useful in identifying the extent of Holocene deposition and erosion in conjunction with analysis of cored sediments. Four echo patterns are recognized based on the reflectivity characteristics of the sediment surface and subbottom. Echo types used in this paper are defined in the same general manner as that of Damuth (1978). However, I have chosen not to use Damuth's numbering scheme, as the relatively few units in this small region compared to those in his much larger region would cause unnecessary confusion in the present study. Examples of each echo type are illustrated in Figures 3.3 to 3.12. The various patterns in this study may be recognized as follows:

1. Transparent sediments (Figure 3.3) Deposits in which internal reflectors are absent. The lower contact with underlying deposits may be conformable or unconformable to the sediment interface. Most commonly these deposits thin away from an identifiable 'depo-center' (e.g., center of South Katla Basin; adjacent to scarp on east flank). Minimum thickness for recognition is 2-3 meters because of the echosounder pulse length. Maximum observed thickness is approximately 20 meters.
2. Laminated sediments (Figure 3.4): Deposits with multiple sub-bottom reflections, typically continuous over several kilometers or more, and normally having 3-4 reflections per 20 meters of penetration.

FIGURE 3.1: Echo character map of Katla Ridge survey area. Numbered sections refer to examples illustrated in the following pages. See text for discussion of various echo types.

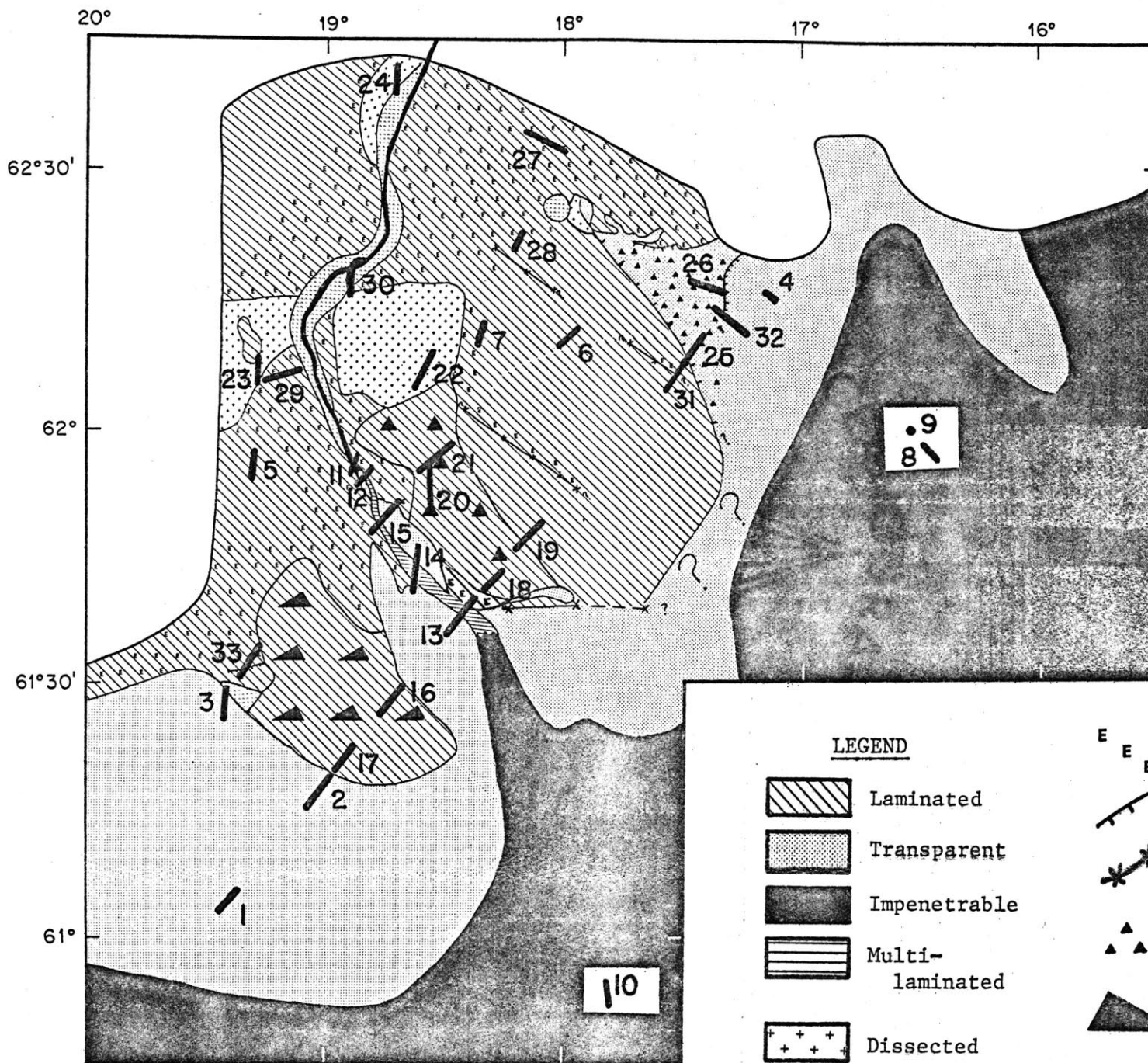
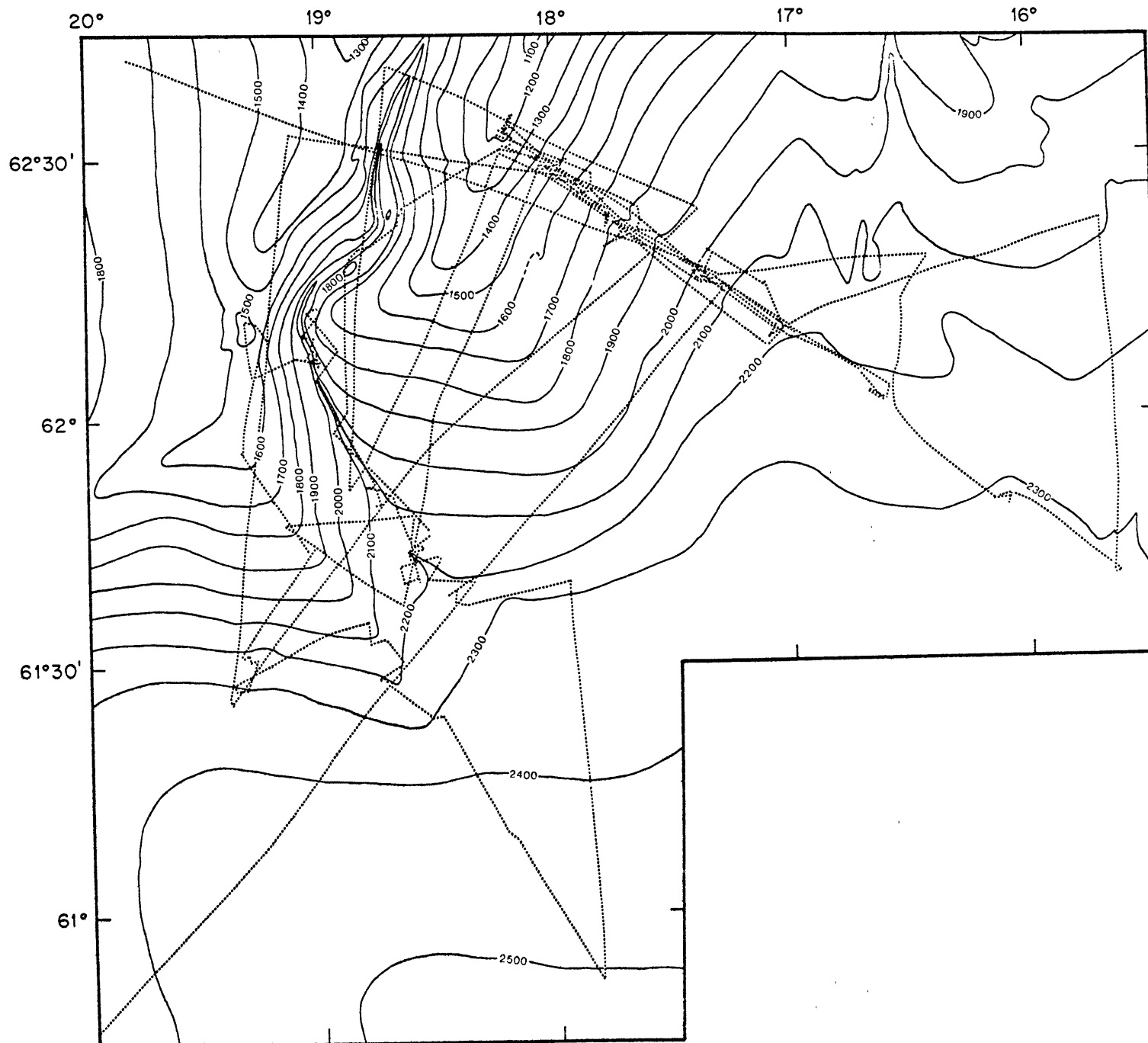


FIGURE 3.2: Bathymetry of Katla Ridge survey area, showing track coverage of AII-94-1. Additional echosounder (3.5 kHz) coverage from Lamont-Doherty cruises was provided by Dr. J. Damuth (cruises V27-06, V28-04, and C 21-12 of R/V Vema and Conrad) for use in constructing the echo character map.



- FIGURE 3.3: Examples of 3.5 kHz echograms: transparent sediments.
- a. Section 1 of Figure 3.1. 1030 - 1100 GMT, 26 June 1977. South Katla Basin.
  - b. Section 2 of Figure 3.1. 1220 - 1255 GMT, 26 June 1977. South Katla Basin (northern margin) where transparent sediments overlie deeper sediment waves on the southern flank of Myrdalsjokull Canyon Levee.
  - c. Section 3 of Figure 3.1. 1745 - 1815 GMT, 28 June 1977. South Katla Basin (northern margin) where transparent sediments overlie slump (?) on lower slope of West Katla Ridge. Arrow indicates position near site of core 12PC.
  - d. Section 4 of Figure 3.1. 0210 - 0235 GMT, 04 July 1977. East flank, East Katla Ridge. Similar to deposits at site of core 4PC.



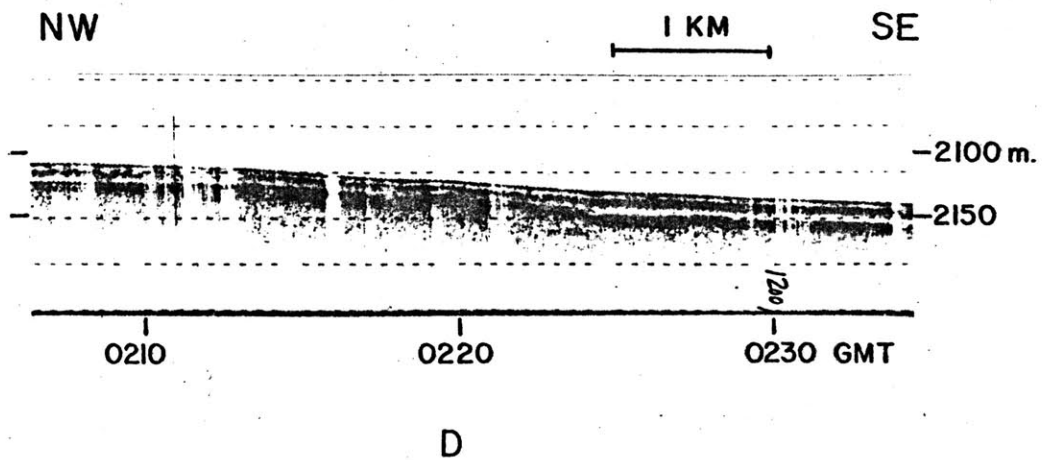
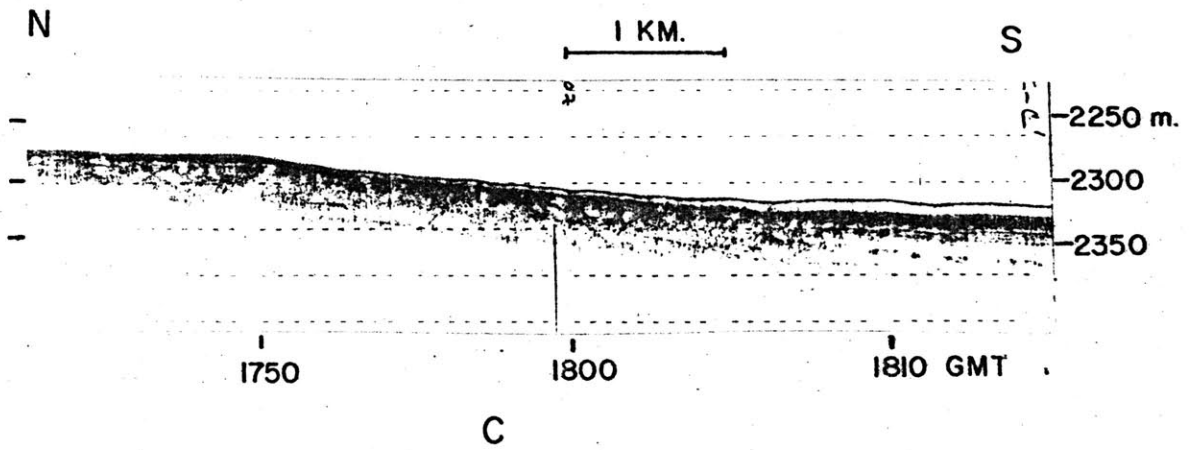
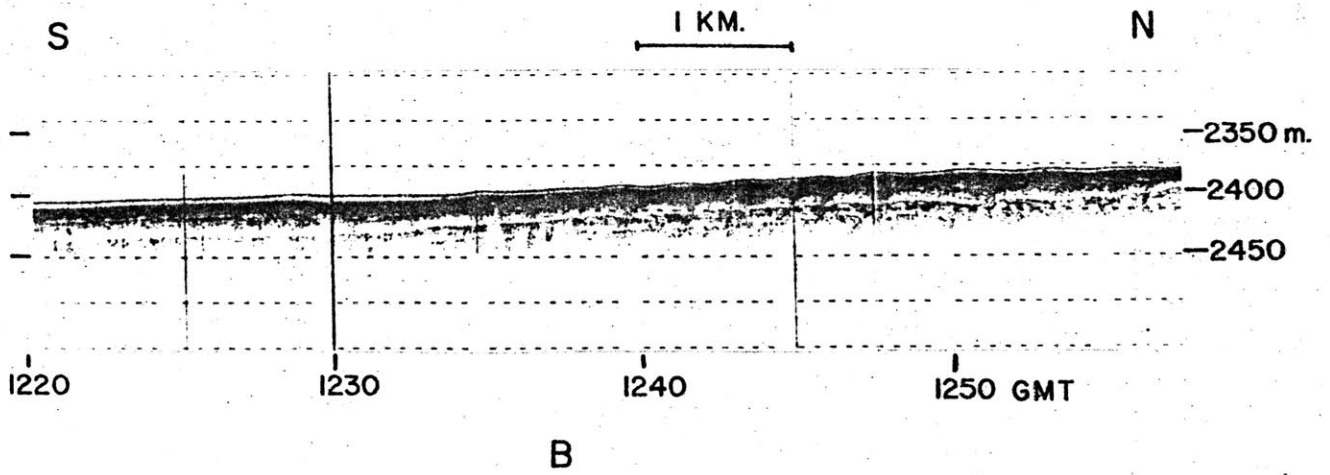
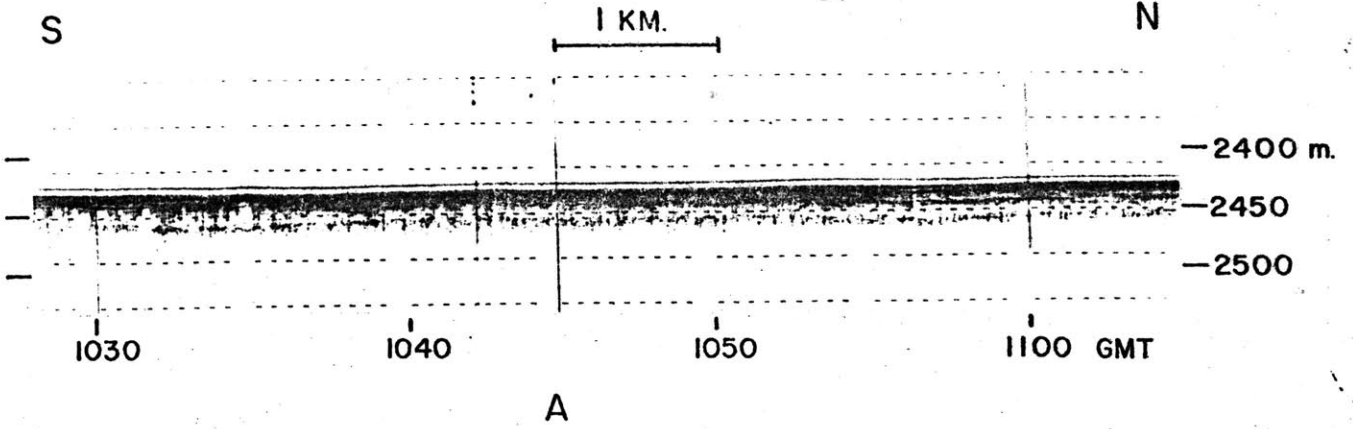
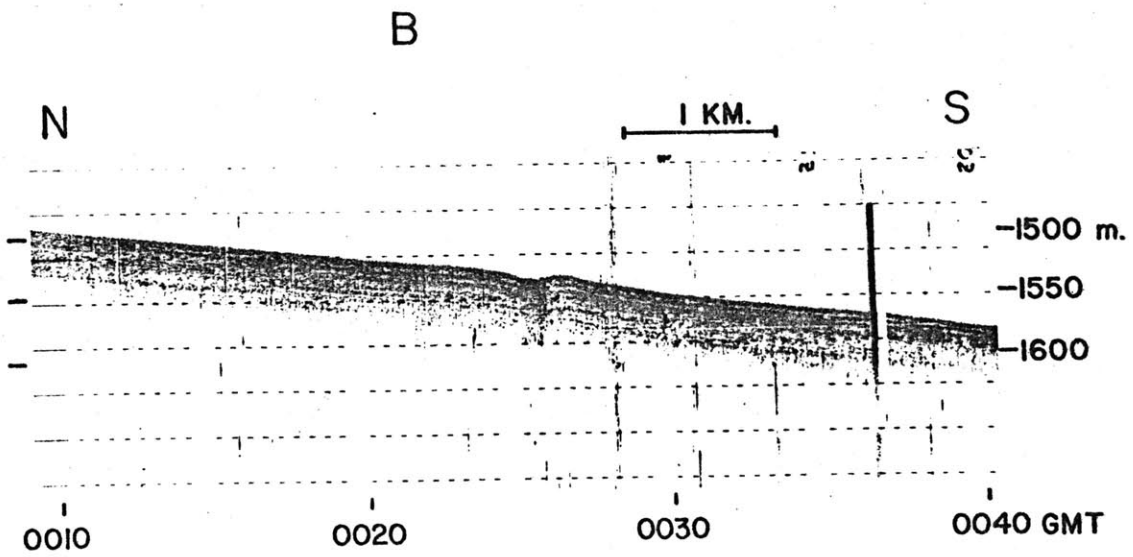
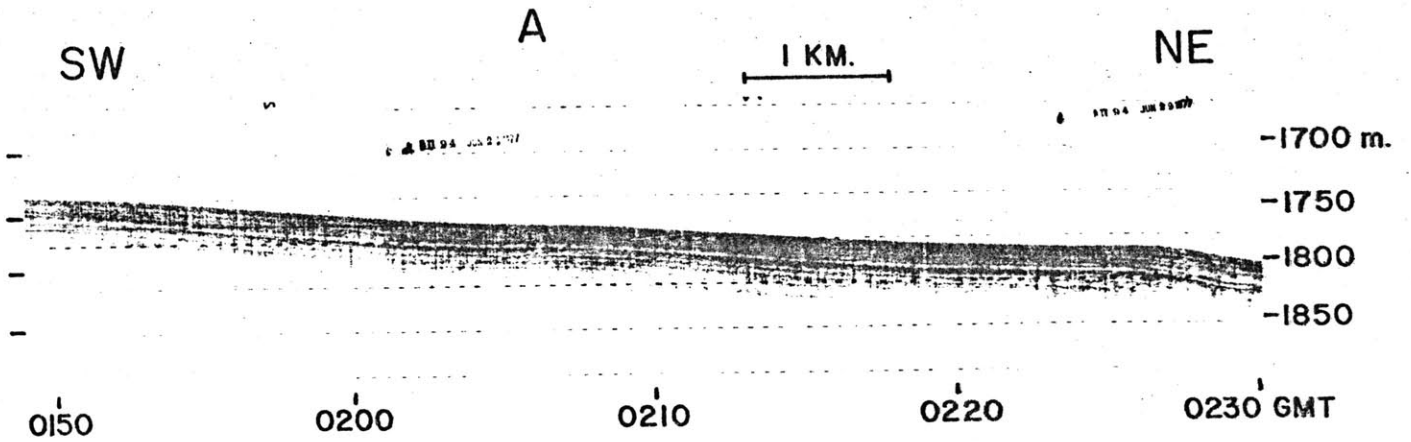
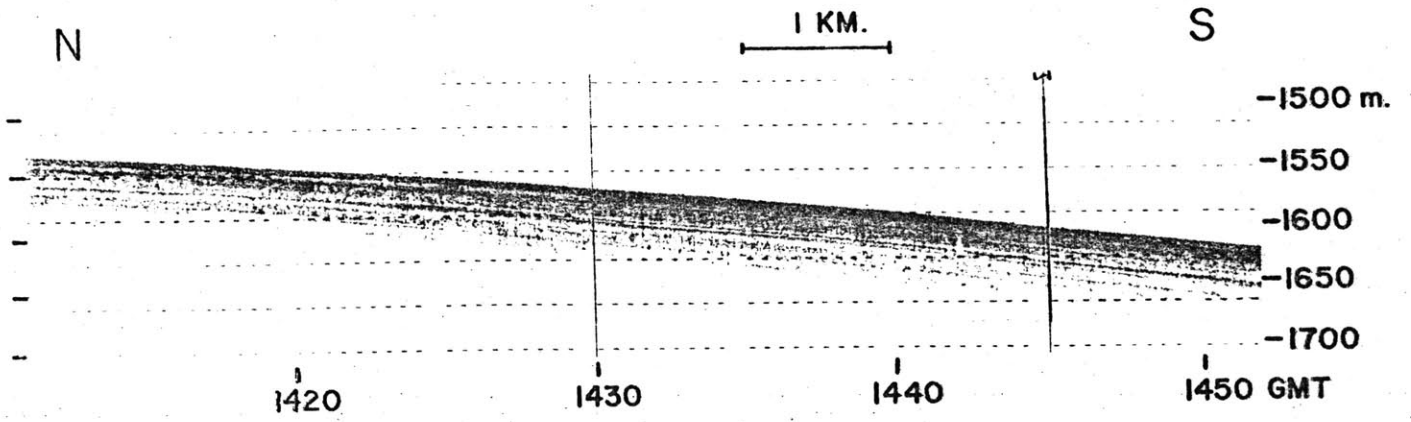


FIGURE 3.4: Examples of 3.5 kHz echograms: laminated sediments.

a. Section 5 of Figure 3.1. 1410 - 1450 GMT, 28 June 1977. East Katla Ridge.

b. Section 6 of Figure 3.1. 0150 - 0230 GMT, 29 June 1977. East Katla Ridge.

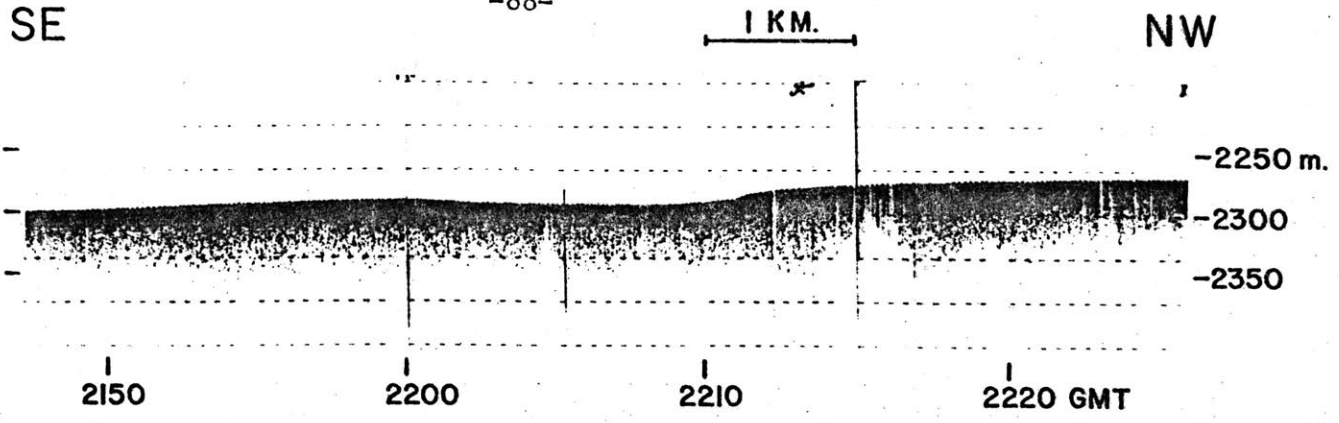
c. Section 7 of Figure 3.1. 0010 - 0040 GMT, 05 July 1977. East Katla Ridge.



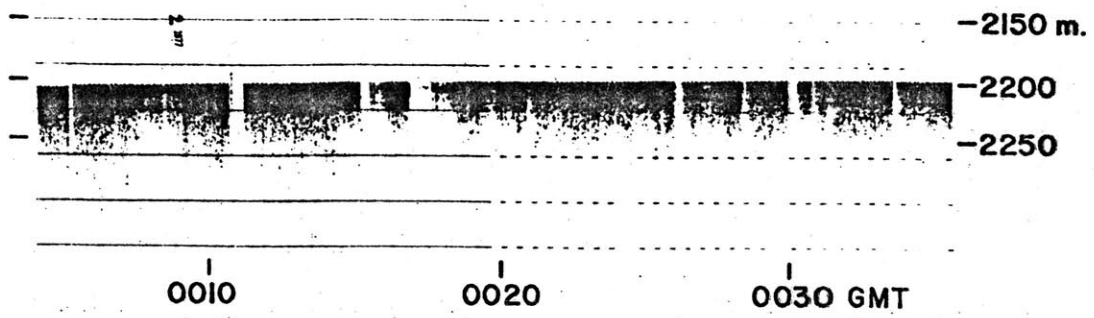
C

FIGURE 3.5: Examples of 3.5 kHz echograms: acoustically impenetrable sediments.

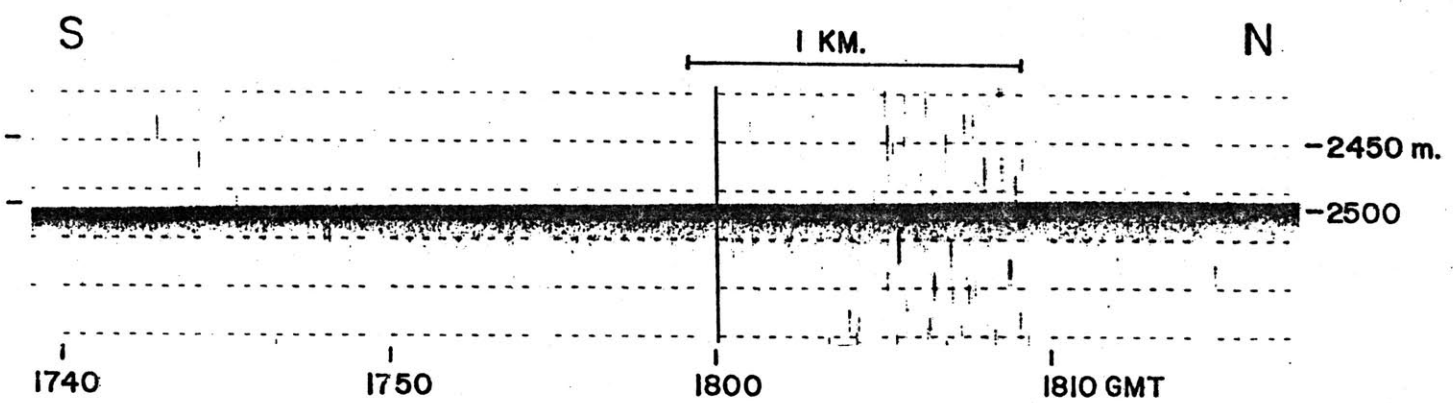
- a. Section 8 of Figure 3.1. 2150 - 2220 GMT, 01 July 1977. Channelized section of basin east of East Katla Ridge.
- b. Section 9 of Figure 3.1. 0005 - 0035 GMT, 02 July 1977. Ship stopped on station at site of core 3PC, lower east flank of East Katla Ridge.
- c. Section 10 of Figure 3.1. 1745 - 1815 GMT, 08 July 1977. Eastern end of South Katla Basin.
- d. Section 11 of Figure 3.1. 1540 - 1550 GMT, 29 June 1977. Turbidites near mouth of Myrdalsjokull Canyon.
- e. Section 12 of Figure 3.1. 1650 - 1700 GMT, 29 June 1977. Near mouth of Myrdalsjokull Canyon. Slumped block in canyon axis, with hyperbolae adjacent.



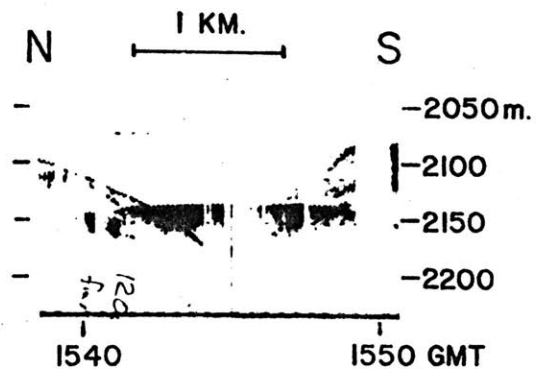
A



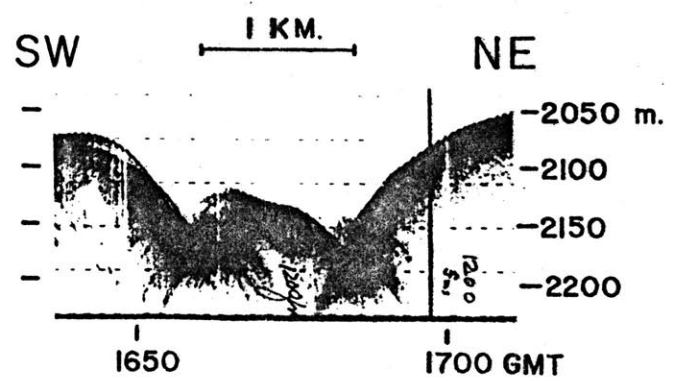
B



C

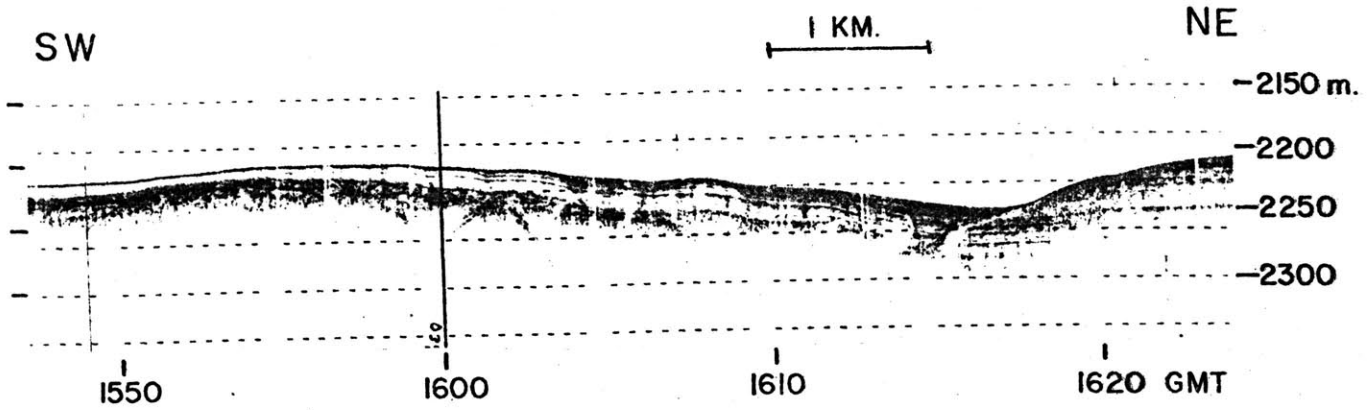


D

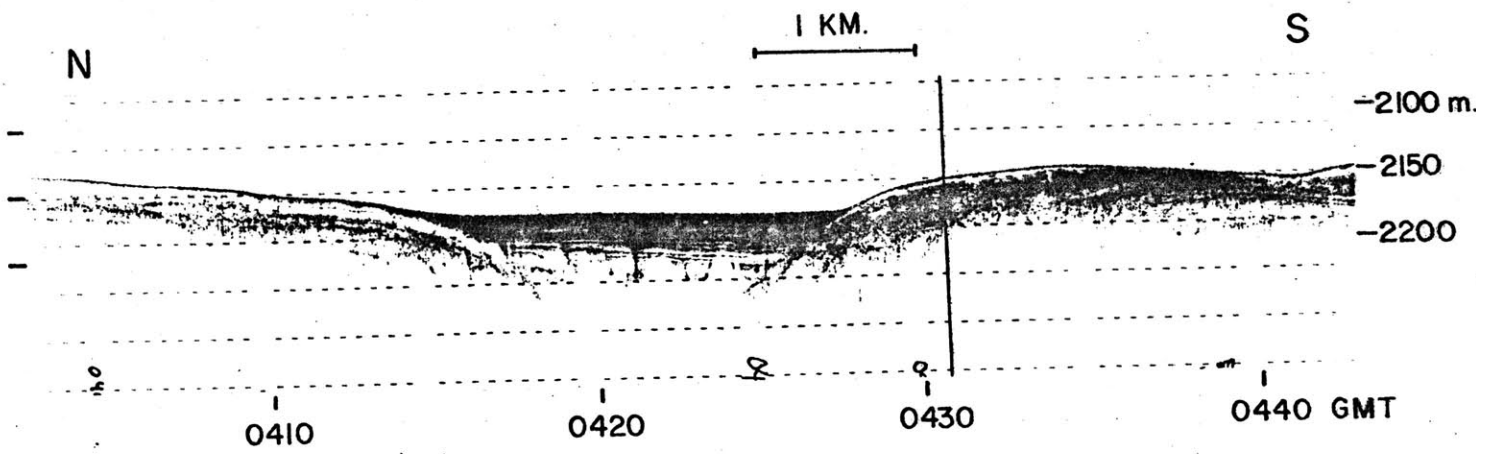


E

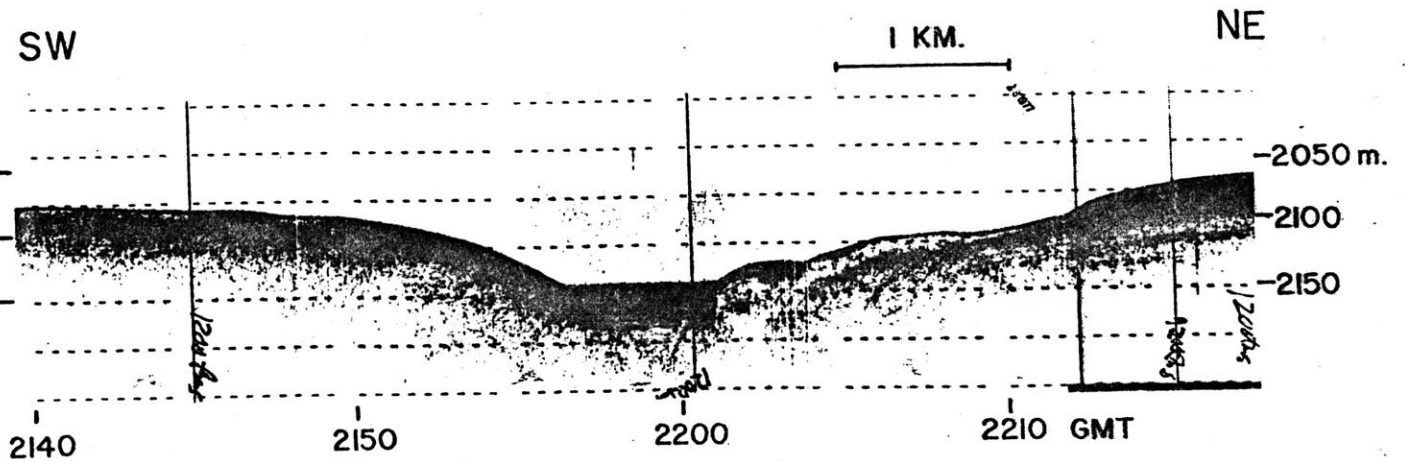
- FIGURE 3.6: Examples of 3.5 kHz echograms: multi-laminated sediments.
- a. Section 13 of Figure 3.1. 1550 - 1620 GMT, 26 June 1977. Myrdalsjokull Channel, near eastern end.
  - b. Section 14 of Figure 3.1. 0405 - 0440 GMT, 05 July 1977. Myrdalsjokull Channel, showing multi-laminated sediments overlying transparent sediments to the north.
  - c. Section 15 of Figure 3.1. 2140 - 2220 GMT, 28 June 1977. Myrdalsjokull Channel, near canyon mouth. Note erosion of channel walls and fill of multi-laminated sediments over transparent sediments to the northeast.



A



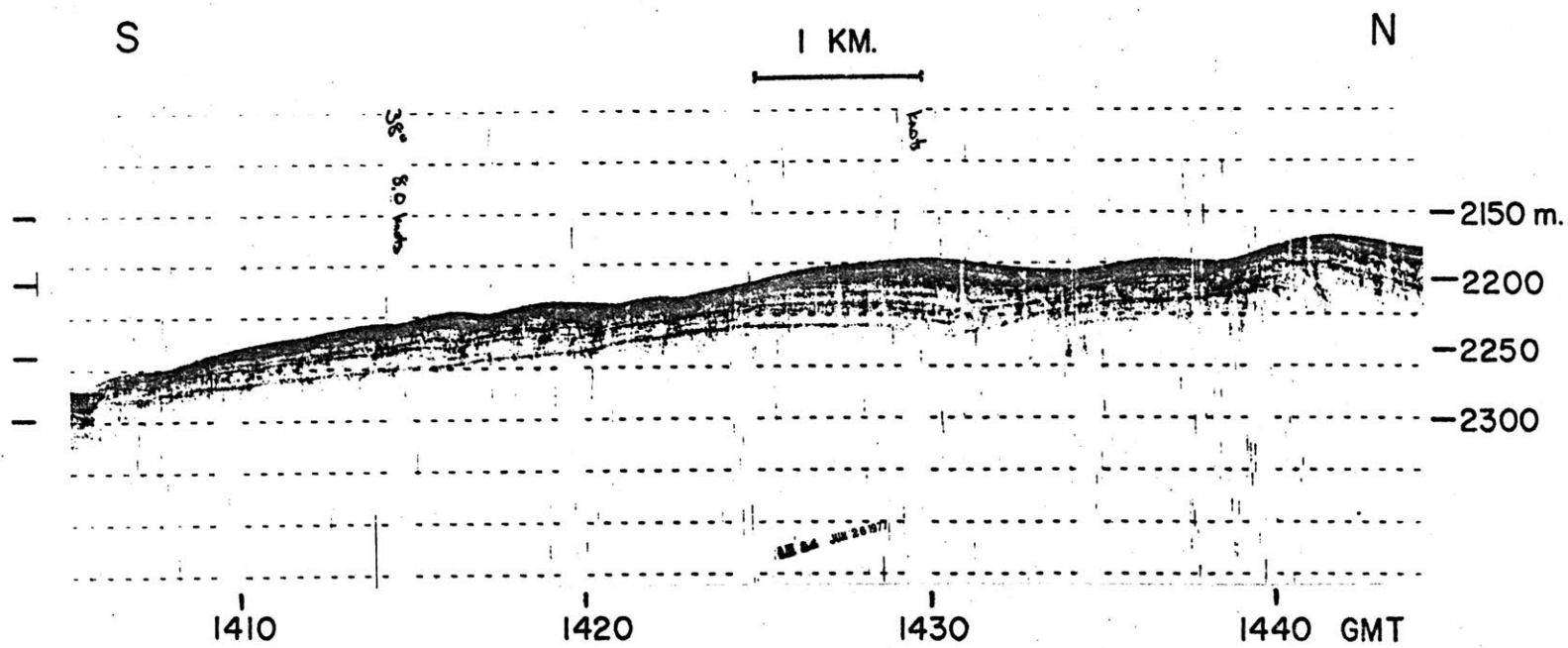
B



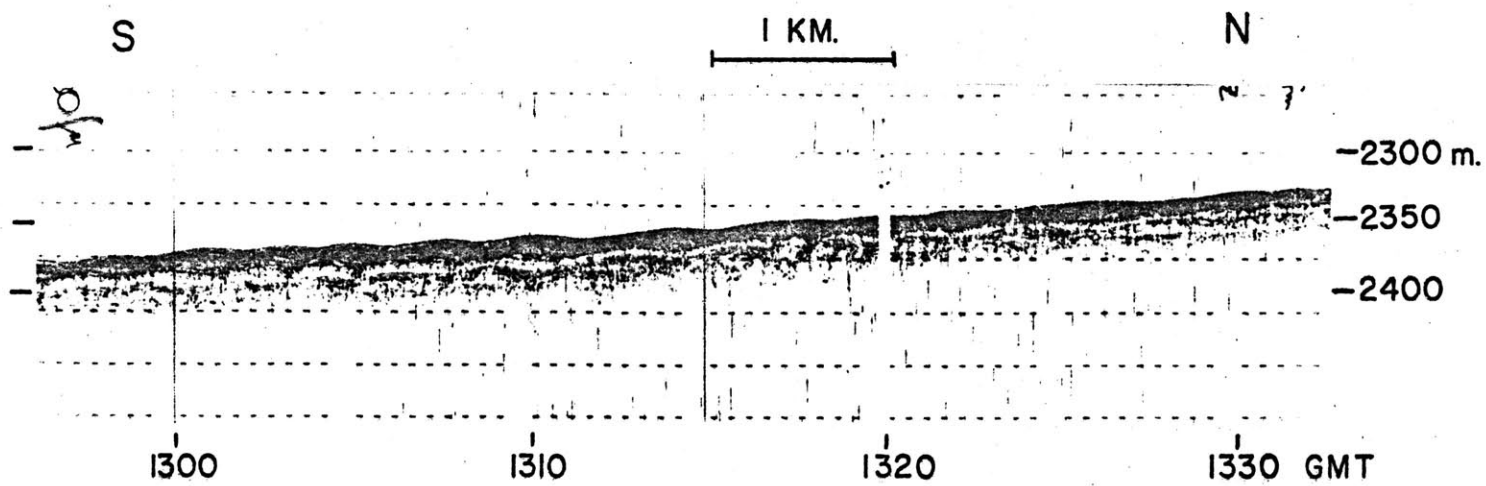
C

FIGURE 3.7: Examples of 3.5 kHz echograms: asymmetric sediment waves.  
a. Section 16 of Figure 3.1. 1405 - 1445 GMT, 26 June 1977. Large waves near crest of Myrdalsjokull Canyon Levee.  
b. Section 17 of Figure 3.1. 1255 - 1330 GMT, 26 June 1977. Small waves on lower southern flank of Myrdalsjokull Canyon Levee.



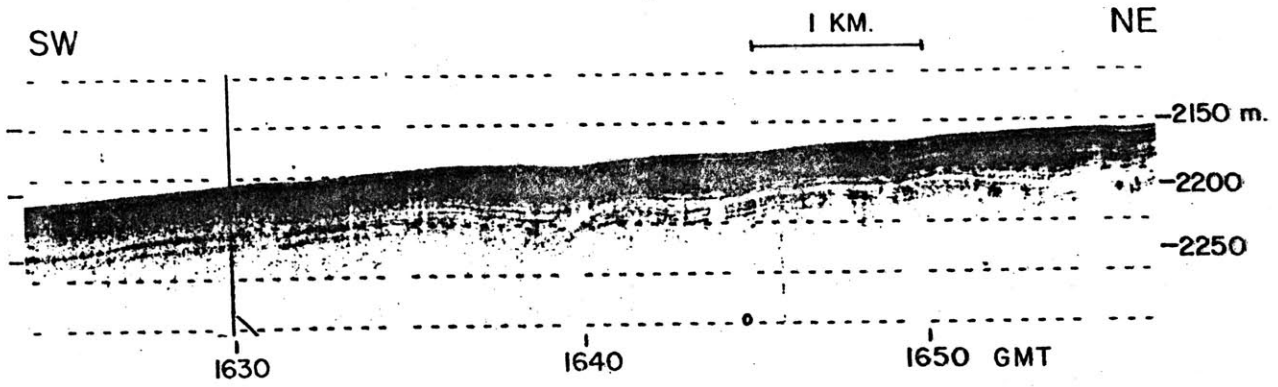


A

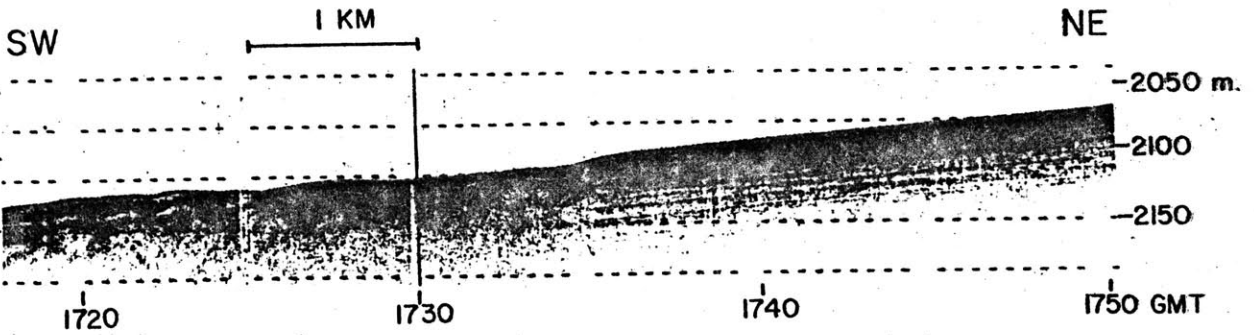


D

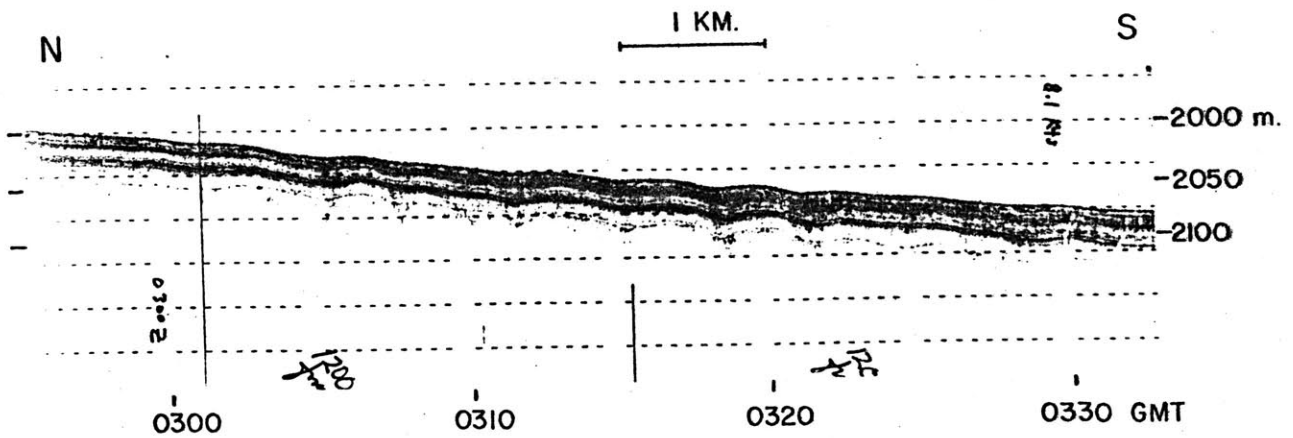
- FIGURE 3.8: Examples of 3.5 kHz echograms: symmetric sediment waves.
- a. Section 18 of Figure 3.1. 1625 - 1700 GMT, 26 June 1977. East Katla Ridge.
  - b. Section 19 of Figure 3.1. 1720 - 1750 GMT, 26 June 1977. Transition from waves to flat-lying laminated deposits. East Katla Ridge.
  - c. Section 20 of Figure 3.1. 0300 - 0330 GMT, 05 July 1977. East Katla Ridge. Note stronger return over troughs due to focussing.
  - d. Section 21 of Figure 3.1. 2250 - 2330 GMT, 28 June 1977. Example of "vertically barred" deposits where surface wave expression is subdued, but focussing is clearly evident.



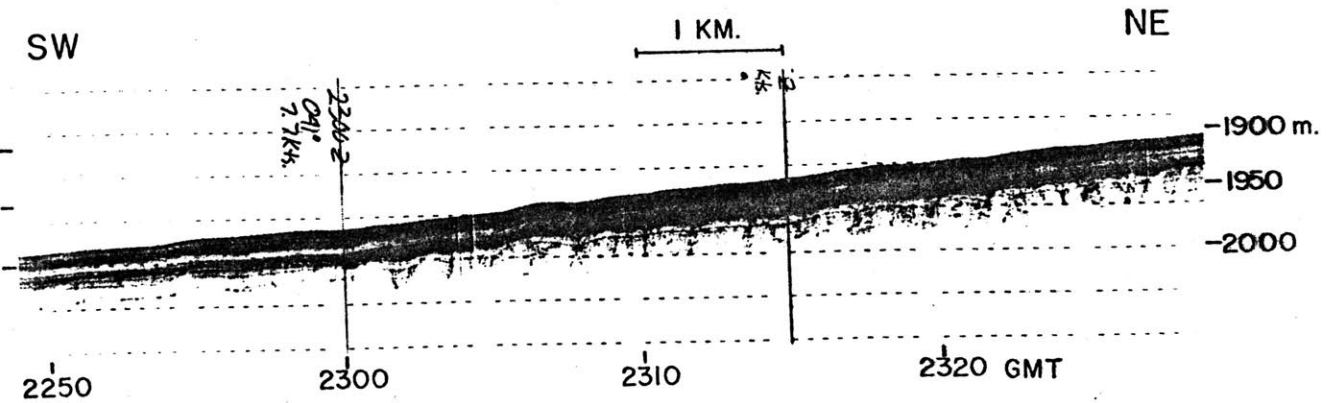
A



B



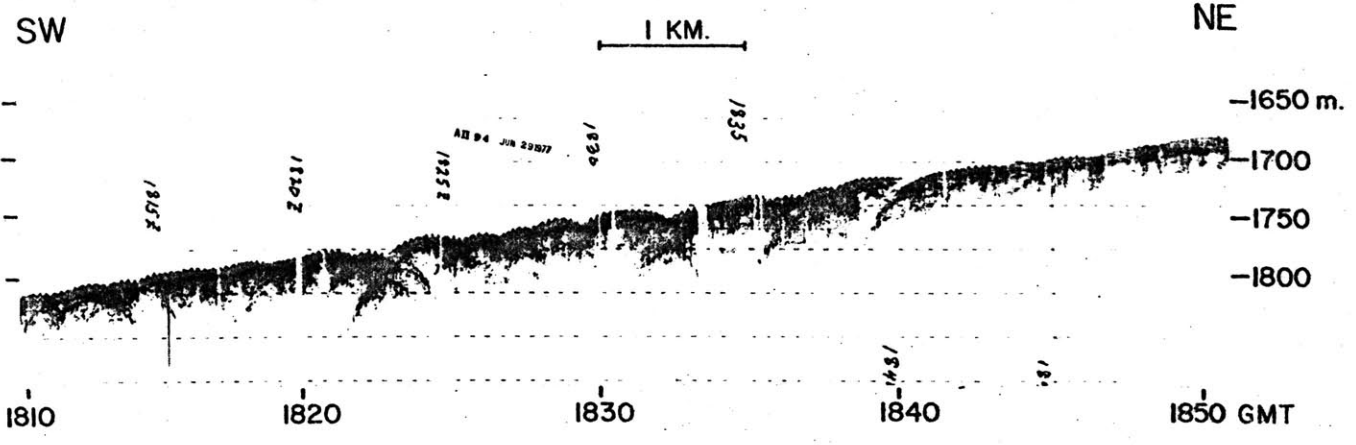
C



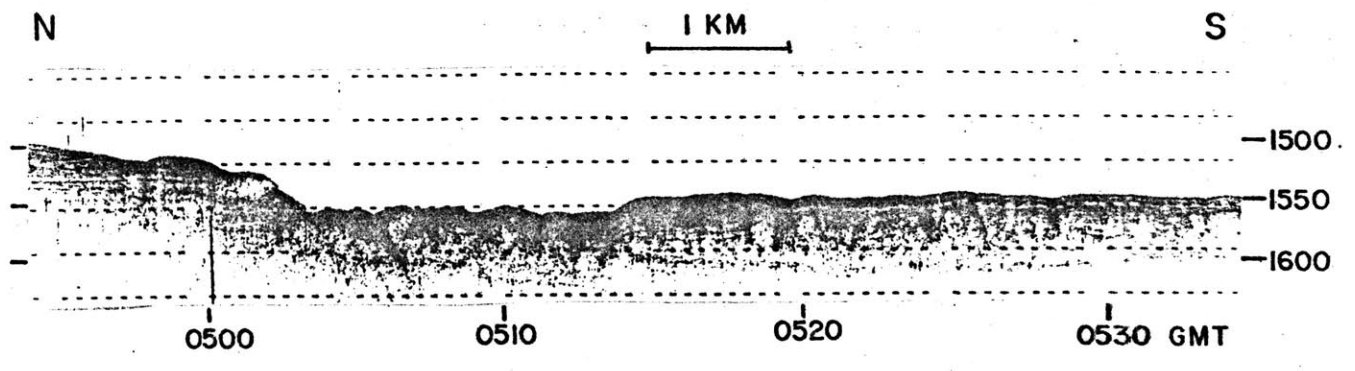
D

FIGURE 3.9: Examples of 3.5 kHz echograms: 'dissected terrain'.

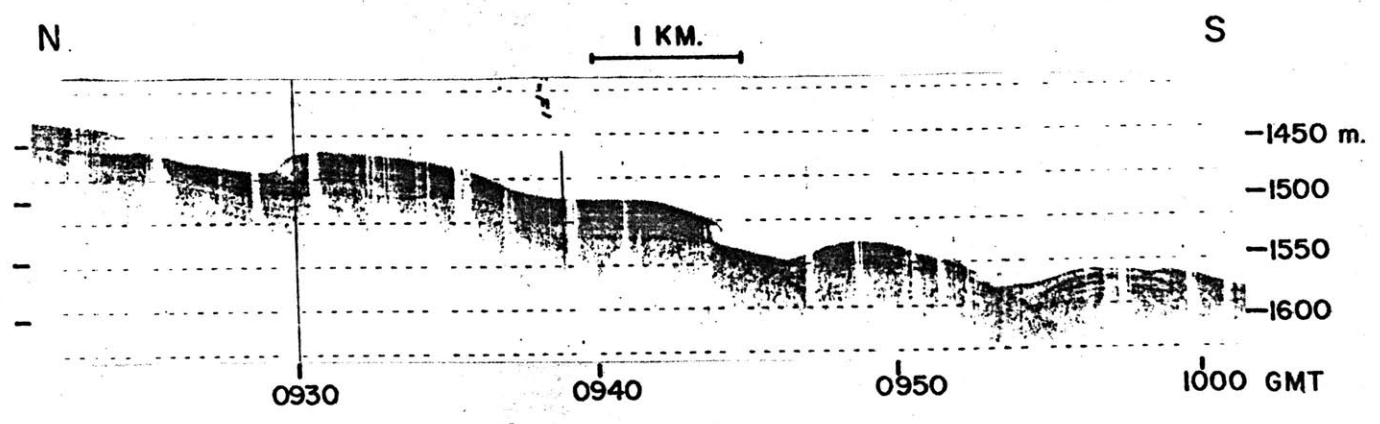
- a. Section 22 of Figure 3.1. 1810 - 1850 GMT, 29 June 1977. South end of East Katla Ridge. This deposit lies within the inferred axis of the ISOC, and may be similar to the abyssal furrows discussed by Flood (1978).
- b. Section 23 of Figure 3.1. 0455 - 0535 GMT, 07 July 1977. Saddle on southern end of West Katla Ridge. This deposit is probably caused by a combination of slumping and subsequent erosion by bottom currents.
- c. Section 24 of Figure 3.1. 0925 - 1000 GMT, 29 June 1977. Wall of Myrdalsjokull Canyon. This type of deposit is inferred to result from slumping.



A



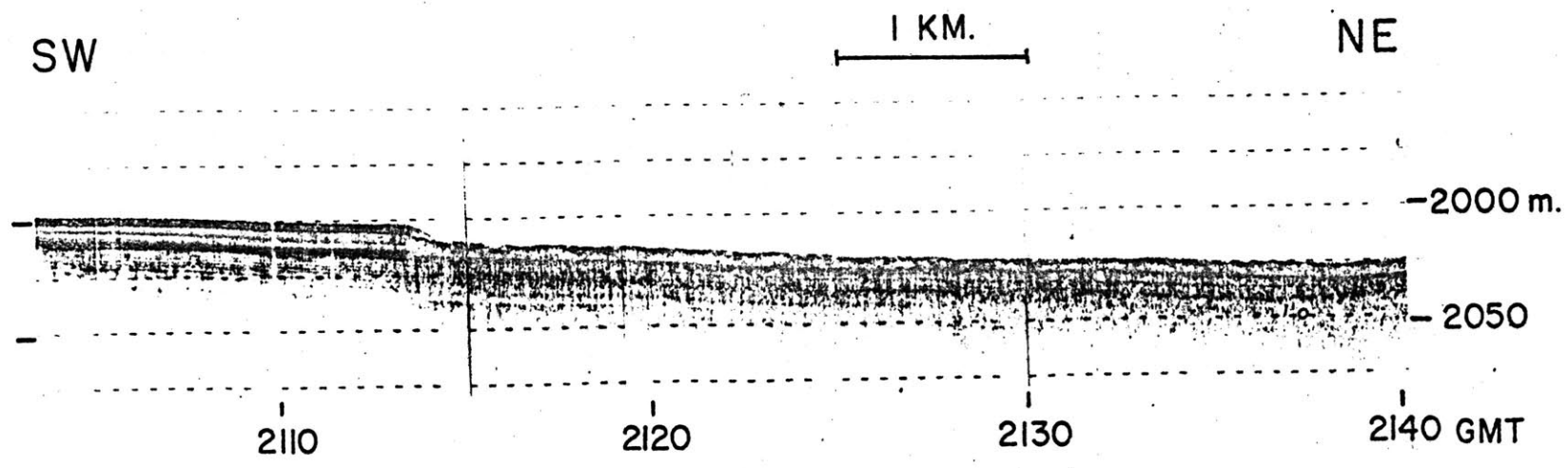
B



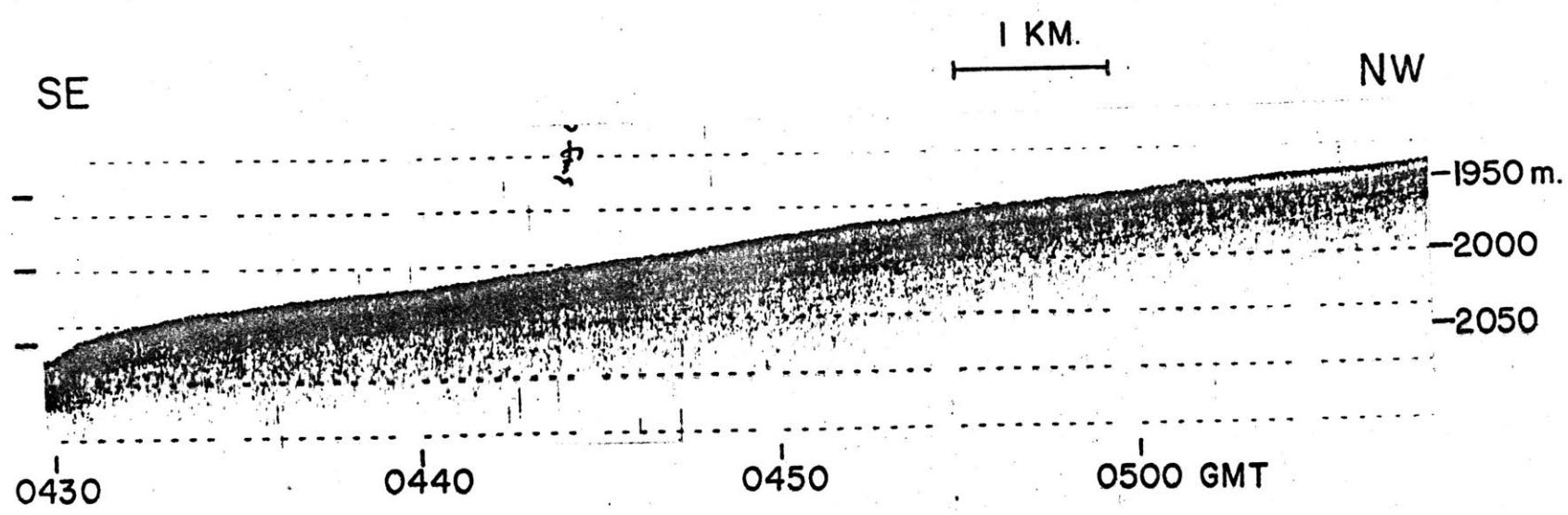
C

FIGURE 3.10: Examples of 3.5 kHz echograms: small-scale surface roughness and hyperbolae.

- a. Section 25 of Figure 3.1. 2105 - 2140 GMT, 26 June 1977. East flank, East Katla Ridge. Near site of core 15BG.
- b. Section 26 of Figure 3.1. 0430 - 0510 GMT, 04 July 1977. East flank, East Katla Ridge.



A



B

- FIGURE 3.11: Examples of 3.5 kHz echograms: surface erosion.
- a. Section 27 of Figure 3.1. 0615 - 0650 GMT, 29 June 1977. East flank, East Katla Ridge. Arrow indicates small scarp (?). These features are common within the region underlying the ISOC axis.
  - b. Section 28 of Figure 3.1. 2230 - 2300 GMT, 04 July 1977. Arrow indicates region of thinning and outcropping of reflectors. Crest of East Katla Ridge, southern end.
  - c. Section 29 of Figure 3.1. 2025 - 2100 GMT, 06 July 1977. Western wall of Myrdalsjokull Canyon.



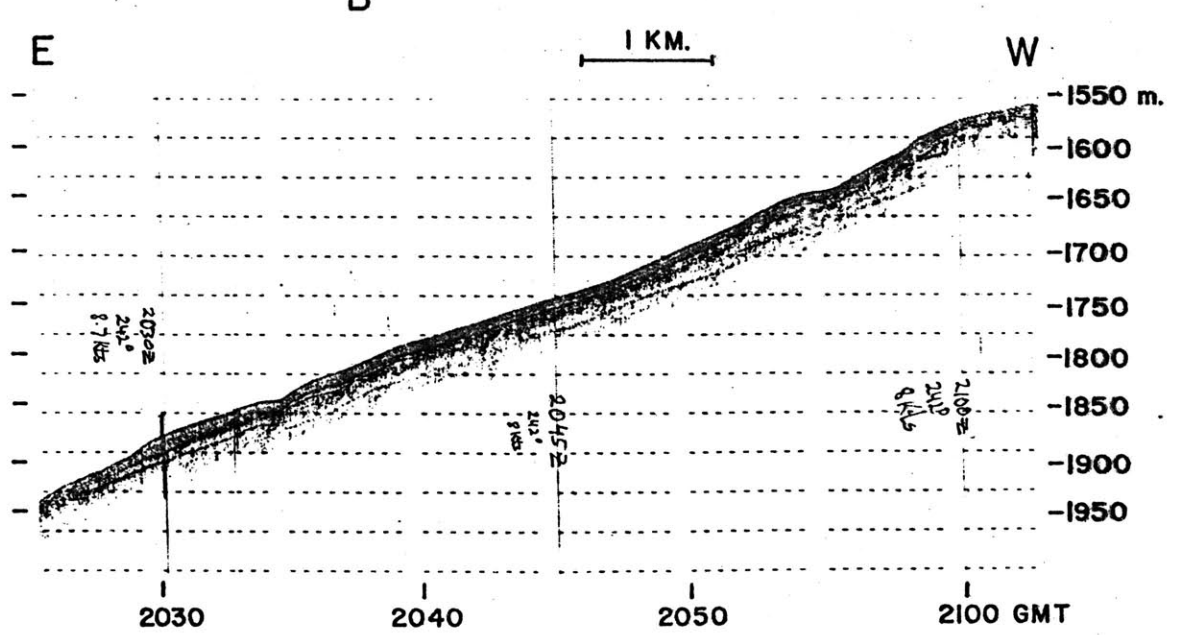
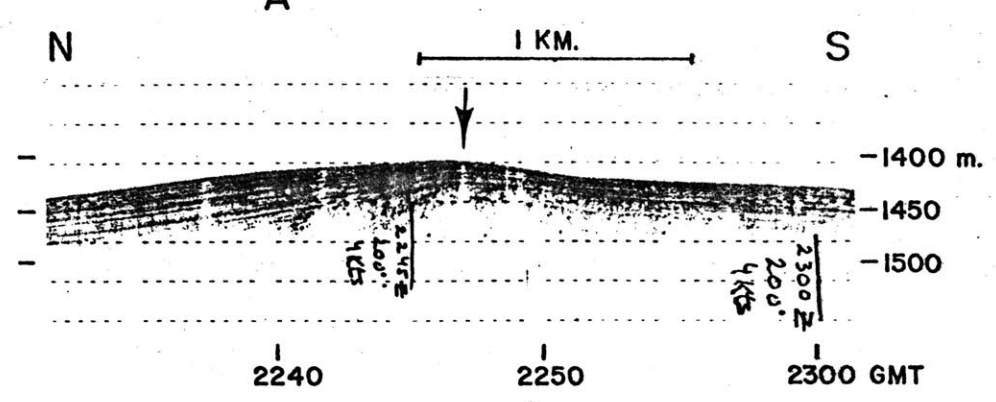
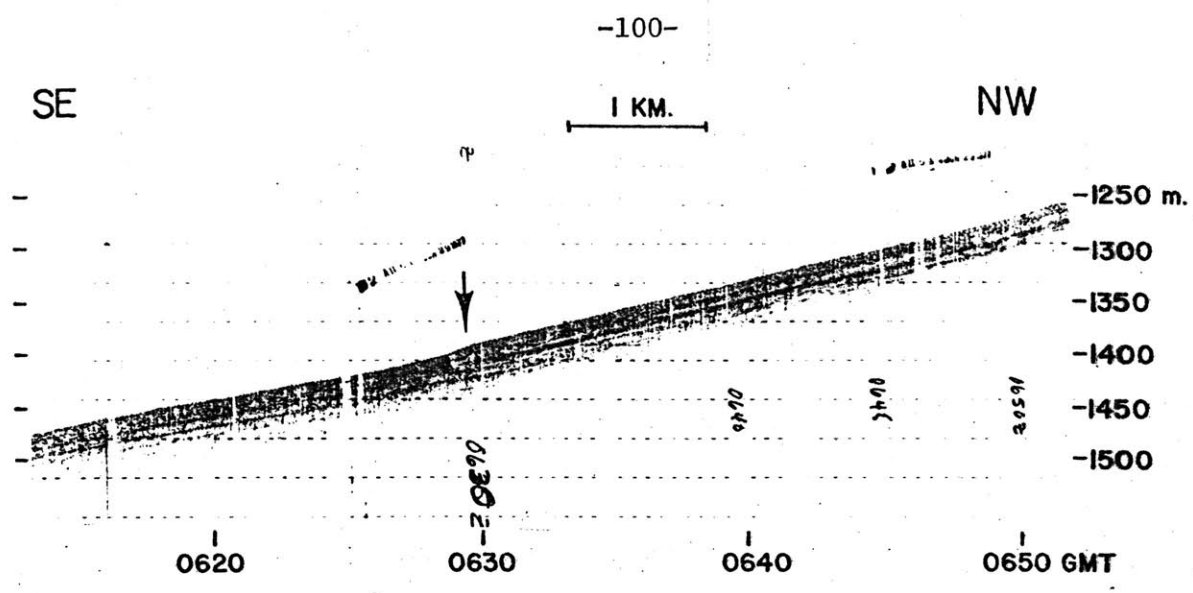
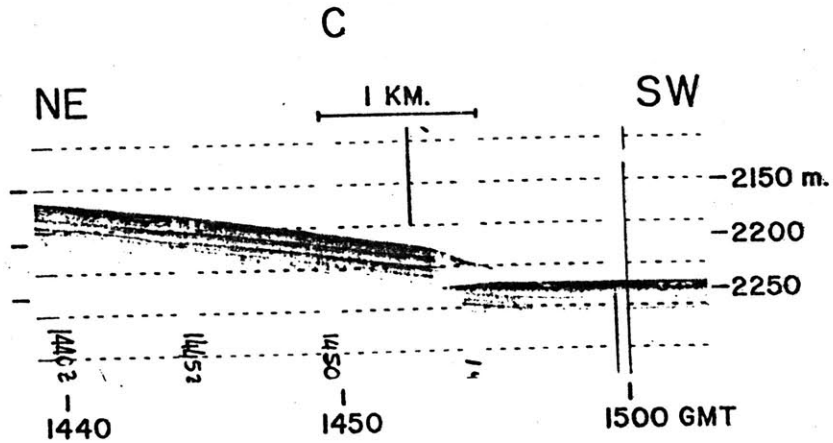
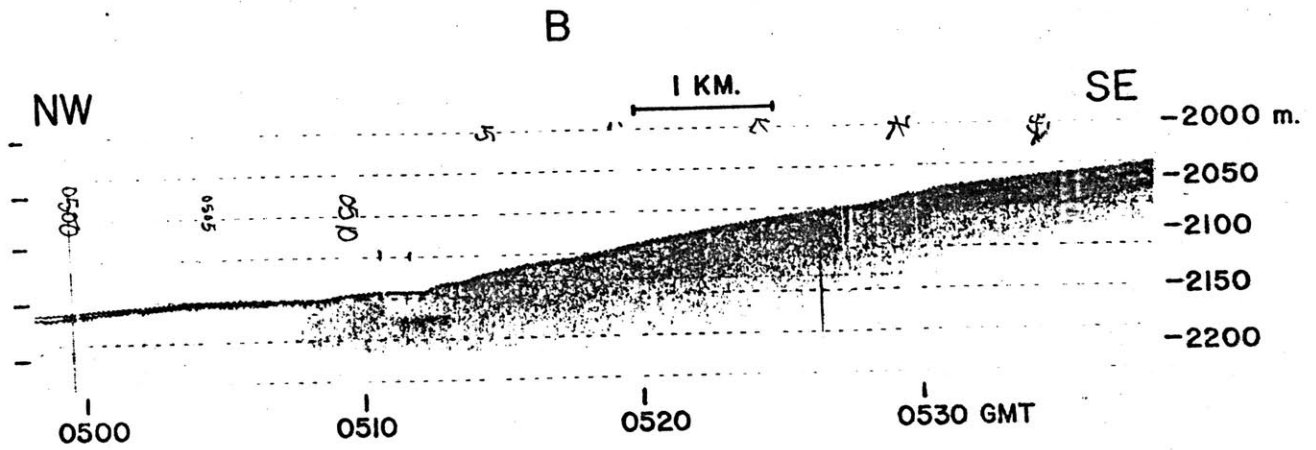
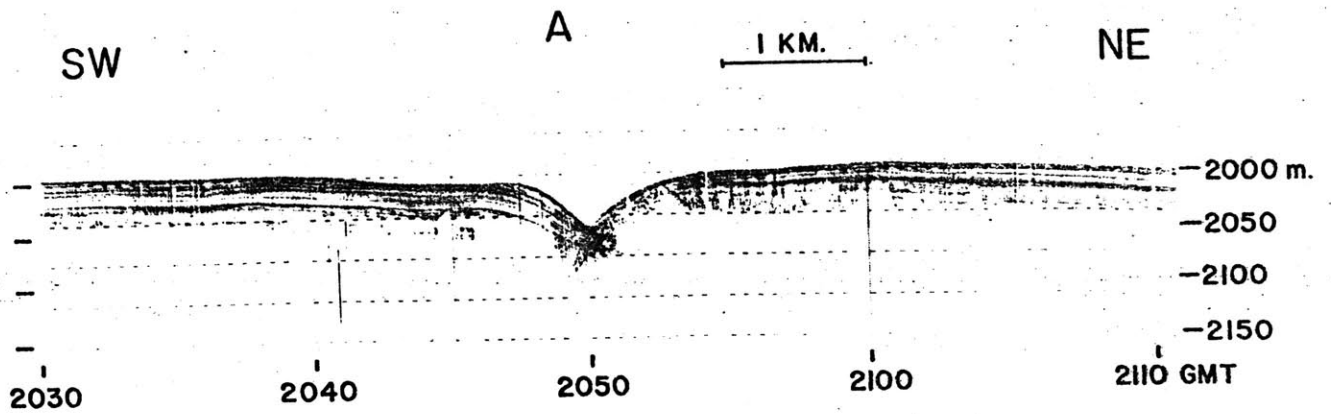
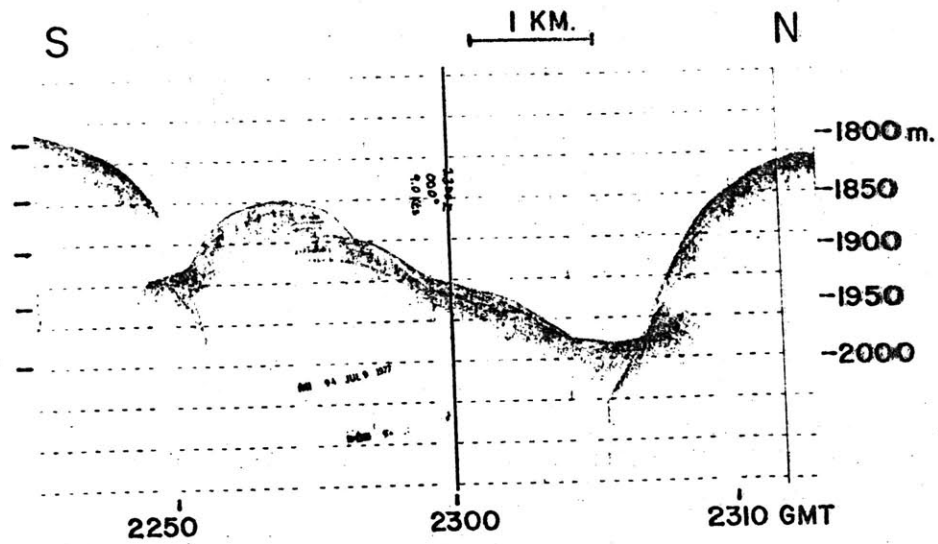


FIGURE 3.12: Examples of 3.5 kHz echograms: slumps, v-channels, and scarps.

- a. Section 30 of Figure 3.1. 2245 - 2310 GMT, 09 July 1977. Large slumped blocks, Myrdalsjokull Canyon.
- b. Section 31 of Figure 3.1. 2030 - 2110 GMT, 26 June 1977. V-shaped channel, east flank of East Katla Ridge. These features are not always continuous from one profile to the next, and may be related to faulting (?).
- c. Section 32 of Figure 3.1. 0500 - 0540 GMT, 03 July 1977. Buried scarp, east flank of East Katla Ridge.
- d. Section 33 of Figure 3.1. 1440 - 1505 GMT, 07 July 1977. Scarp on southern flank of West Katla Ridge. Near sites of cores 11PC, 12PC.



D

Maximum penetration is approximately 60 meters. Subbottom reflectors are generally conformable.

3. Acoustically impenetrable sediments (Figure 3.5): Deposits in which a strong, prolonged surface reflection masks underlying reflectors.

4. 'Multi-laminated' sediments (Figure 3.6): Deposits in which numerous sub-bottom reflections occur, often so closely spaced that individual reflectors may not be followed.

These acoustic patterns show considerable variability, and lateral gradation from one to another is common (particularly between the transparent and multi-laminated deposits). The boundaries on the echo character map (Figure 3.1) are therefore somewhat subjective (as is the case for all such maps). The uppermost acoustic unit only is plotted, although in some cases as many as three echo types may be recognized in a single vertical record section (e.g., Figure 3.6a).

In addition to the four principal echo patterns discussed above, there are five morphologic/acoustic features which result from echo returns from bathymetric elements whose dimensions are near or below the resolving scale of the echosounder (approximately equal to the water depth for a 30° radius sound cone). They are identified as:

1. Asymmetric sediment waves (Figure 3.7): Sedimentary deposits with wave length scales of 300 to 2000 meters, and amplitudes of 3 to 30 meters. They occur in acoustically laminated deposits, with subbottom reflectors indicating upslope migration.

2. Symmetric sediment waves (Figure 3.8): Variable deposits, ranging in amplitude from 1 or 2 meters to approximately 10 meters in laminated

deposits. Wavelength 300 to 1000 meters. Low-amplitude forms commonly develop a 'vertically banded' appearance, apparently due to focussing over troughs.

3. Dissected terrain (Figure 3.9): Regions of rough, irregular morphology, commonly with strong hyperbolic reflections at both the sediment surface and in subbottom returns. Wavelength of individual features is variable, from 200 to 1000 meters or more. Morphologic elements are typically 5 to 25 meters high.

4. Small-scale surface roughness and hyperbolae (Figure 3.10): Overlapping surface-tangent hyperbolae typically 100-200 meters wide. Developed at the surface of a transparent sediment layer approximately 10 meters thick overlying laminated deposits.

5. Surface erosion (Figure 3.11): Regions in which surface irregularities, outcropping reflectors or thinning of acoustic units indicate that removal of surface sediments has occurred. This is the most subjectively defined deposit, with local surface waviness included in the definition.

Additional features recognized on 3.5 kHz records include V-shaped channels and scarps, plus slumped blocks of various sizes (Figure 3.12). Scarps 10 to 20 meters high are common on the East Katla Ridge, but often cannot be traced across adjacent profiles. Only major scarps which may be readily mapped have been indicated on the echo character map.

B. Geographic Distribution of Acoustic Units

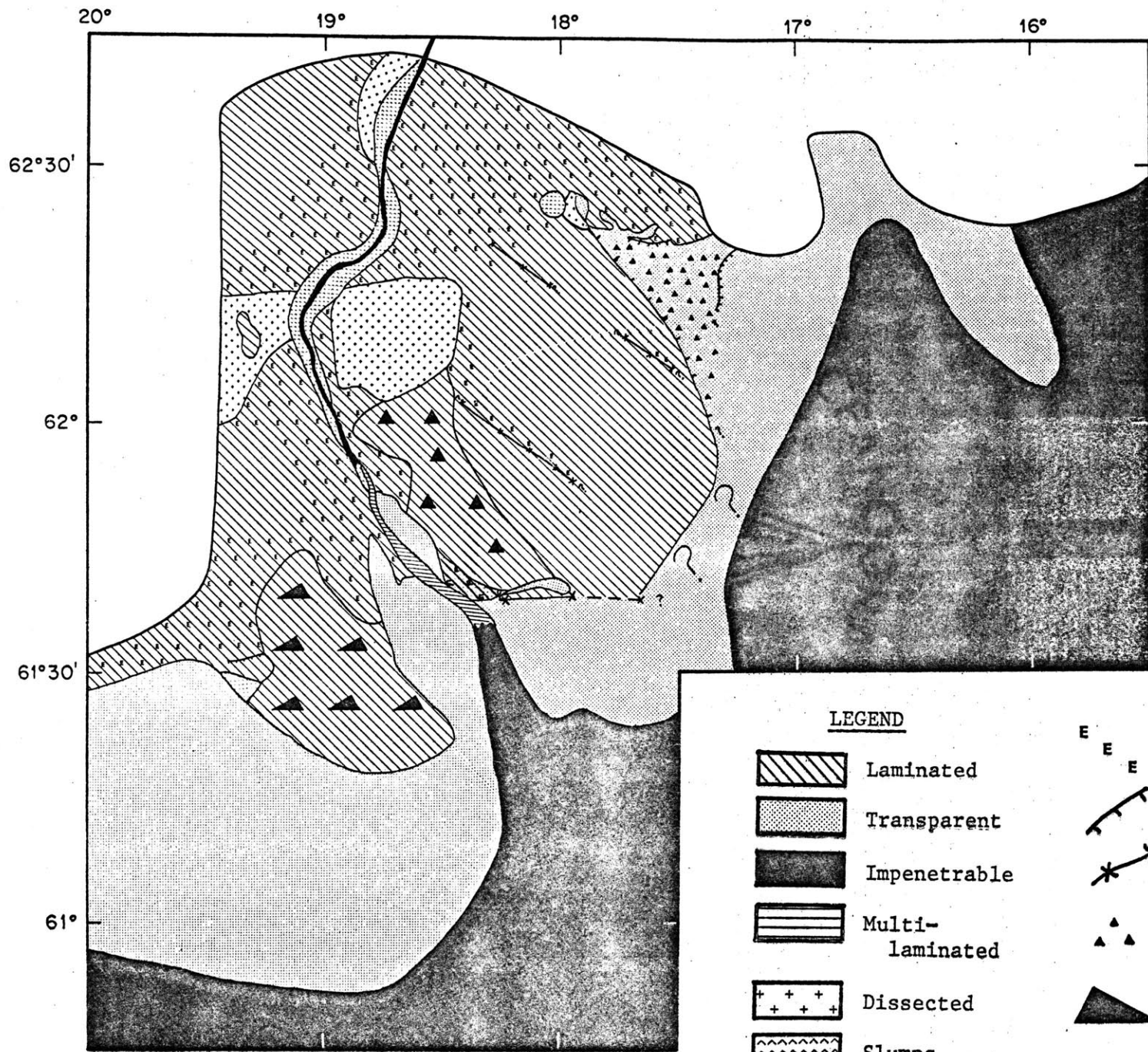
1. Transparent sediments

Transparent sediments are observed in two regions of the study area (Figure 3.13). A broad deposit is located in the cul-de-sac basin (South Katla Basin) immediately south of the East and West Katla Ridge southern flanks. These sediments attain thicknesses of 10 to 20 meters in the center of the basin and thin both to the north and to the south. They overlie the southern end of a field of asymmetric sediment waves on the south flank of the Myrdalsjokull Canyon Levee (Figure 3.3b).

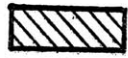





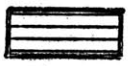

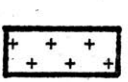



The southern transparent sediment region is continuous with similar deposits flanking the channel emanating from Myrdalsjokull Canyon. Thin deposits of transparent sediments are observed near the point where multi-laminated sediments appear to break across the levee towards the south.

Transparent deposits observed on the eastern flank of East Katla Ridge show somewhat different characteristics than those to the south. An abrupt transition occurs between the region of small-scale hyperbolae and transparent sediments at a scarp (50 to 75 meters high) in the vicinity of 2000 meters depth on the ridge flank. Sediment accumulation is thickest immediately downslope from the scarp, and the sediments rapidly thin towards the east (downslope), becoming indistinguishable from the highly reflective and acoustically impenetrable deposits of the lower flank and basin. It is not clear whether the transparent sediments observed on the northern section are continuous into the southern section, due to the lack of adequate 3.5 kHz echo sounder coverage in the intermediate region.

FIGURE 3.13: Echo character map of Katla Ridge survey area. See text for discussion of various echo types.



**LEGEND**

- |   |                 |   |                  |
|---|-----------------|---|------------------|
|  | Laminated       |  | Surface erosion  |
|  | Transparent     |  | Scarp            |
|  | Impenetrable    |  | Channels         |
|  | Multi-laminated |  | Small hyperbolae |
|  | Dissected       |  | Asymmetric waves |
|  | Slumps          |  | Symmetric waves  |



2. Laminated sediments

Laminated deposits characterize East Katla Ridge at depths shallower than 2000 meters on our northern transect, and to slightly deeper levels in the south. This type of deposit is also common on West Katla Ridge to a depth of approximately 2300 meters, where it is overlain to the south by the transparent sediment of South Katla Basin. The Myrdalsjokull Canyon Levee (the SE spur of West Katla Ridge) is also composed of laminated sediments. The sediments on the southern face of Myrdalsjokull Canyon Levee are characteristically molded into asymmetric sediment waves, which mantle a large section extending from the mouth of the canyon some 50 kilometers to the southeast. The laminated deposits are buried to the northeast by the multi-laminated channel deposits and to the southwest by the thinning wedge of transparent sediments observed in the South Katla Basin.

Minor surface erosion is observed commonly on the upper flanks of East Katla Ridge (Figure 3.13). The northern section shows considerable evidence for slumping as well as current erosion, and some surface irregularities (scarps) are clearly due to slumping. However, some surface erosion is due to the flow of the ISOC (Figure 3.11). Sediment waves and hyperbolae are not developed in these laminated sediments. This contrasts sharply with the sediments of the southern flank of East Katla Ridge, where deep incision and erosion has occurred, resulting in the overlapping hyperbolae of the 'dissected terrain'.

3. Acoustically impenetrable sediments

This type of deposit is observed in the deeper portions of the basin east of East Katla Ridge and within the axis of Myrdalsjokull Canyon. The basin deposits commonly have shallow channels crossing them, originating from canyons north of our survey area.

4. Multi-laminated sediments

The multi-laminated deposits are restricted to the axis of Myrdalsjokull Channel from the mouth of the canyon to a point approximately 40 kilometers downchannel. Tilting of the sediment interface (Figure 3.6a) and the absence of this sediment type to the east indicate that the flow responsible for deposition of this unit crosses the levee towards the south as indicated on the echo character map (Figure 3.13).

Asymmetric sediment waves

Asymmetric sediment waves are restricted to the south-facing slope of Myrdalsjokull Canyon Levee. Similar deposits are observed on the south-facing flank of a levee originating from Reynidsjup Canyon to the south. The waves attain maximum amplitude near  $61^{\circ}30'N$ ,  $18^{\circ}35'W$ , and decrease both towards West Katla Ridge and towards the basin to the east.

Symmetric sediment waves

This bedform is observed most frequently on the southern flank of East Katla Ridge immediately north of Myrdalsjokull Canyon near the canyon mouth. Surface morphology is complex in this region, and distinct sediment waves are observed to grade laterally into both 'vertically banded' deposits (inferred to be low-amplitude waves) and hyperbolae of the adjacent dissected terrain.

'Dissected terrain'

This type of deposit is restricted to three areas. Two lie in approximately 1500-1600 meters water depth on the southern ends of East and West Katla Ridges, and the third is a section on the west wall of Myrdalsjokull Canyon at 62°35'N.

These deposits may have formed from different processes. They are grouped together because they are all characterized by large-scale surface irregularities which are poorly resolved by the surface ship echosounder.

Small-scale surface roughness and hyperbolae

This echo type is restricted to an inferred slump scar on the east flank of East Katla Ridge over a depth range of approximately 1800 to 2100 meters.

Surface erosion

Evidence of surface erosion is observed over a large portion of the region in laminated deposits. Thinned surface units and outcropping reflectors are observed throughout the laminated deposits of our northern survey on East Katla Ridge from 1900 meters to the ridge crest (ca. 1200 meters). Similar features are common at depths shallower than 1500 meters along the East Katla Ridge crest and along the walls of Myrdalsjokull Canyon. Surface erosion is also observed on the south flank of West Katla Ridge.

C. Surface Sediment Lithology

Sediments were sampled at 26 sites in the Katla Ridge region during Atlantis II-94-1. Eleven of 12 piston cores and 10 of 14 box cores were

successful. Locations of core stations are tabulated and figured in Appendix I.

Sediment lithologies are discussed below in the context of the acoustic provinces outlined in the preceding section. Calcium carbonate content and sand content of piston cores are listed in Appendices III and IV, and are summarized in Figures 3.14 and 3.15.

Transparent sediments (Piston cores 4PC, 12PC; Box cores 9BC, 11BC, 12BC)

These deposits are calcareous muds containing 15 to 30%  $\text{CaCO}_3$  and 5 to 25 % sand-size grains ( $>63 \mu$ ). Color is variable, ranging from dark to very dark grayish brown (2.5Y3/2 to 4/2) in core 4PC to olive to olive gray (5Y4/2 to 4/4) in the remaining cores. Sediments are extensively mottled, and burrows are common throughout. The coarse fraction consists mainly of planktonic foraminifera (often small species and juvenile specimens) and brown shards of volcanic glass; the fine fraction consists of fine terrigenous material plus volcanic ash, calcareous nannofossils and clay. Sand layers are present in core 4PC. They are composed of volcanogenic rock fragments plus ash, and planktonic foraminifera are included in distinct laminae in the basal sections. Four layers from 3 to 14 centimeters thick have sharp basal contacts which are eroded but not visibly burrowed. These layers are inferred to be thin turbidites and are discussed in the following chapter.

FIGURE 3.14: Carbonate content of piston core sediments.  
Data plotted as % dry weight, by gasimetric analysis.

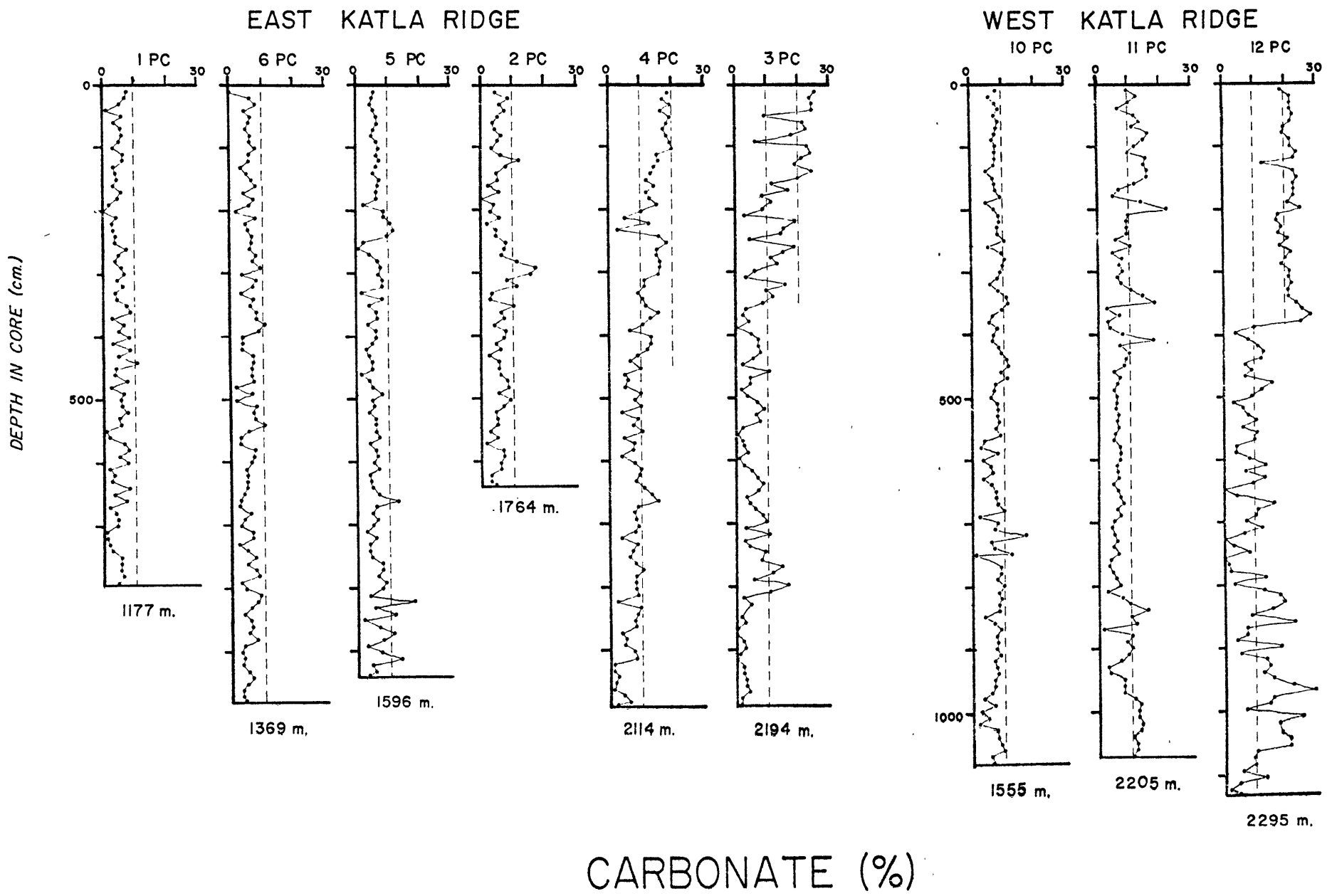
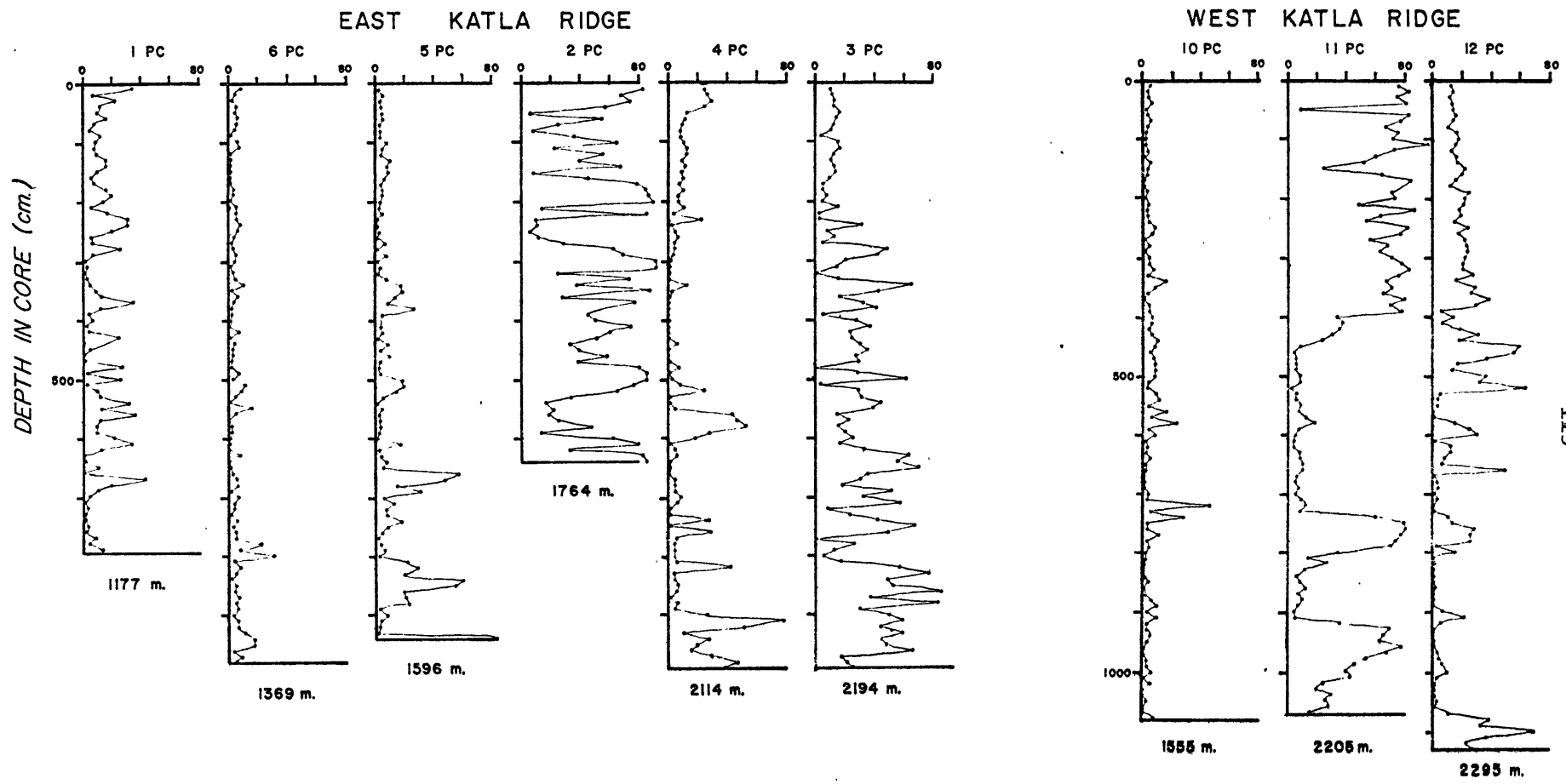


FIGURE 3.15: Sand-size component of piston core sediments.  
Data plotted as % dry weight sediment.



COARSE FRACTION (% > 63 microns)



Laminated sediments (Piston cores 1PC, 2PC, 5PC, 6PC, 11PC; Box cores 3BC, 4BC, 8BC).

Two different sediment types characterize the sediment/water interface in regions of acoustically laminated sediments. Box cores 3BC and 4BC (east flank, East Katla Ridge) each contain a surface layer of muddy sand approximately 1 cm. thick. This poorly sorted deposit contains a mixture of iron-stained rock fragments and planktonic foraminifera, both corroded and fresh, plus minor additional components in the coarse fraction. It is approximately 50% to 80% sand-size ( $>63\mu$ ). The remaining silt and clay-size material is composed mainly of terrigenous silt and clay, volcanic ash, and calcareous nannofossils, with minor biogenic siliceous components and small foraminifera. Benthic foraminifera are also found in the coarse fraction.

None of the piston cores from these regions contains a sand layer at the surface. Several gravity cores attached to the trigger weight, however, do contain a sand layer from less than 1 cm. to 4 cm. thick (gravity cores 1PG and 5PG, located on the east flank of East Katla Ridge, and 11PG on West Katla Ridge). The absence of the sand layer in piston cores 1PC, 5PC, and 11PC is almost certainly due to loss during the coring operation. The sand layers in these three gravity cores are similar to those described above.

Core 8BC (in the asymmetric sediment waves of Myrdalsjokull Canyon Levee) contains an irregular surface layer of sandy mud which contains similar components to the sand layers described above, but which contains only approximately 25% sand-sized grains. This is inferred to result

from bioturbation and downwards mixing of sand into the underlying mud. Core 13BC (east flank, East Katla Ridge, 1198 m.) recovered only a small unoriented surface sample of sandy mud similar to that observed in 8BC.

The second sediment type which is common in laminated deposits beneath the current axis is a 'detrital mud' containing 5 to 15% terrigenous sand, 0 to 5% volcanic ash and approximately 80% silt- and clay-sized terrigenous material. Carbonate is typically about 5% and is mostly planktonic foraminifera, with nannofossils rare or absent. Coarse sand and gravel-size grains are scattered through these deposits and are apparently ice-rafted material; occasional 'ash layers' of black sand (volcanic ash and rock fragments) are present. Induration has occurred in some sections, and the sediments vary in the way they break down when soaked in Calgon<sup>R</sup> plus distilled water for 24 hours. Some samples wet-sieved at 63 $\mu$  contain large percentages of clay clasts which may be an indication of the degree of lithification (dewatering).

The stratigraphy of the cored sediments is discussed in the following chapter. It is worth noting here, however, that the detrital muds are glacial Pleistocene deposits, and that the sand layers overlying them contain a mixture of both interglacial and glacial foraminifera, indicating they are formed both by winnowing of the underlying muds and by addition of younger sediment.

#### Acoustically impenetrable sediments (Piston cores 3PC, 9PC)

A single core (3PC) was obtained from the acoustically impenetrable sediments bordering the east flank of East Katla Ridge. This core contains a layer of calcareous mud from the surface to 350 cm, underlain by

detrital mud. Carbonate content exceeds 20% in the upper 150 cm, decreasing gradually to 10% at 350 cm. Values below this level are approximately 5%.

Four sand layers are observed between 85 and 210 cm in core 3PC. These turbidites are similar to those in core 4PC, and may in fact represent the same events in both cores. The similarity between the upper sedimentary section in 3PC and 4PC is somewhat surprising in light of the difference in the near-surface acoustic properties. The most striking difference between the two cores lies in the amount of sand-size material in the core below 200 cm. While core 4PC contains only a single layer at 500 to 600 cm containing indurated sand-sized fragments, the sediments recovered in core 3PC typically contain 30-60% sand-size components (mainly indurated detrital clay) throughout the section below 200 cm. This suggests that the higher reflectivity of the underlying sediments may result from induration, and that the thin surface layer of calcareous mud in core 3PC may be too thin to resolve with the surface ship 3.5 kHz echosounder.

The second sample of acoustically impenetrable sediments is from piston core 9PC in the axis of Myrdalsjokull Canyon. This core is composed almost exclusively of sand deposits, including both muddy graded units and relatively clean laminated units. Alternate layering of terrigenous and biogenic sands on various scales indicate that multiple sources, and perhaps different processes, are responsible for deposition of the canyon sands.

Sedimentary structures in these units are discussed in the following chapter. Detailed grain size and carbonate studies were not made on these deposits due to the obvious high degree of fine-scale variation. Two samples, one from a graded terrigenous sand layer and one from a laminated biogenic sand, both contain in excess of 60% sand-size material.

Multi-laminated sediments (Piston core 7PC; Box cores 6BC, 7BC, 10BC)

Sediments recovered from the acoustically multi-laminated deposits in the axis of Myrdalsjokull Channel are calcareous silty muds which are compositionally quite similar to the acoustically transparent sediments adjacent to the channel and to the south. Total carbonate exceeds 20% from the surface to 130 cm in gravity core 7PG (maximum depth of core; piston core did not trip properly) and in surface samples from the 3 box cores. Coarse fraction (  $>63\mu$  ) is quite low (5%) and consists principally of planktonic foraminifera and some large diatoms plus volcanic ash. The sediments are olive (5Y4/4) when wet, but dry quickly when exposed to air (as box cores were stored). Silt and sand are concentrated in both layers and lenses, the latter due to benthic organisms reworking the sediment.

Asymmetric waves (Box core 8BC)

This box core contains a sandy surface layer approximately 3 cm thick which contains irregular lenses of sand intermixed with the underlying detrital mud.

Dissected terrain (Piston core 10PC)

This single piston core from the dissected terrain atop West Katla Ridge contains detrital mud with sand and ash layers similar to those

described for the acoustically laminated deposits. Carbonate content is approximately 8%. Sand content ( $> 63 \mu$ ) is generally below 10% throughout the core, consisting mainly of terrigenous (volcanic) rock fragments (apparently ice-rafted) and planktonic foraminifera.

Small-scale surface roughness and hyperbolae (Box core 15 BC)

This core contains a 10 cm. surface layer of structureless muddy sand similar to the thinner sand deposits discussed above. Burrowing has mixed sand into the underlying detrital mud to at least 30 cm in discrete sand-filled holes.

D. Summary of Sediment Distribution

The following characteristics of sediment distribution patterns in the Katla Ridge region may be deduced from the 3.5 kHz echo character of surface deposits plus cored sediment samples:

1) Detrital clays composed of volcanogenic rock fragments, volcanic ash and clay-sized terrigenous material are the dominant lithology over most of the crest and flanks of East Katla Ridge to a water depth of at least 2000 meters. Carbonate content of these sediments is generally in the range 0-8%, and they contain 5 to 10% sand-sized terrigenous sand grains exclusive of lithified mud clasts. The sediments are identified in 3.5 kHz echo sounder profiles as acoustically laminated deposits with conformable subbottom reflectors. Varying degrees of induration are observed, and black, structureless sand layers 5 to 10 cm. thick composed of volcanic glass or basaltic rock fragments are present in some sections.

2) A thin surface layer of muddy sand (50 to 80% sand-size) is present in cores on the east flank and crest of East Katla Ridge between

1180 and 1800 meters water depth. A similar layer is observed in two cores from the southeast flank of West Katla Ridge. In all cases the sandy surface layer overlies the detrital clays discussed in (1) above.

3) The distribution of these two sediment types is similar to that of the regions where measured or inferred bottom flow consistently exceeds approximately 10 to 15 cm/sec.

4) Calcareous muds are observed in cores obtained where the echosounder shows an acoustically transparent surface layer. These deposits contain 15 to 30%  $\text{CaCO}_3$ , and are composed of terrigenous clay-sized material, volcanic glass, calcareous nanofossils, planktonic foraminifera, terrigenous sand/silt and siliceous microfossils, in decreasing order of abundance. Their distribution coincides with that of the eastern margin of the current where flow of 5 to 10 cm/sec is inferred.

5) Acoustically impenetrable sediments lying east of East Katla Ridge contains a surface unit of calcareous clay as described in 4) above. It is underlain by detrital clays containing abundant sand-size detrital clay clasts, suggesting that the acoustic properties may derive from partial induration of the near-surface deposits. Minor channelization in some areas (which were not sampled) suggests that sandy turbidites may be deposited in the central basin area from canyons on the Iceland margin northeast of the Katla Ridges.

6) Sediments in the axis of Myrdalsjokull Canyon are sands. At least two discrete types of deposit are observed: 1) muddy, graded units 10 to 120 cm thick, and 2) cleaner, extensively laminated deposits up to 20 cm thick.

7) Sediments in the axis of Myrdalsjokull Channel seaward of the canyon mouth are calcareous silts, similar in composition to the transparent sediments both adjacent to the channel and outside the fan region. Their 'multi-laminated' acoustic character does not appear to result from either compositional or marked size distribution properties, but rather is probably due to preservation of primary structures resulting from episodic deposition as discussed in the following chapter.

CHAPTER IV: SEDIMENTATION PROCESSES--OBSERVATIONS AND INTERPRETATION

A. Bottom Bedforms: Photographic Evidence

Oblique near-bottom photographs were taken with a pogo camera at 9 stations (Appendix I). Although problems with the film advance severely limited the number of pictures we obtained, we did gain some insight into small-scale surface characteristics in several provinces, including the east flank of East Katla Ridge both within and outside the current-swept region, Myrdalsjokull Canyon axis, Myrdalsjokull Channel, and the incised saddle of West Katla Ridge.

East Katla Ridge, current regime: All photographs from 1194 meters (camera station 3) and 1732 meter (camera station 9) show clear evidence of current shaping of the sediment interface (Figures 4.1, 4.2). Photographs from 1194 meters show a muddy current lineated bottom with abundant pelagic and benthic organisms (including sponges, starfish, fish, worm tubes, and burrow holes and mounds). There is good agreement between the measured current direction ( $282^{\circ}$ ) and the flow direction inferred from surface scouring and bending of benthic organisms in the flow. Occasional large erratic boulders and gravel are visible, often coated with attached organisms. The bottom is clearly visible, and, interestingly, no mud clouds raised by the camera trigger weight are visible. The bottom is thus inferred to be quite compact (which may be responsible for the poor penetration of box cores at sites high on the ridge).



FIGURE 4.1: Bottom photograph, East Katla Ridge crest (camera station 3). Muddy bottom with abundant infauna and evidence of west-flowing currents is characteristic of this province.

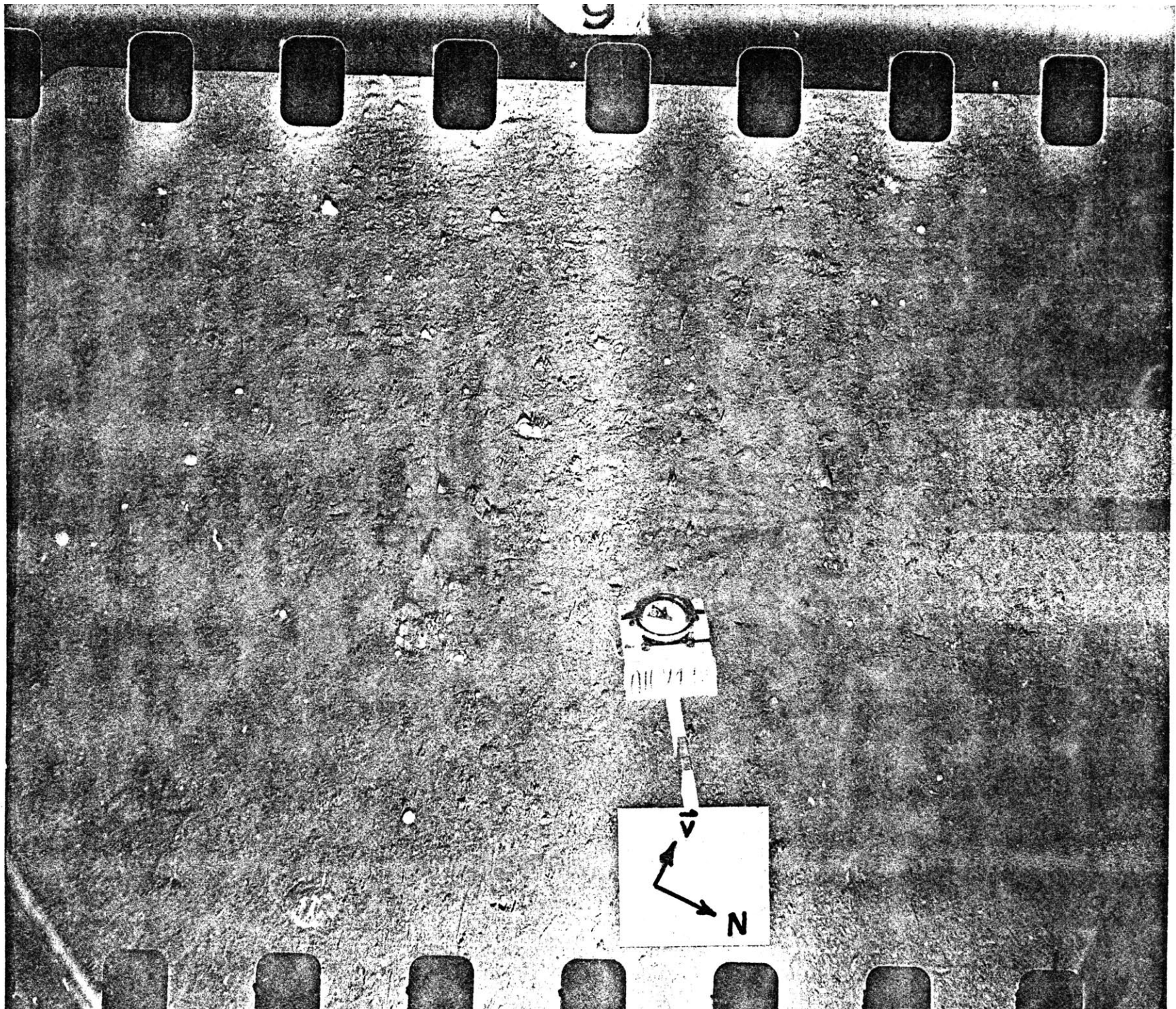
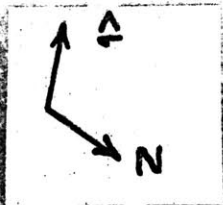


FIGURE 4.2: Bottom photograph, East Katla Ridge current axis (camera station 9). Sand and gravel on the sediment/water interface is characteristic of this province. Subtle bedforms transverse to the measured flow direction may be observed. Infaunal activity is less pronounced than at stations both higher and lower on the ridge flank.



-127-



9

At 1732 meters, where current meters show the strongest flow, photographs show that the bottom is a coarse sand/gravel pavement with bedforms developed transverse to the current direction. A mud cloud in one frame shows southwesterly flow (from a previous camera bounce), which agrees well with the measured flow at adjacent current meters 2 (1600 meters) and 5 (1796 meters). Benthic organisms are rare, with only epifauna (starfish, attached sponges) identified.

East Katla Ridge, downslope from current axis: Three stations (#6, 7, and 8) were occupied on the flank of East Katla Ridge east of the principal region of strong current flow. All three of these stations show a muddy sediment interface littered with fecal coils, tracks, mounds and pits (Figure 4.3). Current directions cannot be determined, as little evidence of flow is indicated. Large mud clouds commonly obscure part of the frame, and at camera station 8 only 4 of 13 photos show the bottom at all. Part of the cloudiness of the water may be due to suspended sediments, although mud clouds from multiple camera hits in a small area are a more likely cause.

Myrdalsjokull Canyon axis: Only a single photograph was obtained in the narrow, incised portion of Myrdalsjokull Canyon. The bottom is dominated by a large block of sedimentary rock, apparently slumped from the adjacent wall, with smaller sedimentary clasts scattered on the adjacent sediment surface. Attached epifauna are common. A large mud cloud obscures much of the sediment interface, suggesting that the bottom is loosely consolidated. No surface structures, either primary or biogenic, are observed in the coarse surface layer.

FIGURE 4.3: Bottom photograph, East Katla Ridge lower east flank. Photographs from the region east of the measured current axis show a soft muddy bottom with abundant evidence of infaunal activity (mounds, pits) and little evidence of current flow.





Myrdalsjokull Channel: Photographs obtained from the channel region show a soft muddy bottom with evidence of current flow and burrowing (Figure 4.4). Mud clouds are common, and obscure the bottom in many frames. Sediments are commonly molded into lag deposits behind burrow mounds, and show northwards flow at the time of observation.

West Katla Ridge: Photographs from the 'dissected terrain' on the nose of West Katla Ridge show a hard, winnowed bottom with coarse clasts and scour indicating westward-flowing currents. Epifauna (brittle stars, starfish) are abundant; infaunal activity appears limited by the hard substrate.

#### B. Stratigraphy: Recognition of Holocene Deposits

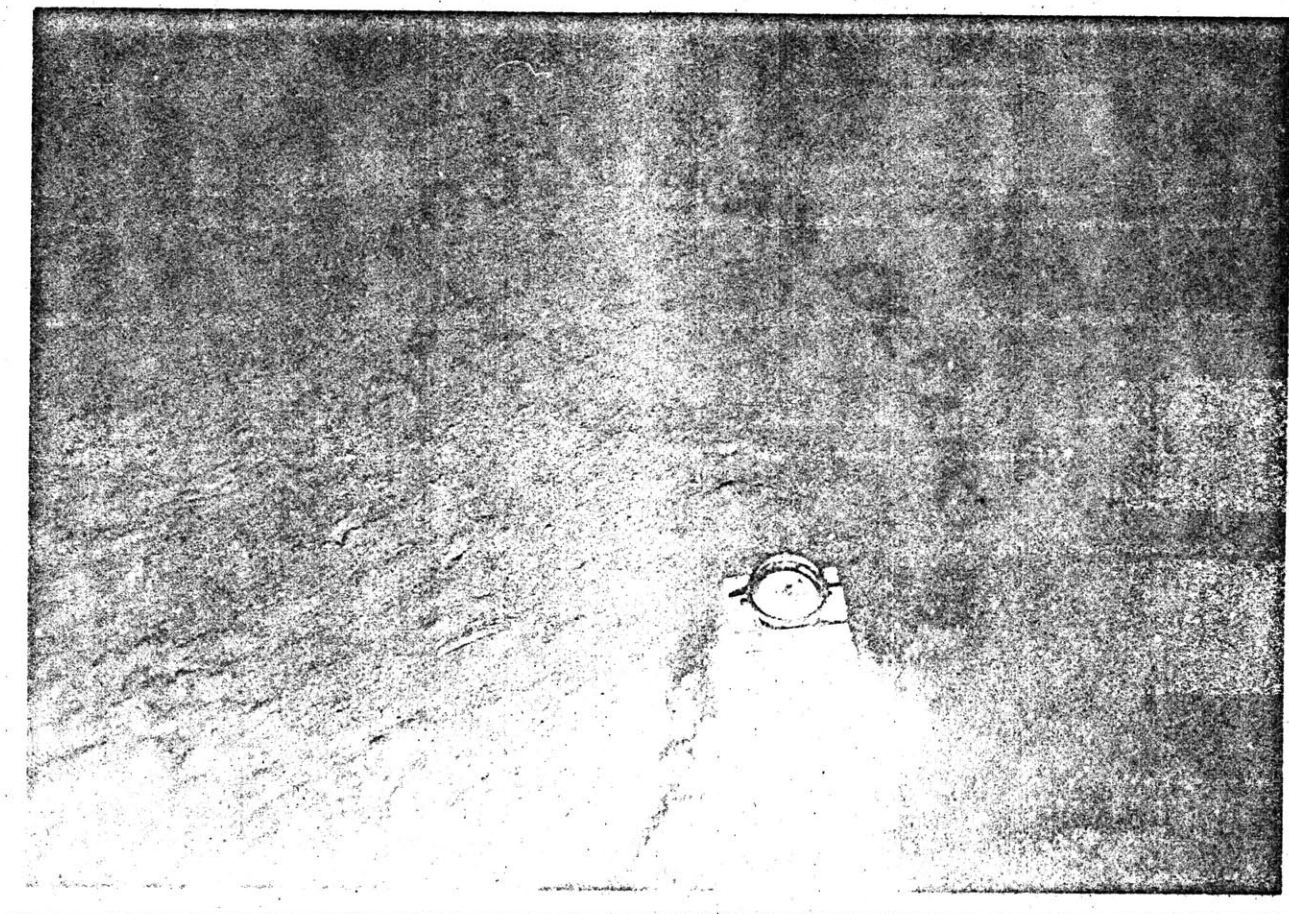
The principal criterion used for recognizing Holocene\* sediments is certain assemblages of planktonic foraminifera (Kipp, 1976). Post-glacial deposits contain a diverse subpolar faunal assemblage dominated by Globigerina bulloides, Globigerina pachyderma (d), and lesser numbers of Globigerina quinqueloba, Globorotalia inflata and Globorotalia scitula. The polar assemblage observed in older glacial deposits is dominated by G. pachyderma (s) with only minor accessory species, usually G. bulloides and G. quinqueloba. G. pachyderma (s) is rarely encountered in post-glacial sediments, and percentage of this morphotype of the total planktonic foraminifera ( $>149\mu$ ) is an excellent means of discriminating Holocene from pre-Holocene deposits at high latitudes.

---

\*The term "Holocene" as used here is synonymous with 'post-glacial', and is inferred to have begun at approximately 13,000 B.P. in this section of the North Atlantic ('Faunal Termination I' of Ruddiman & McIntyre, 1973; Ruddiman & Glover, 1975; Ruddiman and Bowles, 1976).



FIGURE 4.4: Bottom photograph, Myrdalsjokull Channel. Photographs within the channel show a muddy bottom with evidence of northward-flowing currents and only minor evidence of infaunal burrowing.



-133-



Detailed foraminiferal counts were made of two piston cores (4PC, 3PC) on the lower flank of East Katla Ridge which were determined to contain significant accumulations of Holocene sediment. Percentages of G. pachyderma (s) within these cores are illustrated in Figure 4.5. Both cores contain a uniformly low abundance of G. pachyderma (s) in the upper few meters of the core (310 cm. in 4 PC; 230 cm. in 3PC). This unit is underlain in core 4PC by 90 cm. of alternating polar and mixed fauna which is inferred to represent the Younger Dryas cooling event discussed by Ruddiman et al. (1977). A similar cold event in core 3PC is similarly interpreted, although it does not contain the marked fluctuations evident in 4PC. The base of the Holocene section (Termination I, as recognized by Ruddiman and Bowles, 1976) is interpreted to lie at a depth of 450 cm. in core 4PC and 310 cm. in core 3PC.

The stratigraphy of core 12PC (transparent sediments, South Katla Basin) was based on examination of a coarser fraction of the sediment (>250 $\mu$ ), and counts of right-left-coiling G. pachyderma (d+s) were made without discriminating. This shows a quite similar pattern to the two cores above, with low abundance of G. pachyderma from the surface to 370 cm., a short section of slightly higher abundance of G. pachyderma underlain by a single sample with low abundance and then uniformly high values below (Figure 4.6). Termination I is inferred to lie at 425 cm. in this core.

Detailed examination of piston core 1 PC (laminated sediments, crest of East Katla Ridge at 1177 m) shows a clearly polar fauna below 20 cm. (Figure 4.6). Termination I is inferred to lie between 10 and 20 cm.,

FIGURE 4.5: Stratigraphy of cores 3PC, 4PC.

- a. Percentage of left-coiling Globigerina pachyderma (s) in the  $>149\mu$  size fraction of core 3PC. Low abundance indicates subpolar surface waters; high abundance indicates polar (cold) surface waters. The Younger Dryas event discussed by Ruddiman et al (1977) is inferred for the interval 235 to 295 cm.; Termination I (base of Holocene) lies at approximately 310 cm.
- b. Percentage of left-coiling G. pachyderma in core 4PC. Younger Dryas event is inferred to occur at 315 to 405 cm.; Termination I lies at 455 cm. Radiocarbon dates (Table 4.1) are indicated on the right margin.
- c. Silicic bubble-wall shards of clear volcanic ash (Ruddiman and Glover, 1972) plotted as percentage of coarse ( $>63\mu$ ) fraction. Grain counts were by visual estimation. Vertical scale same as for a, b.
- d. Silicic bubble-wall shards plotted as percentage of total sediment dry weight. Note broad low peak centered at 280 cm. lying well above visible ash layer, which could represent maximum of ice-rafted component discussed by Ruddiman and Glover (1972).
- e. Age determinations in core 4PC plotted against depth in the core. Dots are radiocarbon dates by Geochron Laboratories (Table 4.1) relative to the Libby half-life of 5570 years. Star is Termination I, with age estimated as 13,000 years b.p. by Ruddiman and Bowles (1976). Vertical bars are Ash Layer 1 (Ruddiman and Glover, 1972; 1975) which has an age of approximately 9300 years b.p., and the Younger Dryas cooling event (Ruddiman et al, 1977) with an estimated age of 10,200 years b.p. Accumulation rates based on these age estimates are:

13,000 to 24,000 years b.p.: 36.0 cm/1000 yrs.  
Present to 13000 years b.p.: 35.0 cm/1000 yrs.  
to 74.5 cm/1000 yrs.

The higher accumulation rate assumes the radiocarbon date at 10 to 20 cm. of 5910 yrs. The inferred ages of Ash Layer 1 and the Younger Dryas event are more consistent with the lower accumulation rate for Holocene deposition, which assumes that the core top has an age of 0 years.

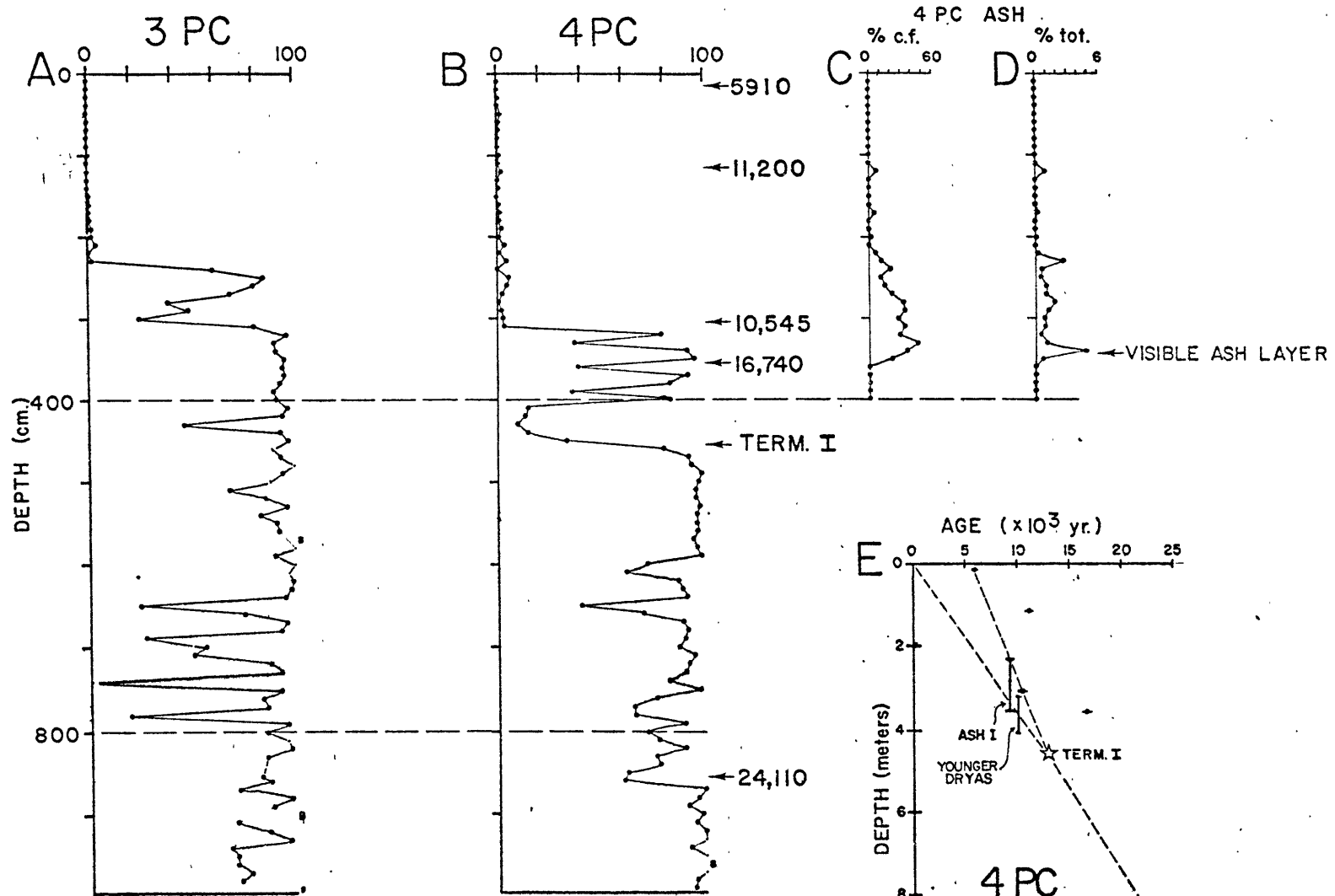
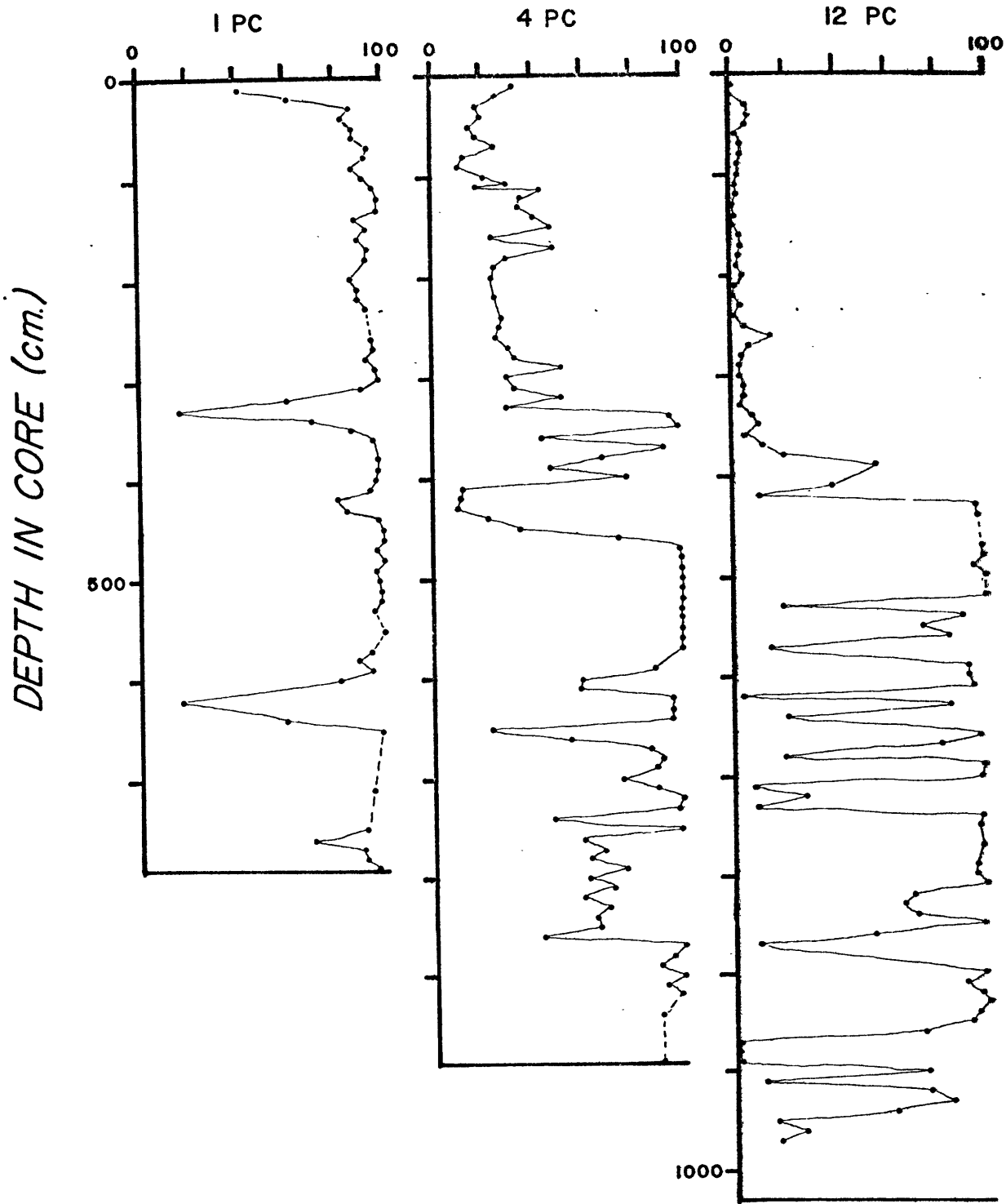


FIGURE 4.6: Globigerina pachyderma abundance in cores 1PC, 4PC, and 12 PC. Total species abundance in the  $>250\mu$  size fraction is plotted. See text for discussion.

### % G. PACHYDERMA (d+s; >250 $\mu$ )



although the high percentage of G. pachyderma at both 10 and 20 cm suggest that bioturbation has mixed glacial and post-glacial sediments at this site.

Faunal counts were not made for the remaining piston cores. Examination of foraminifera in piston cores 6, 2, and 5 PC on the east flank of East Katla Ridge showed polar faunal assemblages in all cores at and below 10 cm. This is true of cores 10 PC and 11 PC on West Katla Ridge as well.

Faunal investigations were not carried out for piston cores 8 PC and 9 PC, both of which contain sandy turbidite sequences originating in Myrdalsjokull Canyon. It was felt that multiple sediment sources from various stratigraphic levels within the canyon would render such an analysis useless. Core 7 PC, located in the Myrdalsjokull Channel axis, failed to trip properly, and the entire core is flow-in. The associated gravity core (7 PG) contains a subpolar faunal assemblage throughout its entire 130 cm. This is true as well for box core samples 6 BC, 7 BC and 10 BC in the acoustically multi-laminated channel deposits and the adjacent cores 9 BC, 11 BC and 12 BC in acoustically transparent deposits bordering the channel.

Box core samples 3BC and 4BC, located beneath the axis of the ISOC on the east flank of East Katla Ridge, contain polar fauna in the detrital muds which are overlain by a thin veneer of sand containing 13 to 15% G. pachyderma(s) (Holocene assemblage with evidence of incorporated reworked pre-Holocene polar material). A similar distribution is observed on the east flank in the region of small-scale hyperbolae (core 15BC) with



Holocene foraminifera in the sand layer overlying pre-Holocene muds. However, a sample of mud at 20 cm contains a subpolar assemblage, and suggests that at least 10 cm of Holocene (?) mud underlies the thick sand layer at this site. It is possible, however, that the subpolar fauna at this site represent a previous interglacial period exposed by slumping. Core 8BC (sediment wave province on Myrdalsjokull Canyon Levee) contains a mixed assemblage (25% G. pachyderma(s)) at the surface; sediments at 19 cm contain a polar assemblage.

#### Radiocarbon dates

Five radiocarbon dates were obtained from Geochron Laboratories on bulk sediment samples in core 4PC (Table 4.1; Figure 4.5). These dates confirm our interpretation that the upper 4.5 meters of sediment in this core is Holocene, although in at least two samples ages appear to be artificially high. This is apparently due to the addition of older carbonate, most likely nannofossils, which are readily transported by bottom currents.

The apparent age of 24110 (+ 1820; - 1480) radiocarbon years (Libby half-life of 5570 yrs.) at 855 cm provides confirmation of the rapid accumulation of sediments on the east flank of lower East Katla Ridge. It is assumed that this is a maximum age estimate, since bioturbation is not likely to admix large amounts of younger sediments deeper than 10 to 20 cm, (equivalent to less than 1000 years) and bottom current transport may add significant amounts of older ( $^{14}\text{C}$ -free) carbonate.

One additional stratigraphic indicator observed in cores 4PC, 3PC and 12PC is a disseminated volcanic ash layer of clear silicic bubble-wall

TABLE 4.1: Radiocarbon Dates, Core 4 PC

<u>Depth in Core (cm)</u>	<u>Age (Radiocarbon Years)</u>
10- 20	5,910 $\pm$ 195
110-120	11,200 $\pm$ 360
300-310	10,545 $\pm$ 310
350-360	16,740 $\pm$ 460
850-860	24,110 (+ 1820; - 1480)

shards (Ruddiman and Glover, 1972). The distribution of these grains are plotted in Figure 4.5 for core 4PC as both % dry weight sediment and as % coarse fraction ( $>63 \mu$ ). It is difficult to assign a precise age to the level of the ash in our cores as has been done by Ruddiman and Glover (1972; 1975) because 1) the samples show ash is spread over more than 130 cm, and 2) we observe a visible layer of the ash at 340 cm. This is the first known occurrence of this ash as a nearly-pure layer. The distribution of silicic bubble-wall shards throughout the upper portion and above deposits inferred to be of Younger Dryas age (Ruddiman et al., 1977) supports the interpretation of Ruddiman and Glover (1972) that the ash is primarily introduced via ice-rafting. The visible ash horizon at 340 cm lies within the interval of colder foraminifera assemblages which is inferred to represent the Younger Dryas event, and may eventually allow a better definition of the age of the volcanic event which produced this unique deposit.

#### C. Accumulation rates of Holocene sediments

Accumulation rates of Holocene deposits are inferred from a combination of faunal stratigraphy in piston cores and 3.5 kHz echo character. Significant thicknesses of Holocene accumulation are indicated for three of the four acoustic units discussed in Chapter 3 (transparent sediments, multi-laminated sediments, and at least some portions of acoustically impenetrable sediments).

##### Transparent sediments

The acoustically transparent surface layer is inferred to consist of Holocene calcareous muds throughout the study area. Piston cores 12PC

(South Katla Basin) and 4PC (East Katla Ridge) each contain a transition from subpolar (Holocene) planktonic foraminifera assemblages above to polar assemblages (glacial Pleistocene) below which approximately corresponds to the base of the transparent layer (Figure 3.3c). In core 4PC this transition occurs at 460 cm; at 12PC it lies at 430 cm, indicating accumulation rates in excess of 30 cm/1000 years at both sites (Figure 4.5)

Box cores recovered from acoustically transparent deposits on the Myrdalsjokull Suprafan contain Holocene faunal assemblages throughout (60-70 cm), providing minimum accumulation rates of approximately 5 cm/1000 yr, although actual rates are inferred to be much higher.

Although one cannot be certain that the transparent layer is strictly Holocene in age, the dramatic climatic changes at this high latitude and the resulting impact on deep-sea sedimentation support this hypothesis, which is based mainly on the apparent correlation between the thickness of Holocene deposits in cores 4 PC and 12 PC with the thickness of acoustically transparent sediments at the core sites where those deposits are quite thin . Holocene accumulation rates in the center of South Katla Basin are inferred to have exceeded 100 cm/1000 years based on the much thicker transparent layer observed there (e.g. Figure 3.3a).

#### Laminated deposits

Accumulation rates in sediments recovered from acoustically laminated sediments are everywhere less than 1 cm per 1000 years. In most cases erosion is inferred; only one core (1 PC) contains (possibly) Holocene muds (<20 cm), while the remainder contain pre-Holocene muds which are

in some cases overlain by a 1 to 4 cm. thick sand layer (1 to 3 mm per 1000 yr. accumulation rate). The sand contains significant amounts of reworked glacial Pleistocene detritus; in most cases an erosional hiatus may be inferred between the sand and underlying mud.

#### Acoustically impenetrable sediments

These deposits may display considerable variability. A sample (3 PC) near the current margin shows accumulation of 310 cm of post-glacial sediments which are quite similar to those recovered at core 4 PC (transparent sediments) immediately upslope. A decrease in accumulation rate of current-derived mud is expected in the deeper sections of the basin adjacent to the east flank. However, turbidity currents from the canyons incised in the Iceland margin north of the survey area apparently travel down the basin via distributary channels, and have probably been active during the Holocene. Thus, no accurate estimate may be made of Holocene accumulation rates in the basin region.

Accumulation rates in Myrdalsjokull Canyon are expected to be highly variable due to local erosion and deposition by turbidity currents.

#### Multi-laminated channel deposits

Deposits in the axis of Myrdalsjokull Channel overlie transparent sediments along the channel margin which are Holocene age. We infer that all of the multi-laminated sediments are Holocene. They vary considerably in thickness, exceeding 40 meters in most channel crossings (e.g. Figure 3.6b,c), which corresponds to local accumulation of 300 cm per 1000 years or more.

Other acoustic units

Deposition in the asymmetric wave province (8 BC), the dissected terrain on West Katla Ridge (10 PC) and the small-scale hyperbolae on East Katla Ridge (15 BC) all occur at low rates (<2 cm per 1000 years). Minor deposition of Holocene mud may have occurred in 8 BC and 15 BC (approximately 10 cm) prior to formation of the surface sand layers at both sites. No Holocene sand or mud is observed at or below 10 cm in core 10 PC.

D. Primary Sedimentary Structures

Parallel laminations, cross-laminations and graded bedding are the most frequently observed primary sedimentary structures observed in sediments in the East Katla Ridge region. These structures, restricted to sand and silt deposits, are most common in the vicinity of Myrdalsjokull Canyon and Channel, although a few examples are observed from the east flank of East Katla ridge.

Graded sand layers which are interpreted as turbidite deposits are encountered most frequently in the axis of Myrdalsjokull Canyon (9 PC) where at least fifteen discrete graded layers are recognized in six meters of core. The units are typically 5 to 30 cm. thick, with the thickest unit lying at the top of the core (in excess of 100 cm.). They characteristically have sharp basal contacts (sometimes obviously erosional) and tend to grade from coarse sands at the base to silts or fine sands near the tops. Some units contain larger clasts, both partially lithified mud clasts and larger gravel sized rock fragments, which are generally restricted to the base of the units. The sediments consist

of both terrigenous sand containing abundant ash and rock fragments, plus biogenic sand containing planktonic foraminifera and pteropods. The sediment is believed to originate primarily from the shelf and slope of southern Iceland, although slumping of sediments from the adjacent canyon walls and erosion of surface deposits may also contribute as potential source areas.

The upper contact of the turbidites is often difficult to distinguish both on visual examination and with x-radiographs. Alternating laminae of terrigenous and pelagic sand are commonly developed above the turbidite units. We interpret these deposits as being winnowed turbidites, reworked by bottom currents. This interpretation is based in part on the extreme abundance of pteropods which are normally rare pelagic planktonic organisms in North Atlantic sediments: they comprise less than 1% of the deposits on the flanks of East Katla Ridge. Their abundance in the canyon deposits suggests either extremely high local productivity in the waters overlying the canyon or, more likely, the removal of all other fine material from the cored sections by current activity. Pteropods are among the largest of the planktonic organisms encountered in the Katla Ridge region, typically ranging in size from 1 to 3 mm in diameter (and occasionally exceeding 1 cm.). The principal additional components of the sediments between discrete turbidite units are generally coarse terrigenous sand and large planktonic foraminifera. This suggests that these sand layers result from episodic current winnowing of all fine sediments up to at least medium sand size from the axis of Myrdaalsjokull Canyon.

Graded sand layers are also observed at a core (8 PC) seaward of the mouth of Myrdalsjökull Canyon, above outcropping reflectors along the south side of the channel. Distinct graded layers are observed in the upper 2.5 m of this core, immediately overlying calcareous mud. The graded layers are of various thickness, with the uppermost consisting of approximately 30 cm. of terrigenous sand and the second consisting of over one meter of primarily volcanigenic sediments, with terrigenous sand and mud clasts in the upper two-thirds of the unit. The calcareous mud immediately underlying the turbidites contains a subpolar planktonic foraminifera assemblage, suggesting that the turbidites are of Holocene age.

The only other graded units observed in Holocene units are found in the east flank of east Katla Ridge, interbedded with the muddy contourite deposits. Four sand layers in core 4 PC and four similar layers in core 3 PC are composed dominantly of volcanic glass and basaltic rock fragments. Laminations are clearly present in the lower two-thirds of one unit (Figure 4.7), but are absent in the upper portion. Laminations are composed of alternations of thin layers of planktonic foraminifera and volcanic sand. There is a sharp, irregular basal interface, and laminae also terminate against the scoured interface, showing that this structure is not due to core deformation. Although sedimentary structures within these turbidites are not always visible on visual examination, parallel lamination and occasional cross-bedding is present in x-radiographs (Figure 4.7). Cross-bedding direction determined from paleomagnetic declination is consistent with downslope flow rather than along-slope or upslope flow (Appendix V).



FIGURE 4.7: X-radiographs of turbidite sand layers, east flank of East Katla Ridge. Figures actual size.

a. Sand layer from 226 to 236 cm. in core 4PC, illustrating sharp erosional lower contact, laminations in basal layer, and uniform upper layer. Note absence of bioturbation of lower contact.

b. Sand layer from 152 to 155 cm. in core 4PC, illustrating cross-lamination. Current direction inferred from cross-laminae is consistent with downslope flow direction (Appendix V).



A



B

Sedimentary structures are also developed in the silty channel sediments from the axis of Myrdalsjokull Channel (seaward of the canyon mouth). These laminations are parallel to the sediment interface, and no cross-laminations were observed (Figures 4.8, 4.9). It proved impossible to determine current directions from oriented box cores because of the absence of directional indicators in the sedimentary structures. Parallel laminations tend to occur in clusters separated by 10 to 20 cm. or more of relatively structureless sediment. Individual laminae are generally less than a few mm thick. We infer that these laminated deposits are silty turbidites emanating from the mouth of Myrdalsjokull Canyon, primarily on the basis of their distribution. The origin of the homogeneous deposits intercalated with the laminated deposits is not entirely clear as all of the sediments recovered from the channel axis are composed of calcareous muddy silts, and there is no clear compositional difference between sediments with and without laminae.

Cross-bedding is observed at two locations in the survey area. The first is within turbidite deposits on the east flank of East Katla Ridge, mentioned above, where downslope-facing cross-bedding may be used in the interpretation of these as turbidites. The second location in which cross-bedding is apparent is in "sandy contourites" observed at the tops of graded turbidite sequences in Myrdalsjokull Canyon. As discussed in following sections, the tops of turbidites merge into laminated deposits which we have interpreted as contourite sands. These units are commonly cross-bedded at various orientations. Examples (x-radiographs of these units) are illustrated in Figure 4.10. Directionality was not determined

FIGURE 4.8: Photograph of face of core 10BC (multi-laminated channel sediments).

AII-94

BC 10

↑ TOP ↑

UPPER

0 cm  
5 cm  
10 cm  
15 cm  
20 cm  
25 cm  
30 cm  
35 cm

f/16 1/2 sec

FIGURE 4.9: X-radiograph of core 10BC (multi-laminated channel sediments) showing deep burrows and silt laminae.

10 BC

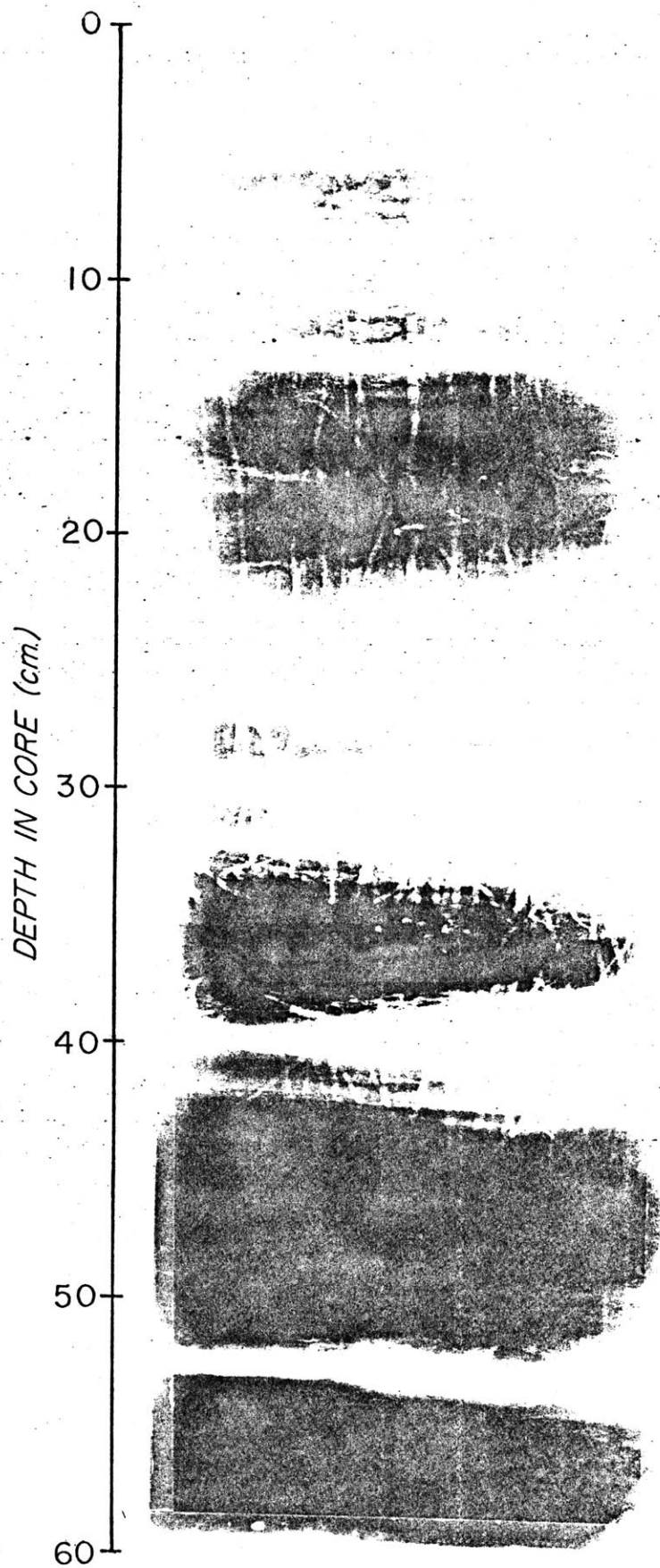
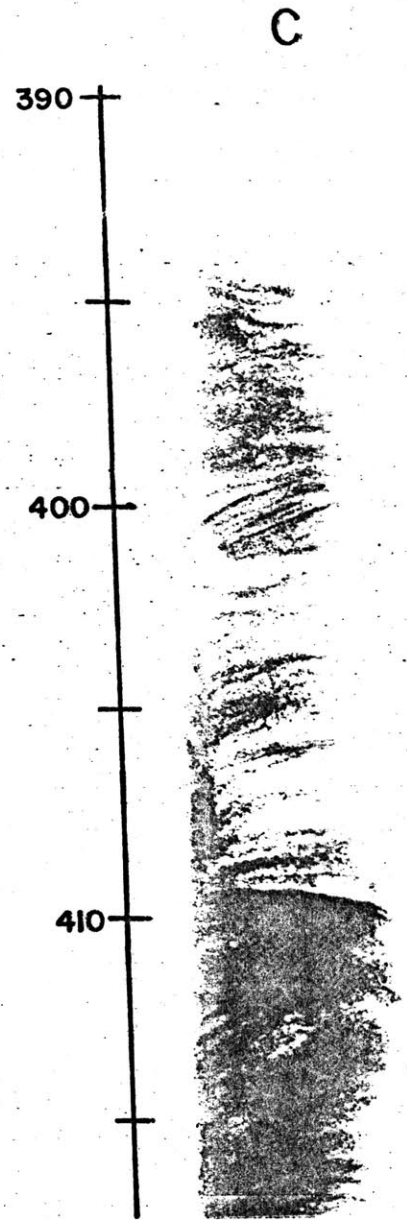
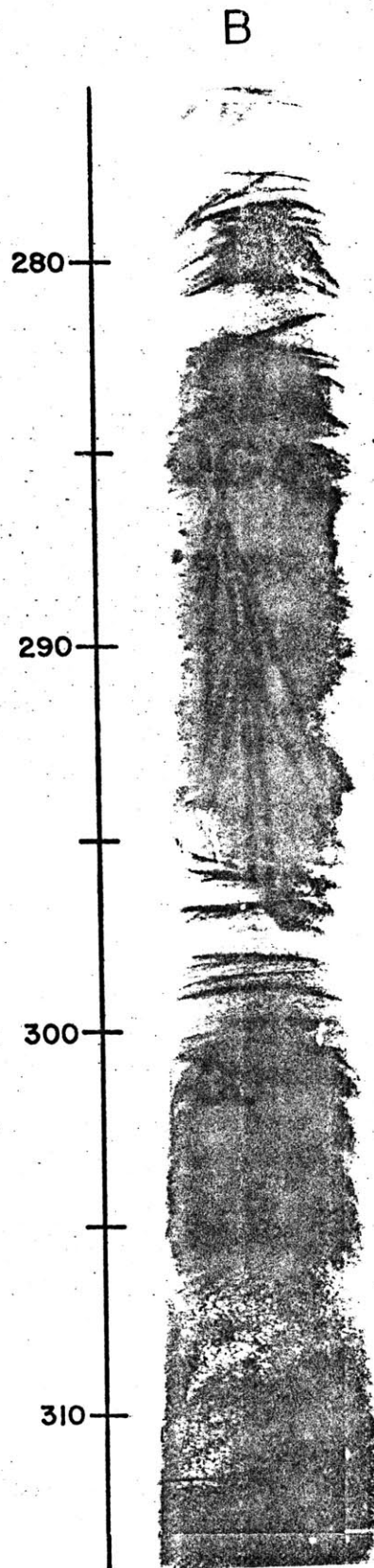
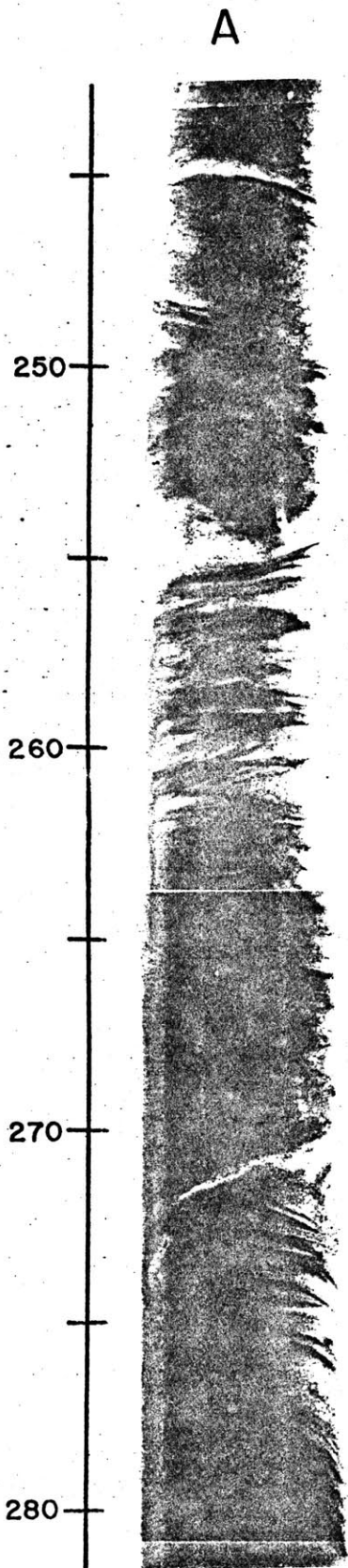


FIGURE 4.10: X-radiograph of core 9PC, showing cross-laminated sands from Myrdalsjokull Canyon axis.



9 PC



for these units because a) they have various orientations as seen in Figure 4.10, and b) the current direction inferred in the axis is both to the north and to the south under M2 tide control. Hence, paleomagnetic orientation would not be likely to yield useful information about flow direction. Laminae are composed of both layers of pteropods and terrigenous sediments. The separation of coarse pteropods into discrete layers suggests that at least occasionally the currents in the canyon attain velocities sufficient for erosion of material in the medium to coarse sand size range.

#### E. Bioturbation

Sediment reworking by benthic organisms, commonly referred to as bioturbation, is clearly seen in split core sections and radiographs. It is extremely common in the muddy deposits on the east flank of east Katla Ridge and in the transparent sediments to the south. This highly productive region apparently supports a host of burrowing animals. Bioturbation is also commonly observed in both channel and channel flank deposits southeast of Myrdalsjokull Canyon. The net result of the activity of benthic infauna on the deposits of muddy contourites has been to erase any primary structures which may have originally been present. The intense reworking of the transparent sediments in the southern section both adjacent to the channel and to the south in the cul-de-sac basin may be largely responsible for the complete absence of current laminations in these sediments.

Several distinct types of infaunal burrowing activity are observed in various portions of the region. Discrete benthic organisms appear to

have adapted to various sedimentary regimes, and these different organisms vary in their ability to disrupt the laminations in the silt and sand layers.

Examples of burrowing activity are illustrated for the transparent sediments immediately adjacent to the Myrdalsjokull Channel (Figures 4.11, 4.12). These silty muds have clearly been highly reworked on numerous occasions by organisms of various sizes. Large (up to one cm. diameter) round burrow traces are observed in box cores (9 BC, 11 BC, and 12 BC; Figures 4.11, 4.12, 4.13). These may be due to gastropods whose shells are observed both in x-ray (Figure 4.12) and as whole specimens recovered from these cores .

A markedly different type of burrowing organism is responsible for vertical and near-vertical branching burrows observed in box cores from the channel axis (Figure 4.9). These burrows, rarely larger than 3 to 4 mm. diameter, extend as much as 40 cm. from the sediment interface downward. They commonly branch upwards, and they appear to result from burrowing activity of tiny pelecypods found in cores 6 BC, 7 BC, and 10 BC. These extremely long burrows are ample evidence of the extent to which sediments may be remobilized by benthic infauna. However, it is noteworthy that the channel sediments have not lost their laminae because of the activity of this type of benthic reworking. It seems likely that the organisms present in the channel sediments are specifically adapted to live in regions in which episodic deposition and erosion may occur, and that the deep burrows may serve more for protection than for searching for food, since only a small percentage of the sediment has been remobilized by their activity.

FIGURE 4.11: X-radiograph of core 9BC, showing bioturbation effects in the transparent sediments adjacent to Myrdalsjokull Channel.

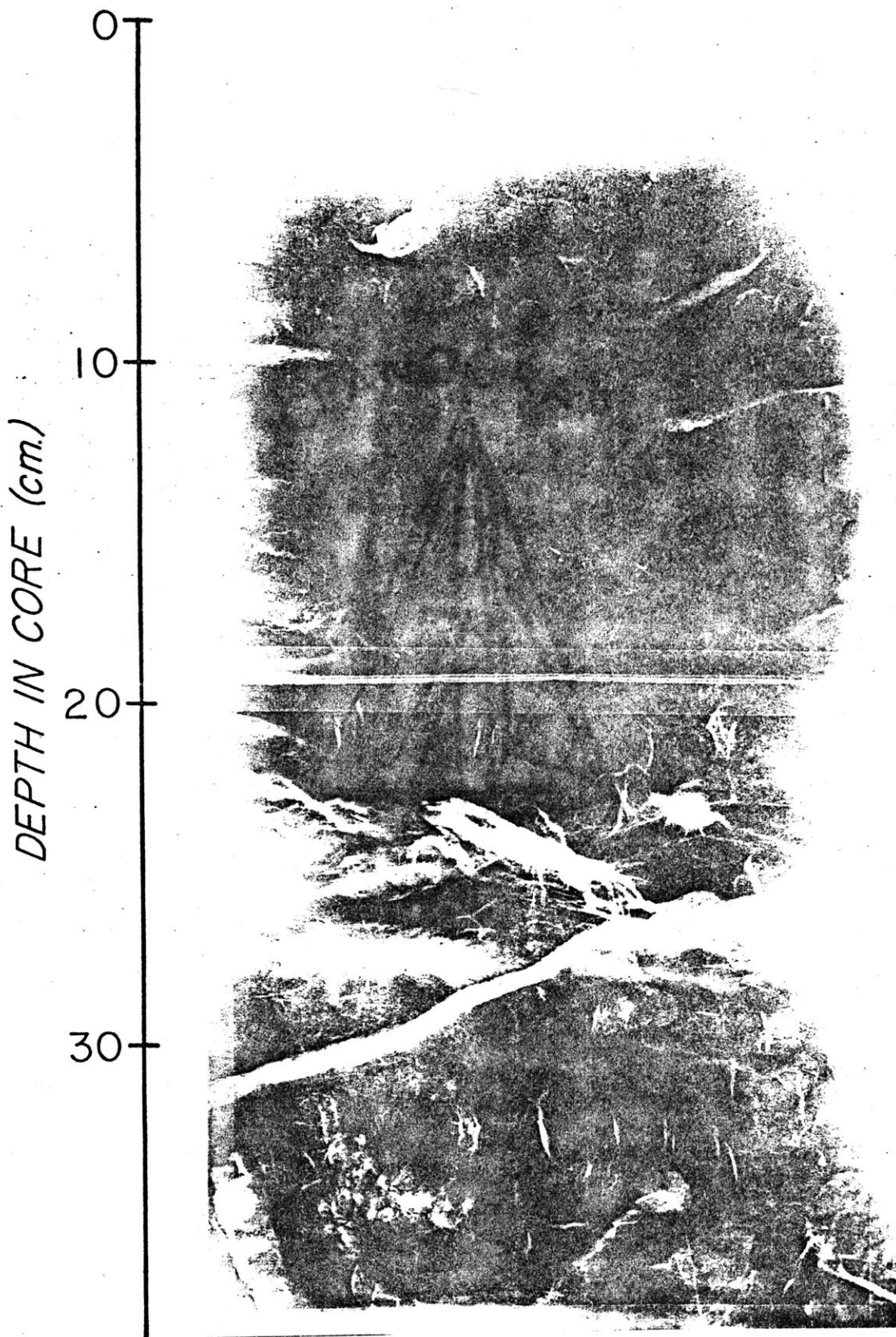


FIGURE 4.12: X-radiograph of core 11BC, showing bioturbation effects in transparent sediments adjacent to Myrdalsjokull Channel.

# II BC

DEPTH IN CORE (cm.)

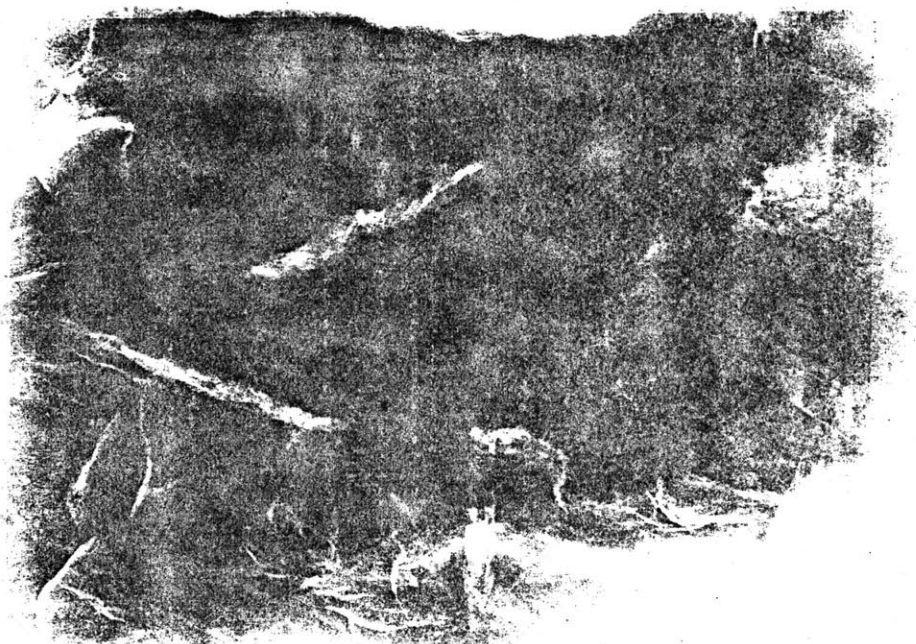
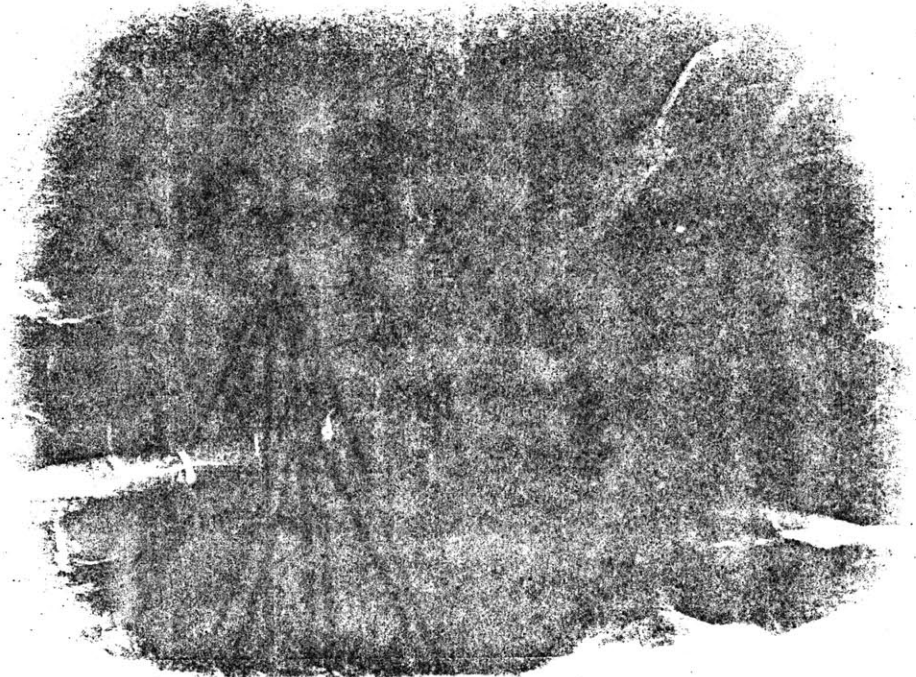


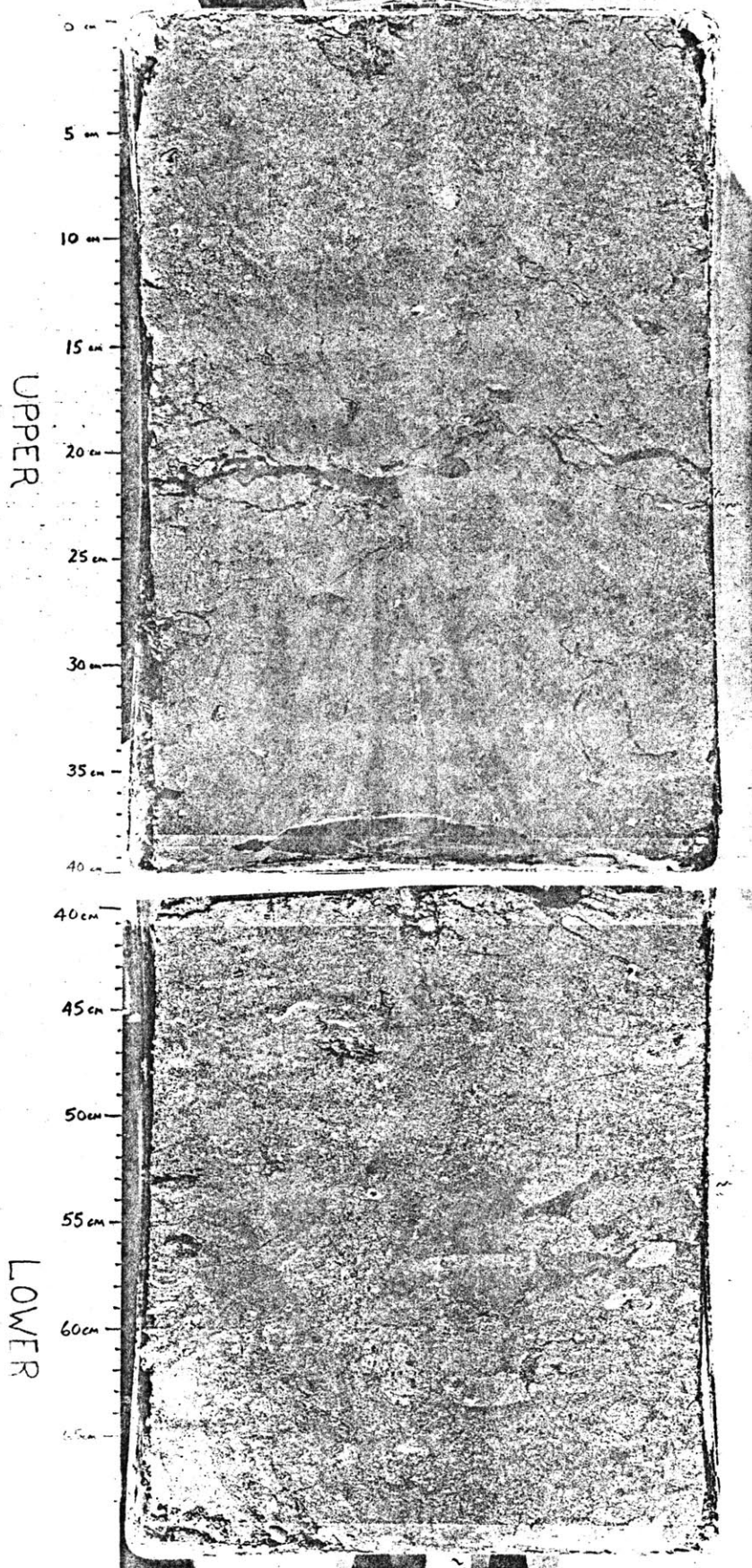
FIGURE 4.13: Photograph of face of core 11BC, showing structureless silt deposit with deep, open burrows.



711-94

BC 11

↑ TOP ↑



A third type of burrowing organism is apparently responsible for the long and wide burrows (20 to 30 cm by 1 to 2 cm) which underlie the thick sand layer at the top of core 15 BC (Figure 4.14). These burrows are unique in the study area in that they are filled with sand which has been burrowed into the previously deposited muddy sediments of the flank of East Katla Ridge. We have no clear idea as to what type of organism is responsible for these burrows. Similar features are notably absent below turbidite sand layers in piston cores located further down the flanks of East Katla Ridge. It may be that the episodic deposition of turbidites (varying from 3 to 14 cm thick in the piston cores) is sufficient to eliminate organisms which are adapted to burrowing the muddy deposits at these locations. This would contrast with the deposits high on the east flank where sand layers are inferred to have been present for several thousand years as a result of persistent current activity. This difference in the degree and type of burrowing activity may prove useful to subsequent investigations of the origin of sand layers in marine sediments and in ancient rocks.

The direct application of bioturbation characteristics to the interpretation of sedimentary depositional regimes is confused by an unfortunate characteristic of the piston coring method. The standard piston corer used in marine research has a diameter of only 6 cm, which is often inadequate to sample burrows of the scale observed in our box cores. In addition, distortion along the walls of piston cores may make the bottom interface of sand or silt layers appear ragged and disturbed when in fact it is flat lying. The routine use of x-ray procedures to analyze piston

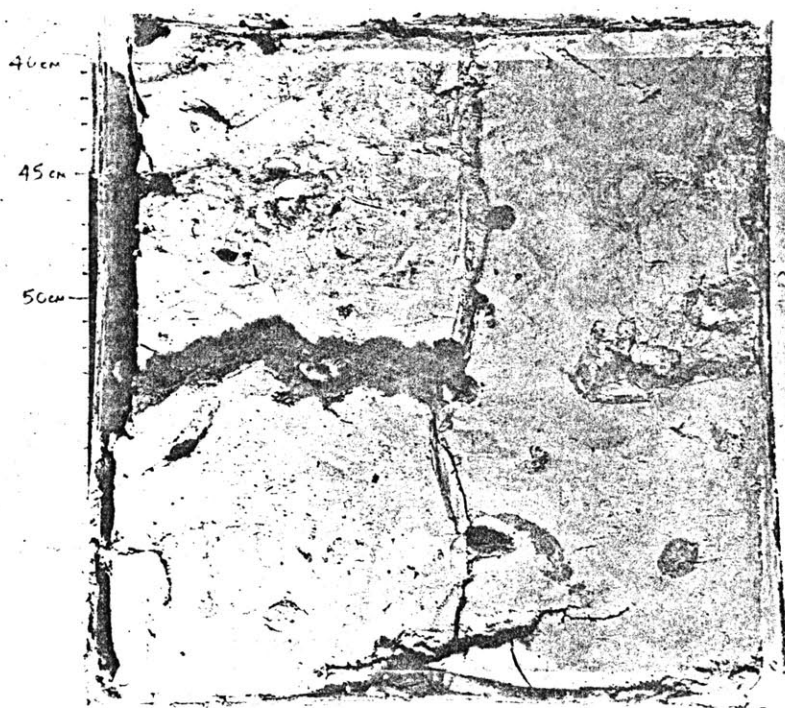
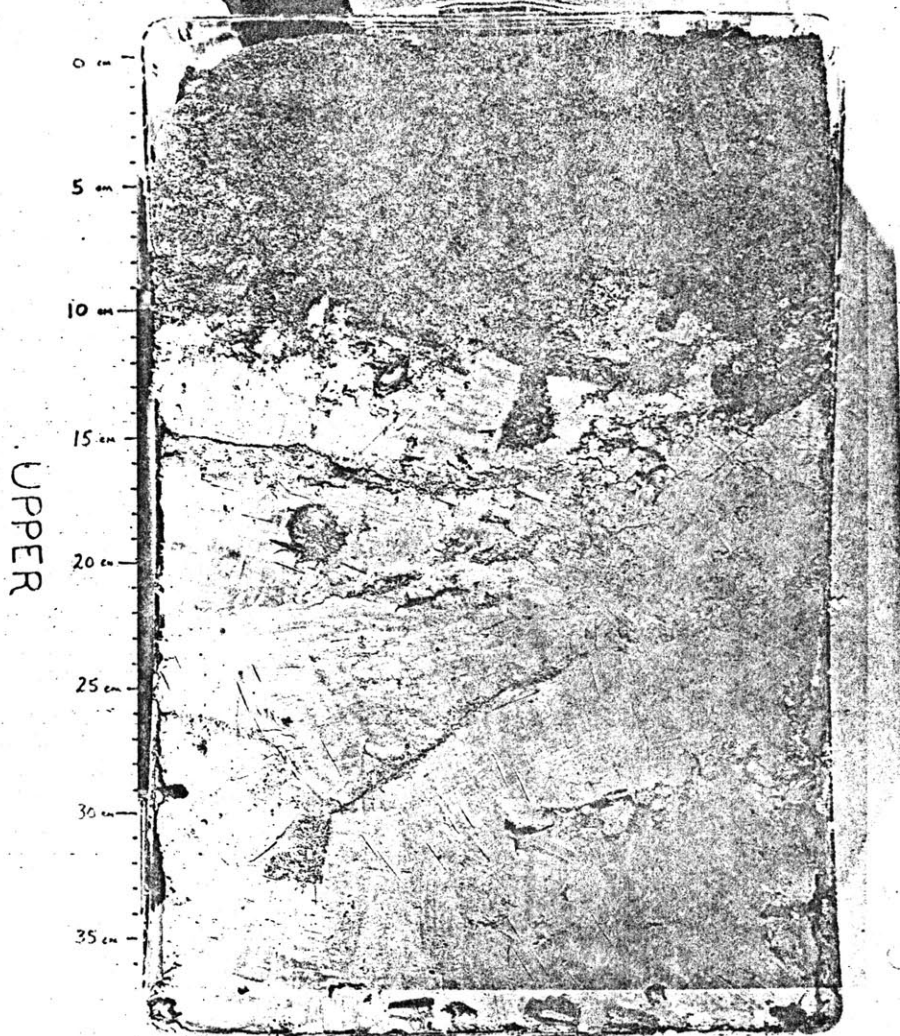
FIGURE 4.14: Photograph of face of core 15BC, showing extensively burrowed muddy sand surface layer.

AII-74

-167-

BC 15

↑TOP↑



cores may provide useful information concerning three-dimensional burrows. However, even this added dimension may not be sufficient for identification of burrowing in the narrow diameter piston cores. The problems inherent in small-diameter piston coring are amplified in contourite mud deposits where parallel "laminations" are apparently often the result of burrowing activity, and it is likely that many burrowing features may not be recognized in such deposits.

Surface sediments observed in bottom photographs and box core tops (Figure 4.15) provide additional evidence that bioturbation is a common feature in regions of muddy surface sediments. Photographs from the crest of East Katla Ridge clearly indicate that the entire sediment/water interface is strongly influenced by benthic infaunal and epifaunal activity (Figure 4.1). Photographs from the lower flank of the ridge, outside of the region influenced by strong currents, show even more extensive and larger burrowing features (mounds, pits, holes) which, although undoubtedly formed over longer time periods, are preserved in large part due to the absence of current activity (Figure 4.3). Photographs obtained over the sandy sediment surface underlying the current axis both on the east flank of East Katla Ridge and on the saddle of West Katla Ridge do not show significant evidence of surface burrowing activity (Figure 4.2). It seems probable that this is a result of sediment reworking under the influence of current flow, and may not adequately represent the degree of burrowing which may be preserved at deeper levels in the sediment column.

FIGURE 4.15: Photograph of core top of core 3BC, showing effects of both winnowing and bioturbation on sediments beneath the bottom current.

a. Photograph of top of full box, showing gravel and burrowed mud outcrops on surface:

b. Closer view of burrow mounds. These features are partially indurated and apparently quite resistant to erosion by strong bottom currents. Sand and gravel on the surface varies from 0 to 2 cm. thick.

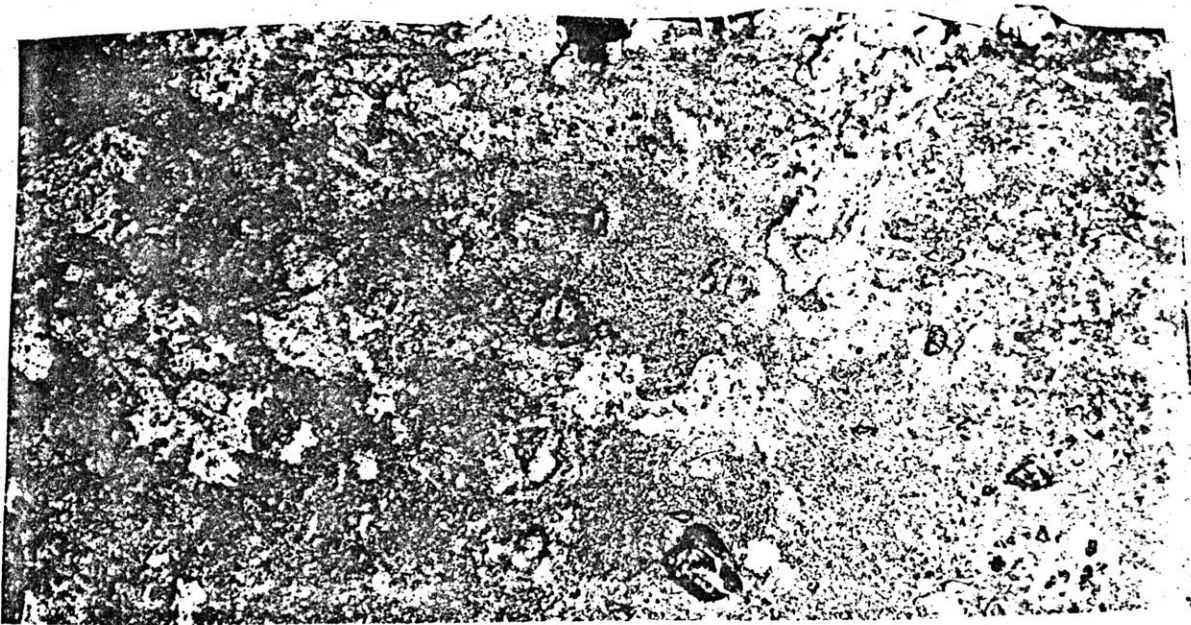
A

-170-



10 cm.

B



10 cm.



Bioturbation occurs less frequently in the sandy deposits from the canyon axis than elsewhere in the region. Although possibly due in part to the above-mentioned problem of recognition of burrowing in piston cores, it seems likely that the reduced preservation of benthic infaunal activity in this region is the result of the episodic and occasionally extremely thick turbidites and slumping activity. Scattered mottles of different colored sediments in the upper layers of graded turbidites are the only evidence to suggest that infaunal burrowing has occurred. Horizontal and cross-laminae are common in the sand layers throughout much of the core, and their undisturbed nature strongly suggests the absence of significant burrowing. Bottom photographs from the canyon axis show extensive epifaunal activity, but do not show the burrowing activity which is common in cores from the muddy deposits on the ridge flanks. Active reworking of surface sediments by tidal currents and the coarse, unconsolidated nature of the sediments are likely causes for the apparent absence of bioturbation features preserved in these sediments.

#### F. Sediment Size Analysis

Size analyses were determined for surface sediments in 11 box cores and gravity cores. Samples were taken from cores in five acoustic sedimentary provinces: laminated sediments from the east flank (1 PG, 3 BC, 5 PG), asymmetric sediment waves (laminated) (8 BC), multi-laminated channel axis sediments (6 BC, 7 BC, 10 BC), transparent sediments adjacent to Myrdalsjokull Channel (9 BC, 11 BC, 12 BC), and the region of small-scale hyperbolae on the east flank (15 BC).



### Method

Size frequency was determined in the following manner:

1) Samples were wet-sieved at 63 micron and weighed to determine percent sand and gravel. Samples were dry-sieved at 2000 micron to separate gravel.

2) Coarse fraction size frequency was determined at 1/2 phi intervals using a Modified Woods Hole Rapid Sediment Analyzer (Schlee, 1966) over the range 63 to 2000 micron (4 to -1 phi).

3) Size frequency of fine sediments was determined with a Model TA Coulter Counter<sup>R</sup> at 1/3 phi intervals over the range 11 to 4 phi (0.5 to 63 micron). Two measuring tubes (200 and 30 micron apertures) were used in Coulter Counter analyses, with intercalibration in overlapping size grades (6.3-8 micron class).

Size frequency data for the 11 surface samples are compiled in Table 4.2. Size frequency data and statistical measures assume an absence of material finer than  $\phi = 11$  (0.5 micron). Intercomparison of Coulter Counter and settling tube size data have not been attempted in these samples.

### Results

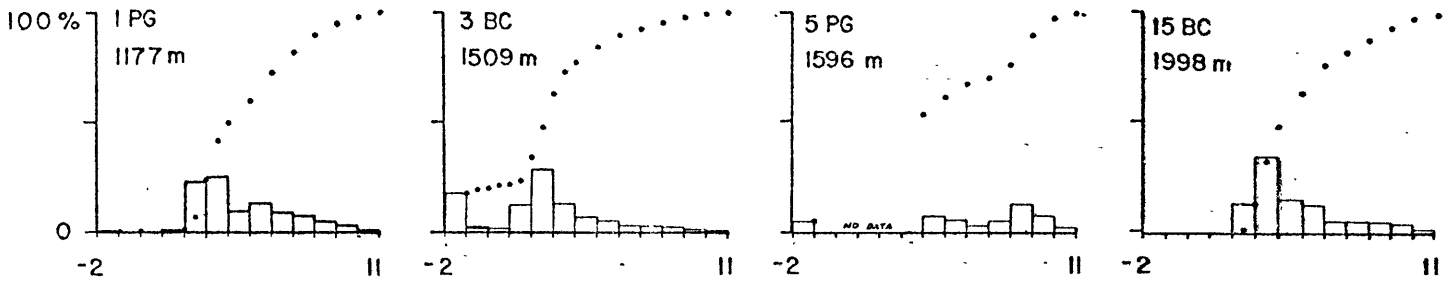
Three samples of surface sand layers obtained on the east flank of East Katla Ridge contain a principal mode in the 2 to 4 phi range (Figure 4.16); two of these contain granule-size basaltic rock fragments, which form a strong secondary mode at 2 to 4 microns (-1 to -2 phi) in core 3 BC. Statistical measures of sorting, skewness and kurtosis (Table 4.2) indicate that the sands are all very poorly sorted ( $\sigma_I > 2$ ) and are both positively (fine-) skewed and moderately peaked.

TABLE 4.2: SUMMARY OF GRAIN SIZE DISTRIBUTION IN SURFACE SEDIMENTS

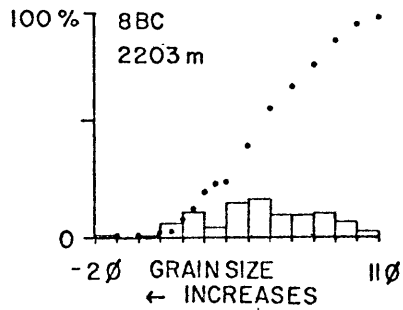
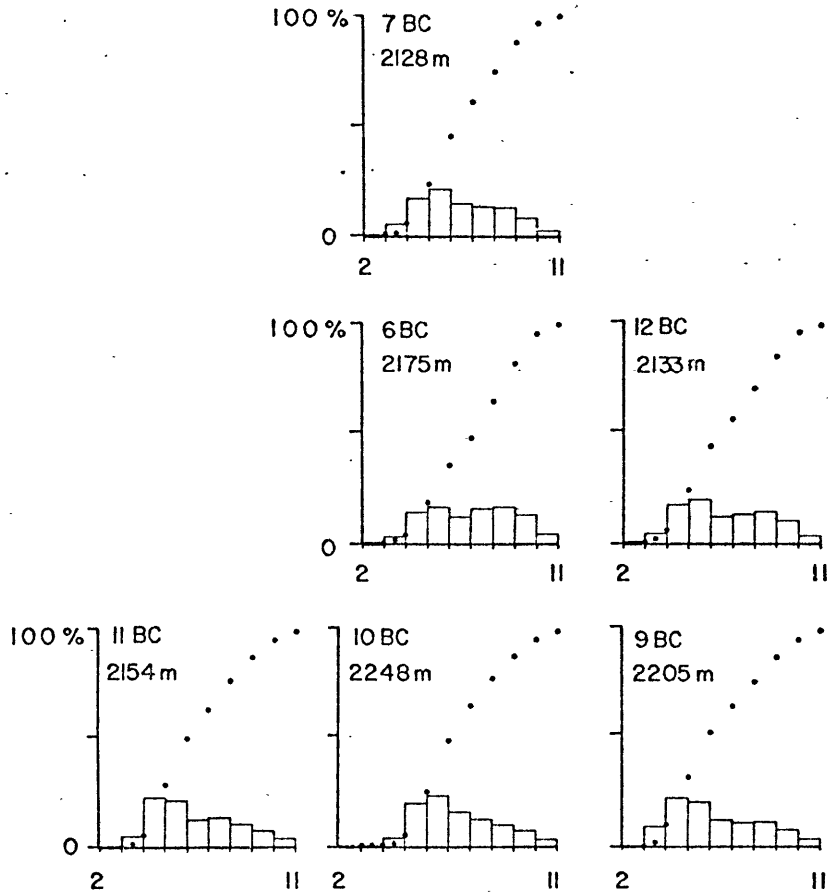
	<u>Sand</u>				<u>Mixed</u>	<u>Multi-laminated</u> <u>Silts</u>			<u>Transparent</u> <u>Silts</u>		
	1PG	3BC	5 PG	15BC	8BC	6BC	7BC	10BC	9BC	11BC	12BC
0 -											
-1	0.3	17.9	5.5	0	1.4	0	0	0	0	0	0
0--1		3.2									
1- 0		1.9			0.8						
2- 1	1.3	12.4			6.3			0.8			
3- 2	22.6	28.6		13.7	11.8	0.6	0.4	0.3	0.3	0.3	1.1
4- 3	25.3	13.1		35.2	4.7	3.7	6.0	4.2	9.6	5.2	4.9
5- 4	9.7	7.0	7.8	15.3	15.7	14.6	17.7	20.2	22.5	23.0	18.0
6- 5	13.4	5.6	5.9	12.9	17.3	17.0	21.8	23.9	20.4	21.5	20.1
7- 6	9.1	3.1	3.3	5.6	10.2	12.5	15.3	16.0	12.2	12.8	12.4
8- 7	7.8	2.7	5.6	5.7	10.1	16.5	13.8	13.0	11.2	13.8	13.7
9- 8	5.2	2.4	13.2	5.3	11.4	17.2	13.4	10.2	11.7	10.9	14.7
10- 9	3.2	1.6	7.9	4.4	7.5	13.6	8.5	7.7	7.9	7.8	11.1
11-10	1.7	0.7	2.3	2.0	3.1	4.7	2.8	3.7	3.8	4.2	3.9

FIGURE 4.16: Size frequency distribution in surface sediment samples.  
See text for discussion.

# EAST FLANK SANDS



MYRDALSJOKULL CHANNEL  
AND VICINITY



# CANYON LEVEE WAVES

Six samples from the channel deposits and adjacent transparent sediments contain a principal mode in the coarse silt range (4 to 6  $\phi$ ). Two samples show a pronounced secondary mode in the clay-size fraction (8 to 9  $\phi$ ). As with the sands, these samples are very poorly sorted. Skewness is variable, although generally positive. Kurtosis (peakedness) is lower than in the sand samples.

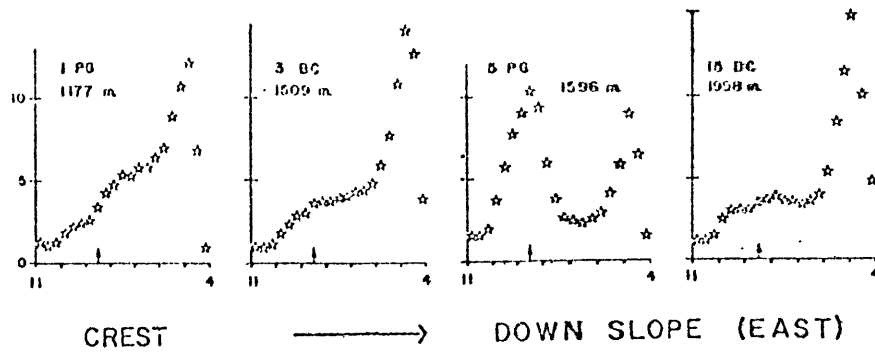
Transparent and multi-laminated deposits are not clearly distinguishable on the basis of grain size (Figures 4.16, 4.17). Adjacent samples show a higher degree of similarity than do samples from similar acoustic sedimentary regimes. Samples from near the canyon mouth (6 BC and 12 BC) both have a well-developed secondary mode in the clay fraction, and samples from cores 6 BC, 7 BC and 12 BC are less peaked than samples from cores 10 BC, 9 BC and 11 BC located further down channel.

Detailed examination of the fine fraction of cores from various provinces provides little clue as to any specific source for the 8.5  $\phi$  peak observed in samples in and around the channel (Figure 4.17). The absence of this mode in Core 10 BC (channel axis) and in 3 of the 4 cores from the sand layers on East Katla Ridge appear to rule out either turbidity currents or bottom currents as being uniquely responsible for its formation. Further study and additional samples will be necessary to determine whether grain size distribution may be used to discriminate fine-grained turbidites from contourites in this region.

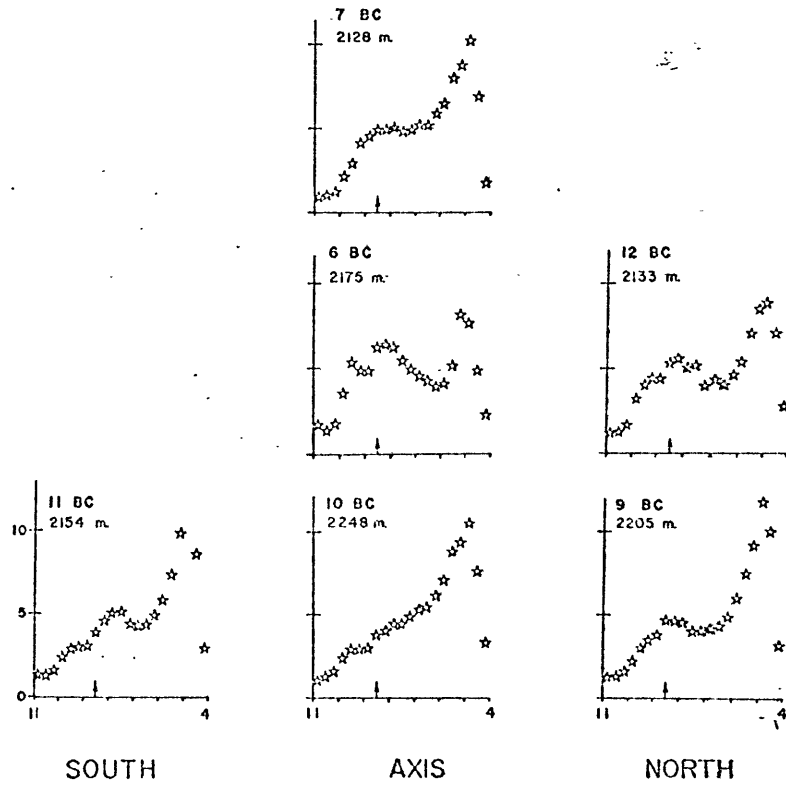
#### Sand layers: interpretation

The poorly sorted surface sand layers observed on the east flank of East Katla Ridge are difficult to explain as simple products of

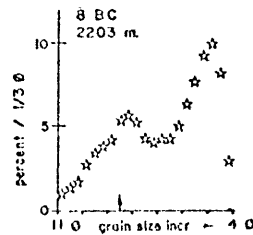
FIGURE 4.17: Size frequency distribution of the fine fraction of surface sediment samples. Size was determined with a Coulter Counter<sup>R</sup> at 1/3 phi intervals from 4 to 11 phi (63 to 0.5 microns diameter). See text for discussion of secondary mode at 8.5 phi.



### EAST FLANK SANDS



### FAN/CHANNEL PROVINCE



### CANYON LEVEE WAVES

mechanical erosion or traction transport. Their formation is probably a complex product of Holocene sand deposition, bedload transport, winnowing of silt and clay from the upper surface by bottom currents, and burrowing by benthic infauna. Grain size distributions support the latter interpretation of a biologic process which introduces mud from below while it is removed by currents at the surface. This mode of formation may be modelled in a simple manner by assuming the observed muddy sand to be a simple mixture of two normally distributed sediments: a mud layer similar to that observed beneath the sand and a well-sorted sand layer. The model assumes that surface winnowing results in the formation of a well-sorted sand layer at the interface; this layer is subsequently disrupted by burrowing organisms which distribute it vertically through the upper several centimeters of the sedimentary column.

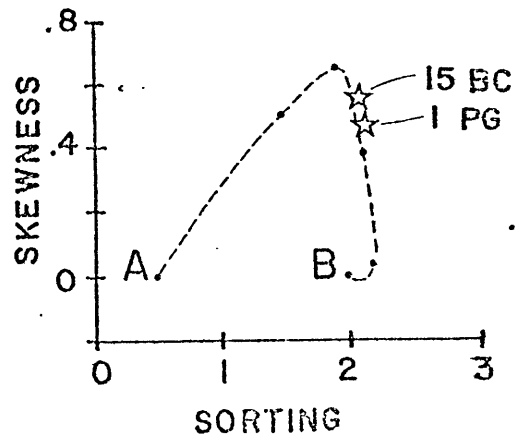
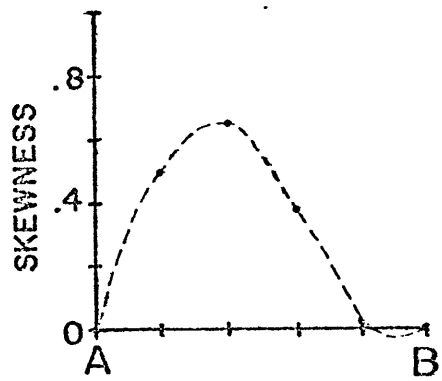
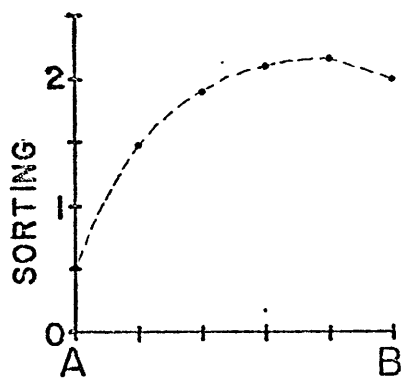
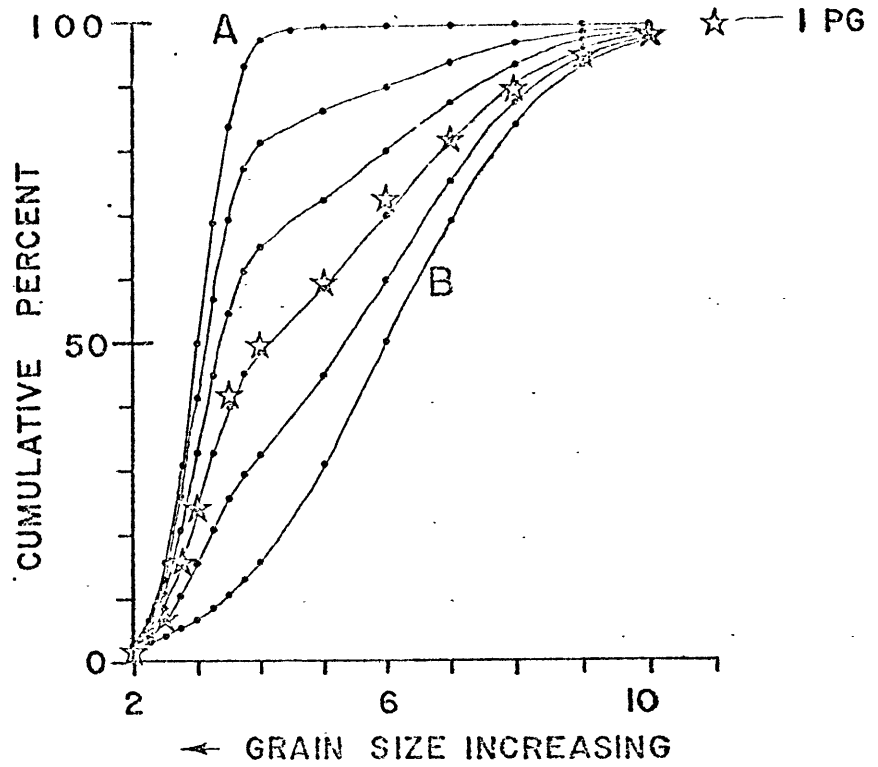
An example of a mixed distribution is illustrated in Figure 4.18. The calculation was based on a normally distributed mud with  $\phi_{50} = 6.0$  and a standard deviation of  $2.0 \phi$  added to a sand layer of  $\phi_{50} = 3.0$  and  $\sigma_I = 0.5$ . These parameters were chosen to coincide with the two modal peaks in core 1 PG.

The resulting sediment size distribution fits the sand layer in core 1 PG quite closely for a ratio of 0.4 sand: 0.6 mud. It is also a reasonable representation of size distribution for cores 15 BC and 3 BC (if gravel mode is removed).

An additional point of interest is that the sorting and skewness parameters (Folk & Ward, 1957) also agree with the mixing model. Examples of sorting ( $\sigma_I$ ) and skewness ( $Sk_I$ ) for various ratios of



FIGURE 4.18: Cumulative frequency and statistics for model mixture of sand plus mud. See text for discussion.



sand and mud are illustrated in Figure 4.18. The mixture of two distinct sediments produces an intermediate maximum in  $\sigma_I$  which must be larger than either endpoint value. In addition, skewness goes through both a maximum and a minimum between 'pure sand' and 'pure mud', with the endpoints defined as having zero skewness (normal distribution). It is intriguing to note that a plot of sorting vs. skewness for such a mixture is therefore not a real function, since values of 50% mud or greater have two skewness values associated with a given sorting index. Sorting and skewness of samples from sand layers fall within the range of 40 to 60% sand, however, which is a close approximation to their observed sand content (Table 4.2).

The preceding discussion is not a proof that mechanical mixing of sand and mud has formed the poorly sorted sand layers beneath the current axis on East Katla Ridge. It is, however, a reasonable mechanism for forming such layers, and it supports the evidence from:

- 1) the correspondence between current flow and sand layer recovery;
- 2) observations of long burrows beneath the sand layers; and
- 3) the patchiness of sand layers on the sediment surface;

that these sand layers were in fact formed by current flow and not some other process.

Grain size parameters in the muddy sands of East Katla Ridge may be compared with those observed in various provinces of the continental margin of eastern North America by Hollister (1973). That study demonstrated that distinct sedimentary provinces could be correlated with various current regimes on the basis of grain size statistics such as mean,

standard deviation, skewness, kurtosis. Samples from the present study have characteristics which are most closely associated with Hollister's 'Gulf Stream Counter Current and Antilles Current' province in which he infers that sand is added to 'an originally well-sorted finer grained material.' (Hollister, 1973, p. M12). These deposits, like those on East Katla Ridge, are characteristically poorly to very poorly sorted and fine-skewed.

G. Contourites: Recognition and Characteristics

A recent synthesis by Stow and Lovell (1979) reviews the literature on modern and ancient "contourite" sediments. These authors propose a set of criteria for recognizing deposits derived from bottom current erosional/depositional processes, and discuss the likelihood of their preservation in the geologic record.

The criteria proposed by Stow and Lovell (1979) differ in a number of respects from those originally proposed by Hollister and Heezen (1972). The essential improvement of the more recent work is in establishing a framework which is suitable for classifying deposits formed under widely differing bottom current velocity regimes. The Stow and Lovell classification includes two major types of contourite deposit, 'muddy' and 'sandy', which may be related to current regimes which are depositional and erosional (or winnowing), respectively. Stow and Lovell recognize at least three types of 'sandy contourites', including 1) coarse lag deposits resulting from restricted flow through deep-sea channels and straits, 2) reworked tops of sandy turbidites, and 3) thin sand/silt laminae interspersed with muddy contourite deposits. Characteristics of 'sandy turbidites' as recognized by these authors are reproduced here (Table 4.3) from their paper (Stow and Lovell, 1979, p. 273).

Circulation and sedimentation: discussion

The results summarized in previous sections concerning distribution of flow properties and sedimentation properties in the Katla Ridge region lead to several lines of reasoning concerning geologic effects of bottom currents. The axis of the steady ISOC, where mean speeds are approximately

TABLE 4.3: (after Stow and Lovell, 1979, p. 273) Sandy contourites: sedimentary characteristics.

	Conclusions from marine-based studies	Comment on potential for presentation, and use in land-based studies
Occurrence	thin lag deposits in muddy contourite sequences reworked tops of sandy turbidites in interbedded sequences coarse lag in deep-sea channels and straits	good, but identification depends on features listed under other headings
Structure	frequently disturbed and bioturbated; irregular coarse layers with little primary structure where undisturbed - horizontal and cross lamination similar to those in turbidites but with no regular structural sequence, and an orientation parallel to the bottom current direction may show reverse grading near the top, and a sharp upper contact	good, especially evidence of current directions, which may well be crucial (Anketell and Lovell, 1976); in the case of the current directions land-based investigations of contourites may prove more fruitful than marine-based studies.
Texture	silt to sand-sized, more rarely gravel may be relatively free of mud and well sorted tendency to low or negative skewness values no offshore trends	not good, likely to be very substantially altered by diagenesis and tectonic deformation
Fabric	indication of grain orientation parallel to the bottom current (along-slope) may show secondary mode of turbidite fabric (? at right angles) may show more polymodal or random fabric (disturbed)	not good, because of diagenesis and tectonic deformation? Scott (1967, p. 274) argues that grain orientations in substantially deformed beds do in at least one case "primarily reflect sedimentation"
Composition	dependent on region and immediate supply of sandy material concentration of grains of higher specific gravity (frequently biogenic lag in muddy contourites) compositional grading in turbidites obscured by reworking some evidence of along-slope reworking	fair, diagenesis may create problems, especially with biogenic material; each region needs to be considered on its merits (see text)

15 cm sec<sup>-1</sup> or greater is presently an area of surficial sand layer formation and surface erosion. The main regions where such erosional activity is observed or inferred include the smooth east flank of East Katla Ridge which is intersected by the west to southwestward flowing ISOC, as well as the southern flanks of both East and West Katla Ridges. In addition, portions of the levee system extending seaward from Myrdalsjokull Canyon protrude high enough into the current to intersect the undeflected and high velocity zones of flow.

Deposition is observed due to bottom current flow in two principal locations. South and east of the main flow axis on the east flank of East Katla Ridge, a region of high accumulation rate Holocene deposition is observed. Stratigraphic evidence suggests that no Pleistocene/Holocene unconformity exists in this region, indicating that persistent, strong flow has been restricted to depths shallower than 2000 meters throughout the Holocene.

The mechanism for deposition of these muddy contourites is inferred to be primarily due to downslope advection of resuspended sediments due to frictional deceleration of the bottom mixed layers. Two pieces of evidence suggest that such a model may apply. The first is the dramatic difference in nepheloid layer shape and intensity between stations shallower and deeper than 2000 meters on the northern section. Shallower stations are characterized by thick, fairly uniform nepheloid layers extending several hundred meters off bottom. Deeper stations, conversely, characteristically show thin (less than 200 meters) and more intense nepheloid layers than the shallower section. Such a pattern

might be expected if detached bottom mixed layers flowing downslope away from the flow axis come to rest in regions in which deposition may occur.

The second line of evidence supporting downslope movement of detached layers is observed in the current meter results. A stall at our current meter at 2000 meters on the east flank section (CM 1) was preceded by 24 hours of eastward flow. A CTD section at this site immediately following the stall shows a highly thickened section of Iceland-Scotland Overflow Water present at this location. This event is simultaneous with westward flow at meters high on the ridge flank, suggesting that flow in the vicinity of the current margin is both episodic and controlled by frictional deceleration.

Deposition of the acoustically transparent sediments in South Katla Basin is inferred to result from reduced current velocities due to the spreading and thinning of the current as it passes southwards out of the complex topography of the canyon into the broad smooth basin. Restricted bottom flow out of this basin to the SW may also be a factor in causing deposition by forcing deeper strata to turn eastwards in a deep cyclonic gyre, depositing part of their load in the basin.

#### 'Sandy contourites' in Iceland Basin sediments

'Sandy contourite' deposits are interpreted as occurring in two regions within the Katla Ridge survey area: 1) beneath the Iceland-Scotland Overflow Current on the flanks of East and West Katla Ridges where measured or inferred current velocities are approximately 15 to 20 cm sec<sup>-1</sup>; and 2) within the axis of Myrdalsjokull Canyon where flow direction and speed may be highly variable, and were not directly measured.



These two types of deposit are analagous to those inferred by Stow and Lovell (1979) to result from 1) flow through restricted channels, and 2) reworking of turbidites, respectively. The third type of deposit discussed by Stow and Lovell, and previously described at length by Hollister and Heezen (1972), is not observed in sediments recovered from the Katla Ridge region. Thin silt layers are observed only in deposits from the axis of Myrdalsjokull Channel, which are inferred to be turbidites.

Evidence as discussed above that the sandy deposits in this study are formed by bottom currents is principally the physiographic setting of the samples relative to the observed current, the type and condition of components in the sand, and the age of the deposits relative to the underlying muds. Criteria based on sedimentary structures, sorting, grain alignment and others suggested by Stow and Lovell (1979) and Hollister and Heezen (1972) did not prove useful in identifying these highly bioturbated deposits. In fact, most features which have been suggested as characterizing sandy contourites are absent (they have been destroyed or greatly modified by the prolific organisms) in the Iceland Basin deposits, as will be discussed below.

The sandy deposit which is encountered in box cores and gravity cores between 1175 and 2000 meters water depth on the east flank of East Katla Ridge is a very poorly sorted muddy sand which varies from a few millimeters to ten centimeters thick. The lower contact is sharp, and in most cases is an unconformity to pre-Holocene terrigenous (volcanic) muds. The contact is extensively burrowed, and sand is disseminated into the

underlying mud as much as 25 centimeters below the base of the sand layer in discrete burrows.

Components of the sand fraction of the east flank deposits include basaltic rock fragments (up to granule size, and apparently ice-rafted), stained and broken planktonic foraminifera (both polar and subpolar forms), 'fresh' well-preserved planktonic foraminifera, volcanic glass, benthic foraminifera (often stained and broken) plus additional minor components. Planktonic foraminifera assemblages are dominantly subpolar, but contain 10 to 20 percent of Globigerina pachyderma (left-coiling) which indicates that substantial amounts of older sediment have been incorporated. Both foraminifera and rock fragments are stained reddish-brown to black in many cases, and the occurrence of numerous broken foraminifera (both planktonic and benthic) indicate that the deposits have had extended contact with flow at the sediment/water interface. The presence of the benthic foraminifer Rupertia stabilis in these deposits in various states of preservation also indicates that the sand deposits have a long history of exposure to bottom current flow, for this species is an attached form which needs a hard substrate of sand or gravel (Phleger et al, 1954). It was originally described from specimens recovered on the H.M.S. Bulldog expedition along the Greenland margin where rapid bottom currents are inferred to be similar or stronger than those observed on East Katla Ridge.

The sandy surface layer represents the total accumulation of Holocene sediment in most cores obtained beneath the rapidly-flowing axis of the ISOC; rates of accumulation are less than 2 cm/1000 yr. This contrasts

markedly with rates in excess of 30 cm/1000 yr observed in cores which are outside of the rapidly-flowing portion of the ISOC.

All of the evidence above points to the concept that the sandy surface deposit observed on the east flank of East Katla Ridge (plus similar deposits on West Katla Ridge) result from a combination of bioturbation plus flow of the Iceland-Scotland Overflow Current, which has prevented deposition of Holocene silt and clay, and has eroded and reworked pre-Holocene muds and mixed them with Holocene sand.

The second type of deposit which is inferred to be 'sandy contourite' is observed in only one piston core from the axis of Myrdalsjokull Canyon, where graded sand layers (turbidites) are separated in many cases by finely laminated and cross-laminated deposits of both terrigenous sand and biogenic sand. The inference that these deposits may be 'contourite' is based primarily on the abundance of pteropod tests in some parts of the core. Pteropods in this core are dominated by the genus Limacina, which is interpreted as an open ocean group rather than a shelf form (Herman, 1968; Herman and Rosenberg, 1969), and which are therefore unlikely to enter the canyon as turbidites originating on the Iceland shelf. The abundance of pteropods in the canyon deposit is particularly remarkable in comparison with cores obtained from other parts of the study area where only scattered occurrence of pteropod layers is noted, and which are invariably less than a few centimeters thick.

Biogenic sand layers in Myrdalsjokull Canyon are of two types: 1) thin (millimeter scale) laminae of pteropods and foraminifera interbedded with terrigenous sand and 2) thick deposits of pteropods and foraminifera

(tens of centimeters) which lack primary structures. In the absence of either direct observation of the current regime within the canyon or additional samples to determine the lateral relationship of these deposits, there is no reliable means of convincingly demonstrating that these deposits are formed by bottom current action. Cross-bedding is observed in both directions relative to the reference frame of the split surface of the piston core in both terrigenous (ungraded) and biogenic sand layers, which would be a result of complex circulation due to a combination of tidal currents and ISOC flow within the canyon; however, it could also result from twisting of the corer during penetration or deformation by the coring process.

The most likely explanation for the fine laminations observed in sand deposits in the canyon deposits appears to be that they are formed by complex flow of bottom currents within the canyon which winnow and segregate low density carbonate tests from the surrounding terrigenous sands; they may be preferentially deposited in the canyon as a result of influx of a steady current which erodes mud from the ridge flank upcurrent and can no longer maintain the coars part of its load in suspension as it exits the canyon. Considerably more study is necessary before the various sand deposits within the canyon axis may be clearly associated with either the process of turbidity currents or of bottom currents.

#### Bioturbation and 'sandy contourite' characteristics

Stow and Lovell (1979) note, in their discussion of sedimentary structures in contourite deposits, that they are likely to provide "...evidence of current directions, which may well be crucial" (p. 273).

However, they also state that 'sandy contourites' are "frequently disturbed and bioturbated [and are often] irregular coarse layers with little primary structure." (p. 273). From the observations of sand layers on the east flank of East Katla Ridge, it seems that the latter statement is more applicable to deposits which are formed beneath the relatively steady currents and very high biologic surface productivity which characterize those high latitude portions of the ocean basins within several hundred kilometers of the point of entrance of dense waters into the basin. At the present time, such persistent flow of bottom water is to be expected along the eastern margin of Greenland, on the Iceland-Faroe Ridge and along the margin of Iceland, at various sites around Antarctica, and perhaps on the continental slope seaward of the Mediterranean outflow at Gibraltar. Similar deposits might also be expected in deep sea channels which serve as conduits for unidirectional flow of bottom water between ocean basins (e.g., Vema Channel in the South Atlantic, (Johnson, et al, 1976) and Samoan Passage (Hollister, et al, 1974) in the South Pacific), although carbonate dissolution at abyssal depths may substantially alter these deposits.

The unusual characteristics of these 'sandy contourites' are interpreted to be due to the prolonged activity of bottom flow and burrowing organisms on the sediment interface, which results in the incorporation of reworked mud in amounts which cannot be satisfactorily explained by models which assume only physical processes acting on the interface. The pronounced effect of bioturbation is likely to eliminate evidence of primary sedimentary structures, grain alignment and unique sorting

characteristics. The most likely characteristics to be preserved are:

1. Mixing of terrigenous and biogenic sands;
2. Stained and broken biogenic tests indicative of prolonged exposure to flow;
3. Sharp, burrowed lower contacts when sand layers overlie silt or clay deposits; and
4. Unconformity between sand layers and underlying sediments.

This type of contourite deposit is most analogous to a soil horizon on land, in which local geomorphology is at least as important as climate in determining the ultimate characteristics of the deposit. It is similar as well in the poor preservation potential of the actual deposit, with a stronger likelihood that a hiatus will result due to the thinness of the sand deposit. This is supported in the Katla Ridge region by both bottom photographs and cores which show muds at the sediment/water interface beneath the flow axis; piston and gravity cores from this regime either contain a surface sand layer or a hiatus of at least 13,000 years. Thus, although the detection of episodes of influx of dense water into the ocean basins is an important problem for understanding the past circulation of the ocean, it would appear to be a problem which is more readily approached by studies of sediments in lower (less productive) latitudes or away from inferred current pathways where depositional processes dominate rather than erosional. Our study of Katla Ridge deposits suggests that persistent currents of 15 to 20 cm sec<sup>-1</sup> may be sufficient to prevent significant deposition, especially in the presence of abundant burrowing activity.

TABLE 4.4: (after Stow and Lovell, 1979, p. 271-272 Muddy contourites: sedimentary characteristics.

	Conclusions from marine-based studies	Comment on potential for presentation, and use in land-based studies
Occurrence	thick sequences of hemipelagic/contourite sediment (sediment ridges) in association with turbidites - over-lying graded muds or sands on the continental rise	good, but identification depends on features listed under other headings
Structure	dominantly homogenous, bedding not well defined bioturbational mottling generally common burrows (? mycelia and pyrite present in many places coarse lag concentrations especially biogenic) reflect composition of coarse fraction in mud primary silt/mud lamination - rare, but where present may be similar to very fine-grained turbidites though lacking structural sequence	good, unless extreme tectonic deformation, but note problem of distinction from very fine-grained turbidites
Texture	dominantly silty mud frequently high sand content (0-15%) of biogenic tests medium to poorly sorted, ungraded no offshore textural trends may show marked textural difference from interbedded turbidite if transport distances are different	not good, likely to be very substantially altered by diagenesis and tectonic deformation
Fabric	mud fabric; smaller, more randomly arranged particle clusters than the large, oriented groupings of mud turbidites (preliminary findings Stow, 1977a) primary silt laminae or coarse lag deposits show grain orientation parallel to the current (along-slope) interbedded, reworked turbidite layers may show widely bimodal grain orientations	not good, because of diagenesis and tectonic deformation coarser layers may preserve useful features (see discussion in Scott, 1967)

TABLE 4.4: (continued)

Conclusions from marine-based studies	Comment on potential for presentation, and use in land-based studies
<p>Composition generally combination of biogenic and terrigenous material (may be distinct from interbedded turbidites)</p> <p>terrigenous material dominantly reflects nearby land/shelf source with some along-slope mixing and small amount of far travelled material (no down-slope trends)</p> <p>biogenic material usually rich - coccoliths, forams, diatoms, radiolaria, etc. (but varies with productivity of surface waters, and depth in relation to CCD)</p> <p>CaCO<sub>3</sub> content often relatively high (10-40%) except where low productivity or below CCD</p> <p>organic carbon content often high (0.5-2%) except as above</p> <p>pyrite (and other iron sulphides) may be common?</p> <p>general absence of shallow-water material; may have broken shallow benthonic forams</p>	<p>fair, diagenesis, especially of biogenic material, likely to create problems; each region needs to be considered on its merits (see text).</p>



'Muddy contourites'

The primary criterion for identification of deposits as 'muddy contourites' is the physiographic setting rather than characteristics ascribed to these deposits by previous workers. However, due in part to the rather weak sedimentological criteria which have been established for recognition of these deposits, there is little disagreement between the characteristics of 'muddy contourites' summarized by Stow and Lovell (1979) and those observed in this study (see Table 4.4, which reproduces their criteria for recognizing 'muddy contourites').

The most widely used criteria for the recognition of the depositional facies associated with abyssal currents have been morphological (e.g., Hollister and Heezen, 1972; Jones et al., 1973; Ruddiman, 1972; and many others). Sedimentological criteria have typically concentrated on inter-layered silt or sand beds rather than on the fine-grained component. The absence of macroscopic sedimentary structures in the clay portion of current deposits is to be expected in cohesive sediments in which the physical controls governing sand and silt deposition break down due to grain-grain adhesion, which effectively prevents the size segregation and density:velocity relationships which result in formation of bedforms in non-cohesive sediments under flow conditions. It has therefore been difficult to establish a reasonable theoretical framework for predicting specific characteristics which would distinguish current-laid deposits of cohesive sediment from those of pelagic settling or fine-grained tails of turbidites.

The one structural criterion which has been proposed for recognition of fine-grained deposits of bottom currents which has proved to be more than locally applicable is the presence of thin sand or silt laminae interbedded with muds. Although often absent, these structures are common in some large and significant areas (e.g., lower continental rise off of eastern North America, as discussed in Hollister and Heezen, 1972). Their absence in other deposits is generally considered to result from bioturbation (Stow and Lovell, 1979). Characteristics of grain fabric such as the size of particle aggregates noted in Stow and Lovell (1979) (Table 4.4) have yet to be convincingly demonstrated to result from flow characteristics rather than post-depositional or biologic processes.

The most convincing lines of evidence that deposits on the lower flank of East Katla Ridge and in South Katla Basin are controlled by bottom circulation, (based on examination of sediments) are 1) the rapid rate of accumulation of these sediments immediately downslope from the rapidly-flowing current, 2) the anomalously high age estimates obtained by radiocarbon dating of Holocene deposits, indicating admixture of fine-grained pre-Holocene carbonate, and 3) the abundance of juvenile and small species of planktonic foraminifera in the sand fraction. The few sand layers observed in the 'muddy contourite' facies are interpreted as thin turbidites rather than 'sandy contourites' based on the downslope flow direction determined from cross-bedding in one sample, and on the graded bedding and absence of bioturbation observed.

Accumulation rates for 'muddy contourites' observed in the Katla Ridge region were determined in three piston cores to be in the range of

25 to 40 cm/1000 years. However, the presence of much thicker deposits of acoustically transparent sediments in South Katla Basin suggest that as much as 20 meters of this material may have accumulated since the last glacial period downcurrent from Myrdalsjokull Canyon, which would indicate that accumulation rates in excess of 1 meter/1000 years may be locally observed. Similarly high rates resulting from current deposition have been proposed for brief periods during deglaciation and renewed bottom circulation following glacial periods beneath the ISOC at 56°N by Ruddiman and Bowles (1978).

H. Summary: 'Contourite' Characteristics in the Katla Ridge Region

The preceding discussion indicates that the best means (at this stage in the field of research) of recognizing deposits of bottom currents is still to establish that 1) a current is present on the basis of other evidence (preferably direct measurement) and 2) to observe the local variability of structure and texture of surface sediments and to correlate these with inferred current variability. Although specific criteria may be established for the recognition of various types of 'contourite' deposits within a given local area, the striking contrast between the surface sand layers on East Katla Ridge and the thin silt laminae which characterize the lower continental rise of eastern North America are ample evidence that bottom currents may give rise to a wide spectrum of deposits, even when current velocities and sediment sources are similar. Velocities of 15-20 cm sec<sup>-1</sup> are not uncommon on the lower continental rise of eastern North America (see Zimmerman, 1971, and Laine, 1977) and both regions are inferred to receive considerable input of terrigenous

sediment via canyons incised in the adjacent slope. The persistence of flow over geologic time, and, perhaps more importantly, the difference in the intensity of bioturbation may be factors which influence the character of 'contourite' deposits more than was previously assumed by Hollister and Heezen (1972) and Stow and Lovell (1979). Further study of surface sediments in regions in which persistent flow over at least several thousand years may be inferred may help to establish more precisely whether the muddy surface sand layers on East Katla Ridge are typical of deposits which might be called 'proximal sandy contourites' and which might be useful in paleocirculation studies.

CHAPTER V: SUMMARY AND CONCLUSIONS

A. Summary

The geologic effects of bottom currents and turbidity currents are well developed in the region of a large, canyon-dissected sediment drift south of Iceland called the East Katla Ridge. It is an elongate sediment deposit trending  $210^{\circ}$  from its intersection with the insular slope of Iceland which slopes gradually to a depth of approximately 1400 meters and, at a sharp break in slope, rapidly deepens to approximately 2100 meters where it merges with the sediments of Myrdalsjokull Suprafan. Sediment thickness beneath the ridge crest exceeds 1.5 km; oceanic basement cannot be identified with confidence beneath East Katla Ridge with a 40 cubic inch airgun system.

In this topographic setting, a rapidly-flowing bottom current was measured that flows along the east flank of East Katla Ridge in water depths from 1200 to 2000 meters. Vector mean velocity exceeded  $18 \text{ cm sec}^{-1}$  at 3 near-bottom current meters deployed at 1400, 1600 and 1800 meters depth for two weeks. Flow at 1200 and 2000 meters exceeded  $10 \text{ cm sec}^{-1}$ ; only one current meter (at 2160 meters) was outside the flow. Flow direction was generally westerly to southwesterly, with instruments on the upper ridge flank showing upslope deviation of up to  $45^{\circ}$  from the isobaths. Flow volume was calculated from 17 CTD stations, forming a closed array, using mass conservation to test the result. A reference level, chosen to coincide with  $\sigma_t = 27.75$ , produced near-bottom velocities which are in reasonable agreement with those measured, and a flow of

$5.0 \times 10^6 \text{ m}^3 \text{ sec}^{-1}$  was calculated under the geostrophic assumption, of which about  $2.0 \times 10^6 \text{ m}^3 \text{ sec}^{-1}$  is Norwegian Sea Deep Water (an influx of dense water from the Norwegian Sea). This value agrees remarkably well with the  $2.2 \times 10^6 \text{ m}^3 \text{ sec}^{-1}$  calculated by Meincke (personal communication) from the comprehensive investigation of outflow from the Norwegian Sea during 'OVERFLOW 73' (ICES).

The flow axis, as defined by both temperature (or density) and velocity, lies at approximately 1600 to 1800 meters water depth on the east flank of East Katla Ridge. The 'uphill' flow directions suggest that the axis crosses the nose of the ridge, and thereupon plunges into the incised (turbidity current-carved) axis of Myrdalsjokull Canyon. A portion of the flow may pass to the west across a saddle at 1500 to 1600 meters on the adjacent sediment drift (West Katla Ridge). However, the most dense water is diverted to the south until it reaches the south-facing slope of West Katla Ridge, whereupon it turns westward and flows toward the northern end of Gardar Drift.

Considerable mixing occurs within the canyon, possibly governed in part by strong tidal flows constrained to the narrow, steep-walled canyon. Bottom mixed layer thickness at two stations in the canyon exceeds 100 meters, and waters at 2237 meters depth on the south flank of West Katla Ridge retain this thick near-bottom layer of density greater than  $\sigma_\theta = 27.96$ . Thick bottom mixed layers (>50 meters) are absent on the east flank of East Katla Ridge, where the current has not yet encountered the canyon. There is some CTD evidence for thin bottom-mixed layers being diverted towards the southeast as they exit the canyon.

This occurs along Myrdalsjokull Canyon Levee, which is a barrier developed along the southern margin of Myrdalsjokull Channel which continues eastward from Myrdalsjokull Canyon. The main body of the current apparently turns westward between 2000 and 2300 meters water depth.

Holocene sediment accumulation patterns throughout the East Katla Ridge region are strongly influenced by this flow of Norwegian Sea source water called the Iceland-Scotland Overflow Current (ISOC). Holocene deposits up to 20 meters thick have accumulated south of the Myrdalsjokull Canyon system in South Katla Basin, and deposits of 3.1 and 4.5 meters have accumulated since 13,000 yBP at two sites east of the current axis on the east flank of East Katla Ridge. The only Holocene sediments lying beneath the main flow axis on the east flank are thin (1-10 cm.) sand layers containing a mixture of Holocene and glacial Pleistocene debris; at sites where the sand layer is absent the surface mud deposits are pre-Holocene in age. A similar thin bioturbated Holocene sandy mud layer observed atop a sediment wave on the south face of the Myrdalsjokull Canyon Levee indicates that this is also a region of winnowing by bottom currents.

Holocene turbidity currents have been relatively minor events compared with turbidity current activity of previous periods. Graded sand layers in one core from the axis of Myrdalsjokull Canyon are typically 5 to 30 cm. thick, with a single unit at the top of the core of 120 cm. Turbidites deposited in the axis of the channel emanating from Myrdalsjokull Canyon are silts containing less than 5% of sand-sized grains. These acoustically highly laminated deposits exceed 40 meters

thickness at some points in the channel axis, but there is no evidence of coarser layers in any of 6 box cores from the channel axis and adjacent acoustically transparent deposits. Only one core, located on outcropping reflectors on the south channel wall near the canyon mouth, contains significant accumulations of sandy turbidites.

The origin of two regions of highly dissected terrain, where 3.5 kHz echosounder records show hyperbolic echos, remain enigmatic. The areas lie between 1500 and 1600 meters depth on the southern end of East Katla Ridge and on a saddle crossing the southern portion of the West Katla Ridge. Overlapping hyperbolae on East Katla Ridge are similar in some respects to morphology in regions of current-eroded abyssal furrows (e.g. Flood, 1978): their location beneath the predicted axis of flow on East Katla Ridge supports such an interpretation. Alternatively, the hyperbolae may be reflections from slump scarps, which have been subsequently modified by bottom current flow.

Using the criteria of Stow and Lovell (1979) the sediments recovered from outside the fan and canyon region are "sandy" and "muddy" contourites. The 'sandy' contourites are reworked deposits containing both iron-stained and broken as well as well-preserved planktonic foraminifera plus ice-rafted rock fragments ranging upwards into the gravel size range. The modal grain size of these poorly-sorted deposits is 2 to 4 phi (1/4 to 1/16 mm.). In contrast to the descriptions of 'contourite' sands by both Hollister and Heezen (1972) and Stow and Lovell (1979), these deposits are very poorly sorted and lack primary sedimentary structures. This anomaly is thought to be due to the importance of extensive



infaunal burrowing beneath a steady flow. Such deposits are predicted to be encountered in box cores recovered from regions where flow exceeds  $20 \text{ cm sec}^{-1}$ , where benthic infauna are abundant, and where local sources of terrigenous muds allowed rapid accumulation of mud during lowered sea levels in the Pleistocene.

A second type of 'sandy contourite' is observed in the deposits in Myrdalsjokull Canyon. Clean (well-sorted) laminations of terrigenous sand alternate with pteropod-rich biogenic sand layers in laminae ranging from less than 1 to several millimeters thick. These layers are common throughout the core below 1.2 meters (a single graded unit lies above). They commonly occur in groups of 'criss-cross' beds, suggesting formations under conditions of alternating current direction.

As discussed by Stow and Lovell (1979), these deposits commonly occur at or near the top of graded turbidite units, indicating that bottom currents actively winnow canyon axis deposits between successive turbidites. The surprising abundance of pteropods (75% in some sections) is evidence for extensive removal of finer sediments, as these pelagic forms are extremely rare in cores outside the canyon.

Deposition of 'muddy contourites' occurs where measured flow is reduced to less than 10 cm/sec. The upcurrent source of the sediments is principally the region underlying the flow axis, where silt-sized and clay-sized material is removed. This source is probably augmented with the finer fraction from sporadic turbidity currents flowing down the canyons. Continuous erosion of the walls of Myrdalsjokull Canyon and winnowing of the turbidites of the canyon floor may also be an important source for these silts and clays.

Primary sedimentary structures are strikingly absent from both 'muddy' and 'sandy' contourite deposits of the Katla Ridge region. Extensive bioturbation seen in x-radiographs appears to have erased what laminations may have been developed in both the 'muddy' and 'sandy contourite' deposits.

#### B. Conclusions

The following conclusions may be drawn from this investigation concerning the geologic effects of bottom currents:

1. The Katla Ridge region of the Iceland margin is the site of both erosion and deposition due to persistent flow of bottom currents. Erosion and thin sand layer formation occurs where measured or inferred velocities exceed  $15 \text{ cm sec}^{-1}$ ; rapid deposition of fine-grained muds characterize the current margin where mean velocities of  $<10 \text{ cm sec}^{-1}$  are observed.
2. Bottom circulation is strongly influenced by the ridge and canyon morphology, which causes homogenization of bottom water properties by mixing in the canyon and broadens the dense bottom strata of the current by guiding dense mixed layers southeastwards away from the canyon mouth along the canyon levee.
3. Bioturbation of both sand and mud current deposits ('sandy' and 'muddy contourites' of Stow and Lovell, 1979) has erased primary sedimentary structures, and has introduced mud into sand layers which makes them both very poorly sorted and fine-skewed.

REFERENCES CITED

- Armi, L., 1978. Some evidence for boundary mixing in the deep ocean. Journal of Geophysical Research, 83, p. 1971-1979.
- Armi, L., and R.C. Millard, Jr., 1976. The bottom boundary layer of the deep ocean. Journal of Geophysical Research, 81, p. 4983-4990.
- Biscaye, P.E., and S.L. Eittreim (1977). Suspended particulate loads and transports in the nepheloid layer of the abyssal Atlantic Ocean. Marine Geology, 23, p. 155-172.
- Bouma, A.H., 1969. Methods for the Study of Sedimentary Structures. John Wiley and Sons, New York. 458 pp.
- Cherkis, N.Z., H.S. Fleming and R.H. Feden, 1973. Morphology and structure of Maury Channel, Northeast Atlantic Ocean. Bull. Geol. Soc. of America, 84, p. 1601-1606.
- Conseil International pour l'Exploration de la Mer, 1979. Proces-Verbal de la Reunion 1978. Charlottenlund Slot, Denmark. 146 pp.
- Crease, J., 1965. The flow of Norwegian Sea Water through the Faeroe Bank Channel. Deep-Sea Research, 12, p. 143-150.
- Damuth, J.E., 1978. Echo character of the Norwegian-Greenland Sea: Relationship to Quaternary sedimentation. Marine Geology, 28, p. 1-36.
- Damuth, J.E., and N. Kumar, 1975. Late Quaternary depositional processes on the continental rise of the western equatorial Atlantic: comparison with the western North Atlantic and implications for reservoir rock distribution. Bulletin of the American Association of Petroleum Geologists, 59, p. 2172-2181.
- Davies, T.A., and A.S. Laughton, 1972. Sedimentary processes in the North Atlantic Ocean. In A.S. Laughton, W. Berggren (editors), Initial Reports of the Deep Sea Drilling Project, 12, U.S. Government Printing Office, Washington, D.C., p. 905-934.
- Egloff, J., and G.L. Johnson, 1979. Erosional and depositional structure of the southwest Iceland insular margin: Thirteen geophysical profiles. In Watkins, J.S., L. Montadert and P.W. Dickerson (editors), Geological and Geophysical Investigations of Continental Margins, AAPG Memoir 29. Tulsa, Oklahoma. p. 43-63.
- Ellett, D.J., and D.G. Roberts, 1973. The overflow of Norwegian Sea deep water across the Wyville-Thompson Ridge. Deep-Sea Research, 20, p. 819-835.

- Ewing, J.I., and C.D. Hollister, 1972. Regional aspects of deep sea drilling in the Western North Atlantic. In C. D. Hollister, J. I. Ewing (editors), Initial Reports of the Deep Sea Drilling Project, 11. U.S. Gov't. Printing Office, Washington, D. C., p. 951-973.
- Ewing, M., S.L. Eittreim, J.I. Ewing and X. Le Pichon, 1971. Sediment transport and distribution in the Argentine Basin. 3. Nepheloid layer and processes of sedimentation. In Physics and Chemistry of The Earth, vol. 8, Pergamon Press, New York, p. 49-78.
- Field, M.E., and O.H. Pilkey, 1971. Deposition of deep sea sands: comparison of two areas of the Carolina continental rise. Journal of Sedimentary Petrology, v. 41, p. 526-536.
- Flood, R., 1978. Studies of Deep-Sea Sedimentary Microtopography in the North Atlantic Ocean. Unpublished Ph.D. dissertation, Massachusetts Institute of Technology/Woods Hole Oceanographic Institution Joint Program in Oceanography, Woods Hole, Massachusetts. 395 pp.
- Folk, R.L., and W.C. Ward, 1957. Brazos river bar: a study in the significance of grain size parameters. J. Sedimentary Petrology, 27, p. 3-26.
- Fritz, S., and O.H. Pilkey, 1975. Distinguishing bottom and turbidity current coarse layers on the continental rise. Journal of Sedimentary Petrology, 45, p. 57-62.
- Fuglister, F.C., 1960. Atlantic Ocean Atlas. Woods Hole Oceanographic Inst. Atlas Series, vol. 1. Woods Hole, Massachusetts. 209 pp.
- Gardner, W.D., 1977. Incomplete extraction of rapidly settling particles from water samplers. Limnology and Oceanography, 22, p. 764-768.
- Garner, D.M., 1972. Flow through the Charlie-Gibbs Fracture Zone, Mid-Atlantic Ridge. Canadian Journal of Earth Science, 9, p. 116-121.
- Heezen, B.C., C.D. Hollister and W.F. Ruddiman, 1966. Shaping of the continental rise by deep geostrophic contour currents. Science, 152, p. 502-508.
- Herman, Y., 1971. Vertical and horizontal distribution of pteropods in Quaternary sequences. In Funnell, B.M., and W.R. Riedel (editors), Micropaleontology of the Oceans. Cambridge University Press, Cambridge, England, p. 463-486.
- Herman, Y., and P.E. Rosenberg, 1969. Pteropods as bathymetric indicators. Marine Geology, 7, p. 169-173.

- Hermann, F., 1967. The T-S diagram analysis of the water masses over the Iceland-Faroe Ridge and in Faroe Bank Channel. In Tait, J.B. (editor), The Iceland-Faroe Ridge International (ICES) "OVERFLOW" Expedition, May-June, 1960 (Rapports et Proces-Verbaux des Reunions, 157). Conseil Permanent International pour l'Exploration de la Mer. Copenhagen, Denmark. p. 139-149.
- Hollister, C.D., 1967. Sediment distribution and deep circulation in the Western North Atlantic. Unpublished Ph.D. Dissertation, Columbia University, New York.
- Hollister, C.D., 1973. Atlantic continental shelf and slope of the United States -- texture of surface sediments from New Jersey to Southern Florida. USGS Professional Paper 529M. 23 pp.
- Hollister, C.D. and B.C. Heezen, 1972. Geologic effects of ocean bottom currents: Western North Atlantic. In A. Gordon, ed., Studies in Physical Oceanography, Gordon and Breach, London, Vol. II, p. 37-66.
- Hollister, C.D., W.D. Gardner, P.F. Lonsdale and D.W. Spencer, 1976. New evidence for northward flowing bottom water along the Hatton sediment drift, eastern North Atlantic, (abstract) EOS, v. 57, p. 261.
- Hollister, C.D., D.A. Johnson and P.F. Lonsdale, 1974. Current-controlled abyssal sedimentation: Samoan Passage, Equatorial West Pacific. Journal of Geology, 82, p. 275-300.
- Ivers, W.D., 1975. The deep circulation in the northern North Atlantic, with especial reference to the Labrador Sea. Unpublished Ph.D. dissertation, Scripps Institution of Oceanography. 179 pp.
- Johnson, D.A., S.E. McDowell, L.G. Sullivan and P.E. Biscaye, 1976. Abyssal hydrography, nephelometry, currents, and benthic boundary layer structure in the Vema Channel, Jour. Geophys. Res., 81, p. 5771-5786.
- Johnson, D.A., and A.N. Shor, 1977. Initial Cruise Report, Atlantis II-94, Leg 1 (Woods Hole Oceanographic Institution Technical Report 77-70). 57 pp. (unpublished manuscript).
- Johnson, G.L., and G. Palmason, in preparation. Observations of the morphology and structure of the sea floor south of Iceland.
- Johnson, G.L., and E.D. Schneider, 1969. Depositional ridges in the North Atlantic. Earth and Planetary Science Letters, 6, p. 416-422.
- Johnson, G.L., P.R. Vogt and E.D. Schneider, 1971. Morphology of the Northeastern Atlantic and Labrador Sea. Deutsche Hydrographische Zeitschrift, 24, p. 49-73.

- Jones, E.J.W., M. Ewing, J.I. Ewing and S.L. Eittreim, 1970. Influence of Norwegian Sea overflow water on sedimentation in the northern North Atlantic and Labrador Sea. Journal of Geophysical Research, 74, p. 1655-1680.
- Kellogg, T., 1976. Late Quaternary climatic changes: Evidence from deep-sea cores of Norwegian and Greenland Seas. In Cline, R.M., and J.D. Hays (editors), Investigation of Late Quaternary Paleoceanography and Paleoclimatology. Geological Society of America Memoir 145, p. 77-110.
- Kellogg, T., 1977. Paleoclimatology and paleo-oceanography of the Norwegian and Greenland Seas: the last 450,000 years. Marine Micropaleontology, 2, p. 235-249.
- Kipp, N., 1976. In Cline, R.M., and J.D. Hays (editors), Investigation of Late Quaternary Paleoceanography and Paleoclimatology. Geological Society of America Memoir 145, p.
- Laine, E.P., 1977. Geological effects of the Gulf Stream system in the North American Basin. Unpublished doctoral dissertation, Massachusetts Institute of Technology/Woods Hole Oceanographic Institution Joint Program in Oceanography, Woods Hole, Massachusetts. 147 pp.
- Laughton, A.S., W.A. Berggren, et al., 1972. Initial Reports of the Deep Sea Drilling Project, 12, Washington (U.S. Government Printing Office), 1243 p.
- Lee, A., and D. Ellett, 1967. On the water masses of the northwest Atlantic Ocean. Deep-Sea Research, 14, 183-190.
- Lonsdale, P.F., and C.D. Hollister, 1979 (in press). Cut-offs at an abyssal meander. Journal of Sedimentary Petrology.
- Lonsdale, P.F., and J.B. Southard, 1974. Experimental erosion of North Pacific red clay. Marine Geology, 17, p. M51-M60.
- Luyendyk, B.P., A.N. Shor and J.R. Cann, 1978. General implications of the Leg 49 drilling program for North Atlantic Ocean geology. In Luyendyk, B.P. and J.R. Cann (editors), Initial Reports of the Deep Sea Drilling Project, 49, Washington (U.S. Government Printing Office), p. 825-839.
- Malmberg, S.-A., 1974. A note on the deep water south of Iceland -- "Overflow '73". ICES Ref. C.M. 1974/c:32 (unpublished manuscript).
- McElhinny, M.W., 1973. Palaeomagnetism and Plate Tectonics. Cambridge University Press, Cambridge, England. 358 pp.
- McIntyre, A., W.F. Ruddiman and R. Jantzen, 1972. Southward penetrations of the North Atlantic Polar Front: faunal and floral evidence of large-scale surface watermass movements over the last 225,000 years. Deep-Sea Research, 19, p. 61-77.

- Meincke, J., 1978. On the distribution of low salinity intermediate waters around the Faroes. Deutsche Hydrographische Zeitschrift.
- Parsons, B., and J.G. Sclater, 1977. An analysis of the variation of ocean floor bathymetry and heat flow with age. Journal of Geophysical Research, 82, p. 803-827.
- Phleger, F.B., F.L. Parker and J.F. Peirson, 1954. North Atlantic Foraminifera (Reports of the Swedish Deep-Sea Expedition, v. VII). Elanders Boktryckeri Aktiebolag, Goteborg (Sweden), 122 pp.
- Ruddiman, W.F., 1972. Sediment redistribution on the Reykjanes Ridge: seismic evidence. Geological Society of America Bulletin, 83, p. 2039-2062.
- Ruddiman, W.F., and F.A. Bowles, 1976. Early interglacial bottom-current sedimentation on the eastern Reykjanes Ridge. Marine Geology, 21, p. 191-210.
- Ruddiman, W.F., and L.K. Glover, 1972. Vertical mixing of ice-rafted volcanic ash in North Atlantic sediments. Bull. Geol. Soc. Amer., 83, p. 2187-2836.
- Ruddiman, W.F., and L.K. Glover, 1975. Subpolar North Atlantic circulation at 9300 yrs. BP: faunal evidence. Jour. Quat. Res., 5, p. 361-389.
- Ruddiman, W.F., and A. McIntyre, 1973. Time-transgressive deglacial retreat of polar waters from the North Atlantic. Jour. Quat. Res., 3, p. 117-130.
- Ruddiman, W.F., C.D. Sancetta and A. McIntyre, 1977. Glacial/Interglacial response rate of subpolar North Atlantic waters to climatic change: the record in oceanic sediments. Phil. Trans. R. Soc. Lond., B, 280, 119-142.
- Schick, G.B., J.D. Isaacs, and M.H. Sessions, 1968. Autonomous instruments in oceanographic research. Marine Sciences Instrumentation, 4, Plenum Press, New York, 203-230.
- Schlee, J., 1966. A modified Woods Hole rapid sediment analyzer. Journal of Sedimentary Petrology, 36, p. 403-413.
- Shor, A.N., 1978. Bottom currents on East Katla Ridge, NW Iceland Basin. ICES Ref. C.M. 1978/c.60 (unpublished ms.).
- Shor, A.N., P. Lonsdale, C.D. Hollister and D. Spencer, 1980 (in press). Charlie-Gibbs Fracture Zone: Bottom-water transport and its geological effects. Deep-Sea Research.
- Shor, A.N., and R.Z. Poore, 1978. Bottom currents and ice rafting in the North Atlantic: Interpretation of Neogene depositional environments of Leg 49 cores. In Luyendyk, B.P., and J.R. Cann (editors), Initial Reports of the Deep Sea Drilling Project, 49. Washington, D.C. (U.S. Government Printing Office). p. 859-872.

- Southard, J.B., R.A. Young and C.D. Hollister, 1971. Experimental erosion of calcareous ooze. Journal of Geophysical Research, 76, p. 5903-5909.
- Stanley, D.J., H. Sherig, and C.P. Pedraza, 1971. Lower continental rise east of the Middle Atlantic States: predominant sediment dispersal perpendicular to isobaths. Bull. Geol. Soc. Amer., 82, p. 1831-1840.
- Stanley, L.T., and H.J. Gray, 1973. Practical Statistics for Petroleum Engineers. Petroleum Engineering Co., Tulsa, Oklahoma. 150 pp.
- Steele, J.H., J.R. Barrett, and L.V. Worthington, 1962. Deep currents south of Iceland. Deep-Sea Research, 9, p. 465-474.
- Stow, D.A.V., and J.P.B. Lovell, 1979. Contourites: their recognition in modern and ancient sediments. Earth Science Reviews, 14, p. 251-291.
- Talwani, M., D. Hayes, W. Pitman and T. Aitken, 1974. Underway Marine Geophysical Data in the North Atlantic June 1961 - January 1971, Parts C, D. Lamont-Doherty Geol. Obs., Palisades, N.Y.
- Thorndike, E.M., 1975. A deep sea photographic nephelometer. Ocean Engineering, 3, p. 1-15.
- Vogt, P.R., and O.E. Avery, 1974. Detailed magnetic surveys in the northeast Atlantic and Labrador Sea. Journal of Geophysical Research, 79, p. 317-424.
- Weyl, P.K., 1968. The role of the oceans in climatic change: a theory of the ice ages. In Mitchell, J.M. (editor), Causes of Climatic Change (Meteorological Monographs, 8), Boston (American Meteorological Society), p. 37-62.
- Worthington, L.V., 1970. The Norwegian Sea as a mediterranean basin. Deep-Sea Research, 17, p. 77-84.
- Worthington, L.V., and G.H. Volkmann, 1965. The volume transport of the Norwegian Sea overflow water in the North Atlantic. Deep-Sea Research, 12, p. 667-676.
- Worthington, L.V., and W.R. Wright, 1970. North Atlantic Ocean Atlas (WHOI Atlas Series, vol. 2), Woods Hole Oceanographic Inst., Woods Hole, Massachusetts.
- Zimmerman, H.B., 1971. Sedimentary Environments and Processes of the Continental Rise, Southeast of New England. Unpublished doctoral dissertation. University of Rhode Island, Kingston, R.I. 121 pp.



APPENDIX I: Station Locations

APPENDIX I  
TABLE AI - 1: CTD Stations

<u>STATION</u>	<u>CTD NO.</u>	<u>DATE</u>	<u>TIME (GMT)</u>	<u>DEPTH (m)</u>	<u>LATITUDE</u>	<u>LONGITUDE</u>
17	7	27 June	1016-1151	1183	62°34.0'N	18°13.0'W
19	8	27 June	1633-1800	1395	62°31.4'N	18°04.4'W
22	9	27 June	2323-0130	1598	62°28.7'N	17°53.1'W
25	10	30 June	0055-0244	1796	62°23.1'N	17°44.1'W
28	11	30 June	0912-1125	1989	62°18.3'N	17°24.8'W
30	12	30 June	1554-2035	2167	62°11.7'N	17°04.5'W
32	13	1 July	0935-1200	2310	61°43.4'N	15°40.2'W
34	14	1 July	1843-2115	2276	61°51.1'N	16°09.8'W
37	15	2 July	2105-2306	2207	62°04.0'N	16°38.7'W
38	16	2 July	2315-0018	2199	62°05.2'N	16°38.5'W
40	17	3 July	2028-2137	1984	62°18.6'N	17°21.6'W
46	18	4 July	1145-1248	1696	62°25.5'N	17°45.7'W
53	19	5 July	1523-1644	2175	61°43.5'N	18°39.9'W
54	20	5 July	1647-1704	2173	61°43.8'N	18°39.4'W
58	21	6 July	0145-0321	2165	61°53.1'N	18°48.6'W
62	22	6 July	1539-1705	2082	62°08.8'N	19°05.0'W
65	23	6 July	2315-0149	1561	62°11.7'N	19°21.3'W
67	24	7 July	0643-0827	1522	61°57.0'N	19°26.7'W
68	25	7 July	1040-1235	1841	61°44.7'N	19°04.3'W
70	26	7 July	1707-1932	2237	61°31.5'N	19°19.9'W
72	27	8 July	0057-0305	2096	61°33.8'N	18°47.9'W
74	28	8 July	0653-0937	2300	61°25.0'N	18°31.8'W
75	29	8 July	1130-1333	2433	61°10.8'N	18°14.0'W
76	30	8 July	1530-1735	2501	60°54.3'N	17°51.1'W
81	31	10 July	0030-0230	1851	62°25.8'N	18°41.6'W
84	32	10 July	2020-2130	1991	62°18.4'N	17°25.3'W

APPENDIX I  
TABLE AI - 2: Nephelometer stations

<u>STATION</u>	<u>CTD NO.</u>	<u>DATE</u>	<u>TIME (GMT)</u>	<u>DEPTH (m)</u>	<u>LATITUDE</u>	<u>LONGITUDE</u>
17	5	27 June	1016-1151	1183	62°34.0'N	18°13.0'W
19	6	27 June	1620-1839	1395	62°31.4'N	18°04.4'W
22	7	27 June	2326-0130	1598	62°28.2'N	17°54.0'W
25	8	30 June	0057-0244	1796	62°23.8'N	17°42.9'W
28	9	30 June	0912-1130	1989	62°18.3'N	17°24.8'W
30	10	30 June	1544-2030	2169	62°11.7'N	17°04.5'W
32	11	1 July	0935-1200	2310	61°42.9'N	15°40.1'W
33	12	1 July	1454-1810	2274	61°51.6'N	16°10.6'W
34	13	1 July	1852-2115	2276	61°51.1'N	16°09.8'W
37	14	2 July	2105-2306	2207	62°04.3'N	16°38.4'W
39	15	3 July	0200-0451	2165	62°10.5'N	17°06.6'W
40	16	3 July	2028-2137	1984	62°18.6'N	17°21.6'W
53	18	5 July	1523-1644	2175	61°43.5'N	18°39.9'W
58	19	6 July	0145-0321	2165	61°53.1'N	18°48.2'W
62	20	6 July	1539-1705	2082	62°08.8'N	19°05.0'W
65	21	6/7 July	2315-0149	1561	62°11.7'N	19°21.3'W
66	22	7 July	0250-0429	1535	62°10.3'N	19°16.3'W
67	23	7 July	0643-0827	1522	61°57.0'N	19°26.7'W
68	24	7 July	1040-1235	1841	61°44.7'N	19°04.3'W
70	25	7 July	1707-1932	2237	61°31.5'N	19°19.9'W
72	26	8 July	0057-0305	2096	61°33.8'N	18°47.9'W
74	27	8 July	0653-0937	2300	61°25.0'N	18°31.8'W
75	28	8 July	1130-1333	2433	61°10.8'N	18°14.0'W
76	29	8 July	1530-1735	2501	60°54.3'N	17°51.1'W
81	30	10 July	0030-0230	1851	62°25.8'N	18°41.6'W
84	31	10 July	2020-2130	1991	62°18.4'N	17°25.3'W

APPENDIX I  
TABLE AI - 3: Hydrocasts

<u>STATION</u>	<u>HYDRO- CAST</u>	<u>DATE</u>	<u>TIME (GMT)</u>	<u>DEPTH (m)</u>	<u>LATITUDE</u>	<u>LONGITUDE</u>
18	1	27 June	1200-1538	118	62°33.6'N	18°13.9'W
20	2	27 June	1813-2016	1387	62°30.7'N	18°05.0'W
23	3	28 June	0154-0340	1544	62°29.0'N	17°57.5'W
26	4	30 June	0252-0443	1798	62°21.9'N	17°48.8'W
29	5	30 June	1213-1418	1993	62°18.0'N	17°23.9'W
31	6	1 July	0654-0931	2310	61°42.9'N	15°40.7'W
33	7	1 July	1504-1810	2276	61°52.0'N	16°10.1'W
36	8	2 July	1720-2041	2214	62°04.3'N	16°43.4'W
39	9	3 July	0200-0451	2165	62°10.5'N	17°06.6'W
40	10	3 July	2033-2230	1984	62°18.6'N	17°21.6'W
47	11	4 July	1330-1610	1700	62°23.9'N	17°50.2'W
55	12	5 July	1724-1950	2171	61°43.8'N	18°39.5'W
59	13	6 July	0321-0555	2119	61°54.0'N	18°49.5'W
63	14	6 July	1800-2020	2082	62°08.0'N	19°03.6'W
65	15	6/7 July	2315-0149	1561	62°11.7'N	19°21.3'W
67	16	7 July	0643-0827	1522	61°57.0'N	19°26.7'W
68	17	7 July	1040-1235	1841	61°44.7'N	19°04.3'W
70	18	7 July	1707-1932	2237	61°31.5'N	19°19.9'W
72	19	8 July	0057-0305	2096	61°33.8'N	18°47.9'W
74	20	8 July	0653-0937	2300	61°25.0'N	18°31.8'W
75	21	8 July	1130-1333	2433	61°10.8'N	18°14.0'W
76	22	8 July	1530-1735	2501	60°54.3'N	17°51.1'W
81	23	10 July	0030-0230	1851	62°25.8'N	18°41.6'W
85	24	10 July	2130-0046	1993	62°17.5'N	17°25.6'W

APPENDIX I  
TABLE AI - 4: Camera Stations

<u>STATION</u>	<u>CAMERA NO.</u>	<u>DATE</u>	<u>TIME (GMT)</u>	<u>DEPTH (m)</u>	<u>LATITUDE</u>	<u>LONGITUDE</u>	<u>REMARKS</u>
18	3	27 June	1200-1537	1194	62°33.6'N	18°13.8'W	3 Exposures
20	4	27 June	1810-2016	1387	62°31.0'N	18°04.3'W	Camera failed
26	5	30 June	0251-0443	1798	62°22.1'N	17°47.6'W	Camera failed
31	6	1 July	0654-0931	2311	61°42.9'N	15°40.7'W	4 Exposures
36	7	2 July	1720-2041	2211	62°04.3'N	15°43.4'W	7 Exposures
39	8	3 July	0200-0451	2162	62°10.5'N	17°06.6'W	13 Exposures
47	9	4 July	1310-1610	1732	62°23.9'N	17°50.2'W	3 Exposures
55	10	5 July	1724-1950	2173	61°43.8'N	18°39.5'W	5 Exposures
59	11	6 July	0321-0555	2145	61°54.0'N	18°49.5'W	2 Exposures
63	12	6 July	1800-2020	2082	62°08.0'N	19°03.6'W	1 Exposure
66	13	7 July	0250-0429	1535	62°10.3'N	19°16.4'W	4 Exposures

APPENDIX I  
 TABLE AI - 5: Current Meters

<u>STATION</u>	<u>CURRENT METER</u>	<u>TIME DEPLOYED (GMT)</u>	<u>TIME RECOVERED</u>	<u>DEPTH (m)</u>	<u>HEIGHT ABOVE BOTTOM</u>	<u>LOCATION</u>
11	1	2300/June 26	1900/July 3	2000 m	10 m	62°17.6'N 17°24.6'W
13	2	0400/June 27	1330/July 3	1600 m	10 m	62°28.3'N 17°52.0'W
15	3	0820/June 27	1000/July 3	1177 m	10 m	62°34.9'N 18°14.7'W
42	4	0300/July 4	1800/July 10	2171 m	10 m	62°11.0'N 17°04.0'W
44	5	0825/July 4	1200/July 10	1796 m	10 m	62°23.2'N 17°42.0'W
49	6	1930/July 4	0800/July 10	1393 m	10 m	62°30.9'N 18°05.4'W

APPENDIX I  
TABLE AI - 6: Sediment Trap Moorings

<u>STATION</u>	<u>MOORING NO.</u>	<u>TIME DEPLOYED (GMT)</u>	<u>TIME RECOVERED</u>	<u>DEPTH (m)</u>	<u>LOCATION.</u>	<u>HEIGHT OF TRAPS ABOVE BOTTOM (m)</u>
12	1	0200/June 27	1500/July 10	1971	62°18.6'N 17°26.2'W	13,103,503
14	2	0630/June 27	1500/July 3	1596	62°28.5'N 17°53.8'W	13,103,493
51	3	1153/July 5	1200/July 9	2146	61°45.4'N 18°39.2'W	13,14,54,104, 494

APPENDIX I  
Table AI - 7: Piston Cores

<u>STATION</u>	<u>CORE No.</u>	<u>DEPTH (m)</u>	<u>LATITUDE</u>	<u>LONGITUDE</u>	<u>PISTON Sample (cm)</u>	<u>PILOT Sample (cm)</u>
16	1-PC	1177	62°34.6'N	18°14.0'W	845	18
27	2-PC	1764	62°24.0'N	17°46.7'W	970	12
35	3-PC	2199	62°05.9'N	16°37.3'W	1010	67
41	4-PC	2114	62°18.4'N	17°08.6'W	1170	136
45	5-PC	1596	62°28.5'N	17°54.1'W	1132	155
50	6-PC	1369	62°31.2'N	18°05.5'W	1138	0
52	7-PC	2173	61°44.2'N	18°40.9'W	814	148
					(Flow-in only)	
57	8-PC	2088	61°53.2'N	18°48.1'W	481	0
61	9-PC	2082	62°07.6'N	19°02.5'W	721	0
64	10-PC	1555	62°09.9'N	19°19.8'W	1128	9
69	11-PC	2205	61°32.0'N	19°21.9'W	1084	49
71	12-PC	2295	61°28.7'N	19°24.4'W	1147	141

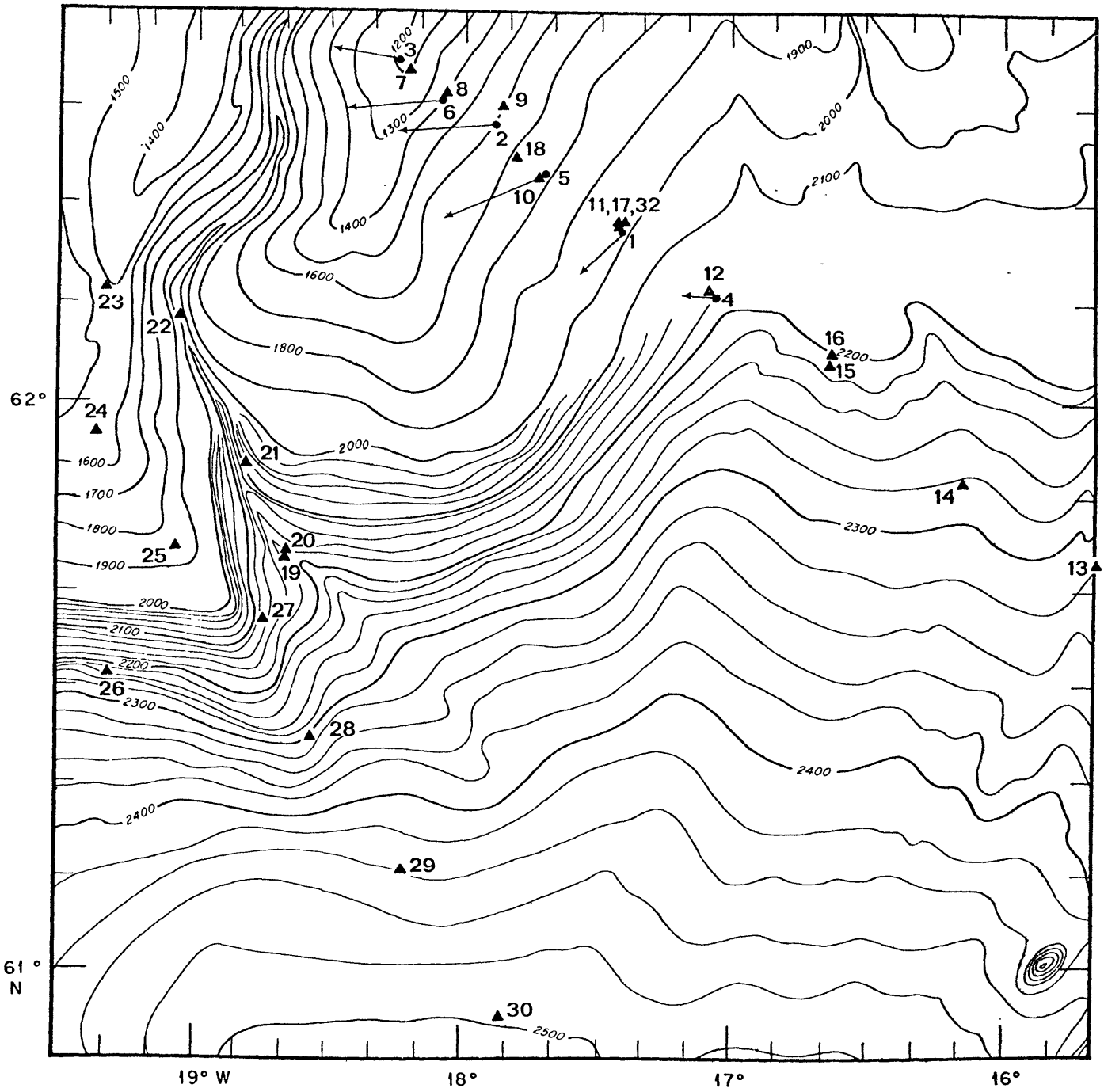


APPENDIX I  
TABLE AI - 8: Box Cores

<u>STATION</u>	<u>CORE No.</u>	<u>DEPTH (m)</u>	<u>LATITUDE</u>	<u>LONGITUDE</u>	<u>REMARKS</u>
21	2-BC	1391	62°30.4'N	18°06.4'W	1 kg sample
24	3-BC	1509	62°29.6'N	17°59.3'W	26 cm sample
43	4-BC	1839	62°22.5'N	17°35.8'W	
48	5-BC	1687	62°26.3'N	17°50.3'W	10 cm sample
56	6-BC	2175	61°44.0'N	18°39.0'W	
60	7-BC	2128	61°50.3'N	18°47.9'W	
73	8-BC	2203	61°31.0'N	18°46.5'W	
77	9-BC	2205	61°41.0'N	18°25.1'W	
78	10-BC	2248	61°40.5'N	18°27.2'W	
79	11-BC	2154	61°41.2'N	18°39.9'W	
80	12-BC	2133	61°45.6'N	18°37.0'W	
82	13-BC	1198	62°33.2'N	18°14.3'W	½ kg sample
83	14-BC	1409	62°31.8'N	18°02.0'W	1 kg sample
86	15-BC	1998	62°17.6'N	17°25.1'W	

(Note: Cores 2BC, 5BC, 13BC, and 14BC were stored in bags on board ship.)

FIGURE A1-1: Station locations: Current meters, CTD lowerings. Cruise AII-94-1.



● CURRENT METERS

▲ CTD PROFILES

CURRENT VELOCITY  
(cm/sec)

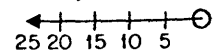


FIGURE AI-2: Station locations: Nephelometer, hydrographic lowerings, sediment trap moorings. Cruise AII-94-1.

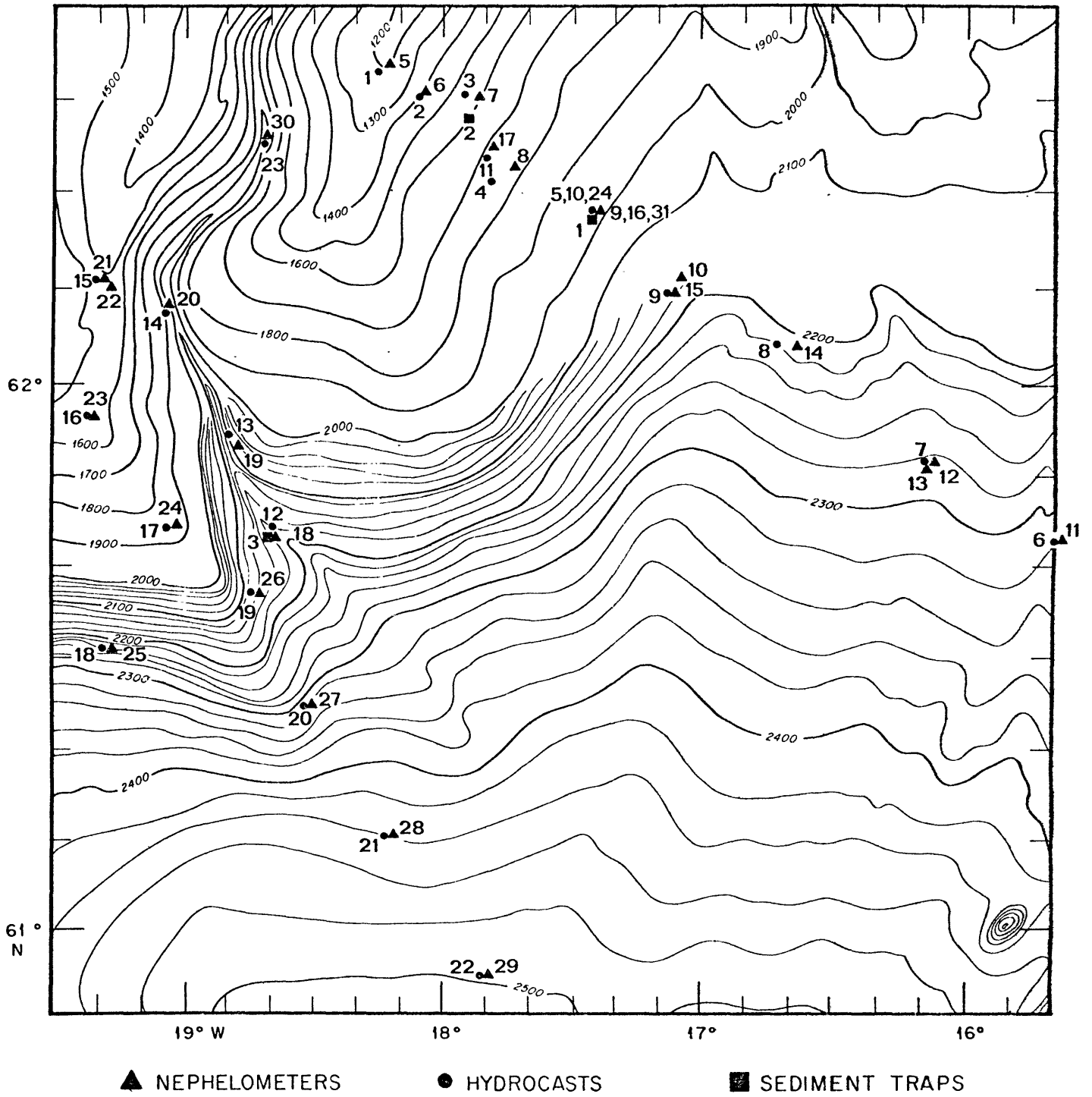
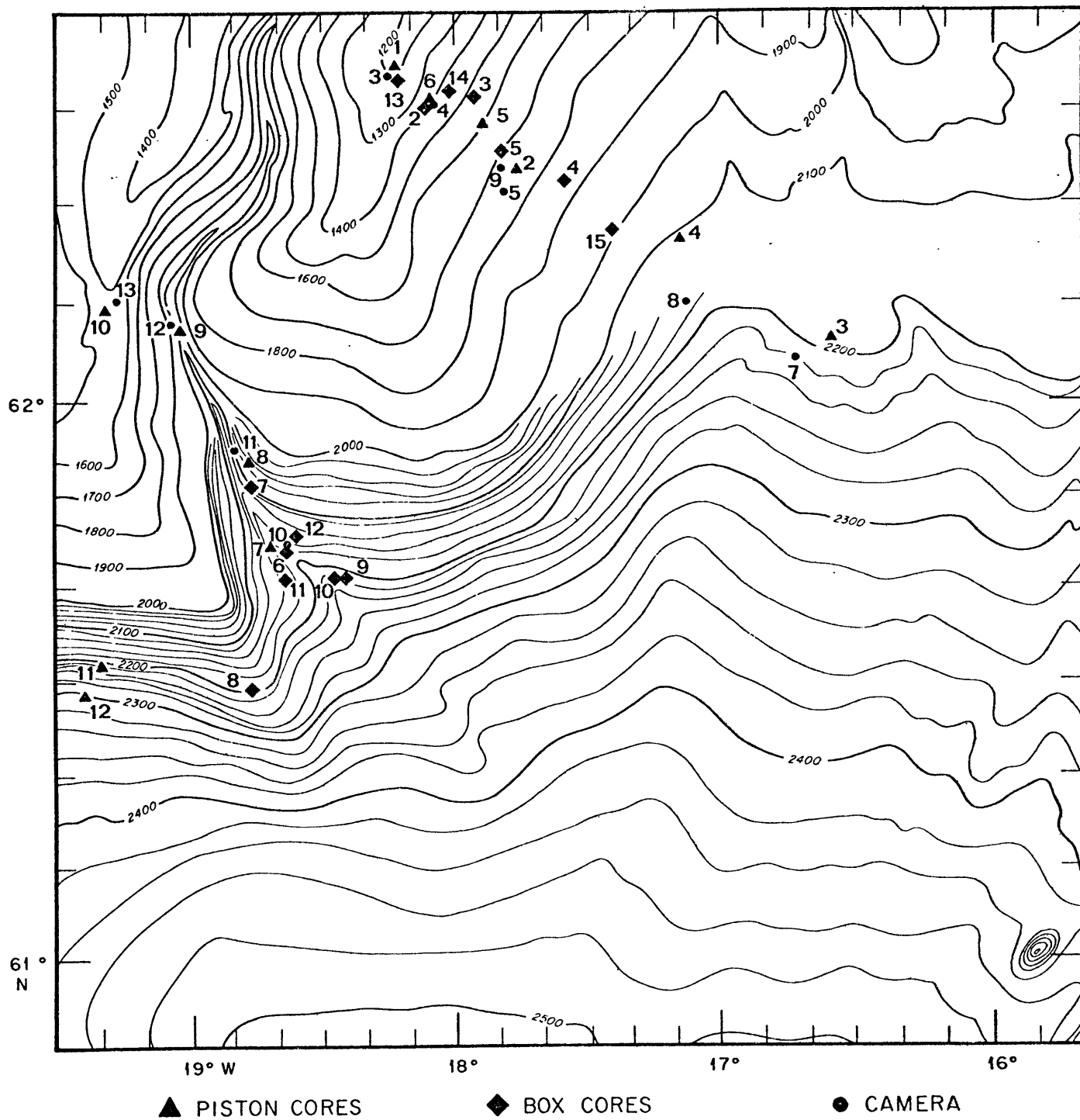


FIGURE AI-3: Station locations: Piston cores, box cores, camera lower-  
ings. Cruise AII-94-1.



APPENDIX II: Flow Calculations



TABLE AII-1: Station Information for Calculations

<u>CTD Station Pair</u>	<u>Station Separation (kms.)</u>	<u>Sine of Latitude</u>	<u>Mean Reference Pressure</u>
7- 8	8.9	.8874	924 db.
8- 9	10.3	.8870	1012
9-10	13.2	.8865	1157
10-32	17.9	.8858	1272
32-12	21.3	.8850	1343
12-15	26.3	.8840	1389
15-14	33.3	.8826	1432
14-13	30.1	.8812	1618
13-30	151.4	.8773	1592
7-31	30.5	.8870	998
31-23	32.1	.8855	1065
23-24	27.4	.8835	1038
24-25	30.8	.8817	1136
25-27	23.2	.8801	1227
27-28	22.1	.8787	1223
28-29	31.0	.8771	1251
29-30	37.2	.8750	1408

TABLE AII-2: Velocity calculations

PRESSURE (dbs.)	CTD STATION PAIRS							
	<u>7-8</u>	<u>8-9</u>	<u>9-10</u>	<u>10-32</u>	<u>32-12</u>	<u>12-15</u>	<u>15-14</u>	<u>14-13</u>
25	-0.2	21.1	18.5	5.1	14.5	-2.5	-1.4	10.0
75	-0.6	21.2	18.1	5.1	13.7	-0.4	-2.2	10.5
125	-1.1	21.9	17.5	4.5	12.1	1.0	-2.3	10.4
175	-0.4	21.7	17.4	3.6	10.4	2.4	-2.3	10.2
225	0.8	21.2	17.4	2.7	9.2	3.4	-2.4	10.0
275	1.8	20.6	17.4	2.0	8.0	4.1	-2.4	9.7
325	3.1	20.0	17.4	1.4	7.1	4.7	-2.4	9.3
375	4.3	19.4	17.4	0.9	6.2	5.0	-2.4	9.0
425	5.6	18.7	17.2	0.4	5.5	5.3	-2.4	8.6
475	7.0	17.8	17.1	-0.4	4.8	5.6	-2.4	8.2
525	8.1	16.8	16.9	-1.0	4.2	5.7	-2.3	7.7
575	8.9	15.7	16.5	-1.6	3.6	5.7	-2.2	7.2
625	9.0	14.4	16.0	-2.1	3.2	5.5	-1.9	6.7
675	8.5	13.1	15.2	-2.3	2.8	5.2	-1.6	6.2
725	7.3	11.6	14.5	-2.6	2.5	4.7	-1.2	5.7
775	5.8	9.6	13.5	-2.7	2.3	4.1	-0.8	5.3
825	4.3	7.7	12.4	-2.6	2.2	3.4	-0.4	4.8
875	0.6	5.6	11.3	-2.3	2.0	2.7	0.0	4.3
925	0.0	3.5	9.9	-1.9	1.9	2.1	0.3	3.9
975	-1.4	1.5	8.0	-1.5	1.8	1.6	0.5	3.4
1025	-2.0	-0.5	6.2	-1.1	1.8	1.1	0.7	3.1
1075	-1.8	-2.4	4.2	-0.7	1.5	0.7	0.8	2.8
1125	-0.9	-4.0	1.6	-0.3	1.2	0.4	0.8	2.6
1175	-0.3	-5.0	-0.9	-0.1	0.9	0.2	0.8	2.4
1225		-5.1	-4.0	0.0	0.6	0.1	0.8	2.2
1275		-3.8	-7.8	0.0	0.4	0.0	0.7	1.9
1325		-2.4	-11.1	-0.4	0.1	0.0	0.4	1.7
1375		-0.8	-13.8	-1.4	-0.2	0.0	0.2	1.4
1425			-15.8	-2.9	-0.5	0.0	0.0	1.1
1475			-17.1	-5.0	-0.7	0.0	-0.2	0.9
1525			-18.2	-7.3	-1.1	0.0	-0.4	0.6
1575			-19.1	-10.0	-1.4	-0.1	-0.7	0.3
1625				-13.0	-1.7	-0.1	-0.9	0.0
1675				-16.3	-2.0	-0.3	-1.2	-0.3
1725				-19.9	-2.1	-0.6	-1.6	-0.7
1775				-24.0	-2.3	-1.0	-2.1	-0.9
1825					-2.5	-1.6	-2.7	-1.2
1875					-3.1	-2.3	-3.3	-1.5
1925					-4.3	-2.7	-4.2	-1.7
1975					-6.0	-3.1	-5.1	-1.9
2025						-3.5	-6.2	-2.2
2075						-3.7	-7.6	-2.5
2125						-3.8	-9.0	-3.0
2175							-10.2	-3.7
2225							-11.3	-4.8

TABLE AII-2: Velocity calculations, continued.

PRESSURE (dbs.)	CTD STATION PAIRS							
	23-24	24-25	25-27	27-28	28-29	29-30	7-31	31-23
25	-2.3	16.4	-3.9	-6.8	14.0	2.8	11.7	-3.3
75	-1.1	15.9	-5.1	-5.8	13.4	2.3	11.4	-3.7
125	-0.8	15.5	-6.2	-5.7	13.2	2.4	11.1	-3.7
175	-0.9	15.1	-7.3	-5.8	13.1	2.4	10.9	-3.6
225	-0.9	14.8	-8.3	-5.9	13.0	2.5	10.8	-3.5
275	-1.0	14.6	-9.3	-6.0	12.7	2.6	10.6	-3.4
325	-1.1	14.3	-10.0	-6.3	12.4	2.6	10.5	-3.2
375	-1.2	14.1	-10.6	-6.6	11.9	2.7	10.4	-3.1
425	-1.3	13.9	-10.9	-6.8	11.2	2.7	10.2	-2.9
475	-1.3	13.6	-11.0	-6.8	10.5	2.6	10.0	-2.7
525	-1.4	13.3	-11.0	-6.8	9.8	2.3	9.8	-2.6
575	-1.4	12.8	-10.8	-6.5	9.1	2.0	9.4	-2.4
625	-1.3	12.1	-10.5	-6.1	8.2	1.7	8.8	-2.3
675	-1.3	11.3	-9.7	-5.7	7.3	1.4	8.0	-2.1
725	-1.1	10.2	-8.6	-5.2	6.4	1.2	7.0	-1.9
775	-0.9	9.0	-7.3	-4.5	5.4	1.1	5.8	-1.7
825	-0.7	7.5	-6.0	-3.6	4.5	1.0	4.6	-1.4
875	0.5	6.0	-4.7	-2.8	3.6	0.8	3.2	-1.1
925	-0.2	4.6	-3.5	-2.1	2.9	0.6	1.7	-0.7
975	-0.1	3.3	-2.4	-1.5	2.3	0.5	0.4	-0.4
1025	0.0	2.1	-1.5	-1.0	1.8	0.3	-0.5	-0.2
1075	-0.1	1.1	-0.9	-0.6	1.3	0.2	-1.2	0.1
1125	-0.1	0.2	-0.3	-0.4	0.9	0.2	-1.9	0.3
1175	-0.3	-0.5	-0.1	-0.2	0.5	0.1	-2.5	0.5
1225	-0.3	-1.1	0.0	0.0	0.2	0.0		0.4
1275	-0.3	-1.6	-0.1	0.1	-0.2	0.0		0.4
1325	-0.4	-2.0	-0.4	0.1	-0.5	0.0		0.6
1375	-0.7	-2.4	-1.0	0.1	-0.8	0.0		0.9
1425	-0.9	-2.8	-1.7	0.0	-1.0	0.0		1.2
1475	-1.0	-3.2	-2.6	0.0	-1.3	-0.1		1.3
1525	-1.1	-3.6	-3.7	0.2	-1.5	-0.1		1.6
1575			-5.0	-0.4	-1.8	-0.1		
1625			-6.4	-0.7	-2.0	-0.1		
1675			-8.0	-1.1	-2.2	-0.2		
1725			-9.5	-1.7	-2.5	-0.2		
1775			-11.2	-2.2	-2.8	-0.2		
1825			-13.1	-3.0	-3.1	-0.3		
1875				-4.0	-3.4	-0.4		
1925				-5.2	-3.7	-0.5		
1975				-6.6	-3.9	-0.7		
2025				-8.3	-4.1	-0.9		
2075				-10.2	-4.5	-1.2		
2125					-4.8	-1.6		
2175					-5.2	-2.1		
2225					-5.8	-2.6		
2275					-6.5	-3.2		
2325					-7.3	-3.8		
2375						-4.6		
2425						-5.7		

TABLE AII-3: Volume transport below reference level (in  $10^3 \text{ m}^3 \text{ sec}^{-1}$ ).

Pressure (dbs.)	CTD STATION PAIRS							
	<u>7-8</u>	<u>8-9</u>	<u>9-10</u>	<u>10-32</u>	<u>32-12</u>	<u>12-15</u>	<u>15-14</u>	<u>14-13</u>
925	0.0							
975	-6.2							
1025	-8.9	-2.7						
1075	-8.1	-12.4						
1125	-3.9	-20.5						
1175	-1.2	-25.9	-5.7					
1225		-26.3	-26.7					
1275		-19.7	-51.5					
1325		-12.4	-73.1	-3.9				
1375		-4.3	-91.2	-12.4	-1.9			
1425			-104.4	-26.0	-5.0			
1475			-112.6	-44.5	-7.8	0.0	-3.5	
1525			-119.9	-65.4	-11.3	-0.4	-7.3	
1575			-126.1	-89.4	-15.1	-0.8	-11.3	
1625				-116.5	-18.2	-1.6	-15.5	-0.5
1675				-145.6	-20.9	-4.0	-20.7	-4.7
1725				-178.5	-22.1	-7.4	-26.8	-9.8
1775				-214.5	-24.1	-13.2	-34.6	-13.7
1825					-26.7	-20.9	-44.3	-18.4
1875					-33.3	-29.9	-55.6	-22.6
1925					-46.1	-35.6	-70.3	-25.7
1975					-63.6	-41.2	-85.4	-29.2
2025						-46.2	-103.4	-32.7
2075						-48.9	-126.4	-37.8
2125						-50.1	-149.7	-44.4
2175							-170.2	-55.7
2225							-187.7	-71.9

TABLE AII-3: Volume transport, continued

PRESSURE (dbs.)	CTD STATION PAIRS							
	<u>23-24</u>	<u>24-25</u>	<u>25-27</u>	<u>27-28</u>	<u>28-29</u>	<u>29-30</u>	<u>7-31</u>	<u>31-23</u>
1025							-7.7	
1075	-0.8						-18.6	1.6
1125	-1.6						-29.0	5.0
1175	-3.5	-7.8					-38.7	7.8
1225	-3.5	-16.7						7.0
1275	-3.5	-24.9	-1.2	0.8	-2.7			7.0
1325	-5.8	-31.1	-5.1	1.2	-7.0			9.3
1375	-10.1	-36.2	-11.6	1.2	-11.7			14.3
1425	-12.8	-42.4	-19.8	0.4	-16.0	-0.4		18.6
1475	-13.6	-49.4	-30.3	-0.4	-19.9	-1.2		20.9
1525	-15.5	-56.0	-43.2	2.0	-23.9	-1.6		25.2
1575			-57.5	-4.3	-27.8	-2.0		
1625			-73.8	-7.8	-31.3	-2.4		
1675			-92.5	-12.5	-34.8	-2.7		
1725			-110.3	-18.3	-38.3	-3.5		
1775			-129.3	-24.6	-42.6	-4.3		
1825			-152.7	-32.8	-47.3	-5.1		
1875				-43.7	-52.0	-6.7		
1925				-57.0	-56.7	-9.0		
1975				-72.6	-61.0	-12.2		
2025				-91.7	-64.1	-16.9		
2075				-112.8	-69.2	-22.3		
2125					-74.3	-29.8		
2175					-80.6	-38.4		
2225					-89.2	-48.2		
2275					-100.1	-58.8		
2325					-113.0	-70.5		
2375						-86.2		
2425						-105.0		

APPENDIX III: Carbonate Content

TABLE AIII-1: CARBONATE SUMMARY

<u>Depth</u> <u>(cm.)</u>	<u>1 PC</u>	<u>2 PC</u>	<u>3 PC</u>	<u>4 PC</u>	<u>5 PC</u>	<u>6 PC</u>	<u>10 PC</u>	<u>11 PC</u>	<u>12 PC</u>
10	7.4	4.0	25.7	18.6	4.7	0.9	8.7	9.9	18.8
20	7.0	8.0	24.5	16.9	4.5	5.8	5.9	13.1	21.8
30	5.4	5.5	24.7	19.1	4.2	7.7	8.1	10.6	21.7
40	1.4	7.2	24.7	15.8	5.4	4.3	9.3	7.2	21.7
50	5.7	5.1	10.3	18.9	6.2	6.0	7.9	11.9	22.9
60	3.5	3.4	22.3	18.1	5.7	5.5	8.9	14.3	21.9
70	5.5	3.8	23.2	17.4	4.7	4.5	8.8	11.5	20.1
80	5.8	6.3	18.7	17.8	4.6	6.1	7.9	16.3	19.5
90	5.0	5.3	7.2	19.2	6.0	5.8	7.1	14.8	22.1
100	3.2	3.0	22.8	19.5	6.5	7.6	8.0	11.7	21.7
110	6.3	5.7	24.2	15.1	6.0	5.4	8.1	9.9	24.3
120	6.2	11.5	21.3	15.6	6.8	5.7	8.2	15.6	23.4
130	3.2	7.7	19.5	14.2	6.1	3.0	7.6	15.3	13.1
140	3.9	4.5	25.5	13.3	5.4	4.8	5.1	16.2	22.7
150	4.4	5.3	20.0	11.6	6.7	6.3	7.0	15.8	23.7
160	3.3	2.1	11.7	14.1	6.5	7.6	7.4	12.1	22.6
170	5.7	5.4	17.2	11.6	6.2	4.0	8.3	7.7	22.9
180	4.6	0.0	8.0	12.6	6.2	6.8	9.6	5.5	22.7
190	1.9	3.6	11.5	15.1	2.9	5.4	5.1	14.3	20.6
200	0.1	2.2	9.0	10.3	8.6	1.7	7.5	21.9	25.2
210	4.3	5.5	2.7	5.1	8.5	7.4	8.8	10.0	18.4
220	2.8	1.3	19.2	12.6	10.7	4.5	9.0	9.6	17.6
230	3.2	4.5	15.5	2.4	11.4	5.2	8.4	9.4	19.1
240	3.9	4.5	14.9	15.4	9.7	6.5	8.6	9.6	17.9
250	3.7	7.6	4.7	18.2	2.3	6.3	10.5	5.9	21.1
260	7.4	6.8	19.0	15.1	0.8	5.9	5.7	10.7	18.6
270	4.8	6.0	15.6	14.8	3.8	7.8	9.5	5.0	21.8
280	3.9	11.1	11.2	15.7	6.6	6.8	11.3	7.7	20.2
290	5.7	16.7	13.6	15.8	7.7	9.1	9.8	7.0	19.3
300	6.6	15.4	6.3	15.4	6.7	3.7	9.0	8.1	21.5
310	4.5	7.7	3.4	11.2	8.3	8.0	8.3	6.6	21.3
320	6.2	11.2	15.8	10.9	8.3	6.7	5.9	7.6	21.8
330	3.9	2.7	10.3	9.2	1.4	2.9	8.3	10.4	21.3
340	4.4	2.6	12.0	10.4	8.1	7.2	11.0	14.4	21.1
350	7.3	10.0	9.3	11.6	4.0	6.1	11.6	17.9	23.6
360	8.6	6.0	3.4	15.5	6.2	8.3	9.6	3.0	25.5
370	2.9	7.2	2.6	13.0	6.4	8.4	6.5	6.9	28.2
380	6.6	4.3	4.3	10.7	3.5	10.9	5.3	3.3	25.3
390	5.0	7.4	0.7	6.3	5.7	8.5	7.7	4.1	10.1
400	8.3	7.0	5.1	13.1	5.7	3.5	6.7	8.3	3.8
410	3.1	4.4	7.7	13.2	5.2	3.5	6.3	17.6	8.1
420	8.5	5.7	7.4	11.9	2.7	3.2	8.5	7.1	10.8
430	4.7	2.4	8.3	8.8	4.2	6.8	9.2	10.1	12.7
440	10.6	5.3	5.7	6.8	4.7	7.1	11.1	9.1	11.9

Depth (cm.)	<u>1 PC</u>	<u>2 PC</u>	<u>3 PC</u>	<u>4 PC</u>	<u>5 PC</u>	<u>6 PC</u>	<u>10 PC</u>	<u>11 PC</u>	<u>12 PC</u>
450	4.1	5.6	2.6	10.3	5.2	6.5	11.5	8.5	7.3
460	3.6	6.0	10.9	5.0	1.3	6.4	9.2	5.3	9.1
470	7.4	8.1	4.7	6.2	4.2	6.9	11.2	6.8	6.8
480	2.5	8.4	4.8	4.8	5.2	1.5	7.6	5.9	15.5
490	6.5	5.4	2.0	9.9	8.3	6.8	7.2	5.1	11.7
500	5.6	9.2	3.7	7.9	5.3	1.9	6.2	6.2	9.2
510	6.0	7.1	6.7	9.9	5.4	7.8	7.9	5.7	2.8
520	7.7	4.4	9.5	3.7	3.7	7.2	8.2	5.6	5.8
530	5.2	5.0	6.7	8.9	6.3	7.7	7.9	6.5	8.3
540	5.6	5.0	8.1	7.6	5.7	10.5	8.6	6.1	10.6
550	1.1	2.4	2.6	10.5	6.1	5.6	7.6	6.4	5.8
560	2.2	5.0	0.0	4.5	6.9	2.4	8.7	5.6	10.7
570	6.7	1.5	1.9	8.0	4.4	2.3	3.6	5.2	9.8
580	8.0	6.7	3.2	7.5	6.1	7.3	3.2	7.2	4.1
590	5.2	6.9	4.2	3.7	6.4	6.8	7.8	7.0	4.1
600	7.8	5.8	1.6	7.8	5.6	6.2	3.6	7.3	7.7
610	2.2	5.8	3.2	10.1	6.7	4.3	6.0	5.9	13.1
620	3.6	2.7	5.5	9.4	3.7	4.9	6.6	6.0	6.7
630	2.8	3.3	6.9	8.6	4.6	4.9	3.5	6.5	13.3
640	8.3	4.7	9.1	11.2	4.7	4.8	5.9	4.8	9.0
650	3.6		7.6	13.5	6.9	3.7	7.6	6.3	0.0
660	7.2		3.5	15.4	12.7	2.9	7.6	7.3	4.2
670	2.3		4.8	8.9	6.2	2.7	8.3	7.8	16.0
680	4.0		6.6	8.3	5.2	5.9	9.8	6.4	11.2
690	4.7		9.3	8.6	6.5	3.9	2.3	6.8	10.1
700	4.5		9.8	9.0	5.0	2.7	8.4	5.2	7.4
710	1.2		3.5	8.2	3.1	6.4	7.0	4.4	12.0
720	1.4		11.0	4.1	5.8	6.6	17.1	5.3	6.4
730	2.2		2.9	8.7	4.2	1.8	6.0	6.3	0.7
740	3.0		4.6	7.3	4.0	5.0	7.1	5.1	3.0
750	5.9		9.7	6.4	4.4	7.6	12.4	6.5	8.0
760	5.8		8.7	8.3	7.7	4.7	10.9	4.0	0.6
770	5.5		15.3	10.7	8.3	7.4	9.3	3.4	1.2
780	6.4		12.1	8.5	6.6	8.4	8.8	4.7	1.8
790	5.0		6.4	8.5	9.0	2.5	7.9	5.5	13.4
800			16.8	8.6	7.0	4.6	9.7	7.0	3.1
810			10.8	9.1	4.0	8.9	8.4	3.3	12.5
820			2.4	2.5	18.2	8.1	9.4	7.6	17.5
830				9.7	5.5	5.9	8.6	10.2	18.8
840				8.8	12.2	3.8	9.2	15.5	14.7
850			1.9	8.2	2.1	6.0	4.2	10.5	8.5
860			3.1	8.7	6.9	6.6	6.7	12.1	22.2
870			0.9	3.7	11.3	5.4	8.8	1.6	7.2
880			0.0	5.4	7.7	7.9	7.4	10.5	6.7
890			2.3	5.0	3.0	4.0	7.7	8.8	3.4
900			2.7	7.9	7.5	3.2	7.5	10.4	18.1
910			1.6	8.7	14.0	4.0	8.5	9.5	4.8





APPENDIX IV: Coarse Fraction

APPENDIX IV  
TABLE AIV - 1: Coarse Fraction

Depth in Core (cm)	1 PC	2 PC	3 PC	4 PC	5 PC	6 PC	10 PC	11 PC	12 PC
10	34.3	83.1	11.3	25.1	2.2	9.4	4.5	75.7	12.9
20	7.5	67.6	11.7	27.2	5.6	4.7	2.8	83.5	13.2
30	22.9	74.3	13.6	30.6	3.0	3.3	3.7	75.4	11.0
40	12.3	57.2	13.0	25.0	4.4	5.6	5.7	81.4	12.6
50	10.6	6.5	16.9	12.9	3.8	5.1	1.8	8.5	13.1
60	16.2	55.0	15.1	12.3	5.4	7.2	3.2	83.8	14.9
70	8.5	24.9	12.6	10.4	3.5	6.5	5.3	77.2	12.5
80	4.8	7.6	11.2	9.5	2.7	4.6	3.3	67.1	9.8
90	11.8	36.4	4.4	9.3	3.3	1.2	1.9	75.0	16.2
100	9.1	64.8	16.4	10.7	8.1	7.0	2.3	72.0	17.4
110	8.0	22.0	17.6	12.9	5.1	8.4	2.3	97.9	14.7
120	9.6	56.2	12.9	13.2	4.0	1.5	2.9	73.1	12.2
130	16.2	40.6	11.4	9.9	10.0	1.8	1.2	60.4	14.9
140	15.9	68.1	12.8	12.3	8.4	1.7	5.4	51.9	16.6
150	10.6	8.1	13.6	9.7	9.0	1.8	2.7	24.3	21.1
160	5.9	45.9	9.8	10.5	6.8	1.3	2.8	64.8	18.9
170	7.9	79.2	5.0	8.1	3.8	2.0	1.3	84.4	15.3
180	16.1	85.6	4.6	11.3	4.6	4.3	1.6	83.7	10.8
190	19.9	87.0	8.5	7.5	4.6	4.1	2.5	70.7	24.4
200	13.8	90.0	5.1	6.7	3.8	1.4	1.6	73.2	21.3
210	6.1	14.5	16.4	11.2	2.8	5.8	3.7	48.5	20.3
220	16.8	86.7	2.9	4.4	5.2	5.9	3.1	87.0	17.0
230	30.7	9.7	3.3	22.7	1.6	5.8	3.3	62.7	17.9
240	31.2	10.9	32.6	2.8	2.4	8.5	4.0	53.2	14.4
250	19.9	5.6	8.0	5.1	3.0	6.8	7.9	81.8	22.9
260	5.9	12.5	13.4	7.2	1.1	4.5	5.7	77.3	17.4
270	7.2	28.8	4.8	4.9	7.0	3.1	1.1	56.2	21.2
280	25.6	63.1	48.8	5.2	1.8	3.9	3.6	68.1	21.7
290	7.6	70.6	42.5	3.8	7.9	5.9	1.5	63.2	23.5
300	1.3	91.9	20.9	2.8	2.0	4.5	3.6	71.3	21.8
310	2.7	91.5	14.9	2.6	3.7	2.1	1.9	78.4	20.2
320	1.7	25.2	1.4	1.7	2.0	4.0	7.2	83.1	20.2
330	3.1	74.3	16.0	2.3	8.1	5.2	3.3	76.4	26.9
340	4.9	37.8	66.3	13.4	18.0	11.1	15.2	67.6	16.2
350	9.6	87.6	43.1	3.2	19.3	2.8	7.6	71.1	28.7
360	13.1	27.9	17.3	0.8	13.5	6.7	2.6	64.9	25.9
370	35.2	75.8	31.2	0.4	9.1	4.5	1.0	79.9	37.9
380	12.2	-	41.7	0.7	27.4	3.5	3.8	70.4	28.5
390	5.1	46.0	6.3	0.9	5.5	2.9	3.7	78.1	4.6
400	5.4	50.8	28.2	0.5	-	2.2	6.0	33.2	14.3
410	2.9	75.1	38.0	0.3	2.6	0.9	5.7	37.7	6.0
420	4.6	61.0	24.1	0.5	4.9	7.9	4.0	35.4	19.4
430	24.7	52.5	25.4	0.5	2.0	1.5	5.6	30.4	31.3

Depth in Core (cm)	1 PC	2 PC	3 PC	4 PC	5 PC	6 PC	10 PC	11 PC	12 PC
440	0.4	33.6	31.5	6.6	9.4	5.1	9.9	23.0	18.0
450	5.4	39.5	36.2	0.5	3.7	3.6	8.2	8.7	60.1
460	0.6	58.9	28.1	0.6	10.4	3.8	5.3	4.4	56.5
470	0.2	39.2	30.3	1.8	4.5	3.3	6.6	5.3	37.4
480	26.7	81.2	0.8	8.4	3.3	2.8	7.8	5.0	17.2
490	3.0	85.7	29.3	2.1	4.4	8.8	8.4	4.7	13.4
500	25.7	85.5	61.9	3.1	19.3	4.0	8.1	7.8	36.1
510	3.0	77.1	4.5	8.6	20.0	11.6	4.1	7.5	32.3
520	9.9	66.0	29.8	25.3	14.7	10.0	3.0	2.4	64.3
530	12.4	34.2	31.7	1.6	6.3	6.1	8.6	6.0	5.6
540	32.0	17.4	44.8	1.9	1.7	1.8	11.5	4.7	2.7
550	13.3	22.0	40.5	5.1	4.9	17.5	4.3	8.3	2.7
560	36.2	19.0	15.2	44.4	3.8	6.4	15.5	6.9	0.3
570	12.0	26.2	22.8	47.4	4.1	0.6	5.8	12.5	1.2
580	10.1	46.7	16.1	53.5	4.1	2.6	23.2	18.7	15.3
590	10.2	13.5	20.5	28.8	3.6	3.1	3.8	6.7	24.9
600	21.9	63.0	25.5	18.6	1.9	1.4	8.2	5.5	30.5
610	33.7	80.4	17.3	1.9	18.7	1.0	1.7	4.4	1.6
620	12.9	33.3	33.9	4.6	2.7	0.6	2.9	3.9	12.2
630	0.5	83.3	63.8	6.3	4.5	9.2	1.6	7.7	12.4
640	1.3	86.0	56.2	1.9	8.4	1.0	4.5	8.8	7.9
650	11.6		71.3	1.8	5.9	2.2	2.1	10.4	6.1
660	1.1		35.8	1.1	57.1	2.1	1.8	10.1	50.2
670	42.9		31.1	4.6	48.1	4.9	0.8	6.4	1.4
680	19.6		9.0	5.0	15.4	5.4	1.2	4.8	3.1
690	10.6		51.5	5.2	31.3	1.5	0.9	7.3	4.3
700	5.4		32.5	9.2	5.8	6.2	4.4	5.7	1.1
710	2.0		58.2	7.7	12.7	2.8	2.5	9.1	3.2
720	3.6		9.3	1.4	8.0	3.3	46.1	12.4	0.2
730	2.3		24.3	1.4	8.4	1.1	4.9	7.7	1.0
740	2.1		42.6	27.5	18.1	4.9	28.0	60.1	11.7
750	4.0		67.9	1.6	8.7	2.2	3.2	79.9	14.6
760	3.6		50.5	28.7	5.0	3.9	2.9	81.1	29.2
770	8.7		0.4	5.8	2.3	4.4	11.1	78.9	25.7
780	4.7		27.2	5.4	3.7	21.4	3.1	74.5	26.5
790	13.5		13.6	5.0	6.8	6.7	3.8	71.4	3.0
800			6.6	5.1	3.3	29.9	1.7	34.1	15.9
810			17.6	5.9	21.8	3.2	2.2	14.5	0.3
820			57.5	42.5	29.3	6.8	1.1	27.1	1.2
830			78.1	4.1	19.7	4.1	1.2	12.7	0.7
840			-	4.8	60.0	0.5	1.8	6.9	1.0
850			49.8	7.5	55.3	4.4	3.5	7.5	0.2
860			52.9	6.3	9.7	3.4	0.4	12.5	2.1
870			85.7	2.3	10.9	6.1	2.3	7.8	0.2
880			37.5	7.7	12.8	4.5	6.3	10.1	0.4
890			83.6	5.3	3.2	5.2	10.6	6.6	0.3



#### APPENDIX V: Paleomagnetic Orientation of Cores

Paleomagnetic determinations were made on 170 samples from eight box cores for the purpose of determining core orientation relative to magnetic north. Measurements were made on a cryogenic magnetometer. Samples were placed in 2 x 2 x 1 cm. plastic boxes which were oriented relative to the framework of the box corer (Figure AV-1). Declinations are given in this framework; inclinations are positive downwards. All samples were demagnetized at 300 Oe. Two additional samples from one piston core are included for the purpose of orienting cross-laminae in sand layers.

Vector mean directions are summarized for each core in Table AV-1. Confidence limits (95) are calculated according to the method described by McElhinny (1973) for determining errors in a spherical coordinate system. Complete listings of paleomagnetic determinations at 300 Oe demagnetization are found in Table AV-2.

FIGURE AV-1: Paleomagnetic orientation of cores. A, B, C, D are faces of box corer clockwise from open front of box. Declination determined by magnetometer is magnetic north in reference frame of box corer, as indicated. Arrows indicate mean direction of samples from 8 measured box cores (Table AI-1). Dashed arrows are samples from piston core 4PC used to orient cross-laminae in a sand layer (Table AI-2).

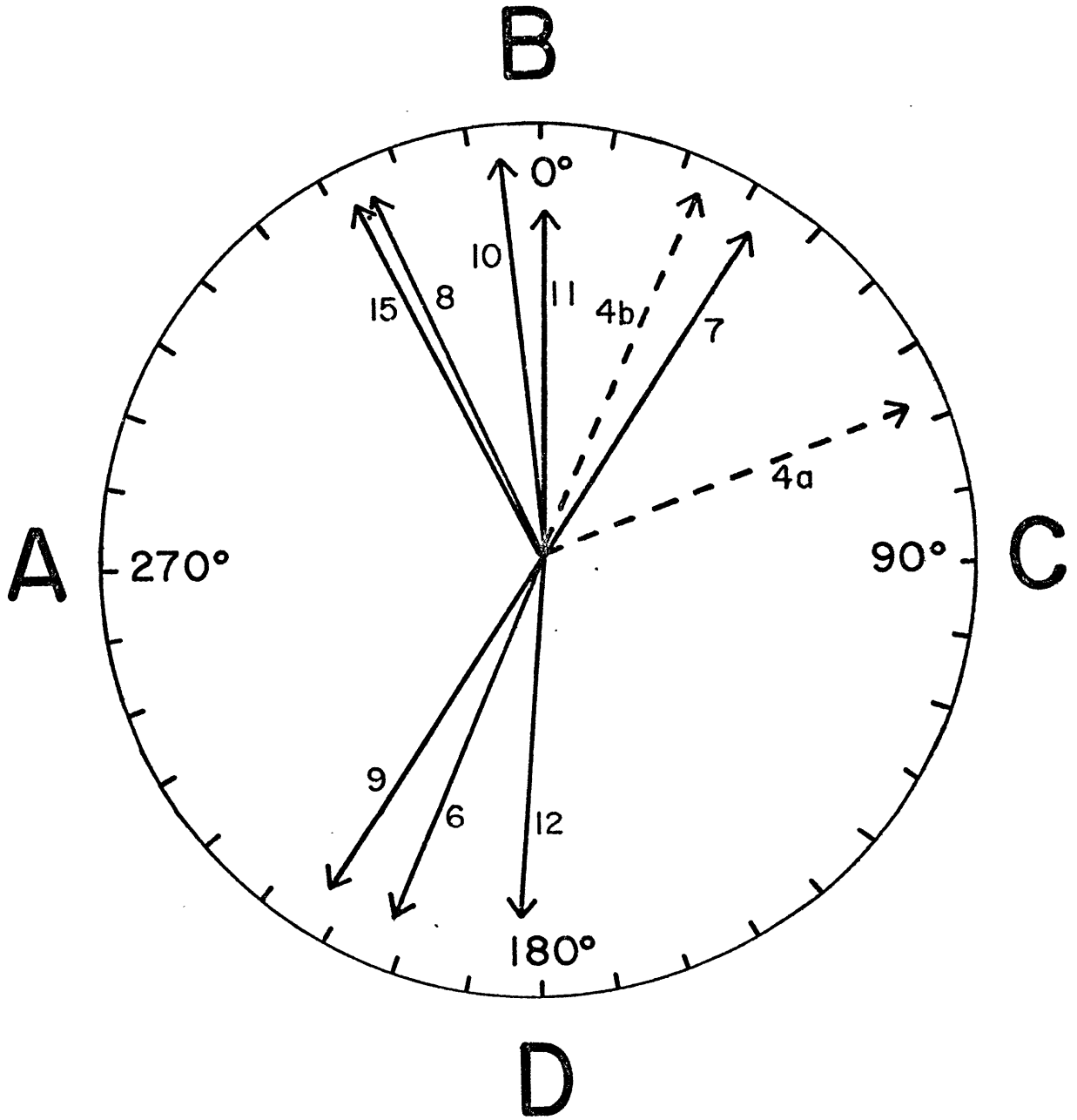




TABLE AV - 1: Summary of mean orientation of box cores.

6 BC

$$I = 64.5^{\circ}$$

$$D = 201.9^{\circ}$$

$$\alpha_{95} = 4.9^{\circ}$$

$$n = 15$$

7 BC

$$I = 81.8^{\circ}$$

$$D = 019.7^{\circ}$$

$$\alpha_{95} = 5.0^{\circ}$$

$$n = 24$$

8 BC

$$I = 74.1^{\circ}$$

$$D = 336.0^{\circ}$$

$$\alpha_{95} = 5.7^{\circ}$$

$$n = 13$$

9 BC

$$I = 72.9^{\circ}$$

$$D = 212.8^{\circ}$$

$$\alpha_{95} = 2.8^{\circ}$$

$$n = 26$$

10 BC

$$I = 70.5^{\circ}$$

$$D = 353.7^{\circ}$$

$$\alpha_{95} = 2.4^{\circ}$$

$$n = 26$$

11 BC

$$I = 73.3^{\circ}$$

$$D = 000.5^{\circ}$$

$$\alpha_{95} = 2.6^{\circ}$$

$$n = 27$$

12 BC

$$I = 73.8^{\circ}$$

$$D = 184.1^{\circ}$$

$$\alpha_{95} = 2.4^{\circ}$$

$$n = 14$$

15 BC

$$I = 74.7^{\circ}$$

$$D = 332.7^{\circ}$$

$$\alpha_{95} = 2.5^{\circ}$$

$$n = 14$$

TABLE AV-2: Paleomagnetic Determinations, Box Cores

<u>6BC</u>			<u>7BC</u>			<u>8BC</u>			<u>9BC</u>		
<u>z</u>	<u>I</u>	<u>D</u>	<u>z</u>	<u>I</u>	<u>D</u>	<u>z</u>	<u>I</u>	<u>D</u>	<u>z</u>	<u>I</u>	<u>D</u>
1	64.4	182.1	4	58.6	311.5	6	69.1	296.1	1	56.8	206.6
4	70.6	178.1	4	61.5	320.1	12	69.3	300.1	4	69.2	204.3
6	71.7	194.4	7	66.0	275.2	19	82.3	328.2	6	78.7	201.4
8	63.6	211.6	10	73.9	033.5	21	80.2	313.3	8	76.0	185.9
10	76.0	219.8	11	82.5	049.1	24	86.5	333.1	11	78.5	181.9
13	71.7	220.1	12	74.5	026.8	29	79.5	342.5	13	78.5	201.7
15	61.4	126.7?	14	77.0	054.6	31	72.2	357.5	16	79.4	187.9
17	62.8	203.2	15	77.8	043.3	33	62.0	344.2	18	80.9	184.1
20	73.1	219.8	16	76.9	042.2	40	63.5	006.0	20	75.5	210.6
23	67.3	212.1	19	73.9	048.1	46	60.8	001.6	22	73.4	180.6
25	61.6	197.1	21	78.7	024.9	50	65.8	318.8	25	72.6	212.3
27	58.7	214.2	24	77.7	050.1	65	80.4	339.3	28	70.7	223.1
29	61.1	198.0	29	71.1	116.3				30	72.5	207.0
32	49.6	201.1	31	75.2	123.8				32	72.1	215.7
35	43.8	191.7	33	70.0	022.6				35	72.8	211.1
			35	73.2	044.2				37	64.5	199.9
			37	71.4	050.4				40	65.1	206.8
			39	74.4	034.0				43	67.9	203.1
			41	80.3	265.9				46	68.1	211.8
			41	75.2	280.4				48	68.4	234.1
			43	76.6	275.1				51	72.2	220.8
			45	75.5	281.1				53	70.8	239.8
			47	80.3	234.7				56	72.5	255.5
									58	80.2	241.4
									61	75.2	236.6
									63	59.8	234.0

z is depth in box core, in centimeters.

I is inclination, positive down, in degrees.

D is declination (direction of magnetic north), in degrees.

TABLE AV-2: Paleomagnetic Determinations, Box Cores, continued.

<u>10BC</u>			<u>11BC</u>			<u>12BC</u>			<u>15BC</u>		
<u>z</u>	<u>I</u>	<u>D</u>	<u>z</u>	<u>I</u>	<u>D</u>	<u>z</u>	<u>I</u>	<u>D</u>	<u>z</u>	<u>I</u>	<u>D</u>
1	84.3	334.7	3	64.7	027.4	1	72.6	219.3	1	77.0	309.0
3	74.7	000.4	5	62.8	010.1	3	74.4	187.2	5	71.2	314.4
5	76.4	307.2	8	72.0	356.0	5	73.9	186.5	7	69.0	310.8
8	78.9	324.1	10	70.6	349.5	8	71.8	189.4	10	69.9	292.1
10	71.0	343.8	12	70.5	350.9	10	73.2	197.3	14	72.2	329.4
13	67.4	355.2	15	68.0	344.8	13	71.2	175.9	17	74.7	356.0
15	71.1	347.7	17	71.3	000.1	15	66.6	168.3	20	73.0	015.2
17	66.6	345.0	19	71.6	335.5	18	73.5	194.7	24	78.7	035.5
20	70.4	344.3	22	74.3	335.4	20	72.6	178.0	26	80.7	021.9
22	71.4	343.8	24	79.3	326.1	23	76.3	172.8	28	75.9	314.0
25	71.5	355.5	26	81.4	027.1	27	70.5	161.4	30	77.5	319.0
30	68.6	341.9	29	81.8	356.4	29	76.1	166.5	32	75.6	332.1
32	62.7	343.4	32	72.8	330.3	32	76.3	197.0	34	72.7	314.3
34	65.8	352.7	34	80.4	354.3	34	76.6	192.5	37	68.8	332.0
37	67.3	351.3	36	76.0	002.3				39	76.6	349.4
39	65.1	341.3	40	68.9	341.7				41	68.9	344.7
41	65.3	347.1	43	62.5	341.9				44	74.0	347.6
44	65.3	355.3	45	70.7	008.9				46	72.2	339.3
46	66.8	358.0	48	70.1	004.8				49	65.8	330.7
48	70.6	012.1	50	69.4	014.2				51	73.0	335.8
50	68.0	016.6	52	68.4	001.1				53	71.9	331.3
53	70.8	012.4	54	73.2	014.2				56	77.5	332.5
55	70.0	016.3	57	67.3	040.4				58	73.6	335.7
57	67.1	021.3	59	73.7	029.0				60	76.2	319.1
59	73.8	018.1	62	75.7	023.9						
62	66.3	353.4	64	77.8	007.5						
			67	79.5	348.3						

Two samples from piston core 4PC were used for orienting a sand layer sample for determination of the orientation of cross-laminae relative to the slope of the ridge. Samples were run twice each (demagnetized at 300 Oe each time):

148 cm: a. I = 56.7 D = 067.4  
 b. I = 60.8 D = 069.3  
 156 cm: a. I = 68.1 D = 028.4  
 b. I = 66.9 D = 017.0

Mean declination gives an orientation of approximately 045° for magnetic north (see Figure AV-1). The piston core was oriented such that the face of the Working half of the piston core was oriented as the "C" face of the box core. The x-radiograph was made of the Archive half of the piston core, and therefore has the opposite orientation (the face seen in Figure 4.7 is the equivalent of the box core "A" face).